National Library
of Canada

Bibliothèque nationale
du Canada

Canadian Theses Service

Services des thèses canadiennes

Ottawa, Canada
K1A 0N4

CANADIAN THESES

THÈSES CANADIENNES

NOTICE

The quality of this microfiche is heavily dependent upon the quality of the original thesis submitted for microfilming. Every effort has been made to ensure the highest quality of reproduction possible.

If pages are missing, contact the university which granted the degree.

Some pages may have indistinct print especially if the original pages were typed with a poor typewriter ribbon or if the university sent us an inferior photocopy.

Previously copyrighted materials (journal articles, published tests, etc.) are not filmed.

Reproduction in full or in part of this film is governed by the Canadian Copyright Act, R.S.C. 1970, c. C-30.

AVIS

La qualité de cette microfiche dépend grandement de la qualité de la thèse soumise au microfilmage. Nous avons tout fait pour assurer une qualité supérieure de reproduction.

S'il manque des pages, veuillez communiquer avec l'université qui a conféré le grade.

La qualité d'impression de certaines pages peut laisser à désirer, surtout si les pages originales ont été dactylographiées à l'aide d'un ruban usé ou si l'université nous a fait parvenir une photocopie de qualité inférieure.

Les documents qui font déjà l'objet d'un droit d'auteur (articles de revue, examens publiés, etc.) ne sont pas microfilmés.

La reproduction, même partielle, de ce microfilm est soumise à la Loi canadienne sur le droit d'auteur, SRC 1970, c. C-30.

THIS DISSERTATION
HAS BEEN MICROFILMED
EXACTLY AS RECEIVED

LA THÈSE A ÉTÉ
MICROFILMÉE TELLE QUE
NOUS L'AVONS REÇUE

NL-339 (r.86/06)

Canada

THE UNIVERSITY OF ALBERTA

NATURAL CONVECTION IN LIQUIDS WITH TEMPERATURE-DEPENDENT PROPERTIES AND SOLIDIFICATION

by

PERIANNA GOUNDER SABHAPATHY

A THESIS
SUBMITTED TO THE FACULTY OF GRADUATE STUDIES AND RESEARCH
IN PARTIAL FULFILMENT OF THE REQUIREMENTS FOR THE DEGREE
OF DOCTOR OF PHILOSOPHY

DEPARTMENT OF MECHANICAL ENGINEERING

EDMONTON, ALBERTA
SPRING 1986

Permission has been granted to the National Library of Canada to microfilm this thesis and to lend or sell copies of the film.

The author (copyright owner) has reserved other publication rights, and neither the thesis nor extensive extracts from it may be printed or otherwise reproduced without his/her written permission.

L'autorisation a été accordée à la Bibliothèque nationale du Canada de microfilmer cette thèse et de prêter ou de vendre des exemplaires du film.

L'auteur (titulaire du droit d'auteur) se réserve les autres droits de publication; ni la thèse ni de longs extraits de celle-ci ne doivent être imprimés ou autrement reproduits sans son autorisation écrite.

ISBN 0-315-30197-X

THE UNIVERSITY OF ALBERTA

RELEASE FORM

NAME OF AUTHOR	PERIANNA GOUNDER SABHAPATHY
TITLE OF THESIS	NATURAL CONVECTION IN LIQUIDS WITH TEMPERATURE-DEPENDENT PROPERTIES AND SOLIDIFICATION

DEGREE FOR WHICH THESIS WAS PRESENTED DOCTOR OF PHILOSOPHY

YEAR THIS DEGREE GRANTED SPRING 1986

Permission is hereby granted to THE UNIVERSITY OF ALBERTA LIBRARY to reproduce single copies of this thesis and to lend or sell such copies for private, scholarly or scientific research purposes only.

The author reserves other publication rights, and neither the thesis nor extensive extracts from it may be printed or otherwise reproduced without the author's written permission.

(SIGNED) ....

PERMANENT ADDRESS:

Pudupatty, Elur (PO),
Puduchatram (Via), Salem (Dt),
Tamil Nadu 636018, INDIA.

DATED 28th February 1986

THE UNIVERSITY OF ALBERTA

FACULTY OF GRADUATE STUDIES AND RESEARCH

The undersigned certify that they have read, and recommend to the Faculty of Graduate Studies and Research, for acceptance, a thesis entitled NATURAL CONVECTION IN LIQUIDS WITH TEMPERATURE-DEPENDENT PROPERTIES AND SOLIDIFICATION submitted by PERIANNA GOUNDER SABHAPATHY in partial fulfilment of the requirements for the degree of DOCTOR OF PHILOSOPHY.

K.C. Cheng

Supervisor

J.D. Dale

Masliyah

E. G. Hauptman

External Examiner

Date February 25, 1986

எப்பொருள் யார்யார்வாய்க் கேட்பினும் அப்பொருள்
மெய்ப்பொருள் காண்ப தறிவு.

To discern the truth in everything,

by whomsoever spoken, is wisdom.

-TIRUKKURAL

To My Father

Abstract

The effects of temperature-dependent properties on the laminar natural convective boundary layer flow along an isothermal vertical flat plate were studied numerically for liquids with Prandtl numbers 1 to ∞. The effects of temperature-dependent viscosity and coefficient of thermal expansion on the stability of the laminar flow were investigated employing linear stability theory. The transient laminar natural convective flow along a smooth vertical circular cylinder subjected to a step change in surface temperature was analyzed numerically for various radii of the cylinder.

Experiments were conducted in water with an isothermal vertical circular pipe (outside diameter 41.3 mm and length 1 m) for various combinations of wall and ambient temperatures in the range 0 to 35°C. The flow was visualized using shadowgraph and dye injection techniques and the points of onset of instability and transition to turbulent flow were obtained for the naturally occurring disturbances. The effects of natural convection on freezing of water over a convectively cooled vertical circular pipe were studied experimentally for ambient temperatures between 8 and 17.5°C and coolant temperatures between -10 and -20°C.

Numerical solutions indicate that for moderate temperature differences between the wall and the ambient liquid, the density can be assumed to be constant in the governing equations except in the buoyancy force term. The

assumption that density varies linearly with temperature in the buoyancy force term underpredicts the surface heat transfer, the surface shear stress, and the total mass flow rate for down flows, and overpredicts them for up flows. The effects are significant for liquids with small as well as large Prandtl numbers. The temperature-dependent viscosity increases the surface shear stress, and decreases the surface heat transfer and the total mass flow rate for a cooled wall, and the reverse is true for a heated wall. Temperature-dependent thermal conductivity, and specific heat at constant pressure also have significant effects on the surface shear stress, the surface heat transfer, and the total mass flow rate.

For liquids, the temperature-dependent viscosity stabilizes the flow along a heated wall and destabilizes it along a cooled wall. The temperature-dependent coefficient of thermal expansion initially stabilizes the flow for a heated wall but farther downstream it destabilizes the flow. For water, the numerical results predict that the critical Grashof number for the onset of instability is discontinous in the region where flow reversals occur due to the density maximum. The trends of experimentally obtained critical values of Grashof number for the onset of instabilty and the transition to turbulence in water agree with the numerical predictions. The temperature measurements and the shadowgraph flow visualization studies reveal that the critical Grashof numbers for the onset of instability and

the transition to turbulent flow are lower during the transient period than at the steady state.

When water freezes over a convectively cooled vertical circular pipe in natural convection, the thickness of the ice layer increases with axial distance in the laminar regime, remains nearly constant in the transition regime, and decreases with axial distance in the turbulent regime. The heat transfer coefficients at the interface obtained from the heat conduction analysis of the solidified region agree fairly well with those given in literature for the natural convective flow along an isothermal vertical flat plate.

Acknowledgement

I would like to thank

- Dr. K. C. Cheng for his expert guidance and financial support through his research grant from the National Science and Engineering Research Council of Canada throughout the course of this thesis,

- Drs. E. Gates, J. D. Dale and J. Masliah, and Dr. E. G. Hauptmann of the University of British Columbia for their helpful suggestions,

- the technical staff members of the Department of Mechanical Engineering, Mr. T. M. Villet, Mr. A. Muir and their colleagues for their assistance in constructing the experimental apparatus and carrying out the experiments, and

- my family members and friends in India, especially my mother and my brother, for their unfailing love and encouragement throughout my stay at the University of Alberta.

Table of Contents

Chapter Page

1. Introduction 1

1.1 Previous Analyses on the Effects of Variable Properties of the Fluid on the Natural Convective Flow Along a Vertical Surface 1

1.1.1 Laminar Flow 1

1.1.2 Stability of Laminar Flow 6

1.2 Previous Analyses on the Transient Natural Convective Flow Along a Vertical Circular Cylinder 11

1.3 Previous Analyses on the Effects of Natural Convection on Solidification and Melting Problems 15

1.4 Present Analysis 17

2. The Effects of Temperature-Dependent Properties on the Laminar Natural Convective Flow Along an Isothermal Vertical Flat Plate 20

2.1 Theoretical Analysis 20

2.1.1 Governing Equations 20

2.1.2 Variation of Density with Temperature 29

2.1.3 Present Treatment of the Buoyancy Force Term 34

2.1.4 Variations of Viscosity, Thermal Conductivity, and Specific Heat with Temperature 42

2.1.5 The Governing Equations for Liquids with Very Large Prandtl Numbers 44

2.2 Results and Discussion 46

2.2.1 The Effects of Variation of Coefficient of Thermal Expansion with Temperature 47

2.2.2 The Effects of Variation of Viscosity with Temperature 55

2.2.3 The Effects of Variation of Thermal conductivity with Temperature 64

2.2.4 The Effects of Variation of Specific Heat with Temperature 72

2.2.5 The Effects of Variable Properties for Liquids with Very Large Prandtl Numbers ...80

2.2.6 The Effects of Variations of Both the Coefficient of Thermal Expansion and the Viscosity with Temperature 82

2.3 Conclusions 89

3. The Effects of Temperature-Dependent Viscosity and Coefficient of Thermal Expansion on the Stability of Laminar Natural Convective Flow Along an Isothermal Vertical Surface 90

3.1 Theoretical Analysis 90

3.1.1 Linear Stability Theory 90

3.1.2 Governing Equations 91

3.1.3 Base Flow Equations 93

3.1.4 Disturbance Equations 95

3.1.5 Numerical Method 97

3.2 Experimental Apparatus and Procedure 100

3.2.1 Experimental Apparatus 104

3.2.2 Flow Visualization Techniques 105

3.2.3 Experimental Procedure 107

3.3 Results and Discussion 108

3.3.1 The Effects of Variation of Viscosity with Temperature 108

3.3.2 The Effects of Variation of Coefficient of Thermal Expansion with Temperature 123

3.3.3 The Effects of Variations of Both the Viscosity and the Coefficient of Thermal Expansion with Temperature 129

3.3.4 Experimental Results 136

3.4 Conclusions 140

4. The Effects of Maximum Density and Temperature-Dependent Viscosity on the Stability of Laminar Natural Convective Flow of Cold Water Along an Isothermal Vertical Surface 142

4.1 Theoretical Analysis 143

4.1.1 Variations of Density and Viscosity of Cold Water with Temperature 143

4.1.2 Governing Equations 144

4.1.3 Numerical Method 146

4.2 Results and Discussion 147

4.2.1 Neutral Stability Curves When Both t_0 and t_∞ are Below or Above t_m 148

4.2.2 Neutral Stability Curves When t_0 and t_∞ are ~~on the~~ Opposite Sides of t_m 156

4.2.3 The Effects of Variation of Viscosity with Temperature 160

4.2.4 Flow Visualization Studies 163

4.3 Conclusions 166

5. Transient Laminar Natural Convective Flow Along a Vertical Circular Cylinder Subjected to a Step Change in Surface Temperature 167

5.1 Theoretical Analysis 167

5.1.1 Governing Equations 167

5.1.2 Numerical Method 171

5.2 Experimental Apparatus and Procedure 173

5.3 Results and Discussion 173

5.3.1 Steady State Temperature and Axial Velocity Profiles 174

5.3.2 Transient Temperature and Axial Velocity Profiles 182

5.3.3 Transient Nusselt Numbers 193

5.3.4 Temperature Measurements 197

5.3.5 Flow Visualization Studies 200

5.4 Conclusions 207

6. Determination of Local Heat Transfer Coefficients at the Solid-Liquid Interface by Heat Conduction Analysis of the Solidified Region 208

6.1 Theoretical Analysis 208

6.2 Results and Discussion 215

6.2.1 Ice Formation Over an Isothermally Cooled Planar Plate 215

6.2.2 Ice Formation Around an Isothermally Cooled Cylinder in Crossflow 216

6.2.3 Ice Formation Inside a Convectively Cooled Pipe 221

6.3 Conclusions 218

7. An Experimental Investigation of Ice Formation Over a Convectively Cooled Vertical Circular Cylinder in Natural Convection 221

7.1 A One-Dimensional Analysis of the Transient Development of the Solid-Liquid Interface 223

7.2 Experimental Apparatus and Procedure 231

7.3 Results and Discussion 233

7.3.1 Transient Development of the Interface ...233

7.3.2 The Local and the Average Heat Transfer Coefficients at the Interface 248

7.3.3 The Effects of Stratification of Ambient Water 250

7.3.4 Cracking of Ice Layer During Melting 252

7.3.5 The Effects of Dissolved Air in Ambient Water 255

7.3.6 The Effects of Artificially-Induced Disturbances 256

7.4 Conclusions 258

8. Conclusions 261

8.1 Scope of Results 261
8.2 Conclusions and Significance 262
8.3 Recommendations 265
References 267
Appendix A 277
Appendix B 282
Appendix C 289
Appendix D 292
Appendix E 297

List of Tables

Table Page

2.1 The effects of variation of density with temperature 30

2.2 The effects of ϵ_f for various Prandtl numbers 54

2.3 The effects of γ_f for various Prandtl numbers 62

2.4 The effects of λ_f for various Prandtl numbers 71

2.5 The effects of ζ_f for various Prandtl numbers 79

2.6 The effects of variable properties for $Pr \to \infty$ 81

2.7 The effects of both ϵ_f and γ_f for $Pr=10$ 88

List of Figures

Figure Page

2.1 The coordinate system 21

2.2 The effects of variation of density with temperature 25

2.3 The dimensionless buoyancy force for different models 38

2.4 The effects of ϵ_f on temperature and velocity profiles for various Prandtl numbers 48

2.5 The effects of γ_f on temperature and velocity profiles for various Prandtl numbers 56

2.6 The effects of λ_f on temperature and velocity profiles for various Prandtl numbers 65

2.7 The effects of ζ_f on temperature and velocity profiles for various Prandtl numbers 73

2.8 Typical temperature and velocity profiles for Pr=10 with opposing or aiding effects of ϵ_f and γ_f 84

3.1 Photograph of the experimental apparatus 101

3.2 Schematic diagram of the experimental apparatus 102

3.3 Typical thermocouple calibration curve 106

3.4 The effects of γ_f on the stability of laminar natural convective flow for Pr=10 109

3.5 The effects of γ_f on the stability of laminar natural convective flow for Pr=20 and Pr=50 117

3.6 The effects of γ_f on the disturbance temperature and velocity profiles for Pr=10 119

3.7 The effects of ϵ_f on the stability of laminar natural convective flow for Pr=10 124

Figure Page

3.8 The effects of ϵ_f on the disturbance temperature and velocity profiles for Pr=10 130

3.9 The effects of both γ_f and ϵ_f on the stability of laminar natural convective flow of water when t_f=20°C and $|t_0-t_\infty|$=20°C 135

3.10 Typical shadowgraph and the experimentally obtained critical values of Ra_x in water 137

4.1 Typical base flow temperature and velocity profiles for various values of t_∞ when t_0=0°C 149

4.2 Typical neutral stability curves when both t_∞ and t_0 are below t_m 150

4.3 Typical neutral stability curves when both t_∞ and t_0 are above t_m 153

4.4 Typical neutral stability curves when t_∞ and t_0 are on the opposite sides of t_m 157

4.5 The effects of temperature-dependent viscosity and the critical values of G and β 161

4.6 Typical dye injection photograph and the experimentally obtained critical values of Ra_x in water for t_0=0°C 164

5.1 The coordinate system 168

5.2 The steady state temperature and velocity profiles for various values of R_0 and Pr when $Gr_x=1 \times 10^7$ 175

5.3 The steady state temperature and velocity profiles for various values of Gr_x and Pr when R_0=10 177

5.4 The steady state temperature and velocity profiles for various values of R_0 and Gr_x when Pr=0.72 179

5.5 The steady state local Nusselt number for various values of ξ 181

Figure Page

5.6 The transient temperature and velocity profiles for Pr=0.1 and Pr=10.0 when $Gr_x = 1 \times 10^7$ and $R_0 = 10$ 183

5.7 The transient temperature and velocity profiles at $Gr_x = 1 \times 10^7$ when $R_0 = 10$ and Pr=0.72 185

5.8 The transient temperature and velocity profiles at $Gr_x = 1 \times 10^6$ when $R_0 = 10$ and Pr=0.72 187

5.9 The transient temperature and velocity profiles at $Gr_x = 1 \times 10^7$, for $R_0 = 2$ and $R_0 = 100$ when Pr=0.72 189

5.10 The transient local Nusselt number for various values of Gr_x, R_0 and Pr 194

5.11 The experimental temperature records at various locations inside the thermal boundary layer when the wall was suddenly cooled 198

5.12 A comparison between the numerical and the experimental temperatures for transient and steady state conditions 201

5.13 Typical transient flow visualization photographs in water 202

6.1 The physical and the transformed planes for ice formation around a cooled cylinder 211

6.2 The local Nusselt number at the interface for freezing of water over an isothermally cooled planar plate 217

6.3 The local heat transfer coefficient at the interface for freezing of water over an isothermally cooled cylinder in cross flow 219

6.4 The local heat transfer coefficient along one wave length for ice surface waves inside a cooled pipe 222

7.1 The coordinate system for a one-dimensional analysis of the ice layer 225

Figure Page

7.2 Photograph of the probe used to measure the ice layer profile 232

7.3 Photographs of ice layer growth for t_{∞}=9.9°C and t_c=-18.6°C 234

7.4 Photographs of ice layer growth for t_{∞}=13.5°C and t_c=-16.7°C 238

7.5 Photographs of ice layer growth for t_{∞}=17.5°C and t_c=-15.0°C 242

7.6 A comparison of experimentally obtained transient ice layer thickness with a one-dimensional analysis 247

7.7 The variation of local Nusselt number, Nu_x with Rayleigh number, Ra_x at the interface 249

7.8 The variation of average Nusselt number, $\overline{Nu}$ with Rayleigh number, Ra_x at the interface 251

7.9 Photographs of ice layer growth in stratified ambient water 253

7.10 Photographs of cracked ice layer 254

7.11 Photograph showing the presence of air bubbles in the ice layer 257

7.12 Photographs showing the artificially induced disturbance on the surface of the ice layer and its recovery process 259

Nomenclature

A,B,C = real constants

B_i = Biot number, $h_c r_0/k_s$

B_1, B_2, B_3 = complex constants

b = width of the plate, m

c = dimensionless wave velocity, Chapters 2 to 4

c_s = specific heat of the solid, kJ/(kg.°C), Chapter 7

c_p = specific heat at constant pressure, kJ/(kg.°C)

$c_{pf}, c_{pr}, c_{p0}, c_{p\infty}$ = specific heat at constant pressure evaluated at temperatures t_f, t_r, t_0 and t_∞, respectively

d = diameter of the pipe, m

f_x = friction factor at x m from the leading edge

F = similarity stream function

g = accleration due to gravity, m^2/s

g = dimensionless stream function, eq. (2.47)

G = dimensionless stream function, eq. (2.50)

G = $4(Gr_x/4)^{1/4}$, Chapters 2 to 4

G = length scale, $[g\beta(t_0-t_\infty)/\nu^2]^{1/3}$, m^{-1}, Chapter 5

G = freezing front speed, $dS/d\tau$, Chapter 7

Gr_x = Grashof number, $g(\rho_0-\rho_\infty)x^3/(\rho_0\nu_f^2)$, Chapters 2 and 3

Gr_x = Grashof number, $g\alpha_t|t_0-t_\infty|^q x^3/\nu_f^2$, Chapter 4

Gr_x = Grashof number, $g\beta(t_0-t_\infty)x^3/\nu^2$, Chapter 5

h = dimensionless temperature, eq. (2.47)

h, h_f = local heat transfer coefficients, $W/(m^2.°C)$

h_c, h_f = heat transfer coefficient at the coolant side and at the interface, respectively, Chapters 6 and 7

$\bar{h}$ = average heat transfer coefficient

H = dimensionless temperature, eq. (2.50)

H = convection parameter at the interface, $h_f r_0/(k_s \theta_c)$, Chapter 7

i = $\sqrt{(-1)}$

J = Jacobian of transformation, $x_\xi y_\eta - x_\eta y_\xi$

k = thermal conductivity, W/(m.°C)

k_s, k_l = thermal conductivity of the solid and the liquid respectively

k_f, k_r, k_0, k_∞ = thermal conductivity evaluated at temperatures t_f, t_r, t_0 and t_∞ respectively

L = latent heat of freezing

L_{pv} = characteristic length, eq. (2.16)

M,N = number of grids in X and Y directions respectively, Chapter 5

M,N = number of grids in the transformed plane, Chapter 6

n = outward normal at the interface

Nu_x = local Nusselt number

$\bar{Nu}$ = average Nusselt number

p, p_∞, p_d = pressure, pressure at the ambient condition and pressure difference $(p-p_\infty)$, respectively

P,Q = coordinate control functions

Pr = Prandtl number

q = constant, Chapter 3

q = exponent of the temperature term, Chapter 4

Q' = total heat transfer rate

r = position of reference temperature, Chapter 2

r = radial coordinate, Chapters 5 to 7

r_f = interface position, Chapters 6 and 7

r_0 = radius of the cylinder, Chapters 5 to 7

R = temperature parameter, $(t_m-t_\infty)/(t_0-t_\infty)$, Chapter 4

R = dimensionless radial coordinate, r/r_0, Chapter 7

R_0 = dimensionless radius of the cylinder, r_0G, Chapter 5

Ra_x = Rayleigh number, $(Gr_x\ Pr)$

Re_x, Re_d = Reynolds numbers, Chapter 6

s = temperature disturbance amplitude function

s_r, s_i = real and imaginary parts of temperature disturbance amplitude function, respectively

S = dimensionless interface position, r_f/r_0

$t, t_c, t_f, t_m, t_r, t_0, t_\infty$ = temperature, coolant temperature, film temperature, temperature at the density maximum, reference temperature, surface temperature and ambient temperature, respectively

T = absolute temperature, K

u, v = velocity component in x and y directions

U, V = dimensionless velocities, $u/\nu G$ and $v/\nu G$, respectively, Chapter 5

w = total mass flow rate, kg/s

W_p, W_v = pressure work and viscous dissipation terms, respectively

x,y = Cartesian coordinates

X,Y = dimensionless distances, xG and yG, respectively, Chapter 5

Greek

α = dimensionless complex wave number, Chapters 2 to 4

α_r,α_i = real and imaginary parts of the complex wave number, Chapters 2 to 4

α = thermal diffusivity, Chapter 5

α_s = thermal diffusivity of the solid, Chapter 7

α,β,γ = transformation factors, $\alpha=x_\eta^2+y_\eta^2$, $\beta=x_\xi x_\eta+y_{\xi\eta}$, $\gamma=x_\xi^2+y_\xi^2$, Chapter 6

α_t = coefficient, $(°C)^{-q}$, eq. (4.1)

β = coefficient of thermal expansion, K^{-1}

$\beta_f,\beta_r,\beta_0,\beta_\infty$

= coefficient of thermal expansion evaluated at temperatures t_f, t_r, t_0 and t_∞, respectively

β = dimensionless frequency, disturbance equations, Chaters 3 and 4

β_r,β_i = real and imaginary parts of the frequency, Chapters 2 to 4

γ_f,γ_r = dimensionless parameters for variation of dynamic viscosity with temperature, Chapters 2 to 4

δ = boundary layer thickness, m

δ = local ice layer thickness, Chapters 6 and 7

Δt = (t_0-t_∞)

ϵ_f, ϵ_r = dimensionless parameters for variation of coefficient of thermal expansion with temperature, Chapters 2 to 3

ϵ = perturbation parameter, $c_s(t_f-t_c)/L$, Chapter 7

ζ_f, ζ_r = dimensionless parameters for variation of specific heat with temperature, Chapter 2

η = similarity variable

θ = dimensionless temperature, $(t-t_\infty)/(t_0-t_\infty)$, Chapter 2

θ = dimensionless temperature, $(\bar{t}-t_\infty)/(t_0-t_\infty)$, Chapters 3 and 4

θ = dimensionless temperature, $(t-t_\infty)/(t_0-t_\infty)$, Chapter 5

θ = dimensionless temperature, $(t-t_c)/(t_f-t_c)$, Chapters 6 and 7

θ_c = cooling temperature ratio, $(t_f-t_c)/(t_\infty-t_f)$

κ = thermal diffusivity

λ_f, λ_r = dimensionless parameters for variation of thermal conductivity with temperature, Chapter 2

λ = constant, Chapters 3 and 4

μ = dynamic viscosity, kg/(m.s)

$\mu_f, \mu_r, \mu_0, \mu_\infty$ = dynamic viscosity evaluated at temperatures t_f, t_r, t_0 and t_∞, respectively

ν = kinematic viscosity

ξ = similarity variable, eq. (2.47)

ξ = curvature parameter, Chapter 5

ξ, η = coordinates in the transformed plane, Chapter 6

Ξ = similarity variable, eq. (2.50)

ρ = density, kg/(m^3)

$\rho_f, \rho_r, \rho_0, \rho_\infty$
= density evaluated at temperatures t_f, t_r, t_0 and t_∞, respectively

τ = time, s, Chapters 2 to 4

$\bar{\tau}$ = time, s, Chapters 5 to 7

τ = dimensionless time, $\nu G^2 \bar{\tau}$, Chapter 5

τ = dimensionless time, $(\bar{\tau}\epsilon\alpha_s)/r_0^2$, Chapter 7

τ_0 = shear stress at the surface, $[\mu(\partial u/\partial y)]_{y=0}$, Chapter 2

ϕ = velocity disturbance amplitude function

ϕ = angular position measured from the forward stagnation point, Chapter 6

ψ = stream function

Subscripts

c = coolant

B.A. = Boussinesq approximations (properties evaluated at $t=t_f$, unless otherwise specified)

f = "film" condition, Chapters 2 to 4

f = freezing front chaters 6 and 7

i = ice

l = liquid

m = density maximum condition

max = maximum value

s = solid

ss = steady state

x = distance x from the leading edge

0 = at the surface, Chapters 1 to 5

∞ = ambient condition

η,ξ = partial derivatives w. r. t. η and ξ respectively, Chapter 6

Superscripts

$-$ = mean value

$\sim$ = disturbance quantity

$\wedge$ = dimensional quantity

$'$ = differentiation with respect to η

1. Introduction

Natural convective flows arise due to the effect of a density difference resulting from a temperature or concentration difference in a body force field such as the gravitational field. In natural convection, there is no externally induced flow field as in forced convection. Natural convective flows are abundant in nature and technology. For example, natural convection plays a vital role in the circulations of atmosphere, oceans, lakes and other water bodies. The predominant mode of heat rejection in many electrical and electronic devices is natural convection. In natural convection, the flow field is linked with and dependent on temperature and concentration fields. Mathematical analysis of natural convective flows over complex geometries is generally difficult. Hence, natural convective flows are normally idealized into flows over simpler geometries with simple boundary conditions. Among these flows, the natural convective flow along an isothermal vertical surface is technically very important.

1.1 Previous Analyses on the Effects of Variable Properties of the Fluid on the Natural Convective Flow Along a Vertical Surface

1.1.1 Laminar Flow

Even for the laminar natural convective flows over idealized geometries, the exact governing equations are usually intractable. Hence, it is customary to make some approximations to the governing equations. The most frequently employed approximations, known as Boussinesq approximations, consist of the following steps:

1. the density of the fluid is assumed to be constant in all terms of the governing equations except in the buoyancy force term where it is assumed to vary linearly with temperature,
2. all other physical properties are assumed to be constant, and
3. the viscous dissipation and the pressure work are neglected.

The laminar natural convective flow along an isothermal vertical flat plate with Boussinesq approximations has been of interest to many investigators for more than 100 years. One of the earliest investigators to attempt a solution of the governing equations for this classical problem was Oberbeck (1879). Lorenz (1881) assumed that the streamlines and the isotherms were parallel to the vertical surface and solved the resulting ordinary differential equations to obtain the local Nusselt number at the surface.

Pohlhausen along with Schmidt and Beckmann (1930) employed boundary layer approximations and similarity variables technique to transform the partial differential equations into a set of ordinary differential equations and obtained approximate solutions for air. Schmidt and Beckmann also performed experiments for the natural convective flow along a heated vertical plate in air and measured velocity and temperature profiles. Saunders (1939) and Schuh (1948) obtained approximate solutions for various Prandtl numbers.

Ostrach (1953) obtained the exact numerical solutions to the governing equations for Prandtl numbers from 0.01 to 1000. His solutions agreed well with the experimental results of Schmidt and Beckmann. Since then there have been a number of studies on the laminar natural convective flow along a vertical surface encompassing a wide range of conditions. These studies are discussed in Jaluria (1980).

Boussinesq approximations are justified only if the temperature differenece between the surface and the ambient medium is small. For example, it was shown by Gray and Giorgini (1976) that at 15°C and 1 atmospheric pressure, Boussinesq approximations are valid only when the temperature difference between the surface and the ambient medium is less than 1.25°C for water and 28.6°C for air. At larger temperature differences the effects of variable properties must be included in the analysis. There have been a number of studies, in the past, on the effects of variable properties of the fluid on the laminar natural convective flow along a vertical flat plate.

Sparrow (1956) and Sparrow and Gregg (1958) investigated perfect gases for different property laws and also considered liquid mercury. They determined reference temperatures for evaluating the properties to be used to calculate the natural convective heat transfer from the constant property relations. They also found that the use of film temperature is adequate for most applications. Hara (1958) employed a perturbation method to study the effects of variable properties for air. Minkowycz and Sparrow (1966) studied the non-ideal gas behaviour of steam and proposed reference temperatures for calculating the natural convective heat transfer at the surface. Nishikawa and Ito (1969) considered the variable property effects in water and in CO_2 near supercritical pressure conditions.

Fujii et al. (1970) proposed two kinds of experimental correlations, one using the physical properties at a reference temperature, and the other using the properties at the ambient temperature with supplementary terms referred to the variation of kinematic viscosity with temperature. Piau (1970,1974) studied the effects of variations of coefficient of thermal expansion and viscosity with temperature for the natural convective flow along an isothermally heated vertical plate in water and in liquids for moderate temperature diffenences (~10 to 30°C) between the wall and the ambient medium. He found that the temperature-dependent viscosity increases the surface heat transfer rate whereas the temperature-dependent coefficient of thermal expansion has little effect on it. He also showed that the effects of variation of the coefficient of thermal exapansion are negligible when $Pr \to \infty$.

Barrow and Seetharamarao (1971) examined the effects of temperature-dependent coefficient of thermal expansion for an isothermal vertical surface in water. They found that it has considerable influence on the local Nusselt number at the surface. They neglected the effects of variable viscosity. Brown (1975) extended the work of Barrow and

Seetharamarao by employing an integral method to include the variation of density with temperature. He concluded that its effects are more complex than the approximations made in the previous investigations.

Ackroyd (1974) showed that the effects of viscous dissipation and pressure work can be neglected under normal conditions and that the variations in the properties of the ambient fluid are important. Ito et al. (1974) considered the effects of variable properties for a uniform heat flux vertical surface in oil and in supercritical CO_2. Carey and Mollendorf (1978) studied the effects of variation of viscosity with temperature for liquids with Prandtl numbers 1 to 1000. They examined both heated and cooled walls and determined the limits of variation of viscosity with temperature for which the Boussinesq approximations are valid within ±5%. They neglected the effects of variation of coefficient of thermal expansion with temperature.

Shaukatullah and Gebhart (1979) considered the effects of variable properties for an isothermal vertical flat surface in water for various combinations of wall and ambient temperatures in the range 0 to 100°C. Their analysis was restricted to specific combinations of wall and ambient temperatures in water. Carey and Mollendorf (1980) extended their earlier work to study the effects of variation of viscosity with temperature for a freely-rising plane plume, a plane wall plume and a uniform heat flux vertical surface.

These studies on the effects of variable properties on the laminar natural convective flow along a vertical surface have mainly been done for a particular fluid or considering the variation of one or two properties in detail. Also, there is disagreement on the effects of variations of density and the coefficient of thermal expansion with temperature (Barrow and Seetaramarao, 1971, Piau, 1974 and Brown, 1975). Hence a further detailed study is necessary to find the effects of variable properties on the laminar natural convective flow along an isothermal vertical flat plate.

1.1.2 Stability of Laminar Flow

Near the leading edge of the vertical flat plate the natural convective flow is always laminar. Away from the leading edge, the laminar flow becomes unstable to ever-present disturbances in the system. The thermal transport is different in laminar, transition, and turbulent regimes of the flow. Hence the knowledge of the nature of the flow is important for estimating the thermal transport. The transition from laminar regime to turbulent regime depends on the stability characteristics of the flow. Stability and transition to turbulence of natural convective flows over vertical surfaces have been extensively studied by many investigators employing Boussinesq approximations.

Eckert and Soehnghen (1951) were among the earliest to perform experiments with the primary purpose of studying the stability and transition to turbulence of laminar natural convective boundary layer flows. Using a Mack-Zehnder interferometer, they were able to observe the naturally occurring disturbance temperature distributions along an isothermal vertical flat plate in air. They observed the formation and amplification of a wave disturbance which was initially two-dimensional and sinusoidal. However as the disturbance amplified further, the wave form became more complex and eventually gave way to a three dimensional disturbance. This experiment established that the natural convective flow becomes unstable to some wave disturbance having a particular wave number.

The first analytical attempt to predict the stability of natural convective bounday layer flows was made by Plapp (1957). Using the linear stability theory, he derived the disturbance momentum and energy equations and obtained a coupled set of equations, one a fourth order, and the other a second order. He found approximate soultions for an isothermal vertical flat plate in air.

Szewczyk (1962) presented a theoretical and experimental study of the stability of natural convective flow along an isothermal vertical flat plate in water. He used an asymptotic technique to obtain solutions about both the inner and the outer critical layers to the uncoupled equations for a Prandtl number of 10. The critical values of Grashof number obtained for the naturally occurring disturbances in his experiments were lower than those obtained from his theoretical analysis.

It appears that Nachtsheim (1963) was the first to obtain a numerical solution of the coupled disturbance equations. He determined both the uncoupled and the coupled neutral stability curves for the natural convective flow of air, and water along an isothermal vertical flat plate. He showed that the temperature coupling can have an appreciable effect on the stability, particularly for lower values of the wave number-Grashof number product. Since then there have been a number of theoretical and experimental studies on the stability of natural convective flows along vertical surfaces for various conditions.

Polymeropoulos and Gebhart (1967), Knowles and Gebhart (1968), and Dring and Gebhart (1968) investigated the stability of laminar boundary layer flow along a vertical uniform heat flux surface. Fujii et al. (1970) studied experimentally the natural convective flow along a vertical circular cylinder for various liquids with Prandtl numbers from 2 to 2600. They visualized the flow for both constant wall temperature and constant surface heat flux conditions and found that the boundary layer develops through laminar, vortex-street, transition to turbulent, and turbulent flow. They suggested that the phenomena of transition to turbulence occur mainly due to the vortices in the outer part of the boundary layer. They also obtained the local Nusselt number for various regimes of the flow.

Colak-Antic and Gortler (1971) visually investigated the three-dimensional transition phenomena in the natural convective boundary layer along a heated plate in water under controlled forced disturbances. They observed discrete longitudinal vortices in the outer part of the boundary layer. The break-down of these vortices causes the transition of the laminar boundary layer into turbulent flow. Hieber and Gebhart (1971) proposed a new numerical method to solve the disturbance equations. Other studies on this subject can be found in the recent literature review by Gebhart and Mahajan (1982).

There has been no comprehensive study, to date, on the effects of variable properties on the stability of laminar natural convective flow along a vertical surface. Piau (1974) analyzed the experimental data for heated walls and concluded that the temperature-dependent viscosity has a stabilizing effect for liquids and destabilizing effect for gases. It is of interest to note that in the forced convective flow of a liquid over a flat plate it was shown theoretically by Hauptmann (1968), and theoretically and experimentally by Wazzan et al. (1968) that the temperature-dependent viscosity destabilizes the flow for a cooled wall, and stabilizes the flow for a heated wall.

The problem of the stability of laminar natural convective boundary layer flow is an interesting combination of the problems of boundary layer stability (hydrodynamic stability) and thermal stability. Since the natural convective flow is a shearing motion, the problem of its stability contains all the features of boundary layer stability. However, as there is a temperature difference between the wall and the ambient medium in the natural convective flow, the essential features of the thermal stability are also inherently present. Hence a detailed theoretical and experimental study is necessary to find the effects of variable properties on the stability of laminar natural convective flow along an isothermal vertical surface.

It is well known that water exhibits a density maximum near 4°C. When the surface and the ambient temperatures are on the opposite sides of the temperature corresponding to the density maximum, the buoyancy force reverses in direction inside the thermal boundary layer. Also, flow reversal and a rapid decrease in surface heat transfer may occur. There have been a number of studies on the effects of maximum density on the laminar natural convective flow along a vertical flat plate and the references can be found in Yuill (1972) and Carey et al. (1980). Recently Padlog and Mollendorf (1983) studied the effects of variable properties on the laminar natural convective flow in water near the density maximum region.

The presence of density maximum, and the process of buoyancy force reversal with the possiblity of convective inversion of the flow complicate the stability characteristics of natural convective flows in cold water. Qureshi (1980) found that the buoyancy induced flow in water at its density maximum along a vertical uniform heat flux surface is initially stable. But farther downstream the disturbance amplification rate increased. The density maximum was also found to delay the beginning of transition to turbulence.

Carey and Gebhart (1981) visualized the flow adjacent to a vertical ice surface melting in cold water and observed bi-directional flow near the maximum density region. Joseberger and Martin (1981) studied experimentally the melting of a vertical ice surface in salt water for various salinities and ambient temperatures. They also obtained an approximate solution for the turbulent flow near the maximum density.

Recently Higgins and Gebhart (1982,1983) studied the stability of buoyancy induced flows in cold water adjacent to an isothermal vertical flat surface for small temperature differences (~5°C) between the surface and the ambient medium. They found that the Boussinesq approximations overpredict the buoyancy force in up flow circumstances and the resulting neutral stability curves lie to the left of the true ones. The reverse is true for down flows. They neglected the effects of temperature-dependent viscosity.

The viscosity of cold water is a strong function of temperature. Hence it is important to study the effects of both the maximum density and the temperature-dependent viscosity on the stability of laminar natural convective flows in cold water.

1.2 Previous Analyses on the Transient Natural Convective Flow Along a Vertical Circular Cylinder

In many situations such as nuclear reactor accidents, cooling of electrical and electronic equipments and heat transfer from a human body, the natural convective flow during the transient period is very important. Many such surfaces can be approximated as vertical circular cylindrical surfaces for theoretical analysis. It is to be noted that the vertical flat plate is a special case of a vertical circular cylinder with an infinite radius.

The steady laminar natural convective flows along vertical flat surfaces have been studied extensively in the past employing similarity variables. For vertical circular cylindrical surfaces the flows do not normally yield similarity solutions, and they have been studied by approximate methods such as heat balance integral (Lefevre and Ede, 1956, and Hama et al., 1959), perturbation expansion (Sparrow and Gregg, 1956, Kuiken, 1968a, Fujii and Uehara, 1970, and Aziz and Na, 1982), local non-similarity (Minkowycz and Sparrow, 1974) and two-point finite difference (Cebeci, 1974). These studies also contain other related works on this subject.

The transient natural convective flow along a vertical surface subjected to a step change in surface temperature or surface heat flux has mainly been studied for a flat plate. For an infinite isothermal vertical flat plate, with a parallel flow assumption, Illingworth (1950) found that the temperature field in the boundary layer is identical to that of unsteady one-dimensional heat conduction into a semi-infinite body. Sugawara and Michiyoshi (1951) carried out a similar analysis and determined the short time for which the parallel flow approximation is valid.

Siegel (1958) analyzed the transient natural convective flow along a semi-infinite vertical flat surface subjected to a step change in surface tempearture or heat flux by employing Von Karman-Pohlhausen integral method and the method of characteristics. He determined the time required for the steady flow to become established at any position along the plate. The boundary layer thickness was found to reach a maximum, and the heat transfer coefficient at the surface a minimum during the transient period. This is due to the fact that at a given position along the plate, the heat conduction process is sufficiently rapid to enable the boundary layer thickness to grow beyond the steady state thickness before the constraints induced by the leading edge can propagate to that location and prevent the growth from continuing as if the plate were infinite in length. The overgrowth in the boundary layer thickness causes a minimum in the heat transfer coefficient at the surface. The experimental analysis in water by Goldstein and Eckert (1960) confirmed the above predictions. Gebhart (1968) investigated the effect of surface thermal capacity. The effect of Prandtl number was investigated by Schetz and Eichhorn (1962), and by Menold and Yang (1962).

Hellums and Churchill (1962) presented a finite difference numerical solution of the governing partial differential equations for the transient flow along a vertical plate subjected to a step change in surface temperature. Their result agreed with the result of earlier investigators that the local heat transfer coefficient at any point on the surface goes through a minimum during the transient period. Goldstein and Briggs (1964) investigated the flows from vertical plates for constant surface heat flux and constant wall temperature, and from cylinders for constant heat flux conditions. They predicted that the difference between the minimum heat transfer coefficient which occurs during the transient period and the steady state value is larger for a step change in surface temperature than that for a step change in surface heat flux. It was also found that the difference is larger for lower Prandtl numbers.

Brown and Riley (1972) reduced the governing equations to a similarity form and obtained approximate analytical solutions for small and large times. They also predicted a time up to which their unsteady solution is applicable. Ingham (1978) reinvestigated the solution obtained by Hellums and Churchill (1962) and concluded that the numerical technique may introduce artificial diffusion in the calculations. Sammakia and Gebhart (1978,1981) and Sammakia et al. (1982) investigated the flow along a vertical flat surface subjected to a step change in surface heat flux by employing a similar numerical method. Their experimental results in water agreed with those obtained numerically. There is little information on the transient natural convective flow along a vertical circular cylinder sujected to a step change in surface temperature or surface heat flux except the approximate analytical study by Goldstein and Briggs (1964) for the case of constant surface heat flux. Hence, a detailed study of the transient natural convective flow along vertical surfaces is necessary.

1.3 Previous Analyses on the Effects of Natural Convection on Solidification and Melting Problems

In many natural convective flow circumstances, when the wall temperature is sufficiently below the freezing temperature of the liquid (less than -5°C for water at 15°C and 1 atmospheric pressure, for example), the liquid solidifies onto the wall. Problems associated with these processes involve heat transfer with phase change. The standard procedure in solidification and melting problems is to find the shape and the position of the solid-liquid interface at different times for the given boundary conditions. These transient problems with a moving boundary are nonlinear in character and hence exact solutions have been found only for problems involving simpler geometries and initial conditions. The early analytical solutions dealt with the problem as a one-dimensional conduction and they are given in Carslaw and Jaeger (1959), and Ozisik (1980).

Tien and Yen (1960) obtained an approximate solution for the solid-liquid moving boundary problem including the buoyancy effects in the liquid. Boger and Westwater (1967) experimentally measured the interfacial velocities and transient and steady state temperature profiles during freezing and melting of water between two isothermal horizontal parallel plates. Szekeley and Chhabra (1970) studied the solidification of lead over an isothermally cooled vertical flat surface. They found that the experimentally obtained shape of the solid-liquid interface was controlled by the natural convection in the liquid.

Lapadula and Mueller (1970) presented an approximate solution for the transient development of the solid-liquid interface when a superheated liquid solidifies onto a cooled vertical wall. They included the effect of natural convective heat transfer adjacent to the interface in their analysis.

Of late, there have been a number of experimental studies on the effects of natural convection on both solidification and melting problems involving various geometries and boundary condtions. Sparrow et al. (1979) studied the freezing of a phase change medium (a paraffin) over a vertical tube and found that the steady state shape and position of the solid-liquid interface was controlled by natural convection. Sparrow et al. (1977) and Bareiss and Beer (1980) studied the influence of natural convection on the shape and the position of the solid-liquid interface in the melting process due to a heated vertical cylinder. A summary of other investigations can be found in the recent literature review by Viskanta (1983).

These investigations were mainly concerned with solidification or melting problems when the natural convective flow adjacent to the interface is in the laminar regime. If the superheating in the liquid or the geometry of the system is large, transition and turbulent regimes will also occur in the natural convective flow adjacent to the interface. It is to be noted that when water freezes over a cooled planar plate or inside a tube in forced convection, transition, and turbulent flows have dramatic effects on the shape of the ice layer profile (Hirata et al., 1979b, Cheng et al., 1981, and Gilpin, 1979,1981). Hence, it is important to study the effects of natural convection on solidification or melting problems when the flow is in transition or turbulent regime.

1.4 Present Analysis

The present study is concerned mainly with the natural convective flow along a vertical surface in a quiescent ambient liquid.

In Chapter 2, the effects of temperature-dependent properties on the laminar boundary layer flow along an isothermal vertical flat plate are studied. The effects of all the relevant properties are considered by employing dimensionless parameters. The effects of variation of density with temperature in various terms of the governing equations are considered in detail. A better approximation of the variation of density with temperature in the buoyancy force term than those employed in previous investigations is considered in the form of a dimensionless parameter. Both heated and cooled walls are examined. Liquids with Prandtl numbers 1 to ∞ are considered. The variable property effects on the temperature and velocity profiles are also studied in detail.

In Chapter 3, the effects of variations of viscosity and coefficient of thermal expansion with temperature on the stability of the laminar boundary layer flow along an isothermal vertical flat plate are studied numerically for various Prandtl numbers. Experiments were also conducted with a copper circular cylinder (outside diameter 41.3 mm and length 1 m) in water for various combinations of wall and ambient temperatures in the range of 5 to 35°C. The flow was visualized with shadowgraph and dye injection techniques.

In Chapter 4, the stability of laminar boundary layer flow along an isothermal vertical flat plate in cold water is studied. The effects of both the maximum density and the temperature-dependent viscosity are examined. Various combinations of wall and ambient temperatures in the range 0 to 20°C are considerd. In particular, the flow from an isothermal wall at 0°C, corresponding to an ice surface, is studied in detail. The stability characteristics of the flow with and without buoyancy force reversals inside the thermal boundary layer are analyzed.

In Chapter 5, the transient flow along a vertical circular cylinder subjected to a step change in surface temperature is investigated numerically for various curvatures of the cylinder and Prandtl numbers 0.1 to 10. Experiments were also conducted in water with a vertical copper cylinder for a step change in surface temperature. The flow was also visualized using shadowgraph technique.

In Chapter 6, the local heat transfer coefficients at the solid-liquid interface are obtained by numerically solving the temperature field inside the solidified region. The solutions are compared with a simple one-dimensional analysis. The example problems, taken from literature, involve freezing of water over a planar plate in longitudinal flow, a cylinder in cross flow and inside a pipe with ice bands.

In Chapter 7, the effects of natural convection in laminar, transition, and turbulent flow regimes are analyzed when water freezes over a convectively cooled vertical circular cylinder. The effects of stratification and dissolved air in ambient water, and the stability of the interface to artificially induced disturbances are investigated. A one-dimensional analysis of the transient development of solid-liquid interface is also presented for the solidification of a liquid over a convectively cooled vertical pipe.

2. The Effects of Temperature-Dependent Properties on the Laminar Natural Convective Flow Along an Isothermal Vertical Flat Plate

In this Chapter, the effects of temperature-dependent properties on the laminar natural convective boundary layer flow of a liquid along an isothermal vertical flat plate are studied numerically for Prandtl numbers from 1 to ∞. The effects of all the relevant properties are considered employing dimensionless parameters. The effects of variation of density with temperature in various terms of the governing equations are analyzed in detail. A better approximation of the variation of density with temperature than those employed in previous investigations is considered in the buoyancy force term. Both heated and cooled walls are examined. The effects of variable properties on temperature and velocity profiles are also studied in detail.

2.1 Theoretical Analysis

2.1.1 Governing Equations

The coordinate system is shown in Fig. 2.1. The quiescent ambient medium and the surface of the vertical flat plate are at constant temperatures t_∞ and t_0, respectively. The flow is assumed to be steady and two-dimensional. The equations governing the conservation of mass, momentum, and energy for the laminar natural

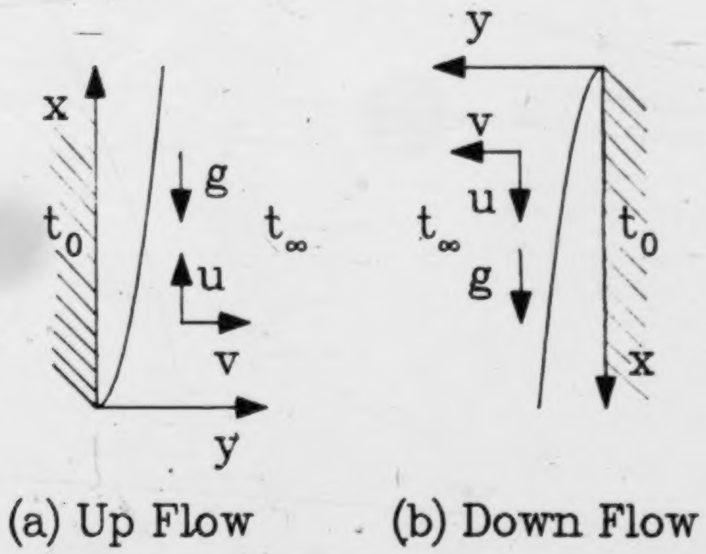
x
g
t_0
t_∞
u
v
y
y
v
u
t_∞
t_0
g
x

(a) Up Flow (b) Down Flow

Fig. 2.1 The coordinate system

convective flow of a Newtonian fluid of variable properties are given by (Batchelor, 1967),

$$\frac{\partial}{\partial x}(\rho u) + \frac{\partial}{\partial y}(\rho v) = 0 \tag{2.1}$$

$$\rho\left(u\frac{\partial u}{\partial x} + v\frac{\partial u}{\partial y}\right) = -\frac{\partial}{\partial x}(p-p_\infty) + g(\rho_\infty-\rho) + \frac{\partial}{\partial x}\left[2\mu\frac{\partial u}{\partial x} - \frac{2}{3}\mu\left(\frac{\partial u}{\partial x} + \frac{\partial v}{\partial y}\right)\right] + \frac{\partial}{\partial y}\left[\mu\left(\frac{\partial u}{\partial y} + \frac{\partial v}{\partial x}\right)\right] \tag{2.2}$$

$$\rho\left(u\frac{\partial v}{\partial x} + v\frac{\partial v}{\partial y}\right) = -\frac{\partial}{\partial y}(p-p_\infty) + \frac{\partial}{\partial y}\left[2\mu\frac{\partial v}{\partial y} - \frac{2}{3}\mu\left(\frac{\partial u}{\partial x} + \frac{\partial v}{\partial y}\right)\right] + \frac{\partial}{\partial x}\left[\mu\left(\frac{\partial u}{\partial y} + \frac{\partial v}{\partial x}\right)\right] \tag{2.3}$$

$$\rho c_p\left(u\frac{\partial t}{\partial x} + v\frac{\partial t}{\partial y}\right) = \frac{\partial}{\partial x}\left(k\frac{\partial t}{\partial x}\right) + \frac{\partial}{\partial y}\left(k\frac{\partial t}{\partial y}\right) - \frac{T}{\rho}\left(\frac{\partial \rho}{\partial t}\right)_p \left(u\frac{\partial p}{\partial x} + v\frac{\partial p}{\partial y}\right) + \mu\phi \tag{2.4}$$

where $\phi = \left[2\frac{\partial u}{\partial x} - \frac{2}{3}\left(\frac{\partial u}{\partial x} + \frac{\partial v}{\partial y}\right)\right]\frac{\partial u}{\partial x} + \left[\frac{\partial u}{\partial y} + \frac{\partial v}{\partial x}\right]^2 + \left[2\frac{\partial v}{\partial y} - \frac{2}{3}\left(\frac{\partial u}{\partial x} + \frac{\partial v}{\partial y}\right)\right]\frac{\partial v}{\partial y}$

For the ambient fluid

$$\frac{\partial p_\infty}{\partial x} = -\rho_\infty g \tag{2.5}$$

In addition to the above equations, an equation of state, relations for the property variations, and the boundary conditions are needed for the complete specification of the problem.

These equations are complex and it is difficult to solve them. Hence some approximations are required to simplify them. Because of the semi-infinite nature of the region, the complete set of boundary conditions is not evident. The boundary layer formulation will simplify the problem and eliminate the necessity of specifying those boundary conditions which are not evident.

The boundary layer equations are obtained after normalizing these equations and performing an order of magnitude analysis. The detailed procedure of normalization, order of magnitude analysis, and the conditions necessary for employing the boundary layer approximations are given in detail in Appendix A. The boundary layer equations governing the flow are given by

$$\frac{\partial}{\partial x}(\rho u) + \frac{\partial}{\partial y}(\rho v) = 0 \tag{2.6}$$

$$\rho\left(u\frac{\partial u}{\partial x} + v\frac{\partial u}{\partial y}\right) = g(\rho_\infty - \rho) + \frac{\partial}{\partial y}\left[\mu\frac{\partial u}{\partial y}\right] \tag{2.7}$$

$$\rho c_p\left(u\frac{\partial t}{\partial x} + v\frac{\partial t}{\partial y}\right) = \frac{\partial}{\partial y}\left[k\frac{\partial t}{\partial y}\right] - \frac{T}{\rho}\left[\frac{\partial \rho}{\partial t}\right]_p u\frac{\partial p}{\partial x} + \mu\left[\frac{\partial u}{\partial y}\right]^2 \tag{2.8}$$

The boundary conditions are,

$$\text{at } y = 0,\ u = v = 0 \text{ and } t = t_0 \text{ for all } x \tag{2.9}$$

$$\text{as } y \to \infty,\ u \to 0 \text{ and } t \to t_\infty \text{ for all } x \tag{2.10}$$

$$\text{at } x = 0,\ u = v = 0 \text{ and } t = t_\infty \text{ all } y > 0 \tag{2.11}$$

The properties of the fluid are functions of temperature and pressure. At moderate pressures, the properties of most liquids are not strong functions of pressure. Hence, the effects of variations of properties with pressure can be neglected normally. But the properties of most liquids are strong functions of temperature. For example, Figs. 2.2(a) and (b) show the variations of properties with temperature at 1 atmospheric pressure for water and ethyl alcohol, respectively. It is seen clearly that the temperature dependence of properties (the coefficient of thermal expansion, the viscosity and the Prandtl number, in particular) are significant. (The variations of properties in Figs. 2.2(a) and (b) are shown with respect to a reference temperature at 0°C, for easy comparison. It will be shown later that the ratios of most properties with reference to a particular temperature rather than the absolute values are important). In this analysis, the film temperature, $t_f = 0.5(t_0+t_\infty)$, will be used as the reference temperature. The analysis can be easily extended to any other reference temperature.

Introducing the following variables,

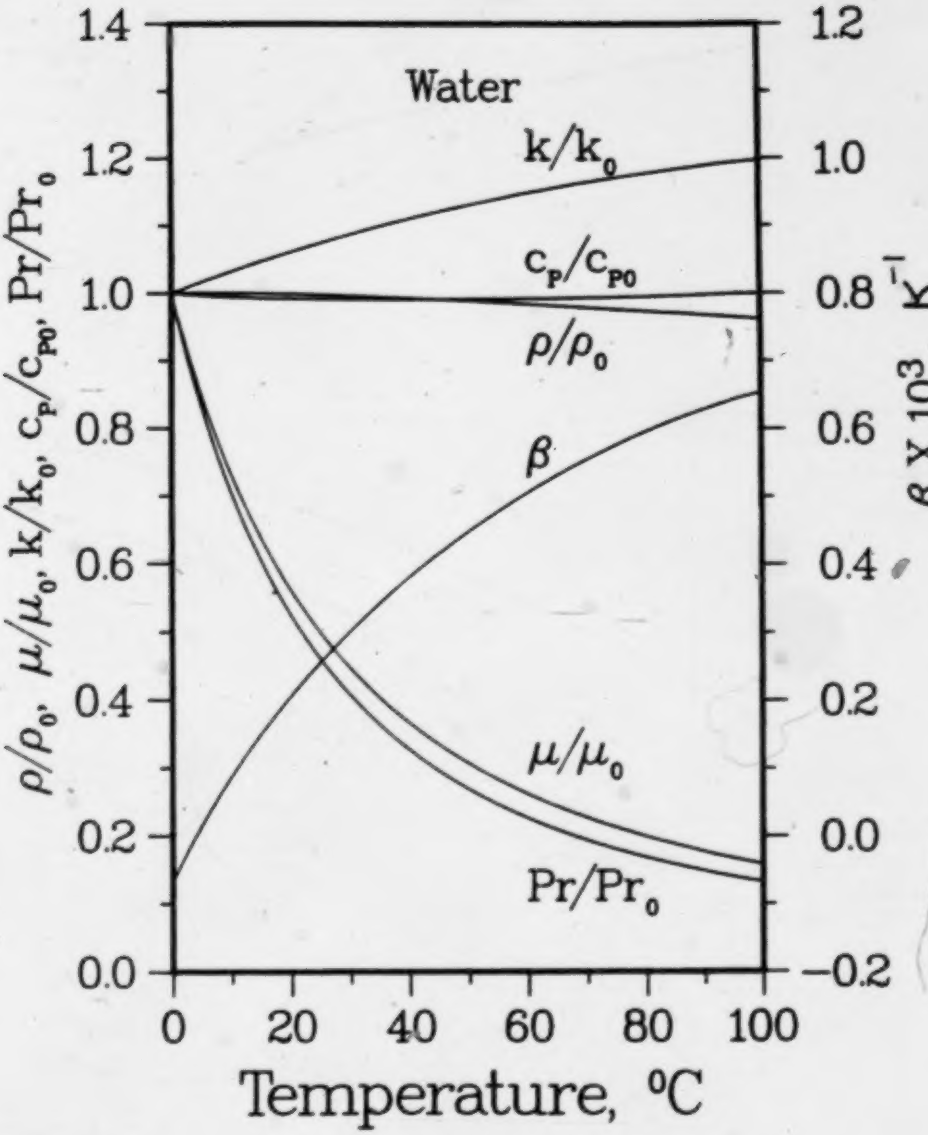

Fig. 2.2(a) The properties of water

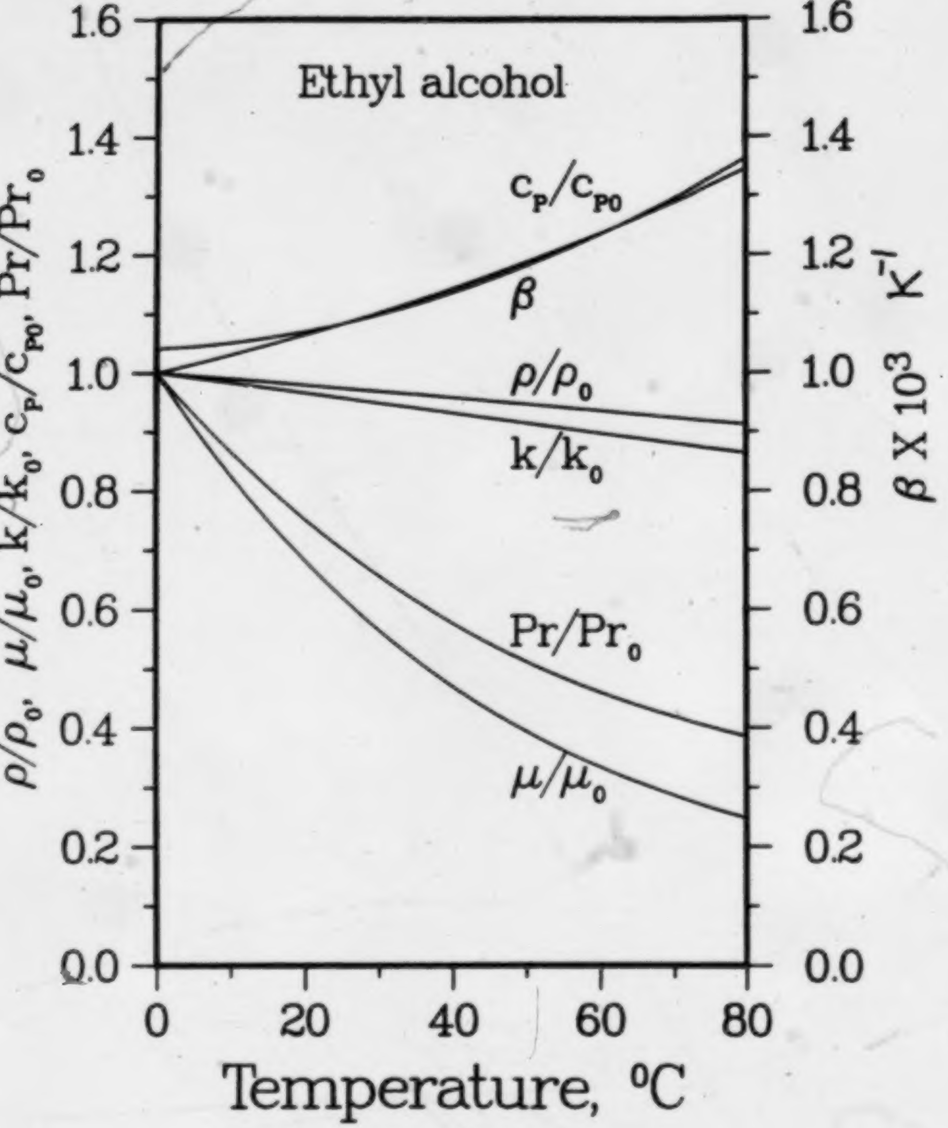

Fig. 2.2(b) The properties of ethyl alcohol

$$Gr_x = \frac{g(\rho_\infty - \rho_0)x^3}{\rho_0 \nu_f^2}, \qquad G = 4\left[\frac{Gr_x}{4}\right]^{1/4} \tag{2.12}$$

$$\eta = \frac{G}{4x}\int_0^y \left(\frac{\rho}{\rho_f}\right)dy, \qquad \psi = \nu_f G\, F(\eta), \qquad t_f = \frac{t_0 + t_\infty}{2} \tag{2.13}$$

$$\theta = \frac{t - t_\infty}{t_0 - t_\infty}, \qquad u = \frac{\partial \psi}{\partial y}, \quad v = -\frac{\partial \psi}{\partial x} \tag{2.14}$$

the equations and the boundary conditions reduce to

$$\frac{d}{d\eta}\left[\frac{\mu\rho}{\mu_f\rho_f} F''\right] + 3FF'' - 2(F')^2 + \frac{\rho_\infty - \rho}{\rho_\infty - \rho_0}\,\frac{\rho_0}{\rho} = 0 \tag{2.15}$$

$$\frac{d}{d\eta}\left[\frac{k\rho}{k_f\rho_f}\,\theta'\right] + \left[\frac{c_p}{c_{pf}}\right]3(Pr)F\theta' - \left[\frac{4x}{L_{pv}}\right](Pr)[W_p - W_v] = 0 \tag{2.16}$$

$$F(0) = F'(0) = \theta(0) - 1 = F'(\infty) = \theta(\infty) = 0 \tag{2.17}$$

where
$$L_{pv} = \frac{c_{pf}\,\rho_0\,\Delta t}{g(\rho_\infty - \rho_0)} \tag{2.18}$$

$$W_p = \frac{\rho_\infty}{\rho_f}\,\frac{\rho_f^2}{\rho^2}\,\frac{T\rho_0}{(\rho_\infty - \rho_0)}\,\frac{\partial}{\partial t}\left[\frac{\rho}{\rho_f}\right]_p F' \tag{2.19}$$

$$W_v = \frac{\mu}{\mu_f}\,\frac{\rho}{\rho_f}\,(F'')^2 \tag{2.20}$$

W_p and W_v are pressure work and viscous dissipation terms respectively, and L_{pv} is a characteristic length. The order of W_p is $\left[\frac{T}{\Delta t}\right]F'$ and that of W_v is $[(F'')^2]$. For liquids under normal conditions, L_{pv} is very large (for example, for water at 1 atmospheric pressure when t_f=20°C and Δt=10°C, $L_{pv} \cong 2400$ m). Hence, in equation (2.16), as (x/L_{pv}) is very small, the pressure work and the viscous dissipation terms can be neglected under normal conditions.

The expressions for the local surface heat transfer rate, the surface shear stress, and the total mass flow rate are given by

$$Nu_x = \frac{hx}{k_f} = \frac{k_0\rho_0}{k_f\rho_f}\left[\frac{Gr_x}{4}\right]^{1/4}[-\theta'(0)] \qquad (2.21)$$

$$f_x = \tau_0/\{\rho_f(\nu_f/x)^2\} = \frac{\mu_0\rho_0}{\mu_f\rho_f}\,4\left[\frac{Gr_x}{4}\right]^{3/4} F''(0) \qquad (2.22)$$

$$w_x = b\int_0^\infty(\rho u)d\eta = 4b\mu_f\left[\frac{Gr_x}{4}\right]^{1/4} F(\infty) \qquad (2.23)$$

It is to be noted that for a given fluid, knowing the functional dependence of properties with temperature, the exact numerical solutions can be obtained for the given wall and ambient temperatures (Shaukatullah and Gebhart, 1979, and Sparrow, 1956). The present analysis considers the effects of variable properties in terms of dimensionless parameters and hence it is not restricted to a particular fluid or specific combinations of wall and ambient temperatures.

2.1.2 Variation of Density with Temperature

The density appears in the form of ρ/ρ_f in viscous force and heat conduction terms, and as a multiplication of ρ/ρ_0 and $(\rho_\infty-\rho)/(\rho_\infty-\rho_0)$ in the buoyancy force term (see eqs. 2.15 to to 2.17). In the case of liquids, for moderate temperature differences between the wall and the ambient medium (~10 to 50°C, for water, for example), ρ/ρ_f is nearly equal to 1. Hence, the variation of density with temperature in viscous force and heat conduction terms can be neglected. This can also be proved rigorously from the solutions to equations (2.15) to (2.17) for typical liquids as shown below.

The equations (2.15) to (2.17) were solved numerically employing a fourth order Runge-Kutta method for typical liquids with $t_f=50°C$ and $|\Delta t|=60°C$ for three different cases

(1) $\mu=\mu(t)$, $k=k(t)$ and $c_p=c_p(t)$, and $\rho=\rho(t)$ in all terms of the equations,

(2) $\mu=\mu(t)$, $k=k(t)$ and $c_p=c_p(t)$, and $\rho=\rho(t)$ only in the buoyancy force term of the equation (2.15)

(3) $\mu=\mu_f$, $k=k_f$ and $c_p=c_{pf}$, and $\rho=\rho(t)$ only in the buoyancy force term of the equation (2.15).

The results are given in Table 2.1. [The functional variations of properties with temperature, $\mu(t)$, $k(t)$, $c_p(t)$ and $\rho(t)$ are given in Appendix B]. The solutions were also

Table 2.1 The effects of variation of density with temperature

(t_0-t_∞)	F''(0)	-θ'(0)	F(∞)	S1	S2	R1	R2	R3	Case
	Water		$t_f=50$		Pr=3.554				
-60	0.34548	0.87909	0.31646	0.63949	0.83311	1.24333	0.96903	0.94227	1
60	0.64211	0.83243	0.36912	0.40970	0.85252	0.79656	0.99161	1.09906	1
-60	0.34776	0.88780	0.31830	0.63716	0.83279	1.23879	0.96867	0.94774	2
60	0.63558	0.82048	0.36780	0.41231	0.85432	0.80164	0.99371	1.09513	2
-60	0.56654	0.90424	0.35994	0.56654	0.90424	1.10149	1.05177	1.07173	3
60	0.46172	0.80443	0.30124	0.46172	0.80443	0.89769	0.93568	0.89695	3
	Benzene		$t_f=50$		Pr-5.827				
-60	0.34605	0.89767	0.25651	0.52440	0.98293	1.12160	0.98422	0.88458	1
60	0.59905	1.10693	0.33414	0.41541	1.00514	0.88849	1.00646	1.15229	1
-60	0.35464	0.92936	0.26043	0.51775	0.98037	1.10736	0.98166	0.89810	2
60	0.58352	1.06733	0.32932	0.42116	1.00874	0.90078	1.01007	1.13566	2
-60	0.47858	1.01154	0.29543	0.47858	1.01154	1.02359	1.01287	1.01879	3
60	0.45637	0.98581	0.28477	0.45637	0.98581	0.97609	0.98710	0.98203	3
	Ethyl Alcohol		$t_f=50$		Pr=11.699				
-60	0.26091	1.08568	0.19568	0.46783	1.18557	1.15303	0.96941	0.81946	1
60	0.57615	1.36813	0.30140	0.34767	1.24341	0.85687	1.01671	1.26220	1
-60	0.26686	1.12098	0.19883	0.46269	1.18368	1.14036	0.96786	0.83266	2
60	0.56162	1.32156	0.29716	0.35204	1.24765	0.86764	1.02017	1.24444	2
-60	0.42049	1.24653	0.24542	0.42049	1.24653	1.03635	1.01926	1.02776	3
60	0.39086	1.19956	0.23266	0.39086	1.19956	0.96333	0.98085	0.97433	3
	Freon R12		$t_f=50$		Pr=3.151				
-60	0.48957	0.69468	0.31897	0.67006	0.90225	1.27374	1.08944	0.91490	1
60	0.55598	1.04057	0.37128	0.40932	0.75288	0.77809	0.90908	1.06494	1
-60	0.52044	0.75601	0.33215	0.64900	0.89462	1.23370	1.08023	0.95270	2
60	0.51496	0.93150	0.35928	0.42792	0.76071	0.81345	0.91853	1.03052	2
-60	0.56523	0.86198	0.36985	0.56523	0.86198	1.07446	1.04081	1.06084	3
60	0.48562	0.79109	0.32596	0.48562	0.79109	0.92313	0.95522	0.93495	3

Note:

$$S1 = \frac{\mu_0 \rho_0}{\mu_f \rho_f} F''(0), \qquad S2 = \frac{k_0 \rho_0}{k_f \rho_f} [-\theta'(0)]$$

$$R1 = \frac{S1}{F''(0)|_{B.A.}}, \qquad R2 = \frac{S2}{-\theta'(0)|_{B.A.}}, \qquad R3 = \frac{F(\infty)}{F(\infty)|_{B.A.}}$$

For cases 1 and 2
$\rho=\rho(t)$, $\mu=\mu(t)$, $c_p=c_p(t)$ and $k=k(t)$.

But for case 1 $\rho=\rho(t)$ in all terms, and for case 2 $\rho=\rho(t)$ in the buoyancy force term only.

For case 3 $\mu=\mu_f$, $k=k_f$, $c_p=c_{pf}$, $k=k_f$, and $\rho=\rho(t)$ in the buoyancy force term only.

B.A.=Boussinesq approximations

compared with that obtained with Boussinesq approximations and are given in the last three columns of the Table. For the Boussinesq approximations, the properties were calculated at the film temperature.

By comparing the local Nusselt number at the surface, the friction factor and the total mass flow rate for the cases (1) and (2), it can be seen that the error in neglecting the density variation with temperature in terms other than the buoyancy force term is small. For example, for water when Δt = -60°C and $\overline{t_f}$ = 50°C,

$$\frac{Nu_x}{Nu_x|_{B.A.}} = 0.96903 \qquad \text{for case 1 and}$$

$$\frac{Nu_x}{Nu_x|_{B.A.}} = 0.96867 \qquad \text{for case 2.}$$

(The subscript "B.A." denotes the solution for Boussinesq approximations). The effects of neglecting the density variation in terms other than the buoyancy force term on velocity and temperature profiles are also small (see Figs. 2.2(c) and (d), for example). This clearly shows that the conclusion arrived at by Brown (1975) that the density variation was very important in all terms of the governing equations is incorrect. Brown neglected the effects of variations of other properties (viscosity, for example) with temperature in his analysis and also his treatment of the buoyancy force term seems to be incorrect.

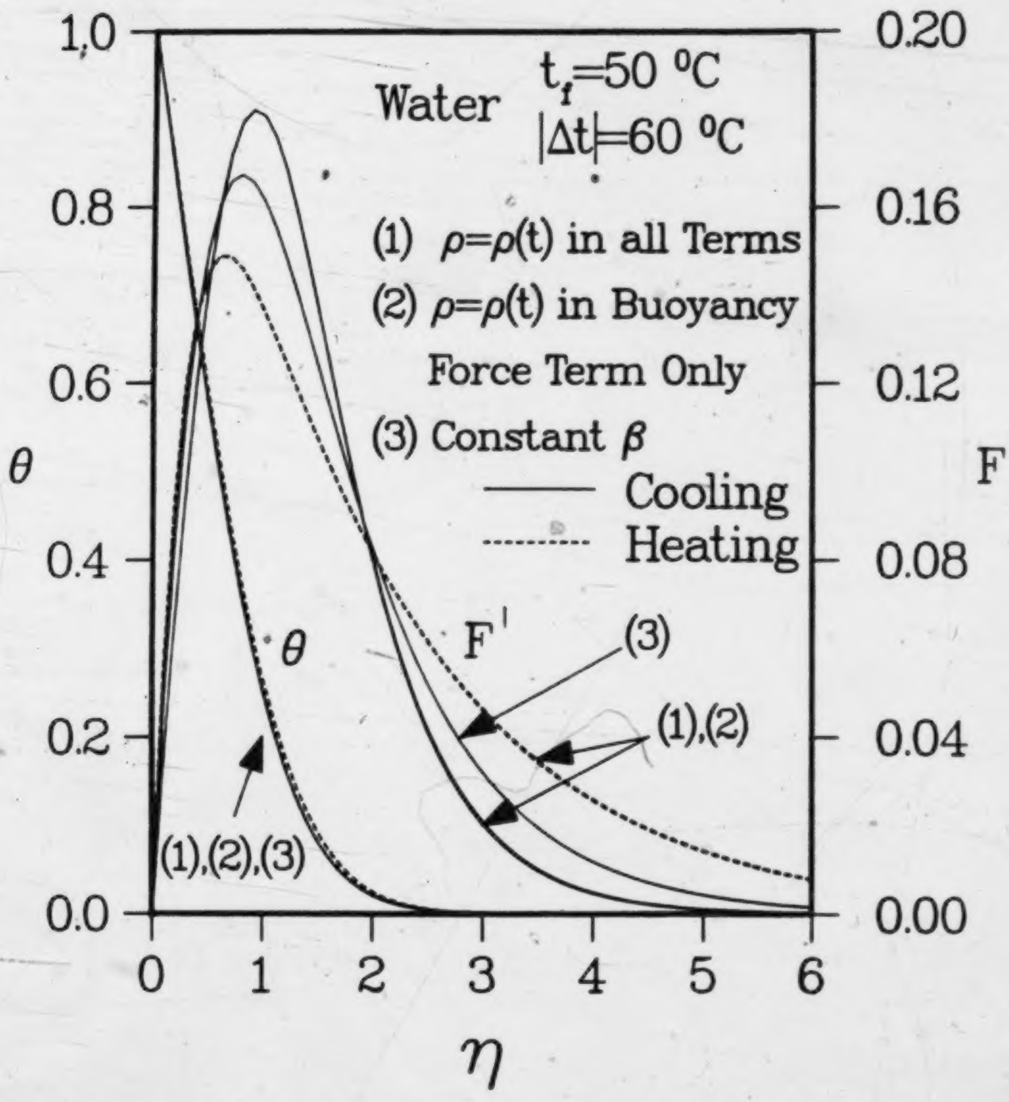

Fig. 2.2(c) The effects of variation of density with temperature for water when t_f=50°C and |Δt|=60°C

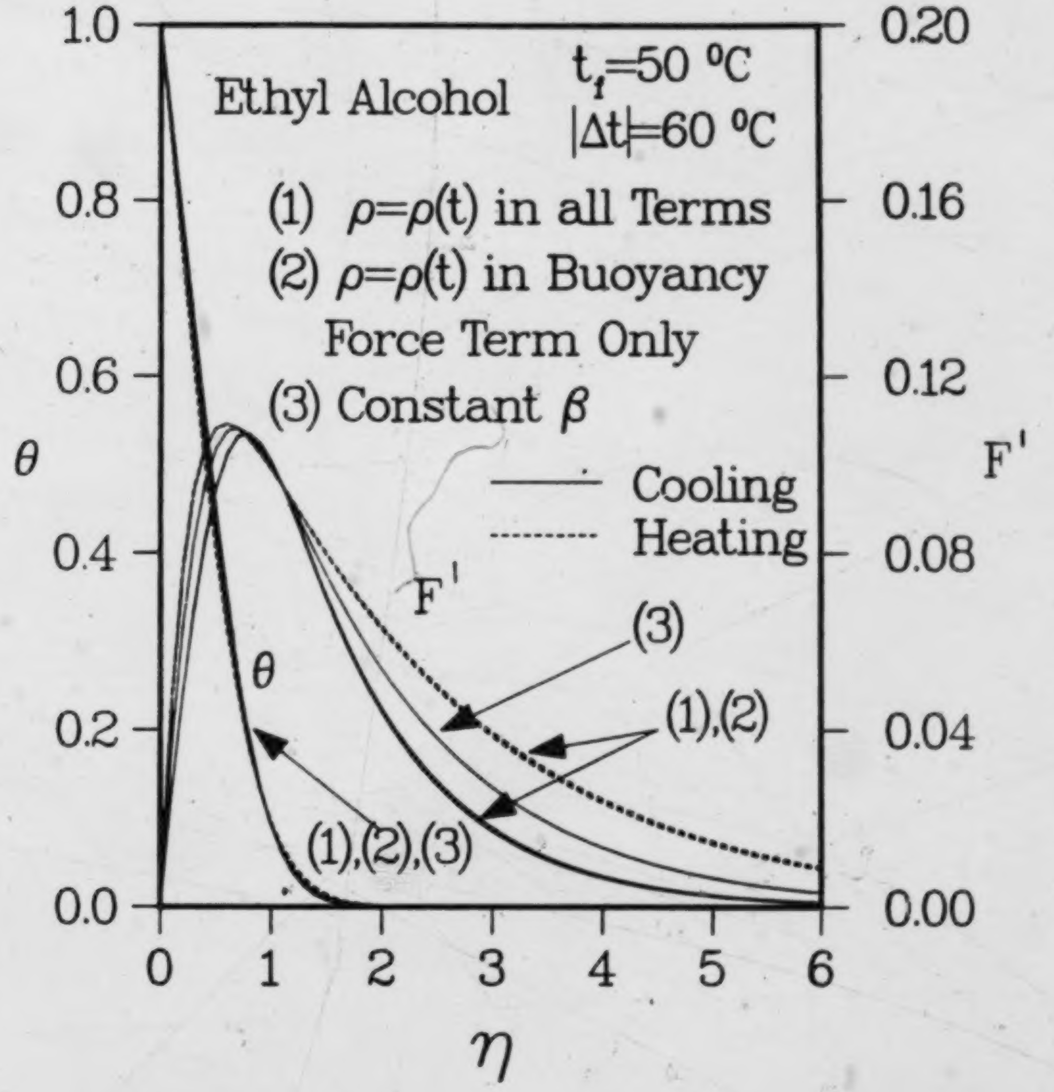

Fig. 2.2(d) The effects of variation of density with temperature for ethyl alcohol when t_f=50°C and |Δt|=60°C

In the buoyancy force term, the conventional assumption that the density varies linearly with temperature is not strictly valid. This can be seen from the solution to case (3). For example, for water when $\Delta t = -60°C$ and $t_f = 50°C$

$$\frac{Nu_x}{Nu_x|_{B.A.}} = 1.05177 \qquad \text{for case 3}$$

As this ratio is different from 1.0, a better approximation of the variation of density in the buoyancy force term than the conventional linear variation is necessary.

Also, by comparing the solutions to cases (2) and (3) for a particular liquid with the same Δt and t_f, it can be seen that it is important to include the variations of viscosity, thermal conductivity and specific heat in the analysis.

2.1.3 Present Treatment of the Buoyancy Force Term

The sole driving force in natural convective flows is the buoyancy force resulting from the variation of density with temperature. Hence, the density cannot be assumed to be constant in the buoyancy force term. As shown before, the conventional assumption that the density varies linearly with temperature in the buoyancy force term is not justified for large temperature differences. Hence, a better approximation of the variation of density with temperature which accomodates a similarity solution is necessary for the buoyancy force term.

When the density of a liquid is monotonically decreasing or increasing between temperatures t_1 and t_2, from the mean value theorem one obtains,

$$\rho_1-\rho_2 = \frac{\partial\rho}{\partial t}\Big|_c(t_1-t_2) \tag{2.24}$$

where c lies between t_1 and t_2. For most liquids, the density varies nonlinearly with temperature and hence $\frac{\partial\rho}{\partial t}$ is a function of temperature. As a first approximation the temperature at c can be taken to be equal to $(t_1+t_2)/2$. This is equivalent to saying that $\rho(t)$ is a second order polynomial. For moderate temperature differences ρ_0/ρ is nearly equal to 1. Hence, the dimensionless buoyancy force term can be written as

$$\frac{\rho_\infty-\rho}{\rho_\infty-\rho_0}\,\frac{\rho_0}{\rho} \cong \frac{\rho_\infty-\rho}{\rho_\infty-\rho_0}$$

$$= \frac{\frac{\partial\rho}{\partial t}\Big|_c(t_\infty-t)}{\frac{\partial\rho}{\partial t}\Big|_d(t_\infty-t_0)} \tag{2.25}$$

where the temperature at c is between t_∞ and t, and the temperature at d is between t_∞ and t_0. Hence, for the parabolic variation of density with temperature it can be easily shown that

$$\frac{\left.\frac{\partial\rho}{\partial t}\right|_c}{\left.\frac{\partial\rho}{\partial t}\right|_f} = 1+\epsilon_f(\theta-1) \qquad (2.26)$$

where
$$\epsilon_f = \frac{\beta_0 - \beta_\infty}{\beta_0 + \beta_\infty} \qquad (2.27)$$

Hence the dimensionless buoyancy force term becomes

$$\frac{\rho_\infty-\rho}{\rho_\infty-\rho_0}\,\frac{\rho_0}{\rho} \cong \theta[1-\epsilon_f(1-\theta)] \qquad (2.28)$$

Had the Grashof number been defined as,

$$Gr_x = \frac{g\beta_r(t_0-t_\infty)x^3}{\nu_r^2} \qquad (2.29)$$

where $$t_r = t_0 - r(t_0-t_\infty) \qquad (2.30)$$

and r is the position of reference temperature,

it could be easily shown that the dimensionless buoyancy force term would become,

$$\frac{\rho_\infty-\rho}{\rho\beta_r(t_0-t_\infty)} \cong \theta[1-\epsilon_r(2-2r-\theta)] \qquad (2.31)$$

where
$$\epsilon_r = \frac{\beta_0-\beta_\infty}{2\beta_r} \tag{2.32}$$

The value of r varies from 0 to 1. The film temperature corresponds to r=0.5.

The parameter ϵ_f (or ϵ_r) depends on the variation of the coefficient of thermal expansion with temperature. It can be seen from eq. (2.27) that the value of ϵ_f normally lies between +1 and -1. The absolute value of the parameter ϵ_f is greater than 1 when there is a density extremum between t_0 and t_∞ and for such a case, the present analysis is not strictly valid. A positive value of ϵ_f corresponds to up flow circumstances and a negative value to down flow. The Boussinesq approximation corresponds to the case when $\epsilon_f=0$.

Piau (1974) proposed the following model to incorporate the temperature-dependent coefficient of thermal expansion. He approximated the dimensionless buoyancy force

$$\frac{\rho_\infty-\rho}{\rho\beta_r(t_0-t_\infty)} \cong \theta[1+\epsilon_p(\theta-0.5)] \tag{2.33}$$

where
$$\epsilon_p = \frac{\rho_f-\rho_0}{\rho_\infty-\rho_f} - 1 \tag{2.34}$$

He did not provide a mathematical explanation for the above approximation.

In Fig. 2.3(a), the dimensionless buoyancy force for different models are compared with the exact value for water

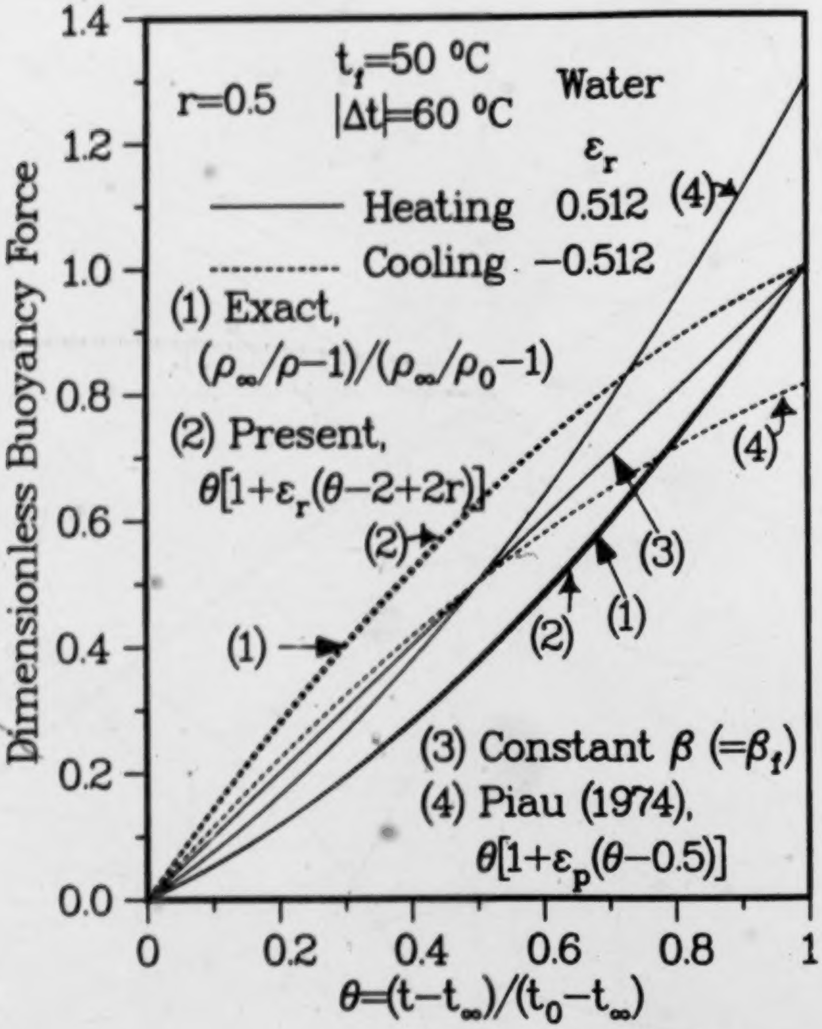

Fig. 2.3(a) The dimensionless buoyancy force for different models when r=0.5

with t_f=50°C and $|\Delta t|$=60°C at all points in the thermal boundary layer. It is seen that the present formulation gives a better approximation of the buoyancy force (and hence an accurate value of local Nusselt number at the surface) than that of Piau (1974) or Boussinesq approximation. For example, for water when t_0=30°C and t_∞=10°C, the error in the local Nusselt number at the surface with the present approximation is less than 1% whereas the errors due to Piau (1974) and the Boussinesq approximations are about 8% and 4% respectively (see also Appendix C).

The assumption that the density varies linearly with temperature underpredicts the buoyancy force for down flows and overpredicts it for up flows. Figs. 2.3(b) and (c) compare the dimensionless buoyancy force for different models for reference temperatures t_∞ and t_0 respectively. The error in the buoyancy force term with Boussineq approximation or that of Piau (1974) is more pronounced when t_∞ or t_0 is chosen as the reference temperature. The present model predicts the buoyancy force fairly well irrespective of the choice of the reference temperature. Eventhough Piau(1974) assumed that the coefficient of thermal expansion varies linearly with temperature, his treatment of the buoyancy force term seems to be incorrect.

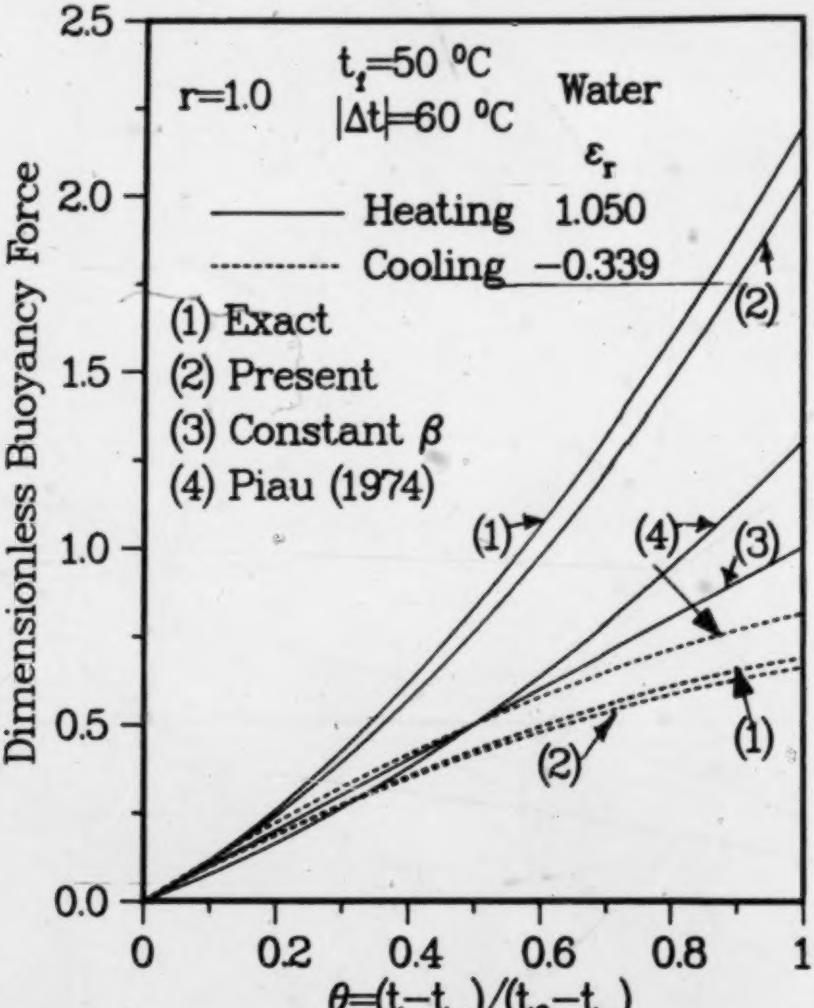

Fig. 2.3(b) The dimensionless buoyancy force for different models when r=1.0

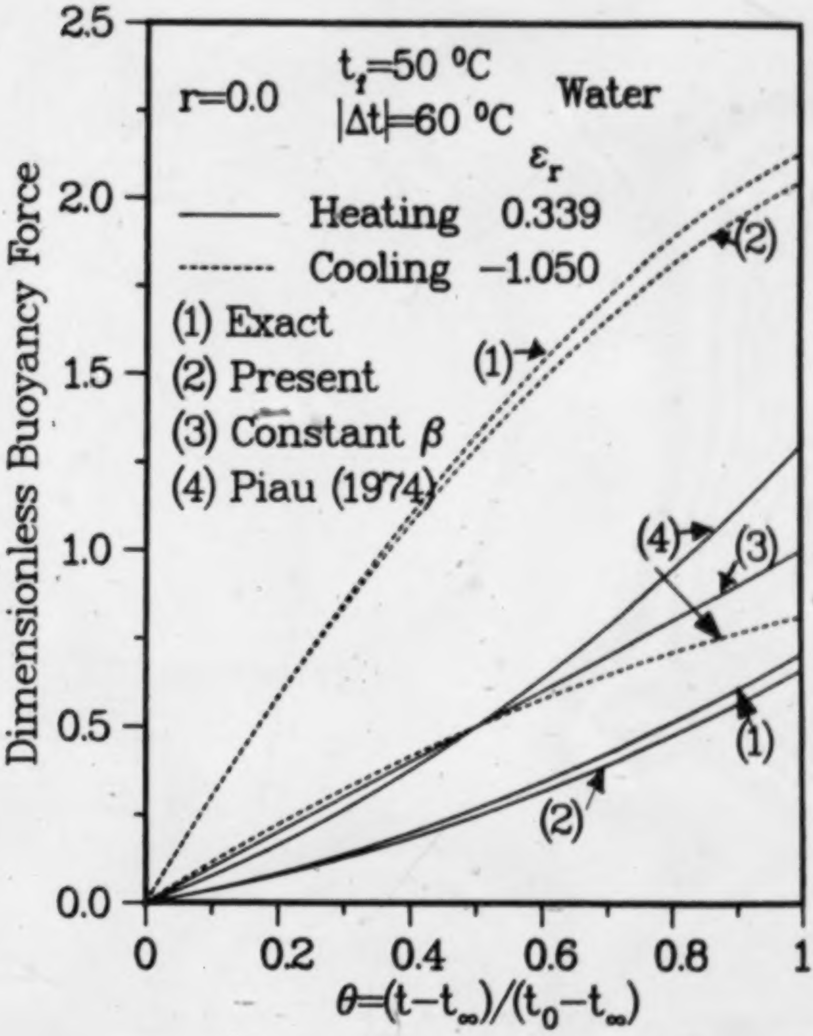

Fig. 2.3(c) The dimensionless buoyancy force for different models when r=0.0

2.1.4 Variations of Viscosity, Thermal Conductivity, and Specific Heat with Temperature

The properties, viscosity, thermal conductivity, and specific heat appear in the governing equations as ratios of μ/μ_f, k/k_f and c_p/c_{pf} respectively. Similarity solutions exist when the ratios are functions of η alone. This is also true if they are functions of θ. A wide variety of functions such as algebraic expressions, exponential forms satisfy this requirement. For moderate temperature differences, each ratio may be approximated by a linearized Taylor series expansion about a reference temperature. They are given by,

$$\frac{\mu}{\mu_r} = 1+\frac{1}{\mu_r}\,\frac{\partial\mu}{\partial t}\Big|_r(t-t_r) = 1+\gamma_r(\theta-1+r) \tag{2.35}$$

$$\frac{k}{k_r} = 1+\frac{1}{k_r}\,\frac{\partial k}{\partial t}\Big|_r(t-t_r) = 1+\lambda_r(\theta-1+r) \tag{2.36}$$

$$\frac{c_p}{c_{pr}} = 1+\frac{1}{c_{pr}}\,\frac{\partial c_p}{\partial t}\Big|_r(t-t_r) = 1+\zeta_r(\theta-1+r) \tag{2.37}$$

where

$$\gamma_r = \frac{1}{\mu_r}\,\frac{d\mu}{dt}\Big|_r(t_0-t_\infty) \tag{2.38}$$

$$\lambda_r = \frac{1}{k_r}\,\frac{dk}{dt}\Big|_r(t_0-t_\infty) \tag{2.39}$$

$$\zeta_r = \frac{1}{c_{pr}} \frac{dc_p}{dt}\Big|_r (t_0 - t_\infty) \qquad (2.40)$$

μ/μ_f, k/k_f and c_p/c_{pf} correspond to the case when r=0.5, that is, when the film temperature is chosen as the reference temperature. If r=0.5 and the properties vary linearly with temperature, it can be easily shown that

$$\gamma_f = 2\frac{(\mu_0/\mu_\infty - 1)}{(\mu_0/\mu_\infty + 1)} \qquad (2.41)$$

$$\lambda_f = 2\frac{(k_0/k_\infty - 1)}{(k_0/k_\infty + 1)} \qquad (2.42)$$

$$\zeta_f = 2\frac{(c_{p0}/c_{p\infty} - 1)}{(c_{p0}/c_{p\infty} + 1)} \qquad (2.43)$$

In the present study, unless explicitly stated, the reference temperature is assumed to be the film temperature. The values of μ_f, λ_f, and ζ_f normally lie between +2 and -2 (see eqs. (2.41) to (2.43)). The case of $\gamma_f = \lambda_f = \zeta_f = 0$, corresponds to Boussinesq approximations. For liquids, the viscosity decreases with an increase in temperature. Hence, a negative value of γ_f corresponds to a heated wall and a positive value, the cooled wall. When the thermal conductivity increases with temperature, a positive value of λ_f corresponds to a heated wall and a negative value, a cooled wall. Similarly, when the specific heat increases with temperature, a positive value of ζ_f means a heated wall and a negative value, a cooled wall.

With the above assumptions and approximations the equations (2.15) to (2.17) become,

$$\frac{d}{d\eta}\left[\{1+\gamma_f(\theta-0.5)\}\ F''\right] + 3FF'' - 2(F')^2 + \theta[1-\epsilon_f(1-\theta)] = 0 \tag{2.44}$$

$$\frac{d}{d\eta}\left[\{1+\lambda_f(\theta-0.5)\}\theta'\right] + \{1+\zeta_f(\theta-0.5)\}\ 3(Pr)F\theta' = 0 \tag{2.45}$$

$$F(0) = F'(0) = \theta(0) - 1 = F'(\infty) = \theta(\infty) = 0 \tag{2.46}$$

2.1.5 The Governing Equations for Liquids with Very Large Prandtl Numbers

For many liquids such as viscous oils, the Prandtl number is far greater than 1. Hence it is of interest to examine the effects of variable properties for the limiting case of Pr → ∞. For liquids with large Prandtl numbers, the natural convection boundary layer has two regions. In the inner region, where there is a tangible temperature difference, buoyancy effect exists (Le Fevre, 1956, and Kuiken, 1968b and 1968c). In the outer region, no buoyancy effect exists. The liquid in this region is flowing due to viscous contact with the inner region. As a direct numerical integration of the equations (2.44) to (2.46) is difficult for very large Prandtl numbers, a singular perturbation technique, similar to the one shown in Kuiken (1968c) is employed.

The Inner Problem

Introducing the following transformations in the equations (2.44) and (2.45) (Kuiken, 1968c)

$$F = Pr^{-3/4}\, g(\xi),\ \theta = h(\xi),\ \eta = \xi\, Pr^{-1/4} \tag{2.47}$$

the governing equations become for Pr→∞,

$$[1+\gamma_f(h-\frac{1}{2})]\, g''' + \gamma_f h'g'' + h[1-\epsilon_f(1-h)]$$

$$+ \frac{1}{Pr}[3gg''-2(g')^2] = 0 \tag{2.48}$$

$$[1+\lambda_f(h-\frac{1}{2})]\, h'' + \lambda_f(h')^2 + 3[1+\zeta_f(h-\frac{1}{2})]gh' = 0 \tag{2.49}$$

The Outer Problem

Introducing the following transformations in the equations (2.44) and (2.45) (Kuiken, 1968c)

$$F = Pr^{-1/4}\, G(\Xi),\ \theta = H(\Xi),\ \eta = \Xi\, Pr^{1/4} \tag{2.50}$$

the governing equations become for Pr→∞,

$$(1-\frac{\gamma_f}{2})\,G''' + 3GG''-2(G')^2 = 0 \tag{2.51}$$

$$H = 0 \tag{2.52}$$

The equations can be solved by a singular perturbation technique. The perturbation parameter is $(Pr)^{-1/2}$. The boundary conditions are (Kuiken, 1968c),

$$g = \frac{dg}{d\xi} = h-1 = 0 \text{ at } \xi = 0 \tag{2.53}$$

$$\frac{dG}{d\Xi} \to 0 \text{ as } \Xi \to 0 \tag{2.54}$$

The remaining boundary conditions have to be obtained from matching the inner and the outer stream functions. For example, for the zeroth order equations, it can be easily shown that (Kuiken, 1968c)

$$\frac{d^2g_0}{d\xi^2} \to 0 \text{ as } \xi \to \infty \tag{2.55}$$

$$G_0 \to 0 \text{ at } \Xi \to 0 \tag{2.56}$$

$$\frac{dg_0}{d\xi}\Big|_{\xi\to\infty} = \frac{dG_0}{d\Xi}\Big|_{\Xi\to 0} \tag{2.57}$$

2.2 Results and Discussion

The equations (2.44) to (2.46) were solved numerically for various values of the parameters ϵ_f, γ_f, λ_f and ζ_f, for Prandtl numbers 1, 2, 10, 20 and 100. For Pr → ∞, solutions to the zeroth order perturbations were obtained for the equations (2.48), (2.49) and (2.51) to (2.57).

2.2.1 The Effects of Variation of Coefficient of Thermal Expansion with Temperature

The effects of variation of coefficient of thermal expansion with temperature on the laminar natural convective flow are given in terms of the dimensionless parameter ϵ_f. The larger the absolute value of ϵ_f, the more pronounced are the effects of temperature-dependent coefficient of thermal expansion on the natural convective flow. The case $\epsilon_f=0$ corresponds to Boussinesq approximations. Figs. 2.4(a) to (f) show the effects of ϵ_f on the temperature and the velocity profiles for Prandtl numbers 1, 10, and 100. Table 2.2 compares its effects on the surface heat transfer, the surface shear stress, and the total mass flow rate for various Prandtl numbers. The parameters γ_f, λ_f and ζ_f were taken to be equal to zero for this case.

The dimensionless buoyancy force is lower for positive values of ϵ_f and it is higher for negative values (see eq. (2.28) and Fig. 2.3(a)). Hence, a positive value of ϵ_f decreases the maximum velocity and the total mass flow rate and a negative value increases them. The thicknesses of thermal and velocity boundary layers are slightly larger for a positive value of ϵ_f and smaller for a negative value. A positive value of ϵ_f decreases the surface heat transfer and the surface shear stress, and a negative value increases them. The larger the absolute value of ϵ_f, the more

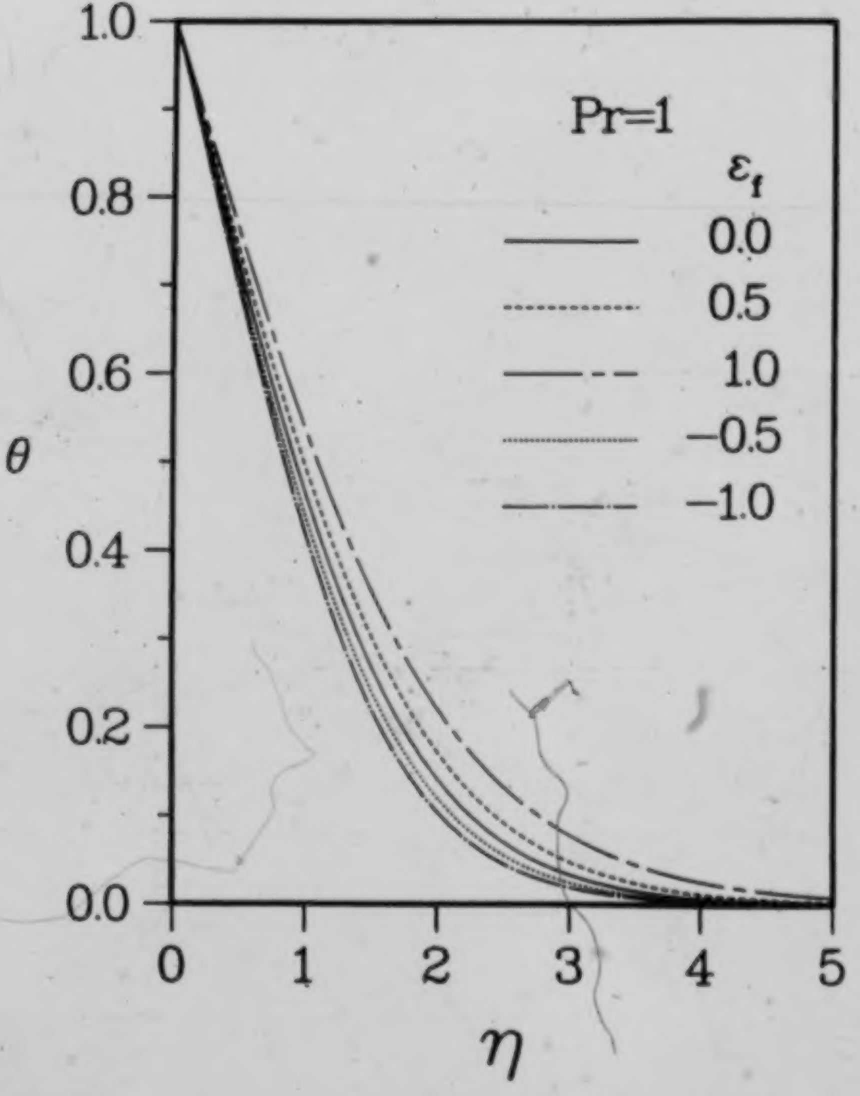

Fig. 2.4(a) The effects of ϵ_f on temperature profile for Pr=1

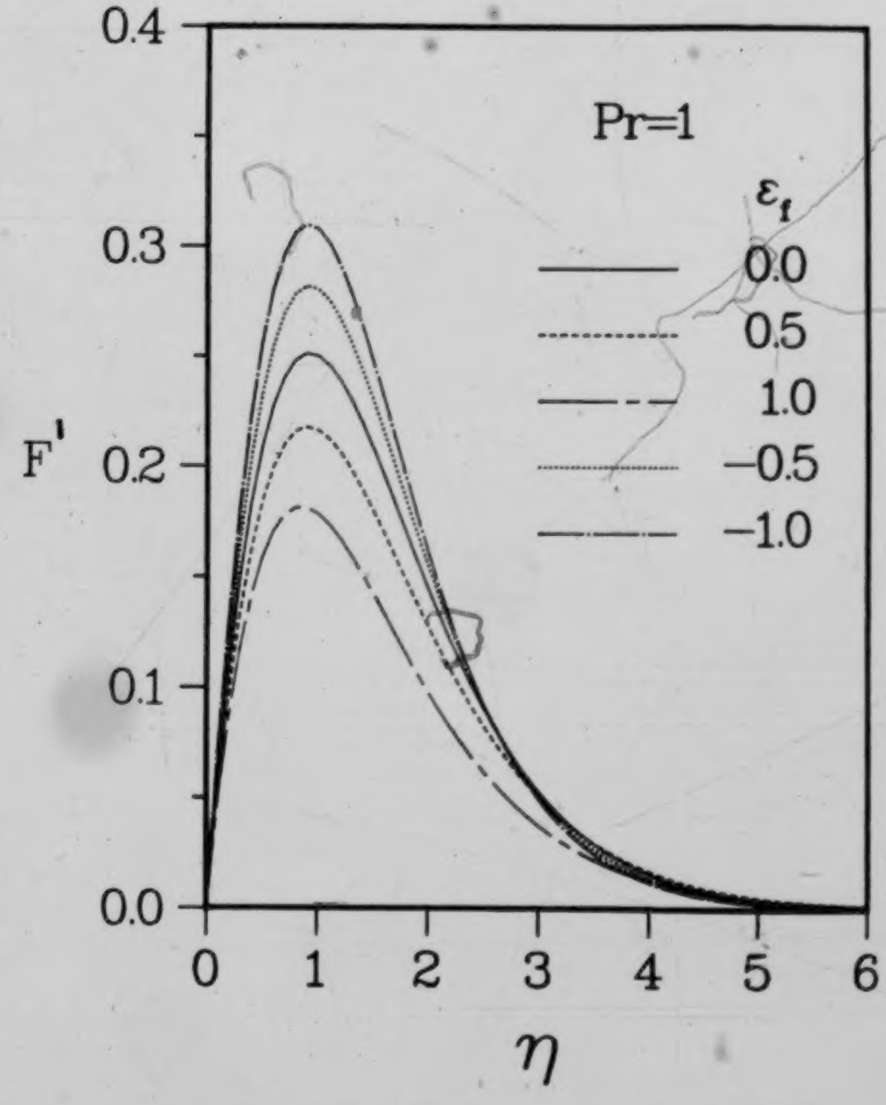

Fig. 2.4(b) The effects of ϵ_f on velocity profile for Pr=1

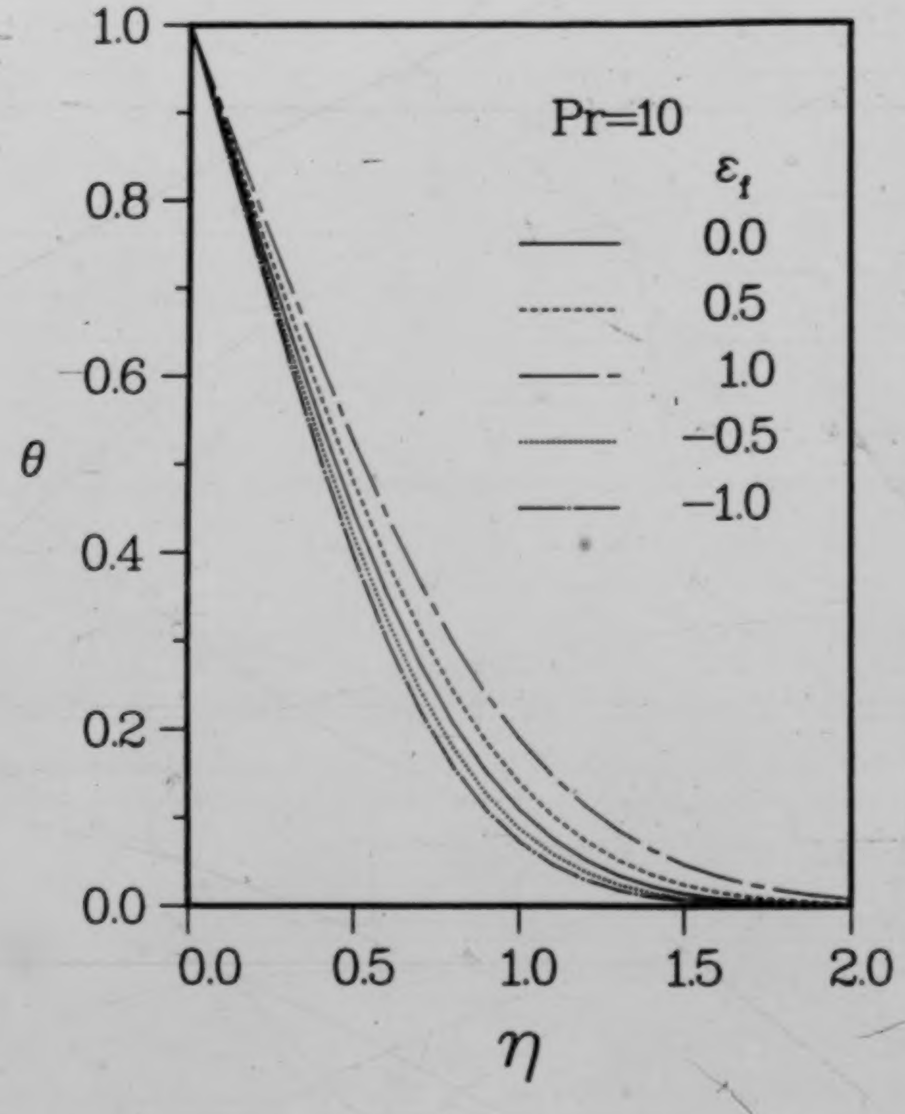

Fig. 2.4(c) The effects of ϵ_f on temperature profile for Pr=10

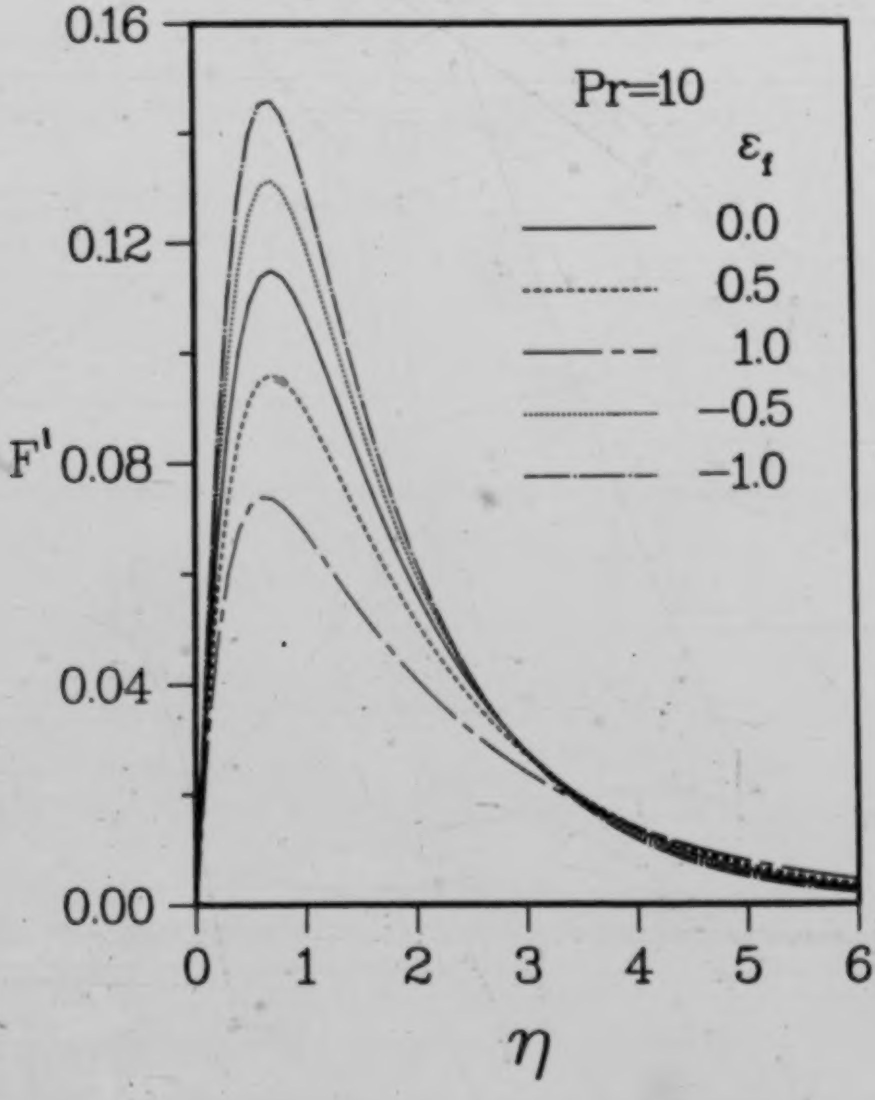

Fig. 2.4(d) The effects of ϵ_f on velocity profile for Pr=10

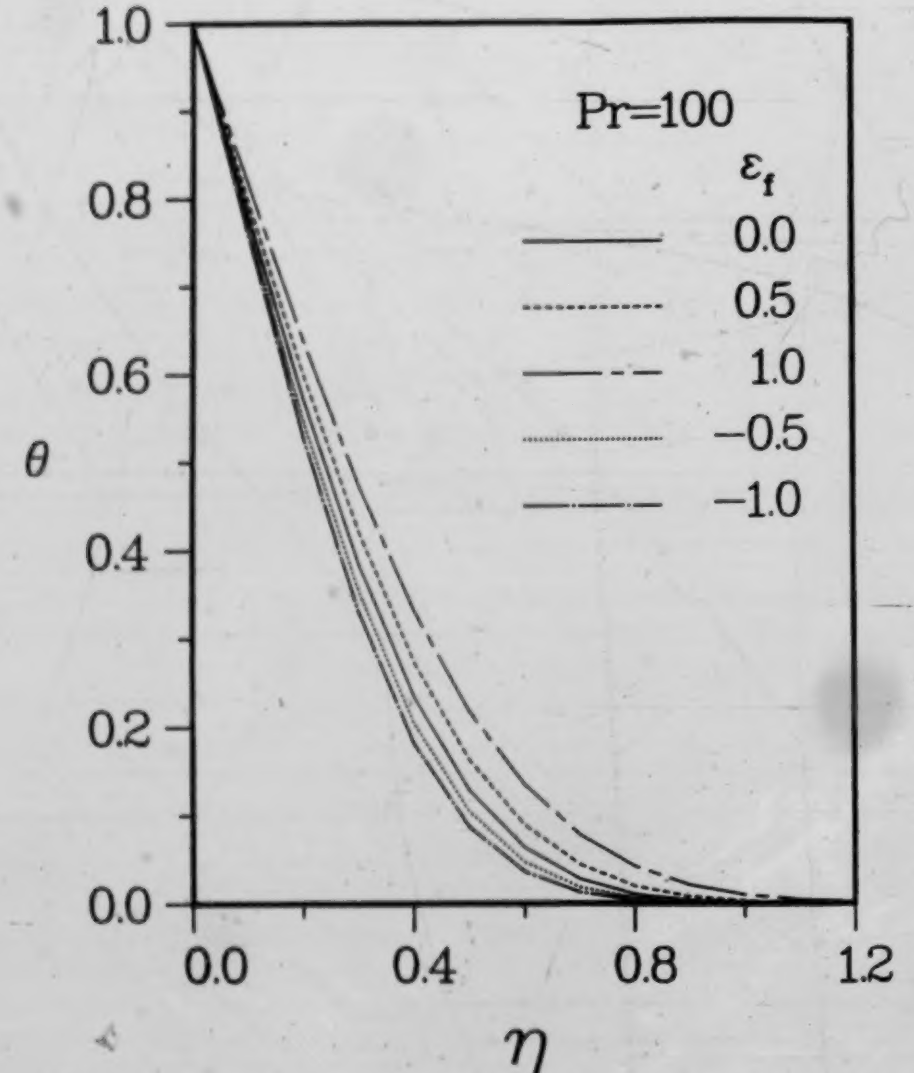

Fig. 2.4(e) The effects of ϵ_f on temperature profile for Pr=100

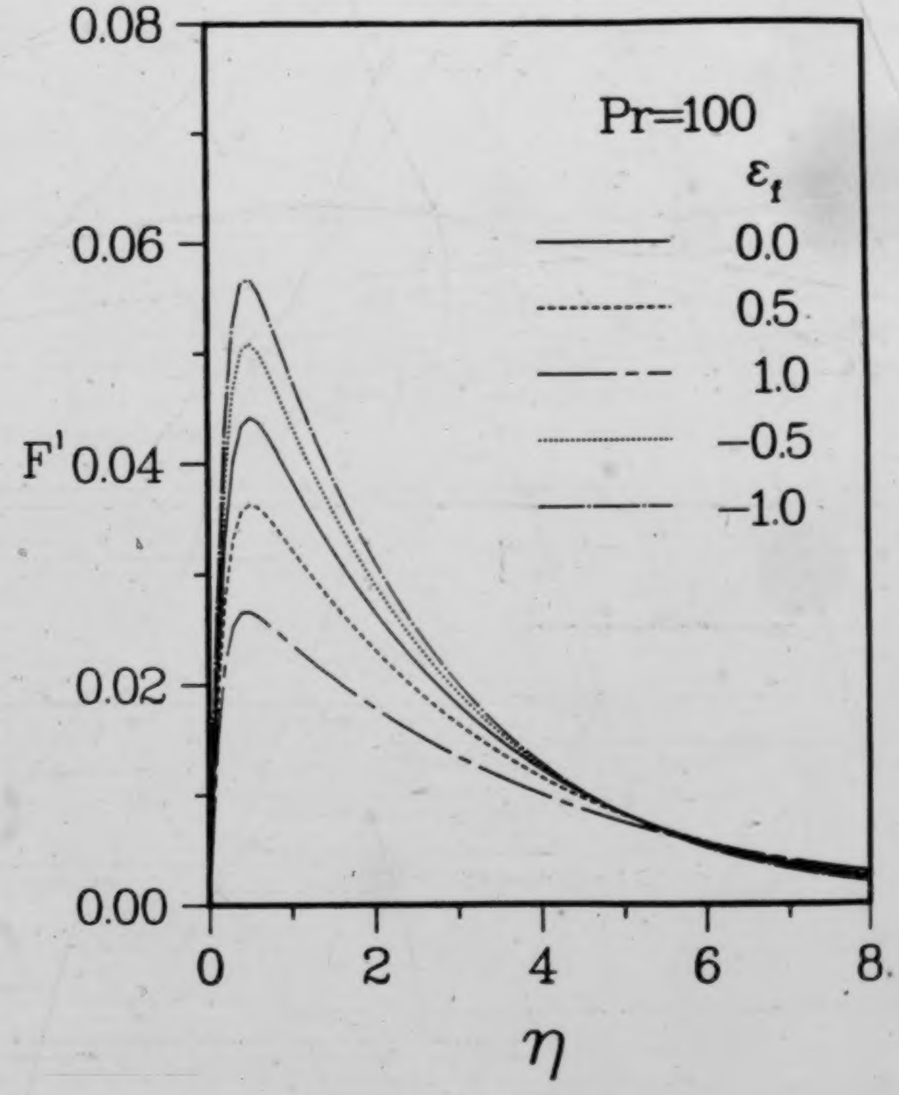

Fig. 2.4(f) The effects of ϵ_f on velocity profile for Pr=100

Table 2.2 The effects of ϵ_f for various Prandtl numbers

Pr	ϵ_f	$F''(0)$	R1	$-\theta'(0)$	R2	$F(\infty)$	R3
1.00	1.00	0.52847	0.82292	0.48444	0.85416	0.37601	0.71897
1.00	0.75	0.55617	0.86606	0.51018	0.89955	0.43001	0.82222
1.00	0.50	0.58470	0.91048	0.53161	0.93733	0.46783	0.89454
1.00	0.25	0.61345	0.95525	0.55034	0.97037	0.49780	0.95186
1.00	0.00	0.64219	1.00000	0.56715	1.00000	0.52298	1.00000
1.00	-0.25	0.67079	1.04453	0.58246	1.02701	0.54487	1.04186
1.00	-0.50	0.69919	1.08875	0.59659	1.05191	0.56434	1.07908
1.00	-0.75	0.72736	1.13262	0.60973	1.07508	0.58194	1.11274
1.00	-1.00	0.75528	1.17610	0.62204	1.09679	0.59805	1.14355
2.00	1.00	0.45856	0.80272	0.61114	0.85299	0.29825	0.73710
2.00	0.75	0.48647	0.85156	0.64348	0.89813	0.33585	0.83004
2.00	0.50	0.51478	0.90112	0.67083	0.93630	0.36345	0.89824
2.00	0.25	0.54310	0.95070	0.69486	0.96985	0.38573	0.95330
2.00	0.00	0.57126	1.00000	0.71647	1.00000	0.40462	1.00000
2.00	-0.25	0.59919	1.04889	0.73617	1.02751	0.42115	1.04084
2.00	-0.50	0.62686	1.09732	0.75435	1.05287	0.43590	1.07730
2.00	-0.75	0.65423	1.14524	0.77126	1.07647	0.44928	1.11036
2.00	-1.00	0.68132	1.19265	0.78709	1.09857	0.46154	1.14068
10.00	1.00	0.32220	0.76861	0.98962	0.84632	0.18824	0.75531
10.00	0.75	0.34663	0.82690	1.04460	0.89333	0.20900	0.83861
10.00	0.50	0.37106	0.88517	1.09136	0.93332	0.22491	0.90244
10.00	0.25	0.39527	0.94293	1.13245	0.96846	0.23800	0.95497
10.00	0.00	0.41920	1.00000	1.16933	1.00000	0.24923	1.00000
10.00	-0.25	0.44281	1.05632	1.20292	1.02872	0.25911	1.03964
10.00	-0.50	0.46610	1.11188	1.23384	1.05517	0.26797	1.07520
10.00	-0.75	0.48907	1.16669	1.26256	1.07973	0.27603	1.10754
10.00	-1.00	0.51174	1.22077	1.28941	1.10269	0.28344	1.13726
20.00	1.00	0.27465	0.75879	1.19920	0.84359	0.15668	0.75719
20.00	0.75	0.29673	0.81978	1.26735	0.89152	0.17371	0.83950
20.00	0.50	0.31873	0.88056	1.32522	0.93223	0.18682	0.90287
20.00	0.25	0.34049	0.94069	1.37602	0.96797	0.19764	0.95514
20.00	0.00	0.36196	1.00000	1.42155	1.00000	0.20692	1.00000
20.00	-0.25	0.38312	1.05846	1.46298	1.02914	0.21510	1.03952
20.00	-0.50	0.40397	1.11607	1.50108	1.05595	0.22244	1.07499
20.00	-0.75	0.42453	1.17286	1.53645	1.08082	0.22911	1.10726
20.00	-1.00	0.44480	1.22885	1.56949	1.10406	0.23525	1.13692
100.00	1.00	0.18731	0.74422	1.83876	0.83909	0.10339	0.75682
100.00	0.75	0.20368	0.80923	1.94727	0.88861	0.11426	0.83639
100.00	0.50	0.21991	0.87374	2.03909	0.93051	0.12336	0.90300
100.00	0.25	0.23592	0.93735	2.11944	0.96718	0.13015	0.95271
100.00	0.00	0.25169	1.00000	2.19137	1.00000	0.13661	1.00000
100.00	-0.25	0.26720	1.06160	2.25663	1.02978	0.14170	1.03725
100.00	-0.50	0.28247	1.12226	2.31663	1.05716	0.14657	1.07290
100.00	-0.75	0.29749	1.18196	2.37219	1.08252	0.15100	1.10533
100.00	-1.00	0.31230	1.24079	2.42410	1.10620	0.15531	1.13688

Note:

For this case

$\gamma_f=\lambda_f=\zeta_f=0$

$$R1 = \frac{F''(0)}{F''(0)|_{\epsilon_f=0}}$$

$$R2 = \frac{-\theta'(0)}{-\theta'(0)|_{\epsilon_f=0}}$$

$$R3 = \frac{F(\infty)}{F(\infty)|_{\epsilon_f=0}}$$

pronounced are the effects.

From Table 2.2, the effect of ϵ_f on the local Nusselt number can be written as,

$$\frac{Nu_x}{Nu_x|_{\epsilon_f=0}} \cong (1-0.5\epsilon_f)^{0.24} \tag{2.58}$$

The above relation is accurate, within ±1% for the range of the parameter ϵ_f and the Prandtl numbers investigated. This also clearly shows that, contrary to Piau (1974), the effects of variation of coefficient of thermal expansion with temperature on the surface heat transfer are significant for small as well as large Prandtl numbers.

2.2.2 The Effects of Variation of Viscosity with Temperature

The effects of variation of viscosity with temperature on the laminar natural convective flow are given in terms of the dimensionless parameter γ_f. The larger the absolute value of γ_f, the more pronounced are the effects of temperature-dependent viscosity on the natural convective flow. The case $\gamma_f=0$ corresponds to Boussinesq approximations. Figs. 2.5(a) to (f) show the effects of γ_f on the temperature and the velocity profiles for Prandtl numbers 1, 10, and 100. Table 2.3 compares its effects on the surface shear stress, the surface heat transfer, and the total mass flow rate for various Prandtl numbers. The parameters ϵ_f, λ_f and ζ_f were taken to be equal to zero for this case.

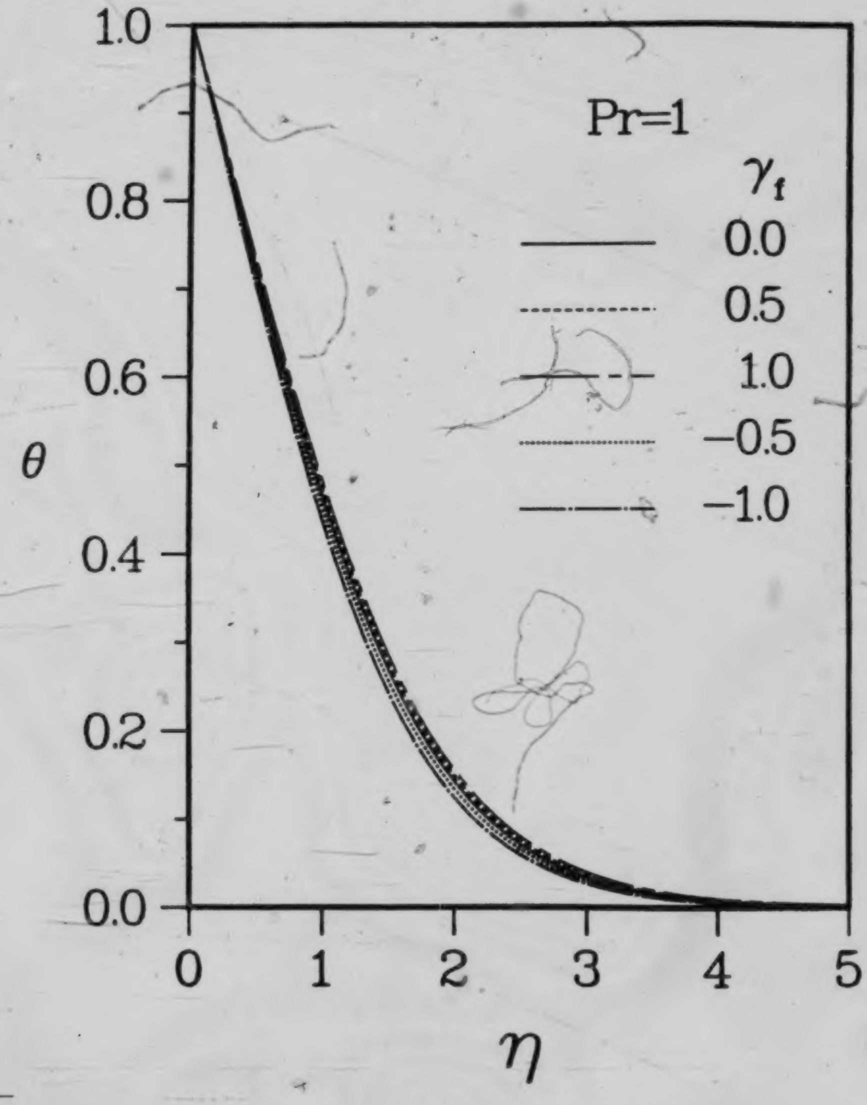

Fig. 2.5(a) The effects of γ_f on temperature profile for Pr=1

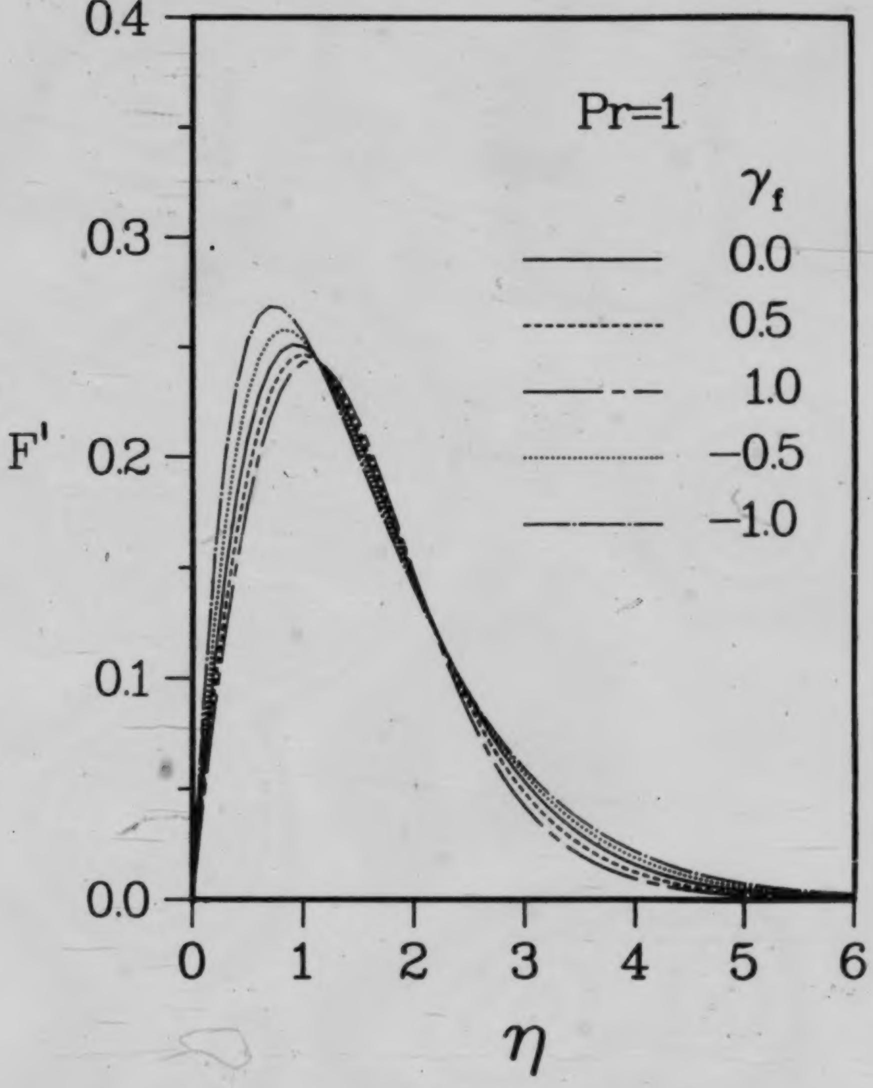

Fig. 2.5(b) The effects of γ_f on velocity profile for Pr=1

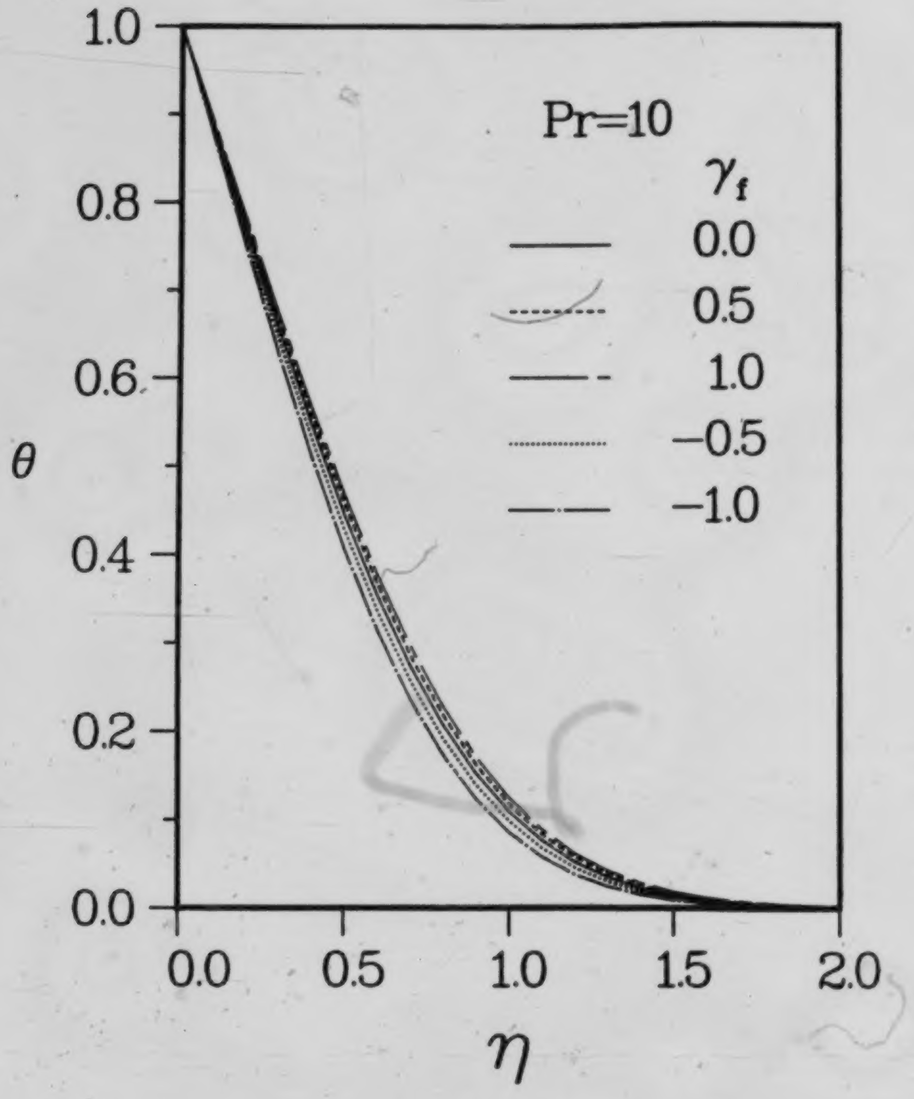

Fig. 2.5(c) The effects of γ_f on temperature profile for Pr=10

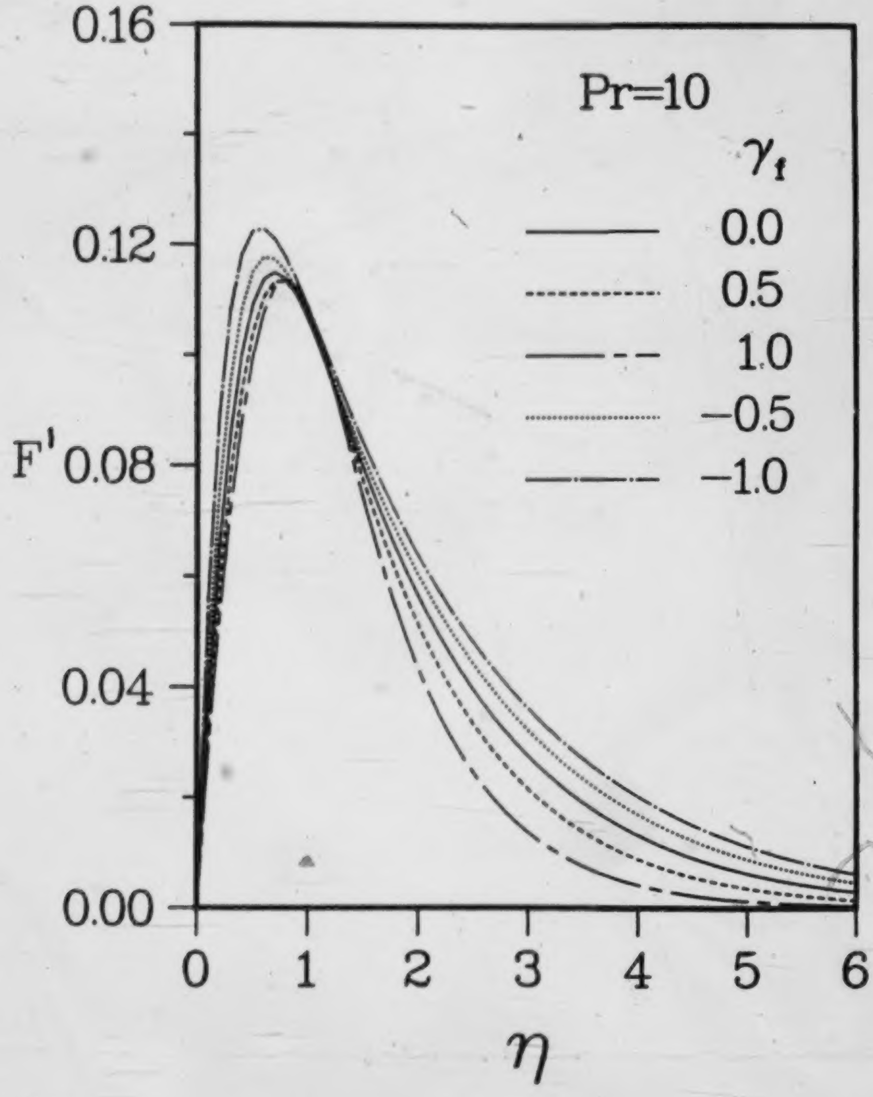

Fig. 2.5(d) The effects of γ_f on velocity profile for Pr=10

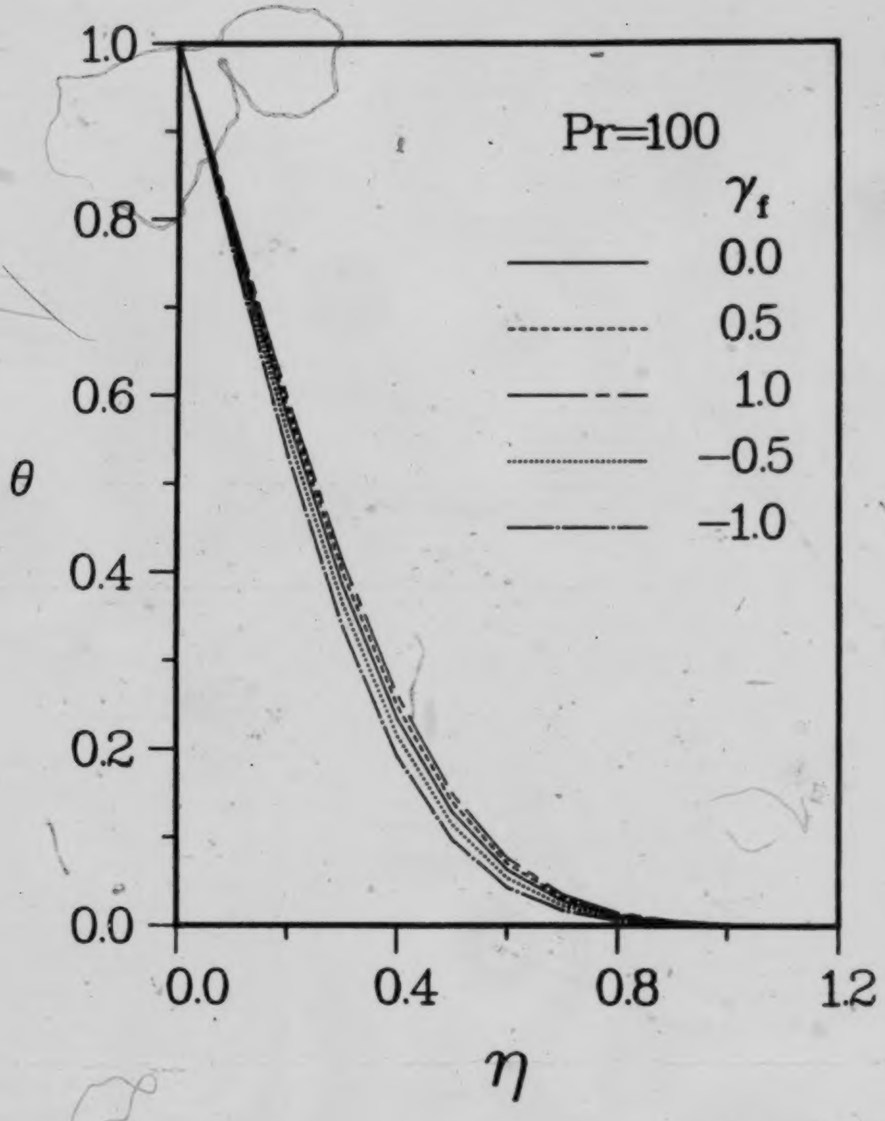

Fig. 2.5(e) The effects of γ_f on temperature profile fo:
Pr=100

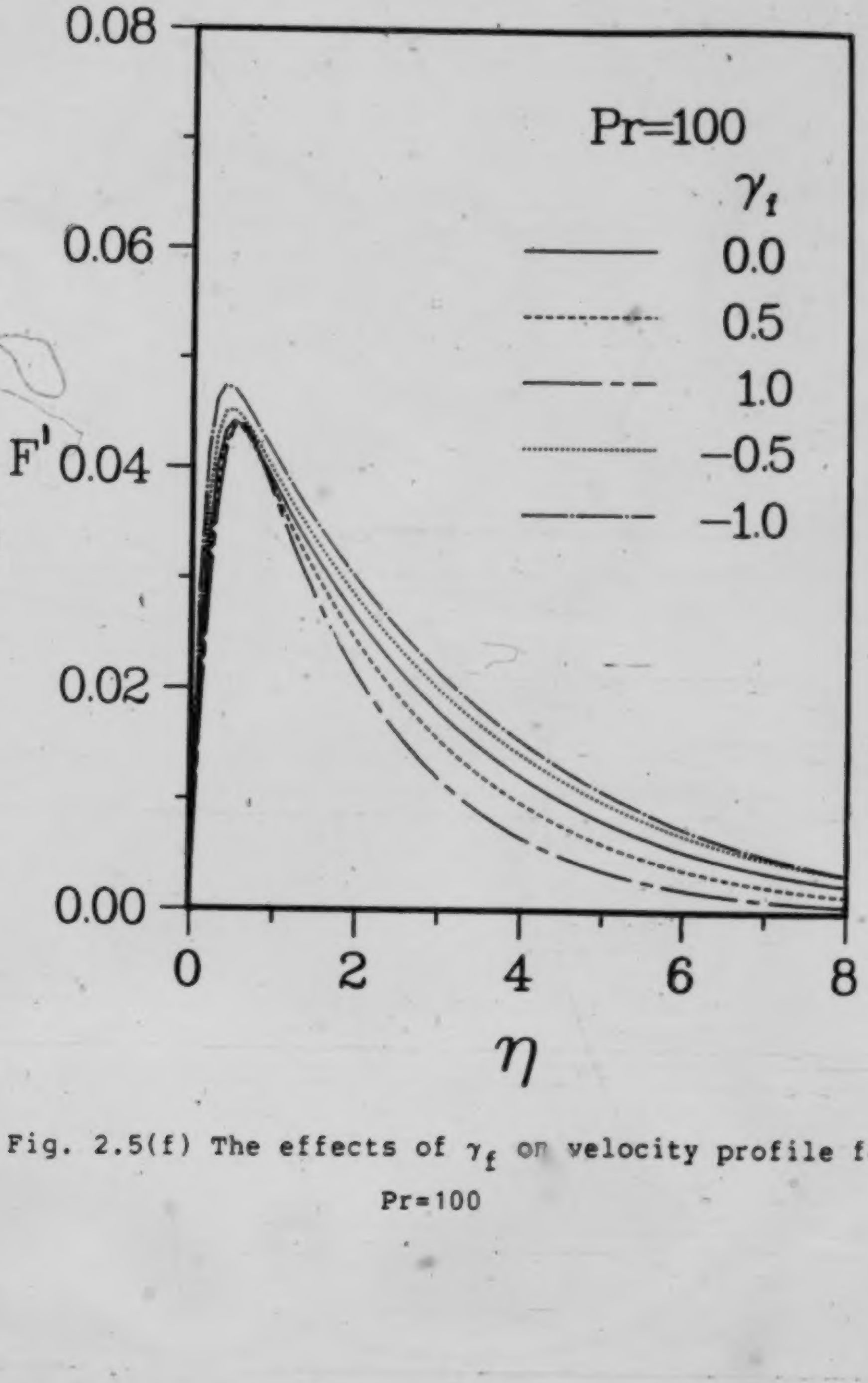

Fig. 2.5(f) The effects of γ_f on velocity profile for Pr=100

Table 2.3 The effects of γ_f for various Prandtl numbers

Pr	γ_f	$F''(0)$	R1	$-\theta'(0)$	R2	$F(\infty)$	R3
1.00	1.00	0.48078	1.12299	0.54273	0.95696	0.48484	0.92708
1.00	0.75	0.51155	1.09528	0.54804	0.96630	0.49393	0.94445
1.00	0.50	0.54755	1.06579	0.55381	0.97648	0.50332	0.96241
1.00	0.25	0.59034	1.03418	0.56014	0.98764	0.51300	0.98093
1.00	0.00	0.64219	1.00000	0.56715	1.00000	0.52298	1.00000
1.00	-0.25	0.70653	0.96266	0.57499	1.01383	0.53326	1.01965
1.00	-0.50	0.78891	0.92135	0.58389	1.02953	0.54387	1.03995
1.00	-0.75	0.89890	0.87484	0.59419	1.04768	0.55489	1.06102
1.00	-1.00	1.05478	0.82124	0.60640	1.06922	0.56643	1.08309
2.00	1.00	0.42375	1.11265	0.68350	0.95399	0.35684	0.88190
2.00	0.75	0.45173	1.08729	0.69057	0.96385	0.36860	0.91098
2.00	0.50	0.48457	1.06030	0.69832	0.97468	0.38051	0.94041
2.00	0.25	0.52371	1.03135	0.70690	0.98665	0.39252	0.97008
2.00	0.00	0.57126	1.00000	0.71647	1.00000	0.40462	1.00000
2.00	-0.25	0.63047	0.96568	0.72726	1.01506	0.41686	1.03023
2.00	-0.50	0.70655	0.92761	0.73961	1.03230	0.42928	1.06095
2.00	-0.75	0.80857	0.88463	0.75401	1.05240	0.44201	1.09240
2.00	-1.00	0.95380	0.83491	0.77126	1.07648	0.45521	1.12502
10.00	1.00	0.30496	1.09123	1.10907	0.94846	0.19707	0.79074
10.00	0.75	0.32648	1.07089	1.12161	0.95919	0.21101	0.84667
10.00	0.50	0.35183	1.04911	1.13566	0.97120	0.22422	0.89965
10.00	0.25	0.38216	1.02560	1.15145	0.98471	0.23690	0.95052
10.00	0.00	0.41920	1.00000	1.16933	1.00000	0.24923	1.00000
10.00	-0.25	0.46557	0.97180	1.18976	1.01747	0.26137	1.04874
10.00	-0.50	0.52558	0.94033	1.21343	1.03771	0.27351	1.09742
10.00	-0.75	0.60671	0.90458	1.24138	1.06162	0.28582	1.14683
10.00	-1.00	0.72347	0.86292	1.27532	1.09063	0.29858	1.19802
20.00	1.00	0.26155	1.08389	1.34498	0.94613	0.15875	0.76722
20.00	0.75	0.28043	1.06527	1.36083	0.95728	0.17181	0.83030
20.00	0.50	0.30268	1.04528	1.37866	0.96982	0.18402	0.88932
20.00	0.25	0.32935	1.02363	1.39876	0.98396	0.19566	0.94556
20.00	0.00	0.36196	1.00000	1.42155	1.00000	0.20692	1.00000
20.00	-0.25	0.40288	0.97392	1.44766	1.01836	0.21799	1.03350
20.00	-0.50	0.45595	0.94475	1.47798	1.03969	0.22904	1.10690
20.00	-0.75	0.52792	0.91156	1.51388	1.06495	0.24027	1.16117
20.00	-1.00	0.63186	0.87282	1.55761	1.09571	0.25194	1.21759
100.00	1.00	0.17979	1.07150	2.06337	0.94159	0.10052	0.73581
100.00	0.75	0.19326	1.05579	2.08988	0.95369	0.11031	0.80748
100.00	0.50	0.20917	1.03883	2.11968	0.96729	0.11957	0.87526
100.00	0.25	0.22827	1.02032	2.15324	0.98260	0.12800	0.93697
100.00	0.00	0.25169	1.00000	2.19137	1.00000	0.13661	1.00000
100.00	-0.25	0.28117	0.97749	2.23503	1.01992	0.14440	1.05702
100.00	-0.50	0.31958	0.95230	2.28594	1.04316	0.15305	1.12033
100.00	-0.75	0.37130	0.92202	2.34630	1.07070	0.16150	1.18219
100.00	-1.00	0.45590	0.90568	2.42210	1.10529	0.17040	1.24734

Note:

For this case

$\epsilon_f=\lambda_f=\zeta_f=0$

$$R1 = \frac{(1+0.5\gamma_f)F''(0)}{F''(0)|_{\gamma_f=0}}$$

$$R2 = \frac{-\theta'(0)}{-\theta'(0)|_{\gamma_f=0}}$$

$$R3 = \frac{F(\infty)}{F(\infty)|_{\gamma_f=0}}$$

The analysis is similar to Carey and Mollendorf (1978), except that the values of γ_f are different and Prandtl numbers 2 and 20 are also included. For liquids, a positive value of γ_f corresponds to a cooled wall and a negative value, a heated wall. For a cooled wall, the liquid near the wall is more viscous than the liquid away from it. Hence a positive value of γ_f increases the shear stress and decreases the surface heat transfer and the total mass flow rate. The thickness of velocity boundary layer is smaller for a positive value of γ_f and that of thermal boundary layer is slightly larger. The maximum velocity is also slightly lower and it occurs farther away from the wall. The effect of γ_f is more pronounced on the velocity profiles than on the temperature profiles. The opposite remarks are true for a negative value of γ_f.

From Table 2.3, the effect of γ_f on the local Nusselt number can be written as,

$$\frac{Nu_x}{Nu_x|_{\gamma_f=0}} \cong (1+0.25\gamma_f)^{-0.28} \tag{2.59}$$

The above relation is accurate within ±2% for the range of the parameter γ_f and Prandtl numbers investigated. (Carey and Mollendorf (1978) did not give a correlation for the local Nusselt number to include the effect of γ_f).

2.2.3 The Effects of Variation of Thermal Conductivity with Temperature

The effects of variation of thermal conductivity with temperature on the laminar natural convective flow are given in terms of the dimensionless parameter λ_f. The larger the absolute value of λ_f, the more pronounced are the effects of temperature-dependent thermal conductivity on the natural convective flow. The case $\lambda_f=0$ corresponds to Boussinesq approximations. Figs. 2.6(a) to (f) show the effects of λ_f on the temperature and the velocity profiles for Prandtl numbers 1, 10, and 100. Table 2.4 compares its effects on the surface shear stress, the surface heat transfer, and the total mass flow rate for various Prandtl numbers. The parameters ϵ_f, γ_f and ζ_f were taken to be equal to zero for this case.

When the thermal conductivity of the liquid increases with temperature, a positive value of λ_f corresponds to a heated wall and a negative value, a cooled wall. For a positive value of λ_f, the thermal conductivity of the liquid near the wall is higher than it is away from the wall. Hence, a positive value of λ_f increases the surface heat transfer and reduces the thickness of the thermal boundary layer slightly. Also, a positive value increases the maximum velocity and the surface shear stress slightly. The opposite remarks are true for a negative value of λ_f. For moderate and large Prandtl numbers, λ_f has little effect on the total mass flow rate due to the small thermal boundary layer thickness (see Table 2.4).

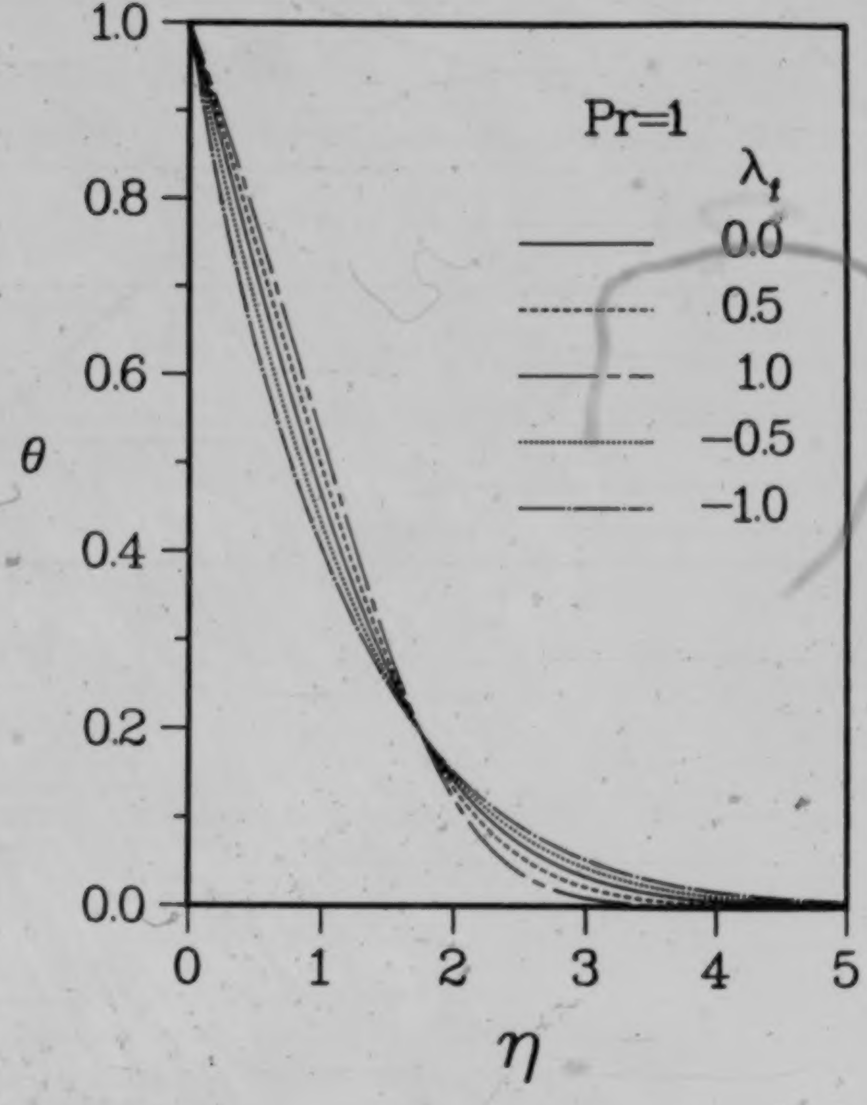

Fig. 2.6(a) The effects of λ_f on temperature profile for Pr=1

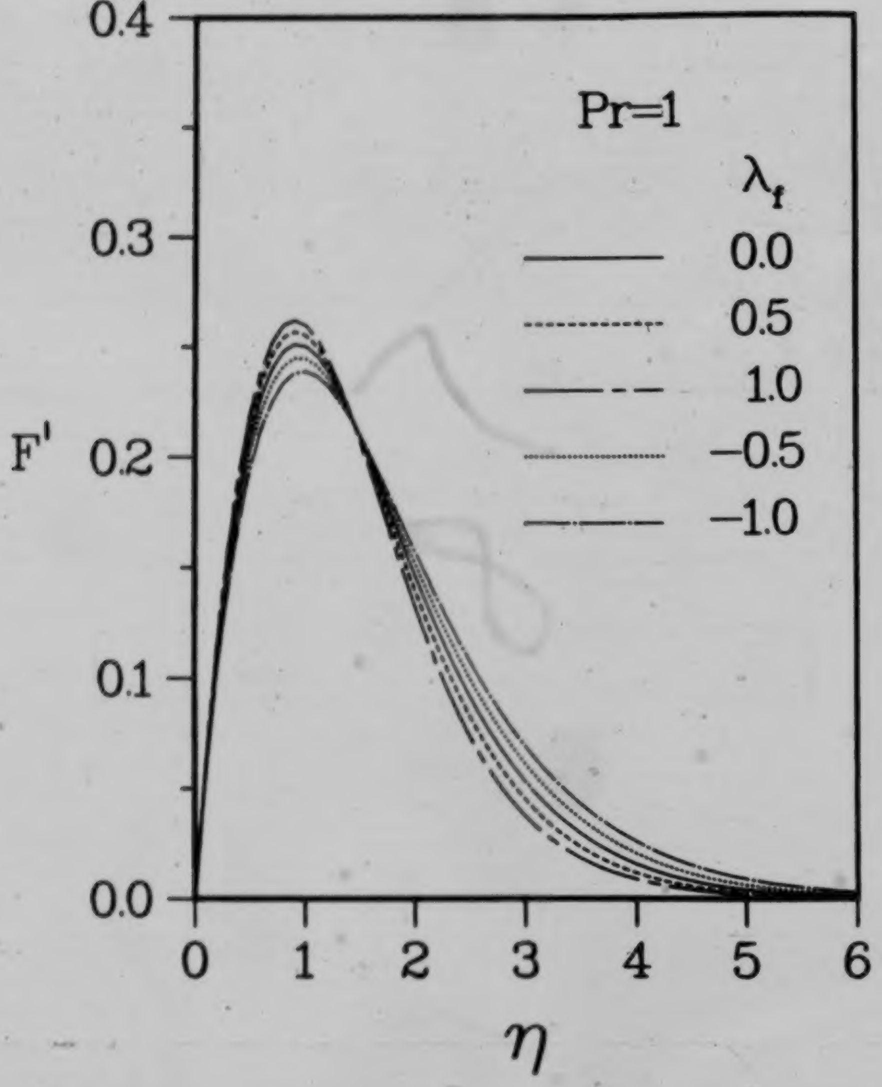

Fig. 2.6(b) The effects of λ_f on velocity profile for Pr=1

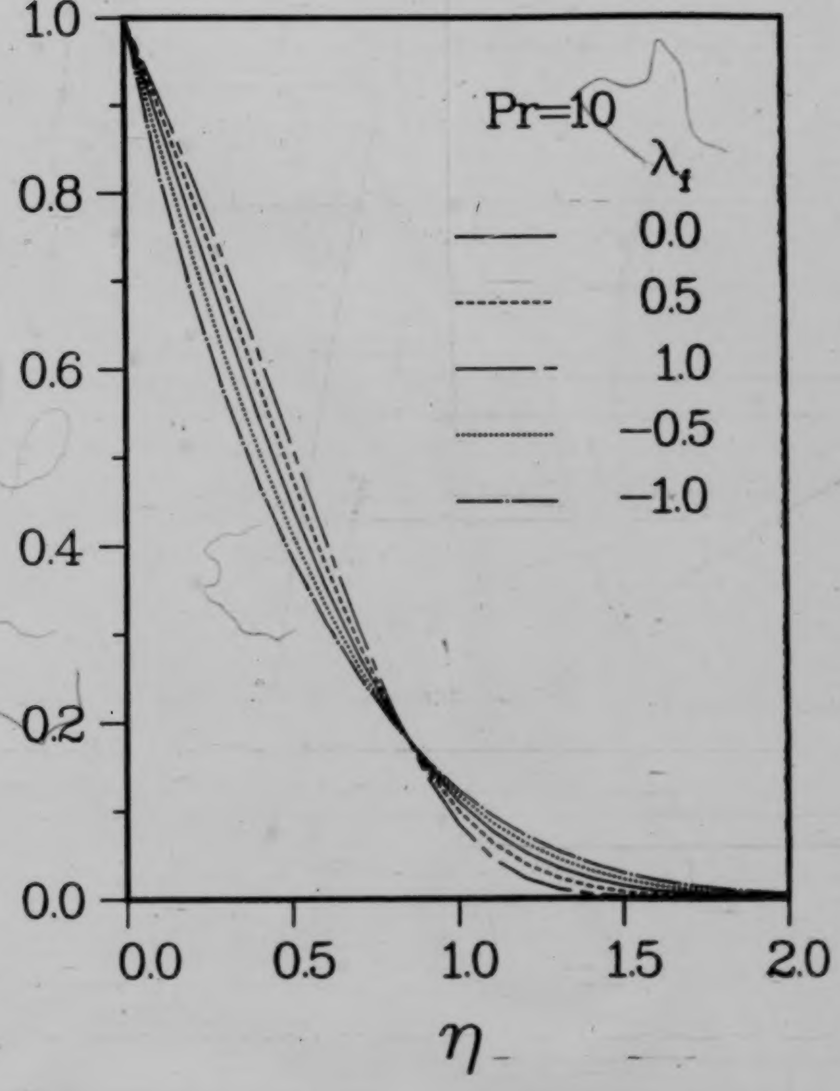

Fig. 2.6(c) The effects of λ_f on temperature profile for Pr=10

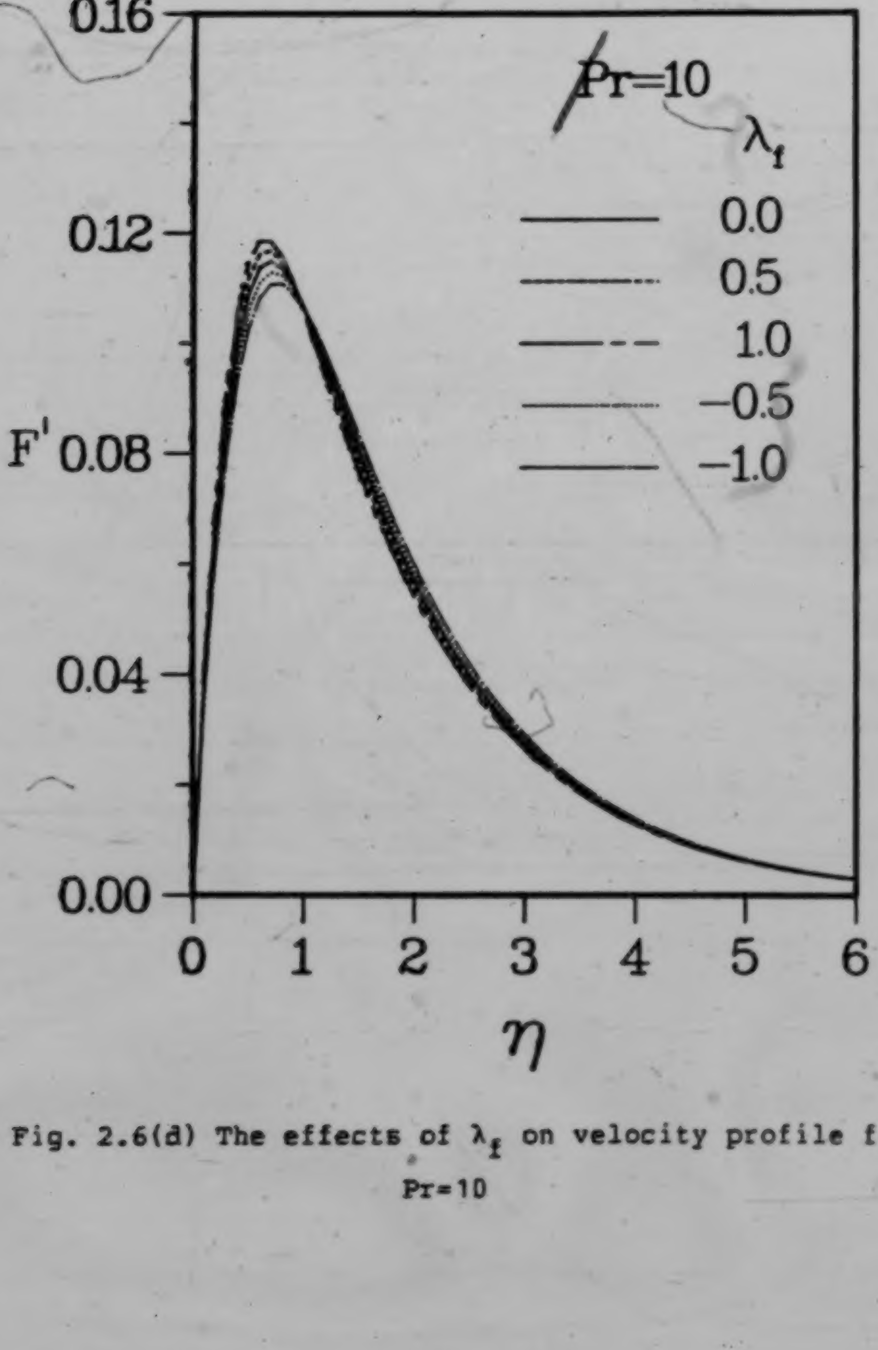

Fig. 2.6(d) The effects of λ_f on velocity profile for Pr=10

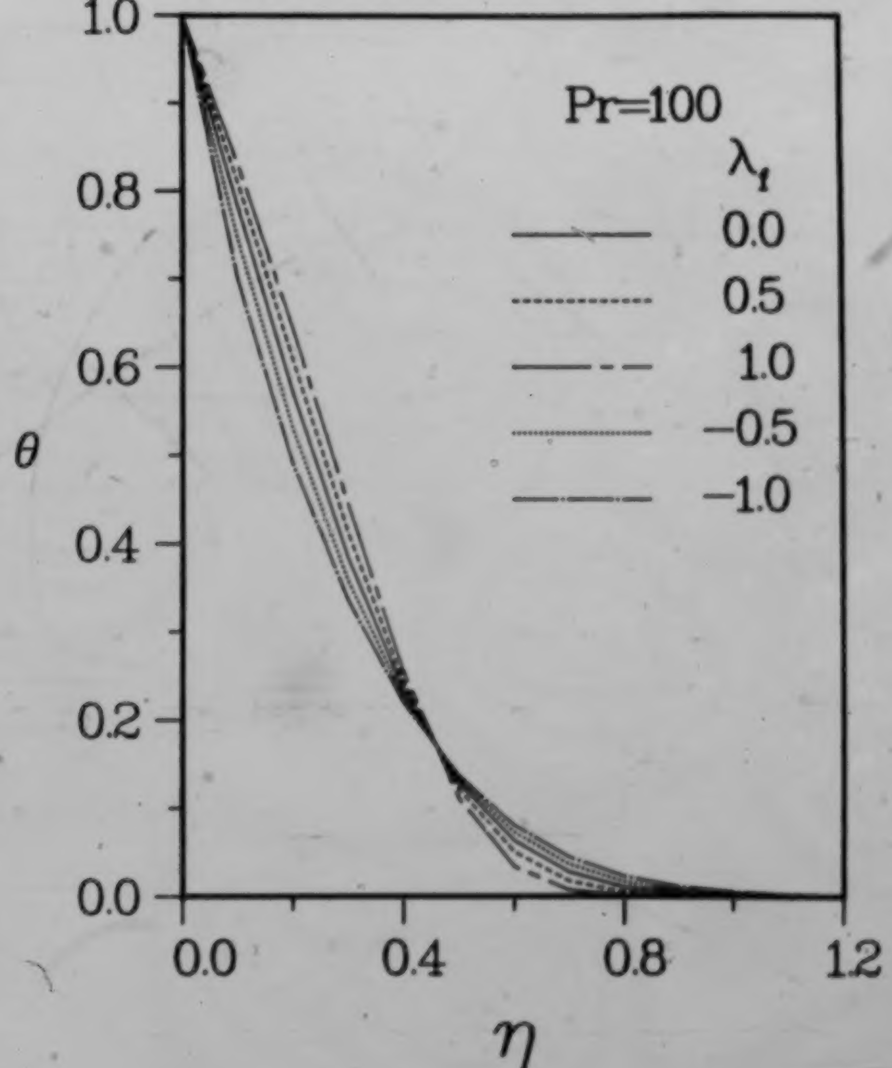

Fig. 2.6(e) The effects of λ_f on temperature profile for Pr=100

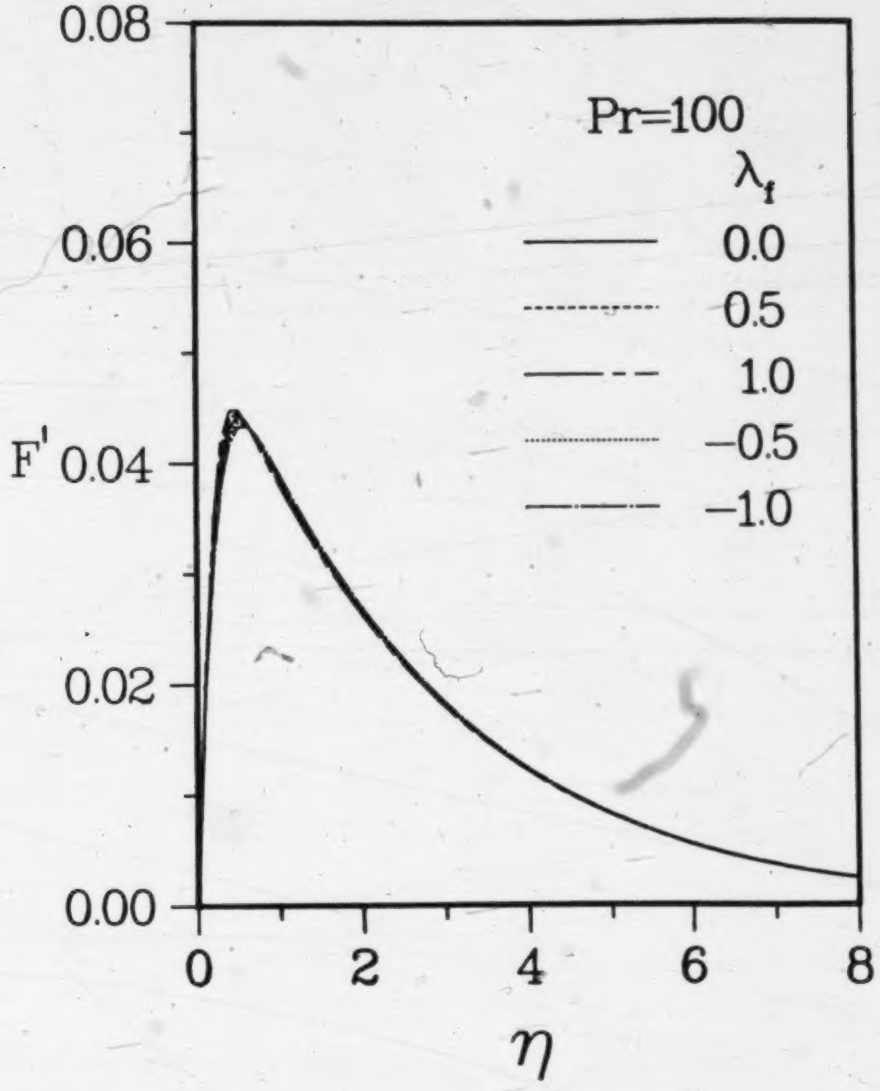

Fig. 2.6(f) The effects of λ_f on velocity profile for Pr=100

Table 2.4 The effects of λ_f for various Prandtl numbers

Pr	λ_f	$F''(0)$	R1	$-\theta'(0)$	R2	$F(\infty)$	R3
1.00	1.00	0.66921	1.04208	0.41581	1.09974	0.49533	0.94713
1.00	0.75	0.66333	1.03292	0.44382	1.07601	0.50175	0.95940
1.00	0.50	0.65691	1.02292	0.47706	1.05145	0.50856	0.97242
1.00	0.25	0.64989	1.01199	0.51729	1.02611	0.51566	0.98601
1.00	0.00	0.64219	1.00000	0.56715	1.00000	0.52298	1.00000
1.00	-0.25	0.63373	0.98683	0.63077	0.97316	0.53044	1.01426
1.00	-0.50	0.62440	0.97230	0.71508	0.94563	0.53797	1.02867
1.00	-0.75	0.61407	0.95621	0.83252	0.91745	0.54553	1.04312
1.00	-1.00	0.60258	0.93832	1.00803	0.88868	0.55307	1.05753
2.00	1.00	0.59716	1.04534	0.52506	1.09928	0.39136	0.96722
2.00	0.75	0.59144	1.03531	0.56045	1.07559	0.39439	0.97471
2.00	0.50	0.58525	1.02448	0.60247	1.05112	0.39763	0.98272
2.00	0.25	0.57854	1.01274	0.65336	1.02591	0.40105	0.99118
2.00	0.00	0.57126	1.00000	0.71647	1.00000	0.40462	1.00000
2.00	-0.25	0.56333	0.98612	0.79706	0.97343	0.40831	1.00912
2.00	-0.50	0.55467	0.97096	0.90394	0.94624	0.41210	1.01848
2.00	-0.75	0.54517	0.95433	1.05291	0.91850	0.41595	1.02800
2.00	-1.00	0.53471	0.93602	1.27569	0.89027	0.41985	1.03764
10.00	1.00	0.44006	1.04976	0.85489	1.09663	0.24667	0.98972
10.00	0.75	0.43537	1.03858	0.91294	1.07351	0.24728	0.99218
10.00	0.50	0.43035	1.02661	0.98192	1.04966	0.24791	0.99472
10.00	0.25	0.42497	1.01378	1.06554	1.02514	0.24856	0.99734
10.00	0.00	0.41920	1.00000	1.16933	1.00000	0.24923	1.00000
10.00	-0.25	0.41298	0.98518	1.30202	0.97429	0.24990	1.00270
10.00	-0.50	0.40628	0.96919	1.47814	0.94807	0.25058	1.00541
10.00	-0.75	0.39903	0.95188	1.72386	0.92139	0.25125	1.00813
10.00	-1.00	0.39115	0.93310	2.09169	0.89440	0.25193	1.01085
20.00	1.00	0.38022	1.05044	1.03836	1.09565	0.20546	0.99294
20.00	0.75	0.37610	1.03907	1.10907	1.07275	0.20583	0.99475
20.00	0.50	0.37171	1.02692	1.19312	1.04913	0.20619	0.99649
20.00	0.25	0.36700	1.01392	1.29502	1.02487	0.20656	0.99824
20.00	0.00	0.36196	1.00000	1.42155	1.00000	0.20692	1.00000
20.00	-0.25	0.35655	0.98505	1.58334	0.97458	0.20728	1.00175
20.00	-0.50	0.35073	0.96897	1.79812	0.94867	0.20764	1.00347
20.00	-0.75	0.34445	0.95161	2.09787	0.92235	0.20799	1.00516
20.00	-1.00	0.33765	0.93283	2.54678	0.89577	0.20833	1.00682
100.00	1.00	0.26448	1.05081	1.59835	1.09408	0.13610	0.99626
100.00	0.75	0.26159	1.03932	1.70772	1.07153	0.13623	0.99721
100.00	0.50	0.25851	1.02707	1.83776	1.04829	0.13636	0.99816
100.00	0.25	0.25521	1.01398	1.99548	1.02443	0.13650	0.99919
100.00	0.00	0.25169	1.00000	2.19137	1.00000	0.13661	1.00000
100.00	-0.25	0.24792	0.98503	2.44193	0.97505	0.13673	1.00087
100.00	-0.50	0.24388	0.96896	2.77467	0.94964	0.13685	1.00175
100.00	-0.75	0.23953	0.95169	3.23930	0.92389	0.13695	1.00248
100.00	-1.00	0.23486	0.93310	3.93653	0.89819	0.13705	1.00321

Note:

For this case

$\epsilon_f=\gamma_f=\zeta_f=0$

$$R1 = \frac{F''(0)}{F''(0)|_{\lambda_f=0}}$$

$$R2 = \frac{-(1+0.5\lambda_f)\theta'(0)}{-\theta'(0)|_{\lambda_f=0}}$$

$$R3 = \frac{F(\infty)}{F(\infty)|_{\lambda_f=0}}$$

From Table 2.4, the effect of λ_f on the local Nusselt number can be written as,

$$\frac{Nu_x}{Nu_x|_{\lambda_f=0}} \cong (1+0.105\lambda_f) \tag{2.60}$$

The above relation is accurate within ±1% for the range of the parameter λ_f and the Prandtl numbers investigated. For most liquids, the thermal conductivity is not a strong function of temperature and hence, the effect of λ_f can be normally neglected.

2.2.4 The Effects of Variation of Specific Heat with Temperature

The effects of variation of specific heat with temperature on the laminar natural convective flow are given in terms of the dimensionless parameter ζ_f. The larger the absolute value of ζ_f, the more pronounced are the effects of temperature-dependent specific heat on the natural convective flow. The case $\zeta_f=0$ corresponds to Boussinesq approximations. Figs. 2.7(a) to (f) show the effects of ζ_f on temperature and velocity profiles for Prandtl numbers 1, 10, and 100. Table 2.5 compares its effects on the surface shear stress, the surface heat transfer, and the total mass flow rate for various values of Prandtl numbers. The parameters ϵ_f, γ_f and λ_f were taken to be equal to zero for this case.

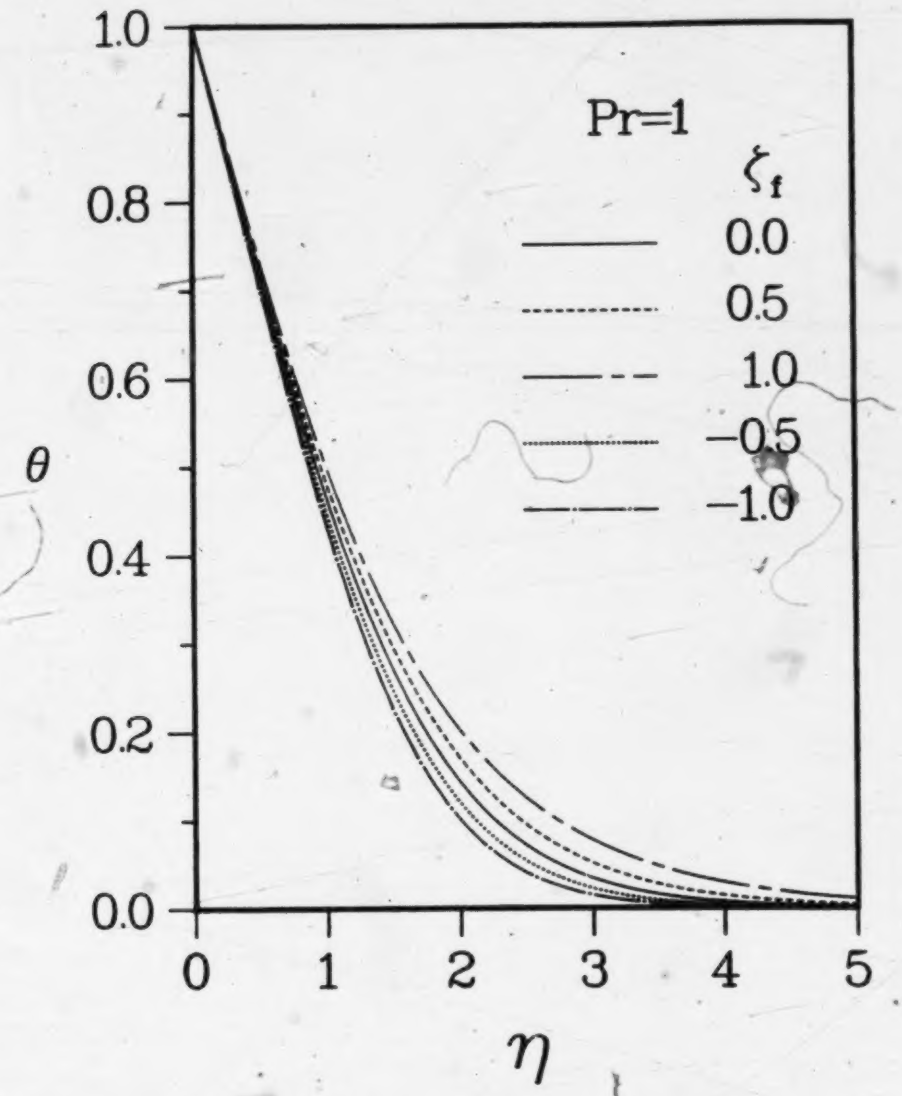

Fig. 2.7(a) The effects of ζ_f on temperature profile for Pr=1

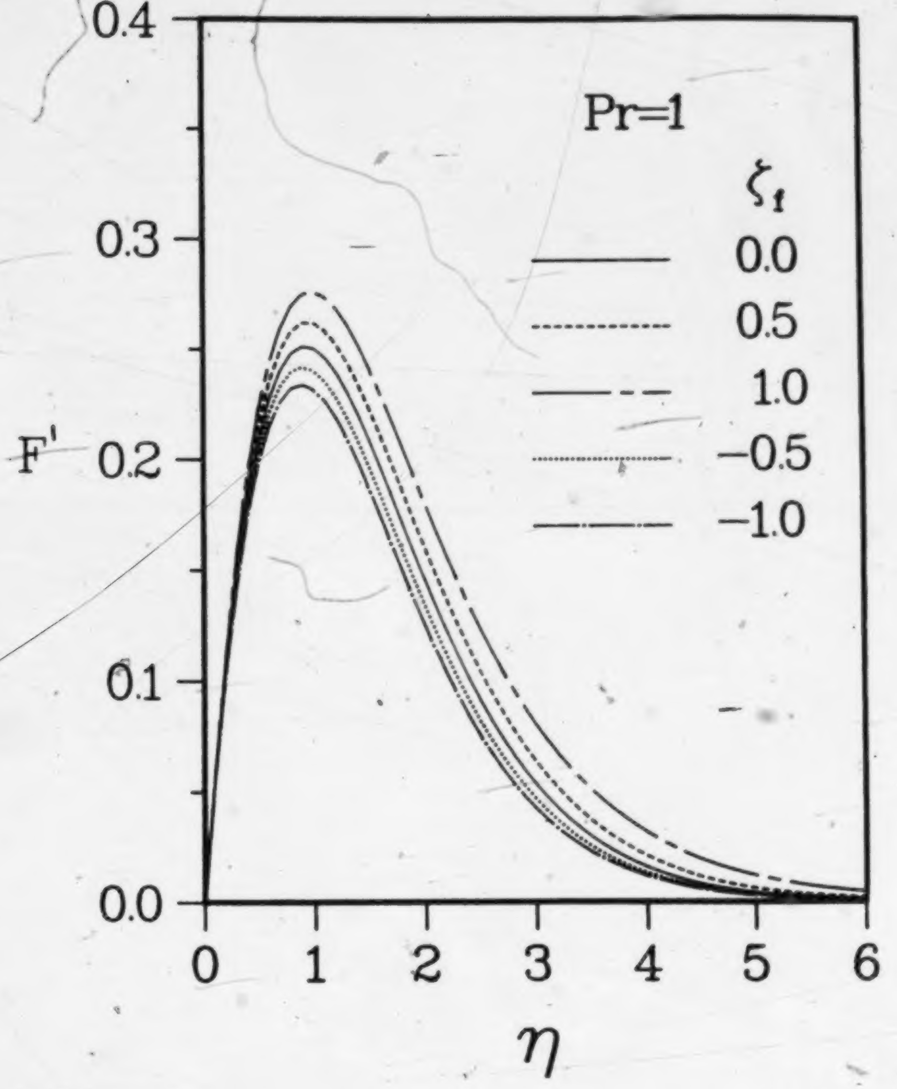

Fig. 2.7(b) The effects of ζ_f on velocity profile for Pr=1

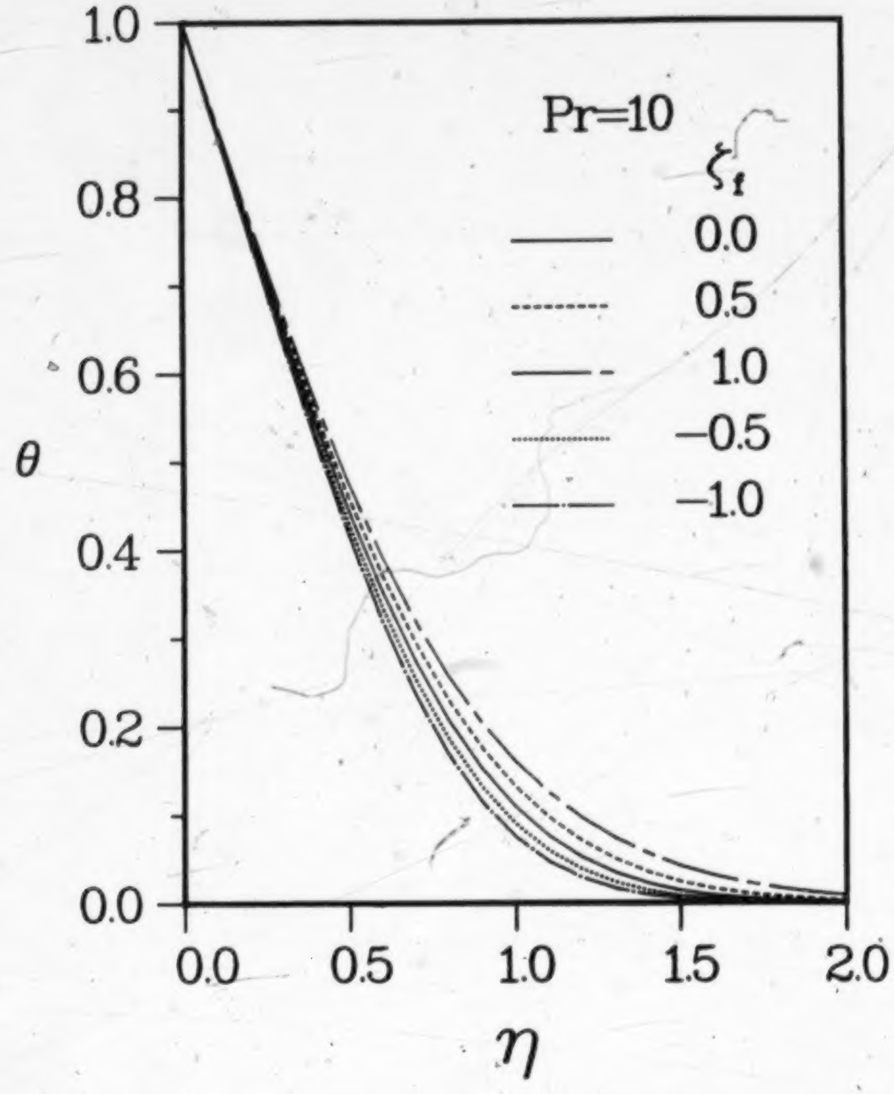

Fig. 2.7(c) The effects of ζ_f on temperature profile for Pr=10

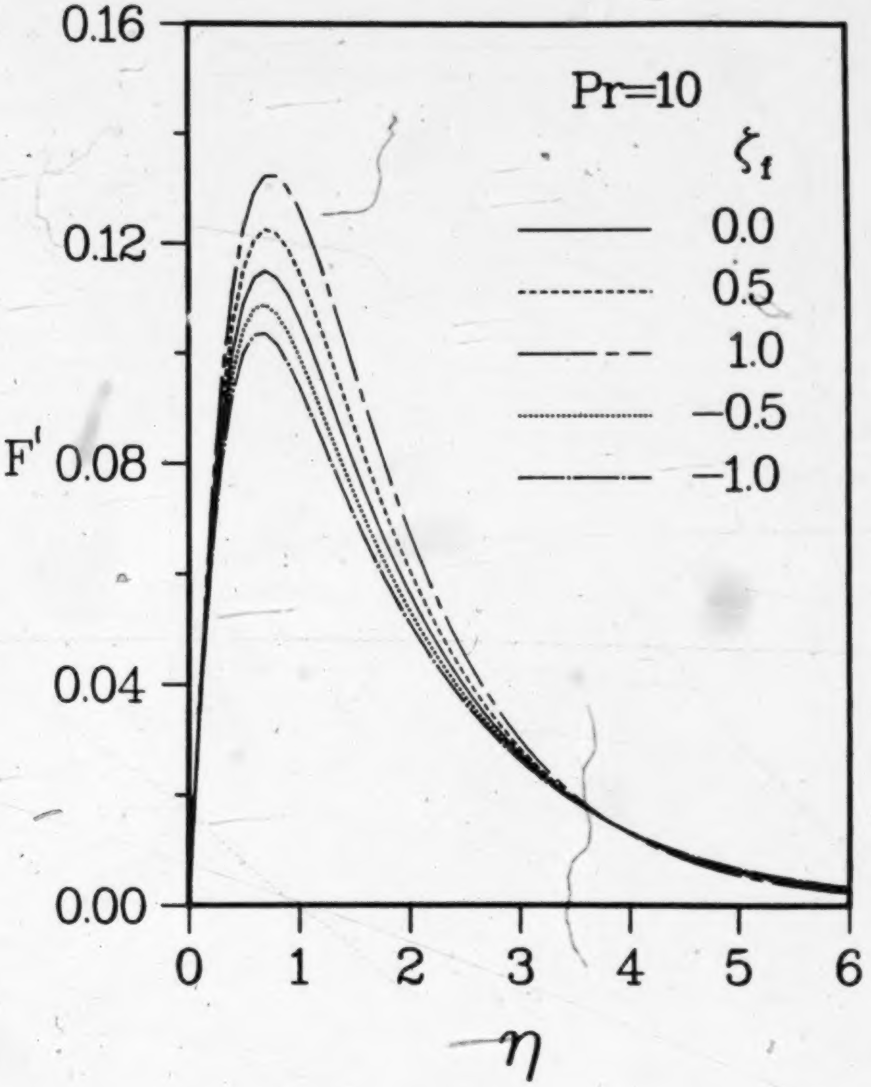

Fig. 2.7(d) The effects of ζ_f on velocity profile for Pr=10

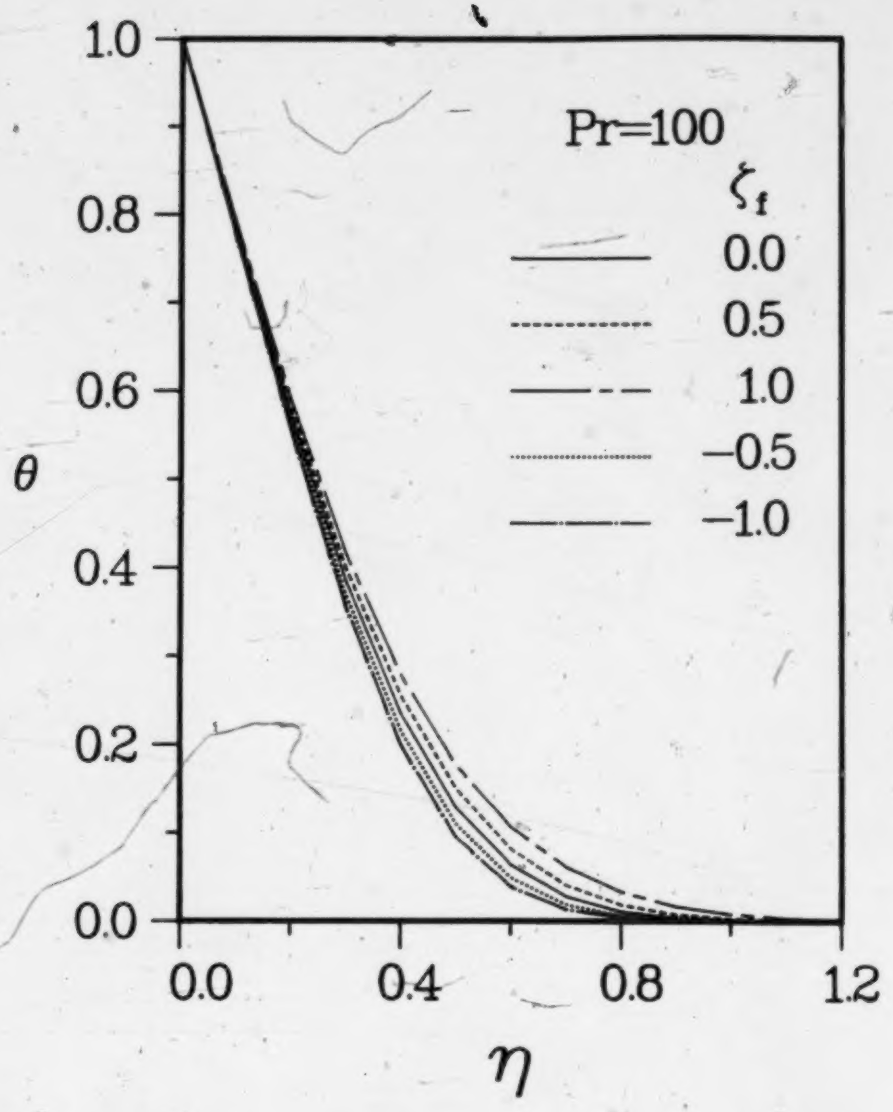

Fig. 2.7(e) The effects of ζ_f on temperature profile for Pr=100

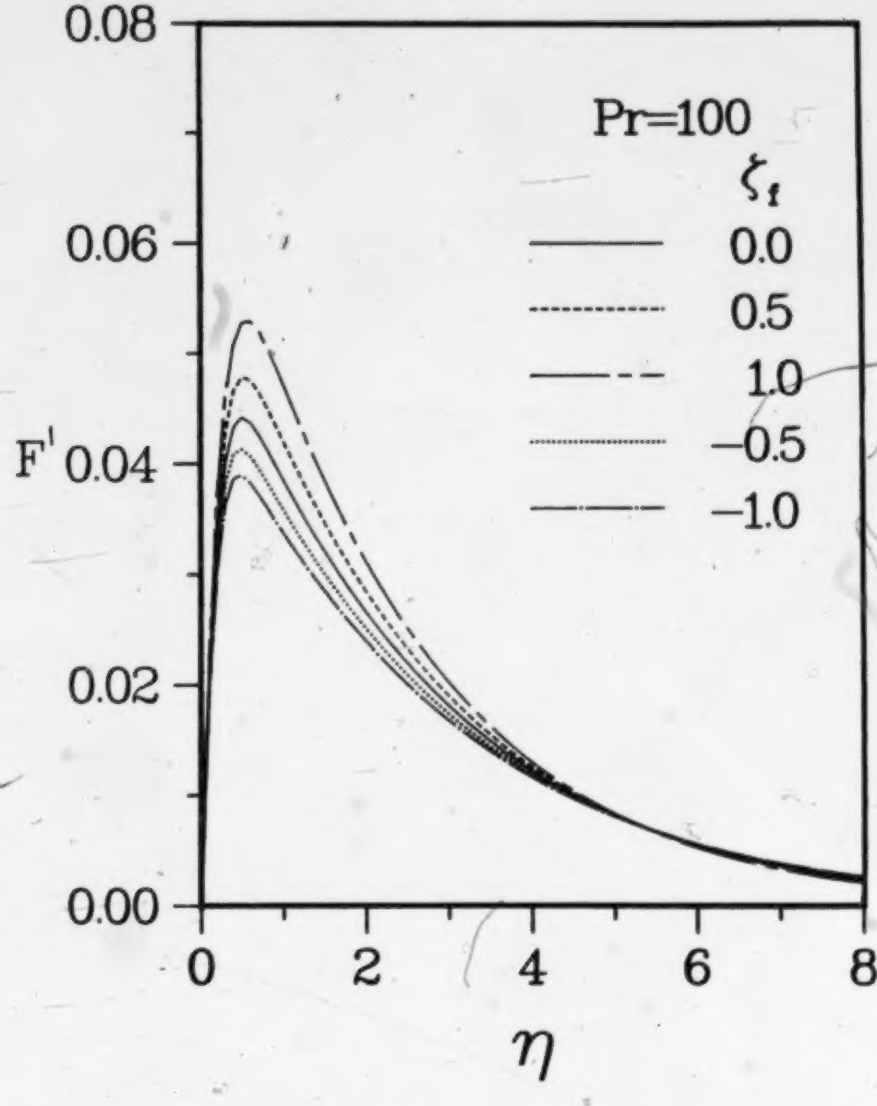

Fig. 2.7(f) The effects of ζ_f on velocity profile for Pr=100

Table 2.5 The effects of ζ_f for various Prandtl numbers

Pr	ζ_f	$F''(0)$	R1	$-\theta'(0)$	R2	$F(\infty)$	R3
1.00	1.00	0.67132	1.04537	0.53843	0.94936	0.64210	1.22776
1.00	0.75	0.66314	1.03263	0.54568	0.96215	0.60077	1.14875
1.00	0.50	0.65564	1.02094	0.55291	0.97491	0.56913	1.08824
1.00	0.25	0.64868	1.01010	0.56008	0.98754	0.54384	1.03988
1.00	0.00	0.64219	1.00000	0.56715	1.00000	0.52298	1.00000
1.00	-0.25	0.63610	0.99052	0.57410	1.01227	0.50537	0.96633
1.00	-0.50	0.63037	0.98160	0.58094	1.02432	0.49023	0.93737
1.00	-0.75	0.62496	0.97317	0.58765	1.03616	0.47701	0.91209
1.00	-1.00	0.61982	0.96517	0.59424	1.04777	0.46532	0.88975
2.00	1.00	0.60188	1.05359	0.68116	0.95072	0.48161	1.19028
2.00	0.75	0.59312	1.03826	0.69017	0.96330	0.45492	1.12431
2.00	0.50	0.58520	1.02439	0.69909	0.97575	0.43452	1.07388
2.00	0.25	0.57795	1.01170	0.70786	0.98799	0.41817	1.03348
2.00	0.00	0.57126	1.00000	0.71647	1.00000	0.40462	1.00000
2.00	-0.25	0.56505	0.98912	0.72489	1.01175	0.39311	0.97155
2.00	-0.50	0.55925	0.97896	0.73312	1.02325	0.38314	0.94691
2.00	-0.75	0.55380	0.96942	0.74117	1.03448	0.37436	0.92522
2.00	-1.00	0.54866	0.96043	0.74904	1.04546	0.36655	0.90590
10.00	1.00	0.44822	1.06923	1.11863	0.95664	0.28290	1.13511
10.00	0.75	0.43969	1.04889	1.13161	0.96774	0.27184	1.09075
10.00	0.50	0.43215	1.03089	1.14443	0.97870	0.26297	1.05516
10.00	0.25	0.42536	1.01471	1.15701	0.98946	0.25557	1.02546
10.00	0.00	0.41920	1.00000	1.16933	1.00000	0.24923	1.00000
10.00	-0.25	0.41354	0.98650	1.18138	1.01030	0.24368	0.97774
10.00	-0.50	0.40831	0.97403	1.19315	1.02036	0.23876	0.95798
10.00	-0.75	0.40345	0.96243	1.20464	1.03019	0.23433	0.94024
10.00	-1.00	0.39890	0.95159	1.21587	1.03980	0.23032	0.92414
20.00	1.00	0.38902	1.07476	1.36328	0.95901	0.23317	1.12688
20.00	0.75	0.38100	1.05261	1.37810	0.96943	0.22468	1.08584
20.00	0.50	0.37396	1.03314	1.39282	0.97978	0.21777	1.05245
20.00	0.25	0.36766	1.01574	1.40732	0.98998	0.21195	1.02431
20.00	0.00	0.36196	1.00000	1.42155	1.00000	0.20692	1.00000
20.00	-0.25	0.35675	0.98561	1.43550	1.00981	0.20250	0.97863
20.00	-0.50	0.35196	0.97237	1.44914	1.01941	0.19855	0.95957
20.00	-0.75	0.34751	0.96009	1.46249	1.02880	0.19500	0.94238
20.00	-1.00	0.34337	0.94865	1.47554	1.03798	0.19176	0.92675
100.00	1.00	0.27289	1.08424	2.11026	0.96299	0.15299	1.11989
100.00	0.75	0.26652	1.05890	2.13050	0.97222	0.14777	1.08168
100.00	0.50	0.26099	1.03692	2.15092	0.98154	0.14346	1.05013
100.00	0.25	0.25609	1.01746	2.17126	0.99082	0.13982	1.02349
100.00	0.00	0.25169	1.00000	2.19137	1.00000	0.13661	1.00000
100.00	-0.25	0.24770	0.98416	2.21118	1.00904	0.13380	0.97942
100.00	-0.50	0.24406	0.96966	2.23065	1.01793	0.13128	0.96098
100.00	-0.75	0.24069	0.95630	2.24976	1.02665	0.12900	0.94429
100.00	-1.00	0.23757	0.94390	2.26850	1.03520	0.12692	0.92806

Note:

For this case

$\epsilon_f=\gamma_f=\lambda_f=0$

$$R1 = \frac{F''(0)}{F''(0)|_{\zeta_f=0}}$$

$$R2 = \frac{-\theta'(0)}{-\theta'(0)|_{\zeta_f=0}}$$

$$R3 = \frac{F(\infty)}{F(\infty)|_{\zeta_f=0}}$$

When the specific heat of the liquid increases with temperature, a positive value of ζ_f corresponds to a heated wall and a negative value, a cooled wall. For a positive value of ζ_f, the specific heat of the liquid near the wall is higher than it is away from the wall. The liquid near the wall having a larger heat capacity aides in conducting heat farther away from the wall. Hence a positive value of ζ_f increases the thicknesses of thermal and velocity boundary layers and the maximum velocity slightly. Also, a positive value of ζ_f increases the surface shear stress and the total mass flow rate, and decreases the surface heat transfer. The opposite remarks are true for a negative value of λ_f.

From Table 2.5, the effect of λ_f on the local Nusselt number can be written as,

$$\frac{Nu_x}{Nu_x|_{\zeta_f=0}} \cong (1-0.045\zeta_f) \qquad (2.61)$$

The above relation is accurate within ±1% for the range of the parameter ζ_f and the Prandtl numbers investigated. For most liquids, as the specific heat is not a strong function of temperature, its effect can be normally neglected.

2.2.5 The Effects of Variable Properties for Liquids with Very Large Prandtl Numbers

Table 2.6 shows the effects of variable properties on the surface heat transfer, the surface shear stress, and the total mass flow rate for $Pr \rightarrow \infty$. Only zeroth order solutions

Table 2.6 The effects of variable properties for Pr → ∞

	$g''(0)$	R1	$-h'(0)$	R2	$G(\infty)$	R3
ε_f			$\gamma_f=\lambda_f=\zeta_f=0$			
1.00	0.60268	0.73095	0.59342	0.83465	0.32520	0.75769
0.75	0.65931	0.79963	0.62977	0.88576	0.36036	0.83961
0.50	0.71530	0.86754	0.66040	0.92885	0.38751	0.90287
0.25	0.77039	0.93436	0.68713	0.96645	0.40993	0.95512
0.0	0.82452	1.00000	0.71099	1.00000	0.42919	1.00000
-0.25	0.87769	1.06449	0.73261	1.03042	0.44617	1.03955
-0.50	0.92996	1.12788	0.75245	1.05832	0.46141	1.07505
-0.75	0.98136	1.19023	0.77081	1.08414	0.47527	1.10736
-1.00	1.03196	1.25160	0.78794	1.10823	0.48819	1.13746
γ_f			$\varepsilon_f=\lambda_f=\zeta_f=0$			
1.00	0.87235	1.05802	0.66552	0.93605	0.30463	0.70976
0.75	0.86209	1.04556	0.67504	0.94944	0.33889	0.78959
0.50	0.85077	1.03184	0.68564	0.96434	0.37047	0.86319
0.25	0.83830	1.01672	0.69753	0.98107	0.40035	0.93279
0.0	0.82452	1.00000	0.71099	1.00000	0.42919	1.00000
-0.25	0.80917	0.98139	0.72643	1.02171	0.45759	1.06617
-0.50	0.79193	0.96048	0.74442	1.04702	0.48611	1.13261
-0.75	0.77227	0.93663	0.76588	1.07720	0.51540	1.20085
-1.00	0.74935	0.90884	0.79228	1.11433	0.54634	1.27295
λ_f			$\varepsilon_f=\gamma_f=\zeta_f=0$			
1.00	0.86610	1.05043	0.77676	1.09250	0.42815	0.99756
0.75	0.85668	1.03901	0.76099	1.07032	0.42844	0.99823
0.50	0.84664	1.02684	0.74474	1.04747	0.42871	0.99887
0.25	0.83594	1.01385	0.72806	1.02401	0.42896	0.99946
0.0	0.82452	1.00000	0.71099	1.00000	0.42919	1.00000
-0.25	0.81231	0.98519	0.69356	0.97549	0.42940	1.00049
-0.50	0.79923	0.96933	0.67583	0.95054	0.42959	1.00091
-0.75	0.78519	0.95231	0.65783	0.92523	0.42974	1.00127
-1.00	0.77009	0.93399	0.63963	0.89963	0.42987	1.00156
ζ_f			$\varepsilon_f=\gamma_f=\lambda_f=0$			
1.00	0.90239	1.09445	0.68760	0.96710	0.47954	1.11730
0.75	0.87859	1.06558	0.69325	0.97505	0.46355	1.08004
0.50	0.85821	1.04086	0.69911	0.98329	0.45031	1.04921
0.25	0.84038	1.01924	0.70505	0.99164	0.43903	1.02291
0.0	0.82452	1.00000	0.71099	1.00000	0.42919	1.00000
-0.25	0.81023	0.98268	0.71689	1.00830	0.42049	0.97972
-0.50	0.79725	0.96692	0.72273	1.01651	0.41269	0.96153
-0.75	0.78534	0.95248	0.72849	1.02461	0.40562	0.94507
-1.00	0.77435	0.93916	0.73416	1.03258	0.39916	0.93003

Note:

$$R1 = \frac{(1+0.5\gamma_f)g''(0)}{g''(0)|_{B.A.}}$$

For this case

$$R2 = \frac{-(1+0.5\lambda_f)h'(0)}{-h'(0)|_{B.A.}}$$

$$R3 = \frac{G(\infty)}{G(\infty)|_{B.A.}}$$

were obtained. Higher order solutions, if necessary, can be obtained in a similar manner. The effects of the dimensionless parameters, ϵ_f, γ_f, λ_f and ζ_f on the natural convective flow are the same as discussed in the previous paragraphs. It can be seen that, contrary to the conclusions arrived by Piau (1974), the effects of ϵ_f as well as γ_f, λ_f and ζ_f on the surface heat transfer, the surface shear stress and the total mass flow rate are important for liquids with very large Prandtl numbers. For example, when $\epsilon_f=1.0$, and $\gamma_f=\lambda_f=\zeta_f=0.0$, for $Pr \to \infty$,

$$\frac{Nu_x}{Nu_x|_{\epsilon_f=0}} = 0.83465$$

When $\lambda_f=1.0$, and $\epsilon_f=\gamma_f=\zeta_f=0.0$, for $Pr \to \infty$,

$$\frac{Nu_x}{Nu_x|_{\lambda_f=0}} = 1.09250$$

2.2.6 The Effects of Variations of Both the Coefficient of Thermal Expansion and the Viscosity with Temperature

For most liquids, especially for water and aqueous solutions, both the coefficient of thermal expansion and the viscosity are strong functions of temperature (see Figs. 2.2(a) and (b)). Hence, it is important to study their effects together. For most liquids, and for water when both t_0 and t_∞ are larger than t_m (the temperature corresponding to the density maximum), ϵ_f is positive and γ_f is negative for a heated wall, and ϵ_f is negative and γ_f is positive for a cooled wall. For water, when both t_0 and t_∞ are lower than t_m, both ϵ_f and γ_f are negative for a heated wall and positive for a cooled wall.

Figs. 2.8(a) to (d) show the effects of both ϵ_f and γ_f, for typical combinations, on temperature and velocity profiles for a Prandtl number of 10. Table 2.7 compares their effects on the surface shear stress, the surface heat transfer, and the total mass flow rate. The parameters λ_f and ζ_f were taken to be equal to zero for this case. When the signs of ϵ_f and γ_f are different, their effects oppose each other. When the signs are the same, their effects add to each other.

From Table 2.7, the effects of ϵ_f and γ_f on the local Nusselt number can be written as,

$$\frac{Nu_x}{Nu_x|_{\epsilon_f=\gamma_f=0}} \cong \frac{(1.0-0.5\epsilon_f)^{0.24}}{(1+0.25\gamma_f)^{0.28}} \tag{2.62}$$

The above relation is accurate within ±1.5% for the range of the parameters ϵ_f and γ_f investigated. As explained before, that ϵ_f and γ_f have opposite signs normally. Under these conditions, it is seen from eq. (2.62) that their effects on the surface heat transfer oppose each other. Hence, the Boussinesq approximations may give fairly accurate results even for larger temperature differences between the wall and the ambient medium than the one below which these approximations have been shown to be valid by Gray and Giorgini (1976).

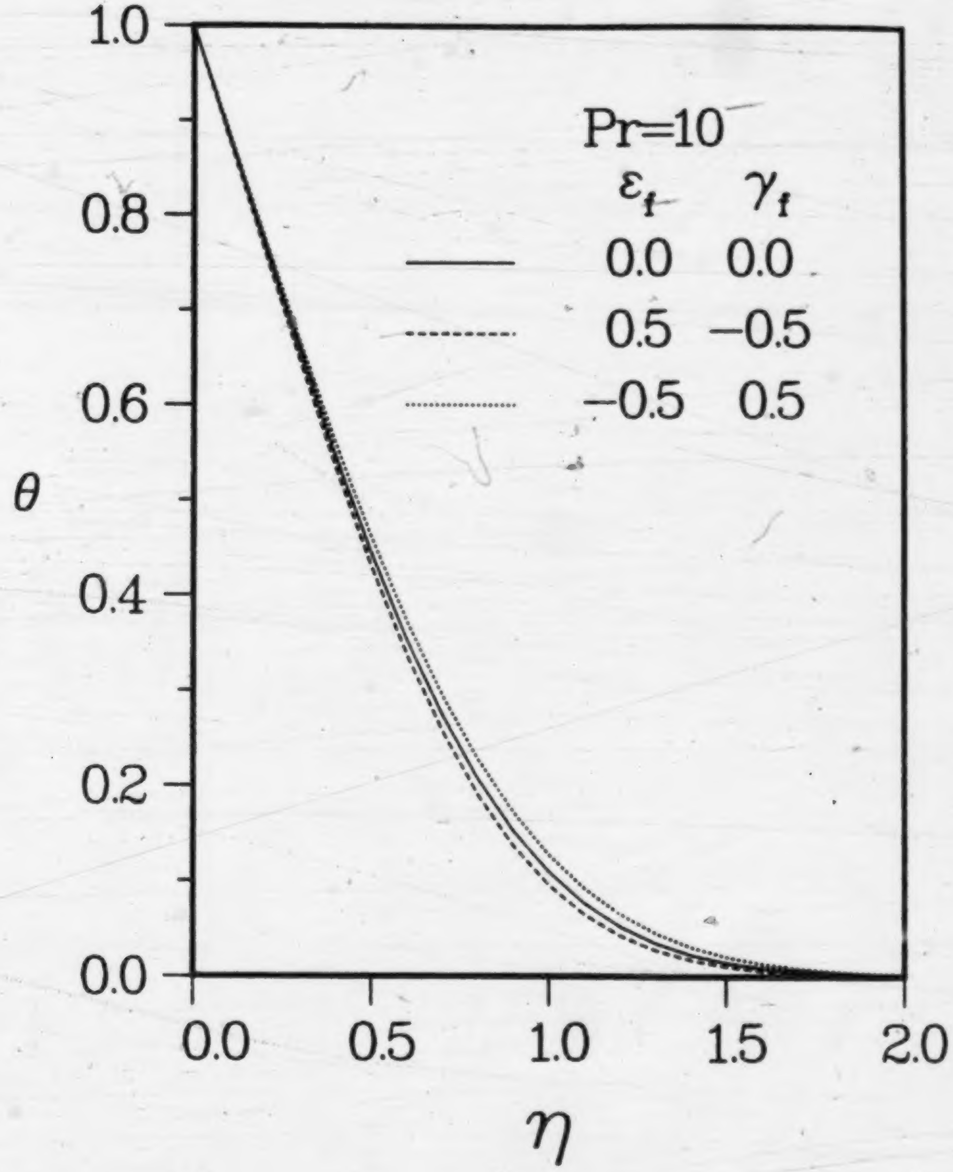

Fig. 2.8(a) Typical temperature profiles for Pr=10 with opposing effects of ϵ_f and γ_f

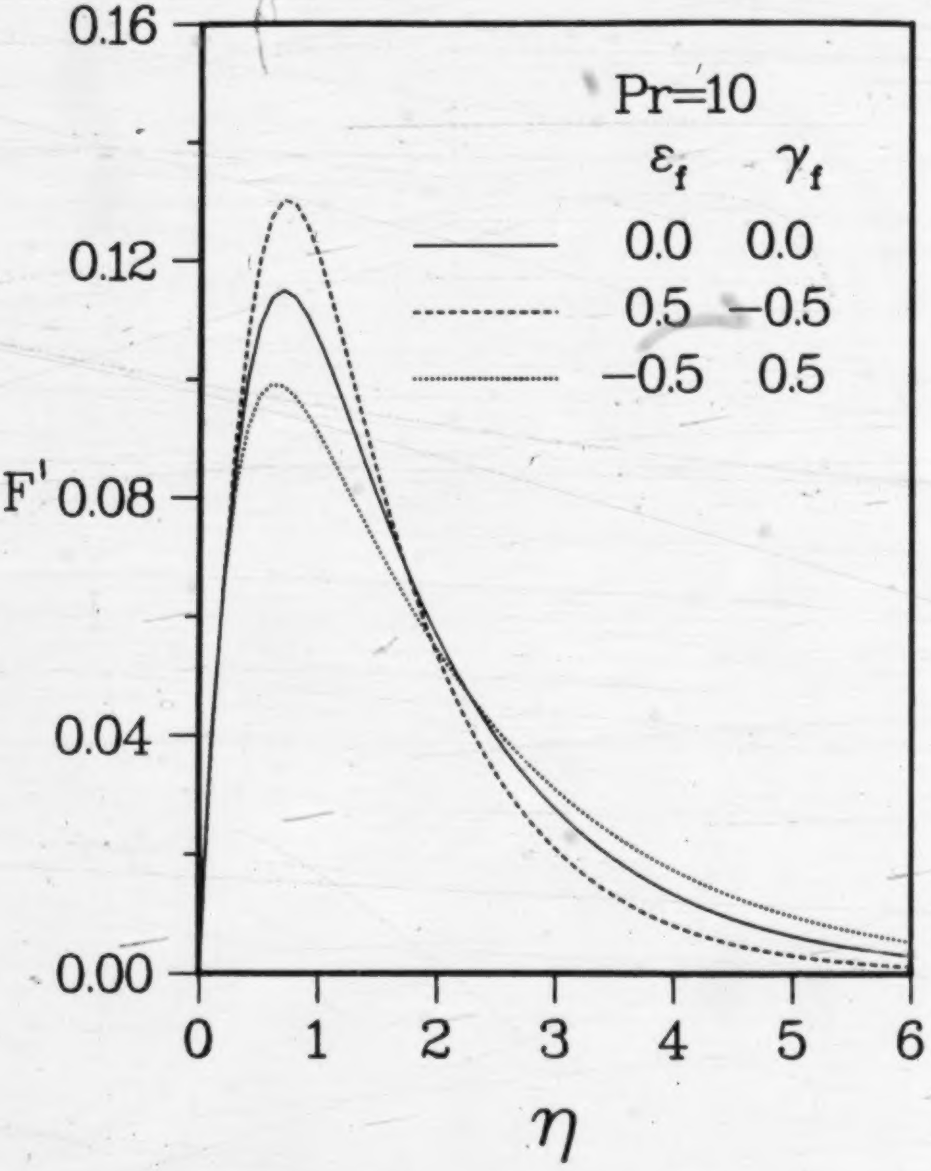

Fig. 2.8(b) Typical velocity profiles for Pr=10 with opposing effects of ϵ_f and γ_f

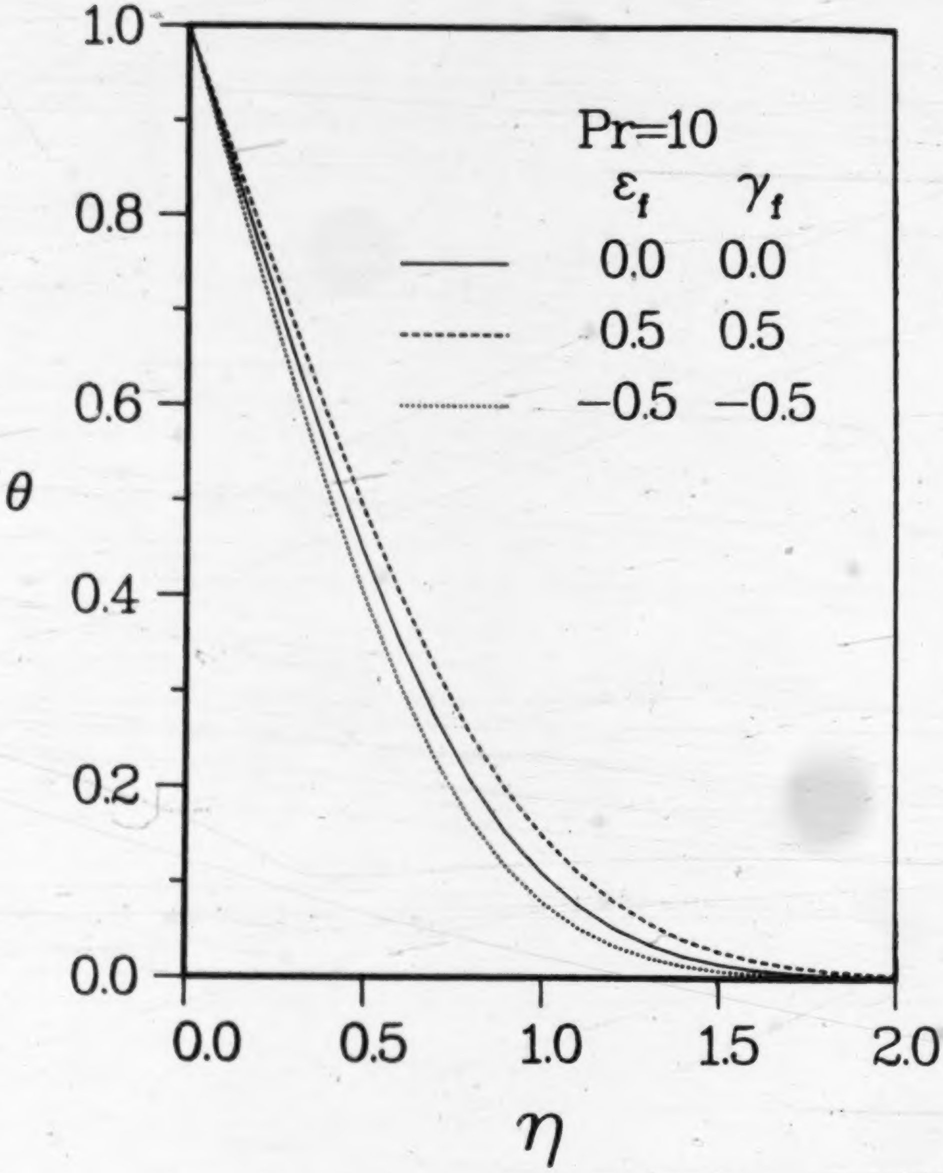

Fig. 2.8(c) Typical temperature profiles for Pr=10 with aiding effects of ϵ_f and γ_f

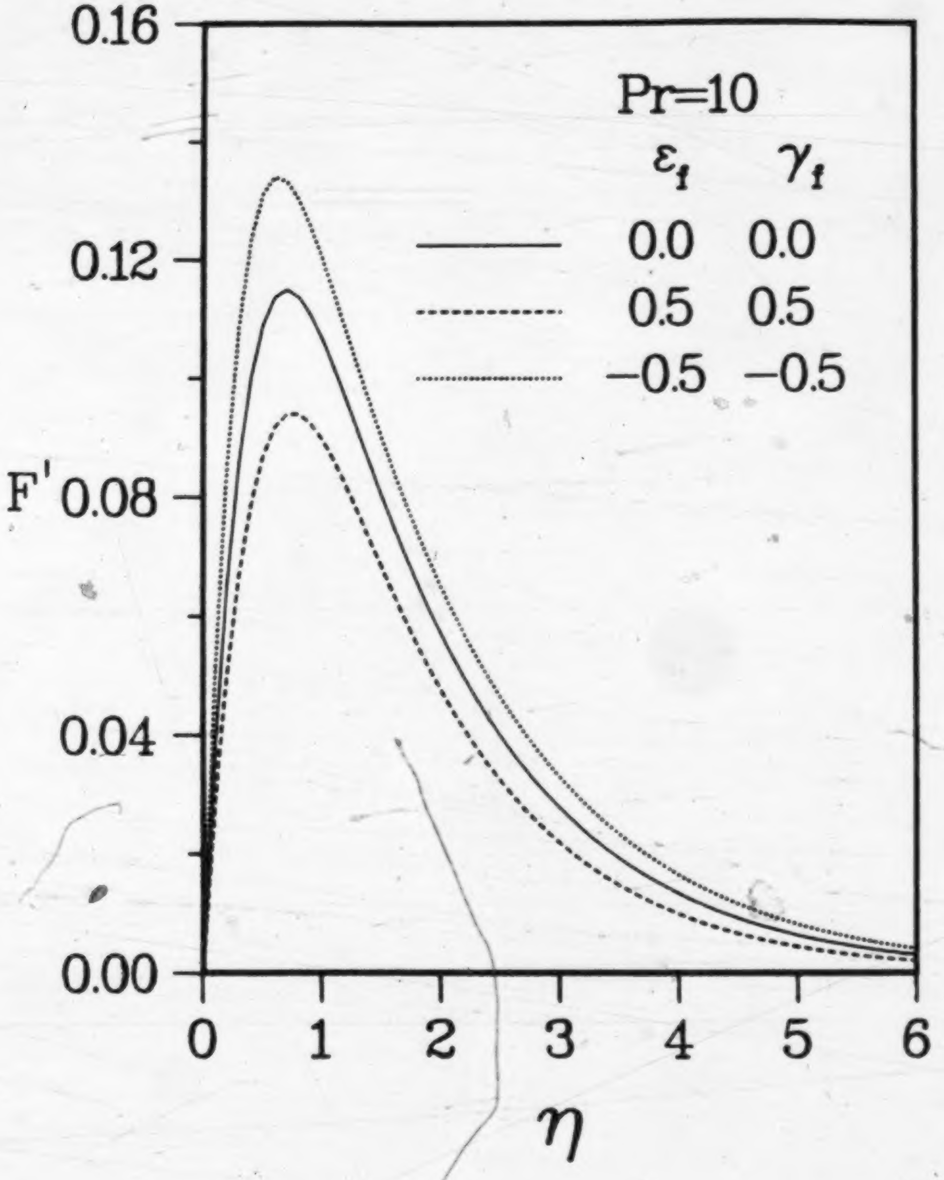

Fig. 2.8(d) Typical velocity profiles for Pr=10 with aiding effects of ϵ_f and γ_f

Table 2.7 The effects of ϵ_f and γ_f for Pr=10

ε_f	γ_f	$F''(0)$	R1	$-\theta'(0)$	R2	$F(\infty)$	R3
0.0	0.0	0.41920	1.00000	1.16933	1.00000	0.24923	1.00000
0.50	1.00	0.27005	0.96632	1.03300	0.88341	0.17653	0.70833
0.50	0.50	0.31149	0.92884	1.05881	0.90548	0.20161	0.80895
0.50	0.0	0.37106	0.88517	1.09136	0.93332	0.22491	0.90244
0.50	-0.50	0.46512	0.83216	1.13389	0.96969	0.24774	0.99401
0.50	-1.00	0.64007	0.76345	1.19355	1.02071	0.27156	1.08962
1.00	1.00	0.23492	0.84061	0.93242	0.79740	0.14410	0.57817
1.00	0.50	0.27072	0.80727	0.95790	0.81918	0.16679	0.66921
1.00	0.0	0.32220	0.76861	0.98962	0.84632	0.18824	0.75531
1.00	-0.50	0.40348	0.72189	1.03083	0.88155	0.20966	0.84123
1.00	-1.00	0.55465	0.66156	1.08848	0.93085	0.23250	0.93290
-0.50	1.00	0.33906	1.21325	1.17166	1.00199	0.21265	0.85323
-0.50	0.50	0.39117	1.16644	1.19905	1.02542	0.24150	0.96901
-0.50	0.0	0.46610	1.11188	1.23384	1.05517	0.26797	1.07520
-0.50	-0.50	0.58440	1.04558	1.27945	1.09417	0.29353	1.17777
-0.50	-1.00	0.80446	0.95953	1.34345	1.14890	0.31976	1.28300
-1.00	1.00	0.37229	1.33214	1.22540	1.04794	0.22539	0.90436
-1.00	0.50	0.42949	1.28071	1.25357	1.07204	0.25571	1.02602
-1.00	0.0	0.51174	1.22077	1.28941	1.10269	0.28344	1.13726
-1.00	-0.50	0.64162	1.14794	1.33642	1.14289	0.31013	1.24436
-1.00	-1.00	0.88319	1.05343	1.40239	1.19930	0.33740	1.35379

Note:

For this case

$\lambda_f=\zeta_f=0$

$$R1 = \frac{(1+0.5\gamma_f)F''(0)}{F''(0)|_{\epsilon_f=\gamma_f=0}}$$

$$R2 = \frac{-\theta'(0)}{-\theta'(0)|_{\epsilon_f=\gamma_f=0}}$$

$$R3 = \frac{F(\infty)}{F(\infty)|_{\gamma_f=0}}$$

2.3 Conclusions

The effects of temperature-dependent properties on the laminar natural convective boundary layer flow along an isothermal vertical flat plate were studied numerically for liquids with Prandtl numbers from 1 to ∞. Numerical solutions indicate that for most liquids when the temperature difference between the wall and the ambient medium is moderate (~10 to 50°C, for water, for example), the density can be assumed to be constant in all terms of the governing equations except in the buoyancy force term.

The assumption that the density varies linearly with temperature in the buoyancy force term underpredicts the surface heat transfer, the surface shear stress, the total mass flow rate and the maximum velocity for down flows, and overpredicts them for up flows. The effects are more pronounced for large temperature differences between the wall and the ambient medium. The effects are significant for liquids with small as well as large Prandtl numbers.

The temperature-dependent viscosity increases the surface heat transfer and the total mass flow rate for a heated wall and decreases them for a cooled wall. The value of surface shear stress is lower for a heated wall and higher for a cooled wall. The effects of variable viscosity and coefficient of thermal expansion normally oppose each other and hence the Boussinesq approximations give fairly accurate results even for moderate temperature differences between the wall and the ambient medium.

3. The Effects of Temperature-Dependent Viscosity and Coefficient of Thermal Expansion on the Stability of Laminar Natural Convective Flow Along an Isothermal Vertical Surface

In this Chapter, the effects of temperature-dependent viscosity and coefficient of thermal expansion on the stability of laminar natural convective boundary layer flow of a liquid along an isothermal vertical flat plate are studied numerically for various Prandtl numbers. Experimental results for the onset of instability and the transition to turbulence are also presented for the natural convective flow of water along an isothermal vertical circular cylinder (outside diameter 41.3 mm and length 1 m) for various combinations of wall and ambient temperatures in the range 5 to 35°C.

3.1 Theoretical Analysis

3.1.1 Linear Stability Theory

Mathematical analysis of the stability of laminar natural convective flow over a vertical surface has been done mainly from the standpoint of linear stability theory. Small two dimensional velocity, temperature, and pressure disturbances are applied on the two dimensional laminar flow equations. The base flow is assumed to be steady and it is taken as the first order laminar boundary layer equations. The disturbance equations are obtained from the two dimensional equations after substracting the base flow equations. Only the first order terms in disturbances are retained as the disturbances are assumed to be small. The disturbance equations are further simplified by applying the parallel flow approximation. This translates into neglecting the gradients of the base flow in the longitudinal direction and the base flow velocity component normal to the surface. Then the disturbances are postulated to be travelling waves whose amplitudes are functions of the coordinate normal to the surface alone. This leads to a set of linear stability equations for the natural convective flow and were first derived by Plapp (1957).

3.1.2 Governing Equations

The coordinate system is the same as the one shown in Fig. 2.1. The quiescent ambient medium and the surface of the vertical flat plate are at constant temperatures t_∞ and t_0, respectively. The absolute viscosity μ and density ρ are assumed to be functions of temperature alone. The thermal conductivity k and specific heat c_p are assumed to be constant. The dissipation terms due to pressure and viscosity are neglected. As demonstrated in the previous chapter, ρ is assumed to be constant in all terms of the governing equations except the buoyancy force term. The resulting equations governing the conservation of mass, momentum, and energy for the two dimensional natural convective flow are given by

$$\frac{\partial u}{\partial x} + \frac{\partial v}{\partial y} = 0 \tag{3.1}$$

$$\rho(\frac{\partial u}{\partial \tau} + u\frac{\partial u}{\partial x} + v\frac{\partial u}{\partial y}) = -\frac{\partial p_d}{\partial x} + g(\rho_\alpha - \rho) + \frac{\partial}{\partial x}\left[2\mu\frac{\partial u}{\partial x}\right] + \frac{\partial}{\partial y}\left[\mu(\frac{\partial u}{\partial y} + \frac{\partial v}{\partial x})\right] \tag{3.2}$$

$$\rho(\frac{\partial v}{\partial \tau} + u\frac{\partial v}{\partial x} + v\frac{\partial v}{\partial y}) = -\frac{\partial p_d}{\partial y} + \frac{\partial}{\partial y}\left[2\mu\frac{\partial v}{\partial y}\right] + \frac{\partial}{\partial x}\left[\mu(\frac{\partial u}{\partial y} + \frac{\partial v}{\partial x})\right] \tag{3.3}$$

$$\rho c_p(\frac{\partial t}{\partial \tau} + u\frac{\partial t}{\partial x} + v\frac{\partial t}{\partial y}) = k(\frac{\partial^2 t}{\partial x^2} + \frac{\partial^2 t}{\partial y^2}) \tag{3.4}$$

$$\frac{\partial p_\alpha}{\partial x} = \rho_\alpha g \tag{3.5}$$

where $p_d = (p_\alpha - p)$

The four dependent variables u, v, t, and p_d, and density ρ can be written as the sum of their mean and disturbance quantities, as follows,

$$u(x,y,\tau) = \bar{u}(x,y) + \tilde{u}(x,y,\tau) \tag{3.6}$$

$$v(x,y,\tau) = \bar{v}(x,y) + \tilde{v}(x,y,\tau) \tag{3.7}$$

$$t(x,y,\tau) = \bar{t}(x,y) + \tilde{t}(x,y,\tau) \tag{3.8}$$

$$p_d(x,y,\tau) = \bar{p}_d(x,y) + \tilde{p}_d(x,y,\tau) \tag{3.9}$$

$$\rho(x,y,\tau) = \bar{\rho}(x,y) + \tilde{\rho}(x,y,\tau) \tag{3.10}$$

The disturbance equations are obtained by substituting these relations into the equations (3.1) to (3.5) and employing the assumptions in linear stability theory.

3.1.3 Base Flow Equations

The base flow equations are,

$$\frac{\partial \bar{u}}{\partial x} + \frac{\partial \bar{v}}{\partial y} = 0 \tag{3.11}$$

$$\bar{\rho}(\bar{u}\frac{\partial \bar{u}}{\partial x} + \bar{v}\frac{\partial \bar{u}}{\partial y}) = g(\rho_\infty - \bar{\rho}) + \frac{\partial}{\partial y}\left[\mu\frac{\partial \bar{u}}{\partial y}\right] \tag{3.12}$$

$$\bar{\rho}c_p(\bar{u}\frac{\partial \bar{t}}{\partial x} + \bar{v}\frac{\partial \bar{t}}{\partial y}) = k\frac{\partial^2 \bar{t}}{\partial y^2} \tag{3.13}$$

The boundary conditions are

$$\text{at } y = 0,\ \bar{u} = \bar{v} = 0 \text{ and } \bar{t} = t_0 \text{ for all } x \tag{3.14}$$

$$\text{as } y \rightarrow \infty,\ \bar{u} \rightarrow 0 \text{ and } \bar{t} \rightarrow t_\infty \text{ for all } x \tag{3.15}$$

$$\text{at } x = 0,\ \bar{u} = \bar{v} = 0 \text{ and } \bar{t} = t_\infty \text{ for all } y > 0 \tag{3.16}$$

The equations (3.11) to (3.13) are simplified by employing similarity variables technique. Introducing the following variables,

$$Gr_x = \frac{g(\rho_\infty - \rho_0)x^3}{\rho_0 \nu_f^2}, \quad G = 4\left[\frac{Gr_x}{4}\right]^{1/4} \tag{3.17}$$

$$\eta = \frac{Gy}{4x}, \quad \bar{\psi} = \nu_f G\, F(\eta) \tag{3.18}$$

$$\theta = \frac{\bar{t} - t_\infty}{t_0 - t_\infty}, \quad \bar{u} = \frac{\partial \bar{\psi}}{\partial y}, \quad \bar{v} = -\frac{\partial \bar{\psi}}{\partial x} \tag{3.19}$$

the equations (3.11) to (3.16) become,

$$\frac{d}{d\eta}\left[\frac{\mu}{\mu_f} F''\right] + 3FF'' - 2(F')^2 + \frac{\rho_\infty - \bar{\rho}}{\rho_\infty - \rho_0}\frac{\rho_0}{\bar{\rho}} = 0 \qquad (3.20)$$

$$\theta'' + 3PrF\theta' = 0 \qquad (3.21)$$

$$F(0) = F'(0) = \theta(0) - 1 = F'(\infty) = \theta(\infty) = 0 \qquad (3.22)$$

For liquids, when the temperature difference between the surface and the ambient medium is moderate (~10 to 50°C for water, for example), as shown in the previous chapter, the dimensionless buoyancy force and the ratio μ/μ_f can be written as,

$$\frac{\rho_\infty - \bar{\rho}}{\rho_\infty - \rho_0}\frac{\rho_0}{\bar{\rho}} \cong \theta[1 - \epsilon_f(1-\theta)] \qquad (3.23)$$

$$\frac{\mu}{\mu_f} = 1 + \frac{1}{\mu_f}\frac{d\mu}{d\bar{t}}\Big|_f(\bar{t} - t_f) = 1 + \gamma_f(\theta - \frac{1}{2}) \qquad (3.24)$$

where $\epsilon_f = \dfrac{\beta_0 - \beta_\infty}{\beta_0 + \beta_\infty}$ and $\gamma_f = \dfrac{1}{\mu_f}\dfrac{d\mu}{d\bar{t}}\Big|_f(t_0 - t_\infty)$

For most liquids, and for water when both t_0 and t_∞ are larger than t_m, the value of ϵ_f varies from +1 to -1, positive for up flows (heated walls) and negative for down flows (cooled walls). The viscosity of liquids decreases with an increase in temperature. Hence, for the linear variation of viscosity with temperature, the value of γ_f varies from +2 to -2, positive for a cooled wall and negative for a heated wall. The case $\gamma_f=\epsilon_f=0$ corresponds to Boussinesq approximations.

3.1.4 Disturbance Equations

The disturbance equations are,

$$\frac{\partial \tilde{u}}{\partial x} + \frac{\partial \tilde{v}}{\partial y} = 0 \tag{3.25}$$

$$\bar{\rho}\left(\frac{\partial \tilde{u}}{\partial \tau} + \bar{u}\,\frac{\partial \tilde{u}}{\partial x} + \tilde{v}\,\frac{\partial \bar{u}}{\partial y}\right) = -\,\frac{\partial \tilde{p}_d}{\partial x} - g\tilde{\rho} + \frac{\partial}{\partial x}\left[2\mu\frac{\partial \tilde{u}}{\partial x}\right] + \frac{\partial}{\partial y}\left[\mu\left(\frac{\partial \tilde{u}}{\partial y} + \frac{\partial \tilde{v}}{\partial x}\right)\right] \tag{3.26}$$

$$\bar{\rho}\left(\frac{\partial \tilde{v}}{\partial \tau} + \bar{u}\,\frac{\partial \tilde{v}}{\partial x}\right) = -\,\frac{\partial \tilde{p}_d}{\partial y} + \frac{\partial}{\partial y}\left[2\mu\frac{\partial \tilde{v}}{\partial y}\right] + \frac{\partial}{\partial x}\left[\mu\left(\frac{\partial \tilde{u}}{\partial y} + \frac{\partial \tilde{v}}{\partial x}\right)\right] \tag{3.27}$$

$$\bar{\rho}c_p\left(\frac{\partial \tilde{t}}{\partial \tau} + \bar{u}\,\frac{\partial \tilde{t}}{\partial x}\right) = k\left(\frac{\partial^2 \tilde{t}}{\partial x^2} + \frac{\partial^2 \tilde{t}}{\partial y^2}\right) \tag{3.28}$$

The boundary conditions are

$$\text{at } y = 0,\ \tilde{u} = \tilde{v} = \tilde{t} = 0 \tag{3.29}$$

$$\text{as } y \to \infty,\ \tilde{u} = \tilde{v} = \tilde{t} = 0 \tag{3.30}$$

The velocity and temperature disturbances are assumed to be travelling waves, as shown below.

$$\tilde{\psi} = \hat{\phi}(y)\, e^{i(\hat{\alpha}x-\hat{\beta}\tau)} \tag{3.31}$$

$$\tilde{t} = \hat{s}(y)\, e^{i(\hat{\alpha}x-\hat{\beta}\tau)} \tag{3.32}$$

$$\text{and } \tilde{u} = \frac{\partial\tilde{\psi}}{\partial y}, \qquad \tilde{v} = -\frac{\partial\tilde{\psi}}{\partial x}$$

The disturbances are composed of a number of discrete partial fluctuations, each of which consists of a wave propagatig in x direction. In general, both $\hat{\alpha}$ and $\hat{\beta}$ are complex. $\hat{\alpha}_r$ (the real part of $\hat{\alpha}$) denotes the wave number, $\hat{\beta}_r$ (the real part of $\hat{\beta}$), the frequency and $\hat{\alpha}_i$, $\hat{\beta}_i$ (the imaginary parts), the amplification rates ($\hat{\beta}_i>0$ denotes temporal amplification while $\hat{\alpha}_i<0$ denotes spatial amplification in the positive direction of x).

The two cases of interest are those in which either $\hat{\alpha}$ or $\hat{\beta}$ is wholly real. The theoretical analysis can be done either for spatial amplification ($\hat{\alpha}$ complex and $\hat{\beta}$ real) or for temporal amplification ($\hat{\alpha}$ real and $\hat{\beta}$ complex). But in experiments (when forced disturbances are introduced), a spatially growing (or decaying) wave pattern is normally generated by a localized oscillating source, such as a ribbon. Hence, it is important to do the theoretical analysis for the spatial amplification of unstable disturbances. It is to be noted that whether the disturbance growth occurs temporally or spatially, the neutral stability curve ($\hat{\alpha}_i=\hat{\beta}_i=0$) is always the same. The relation between temporal and spatial amplification (or damping) of unstable disturbances has been discussed in detail by Gaster (1962,1965). In this analysis, the disturbances are assumed to grow spatially ($\hat{\alpha}$ complex and $\hat{\beta}$ real).

Employing the linear stability theory and introducing the following dimensionless variables (Jaluria, 1980),

$$\delta = \frac{4x}{G}, \quad \alpha = \hat{\alpha}\,\delta, \quad \beta = \frac{4\hat{\beta}\,\delta x}{\nu_f G^2}, \quad c = \frac{\beta}{\alpha} \tag{3.33}$$

$$\phi(\eta) = \frac{4\hat{\phi}\,x}{\delta \nu_f G^2}, \quad s(\eta) = \frac{\hat{s}}{(t_0 - t_\infty)} \tag{3.34}$$

the equations (3.25) to (3.30) become,

$$\begin{aligned}[\phi'''' - 2\,\alpha^2\phi'' + \alpha^4\phi]\,[1 + \gamma_f(\theta - \tfrac{1}{2})] = \\ i\alpha G[(F'-c)(\phi''-\alpha^2\phi) - F'''\phi] - 2\gamma_f\theta'(\phi'''-\alpha^2\phi') \\ - \gamma_f\theta''(\phi''+\alpha^2\phi) - 2\epsilon_f\theta' s - [1+2\epsilon_f(\theta-\tfrac{1}{2})]s'\end{aligned} \tag{3.35}$$

$$s'' - \alpha^2\, s = i\alpha G Pr[(F'-c)s - \phi'\theta'] \tag{3.36}$$

$$\phi(0)=\phi'(0)=s(0)=\phi(\infty)=\phi'(\infty)=s(\infty)=0 \tag{3.37}$$

3.1.5 Numerical Method

At large η, the solutions to the base flow equations (3.20) to (3.24) are given by (see Appendix E),

$$F = A + C\, e^{-3A\eta/\lambda} + \frac{Bq}{[27A^3 Pr^2(\lambda Pr - 1)]}\, e^{-3APr\eta} \tag{3.38}$$

$$\theta = B\, e^{-3APr\eta} \tag{3.39}$$

where $\lambda = 1-\frac{\gamma_f}{2}$, $q = 1-\epsilon_f$, and A, B, and C are real constants.

The equations (3.20) to (3.24) were integrated numerically across the boundary layer from the outer edge to the wall, assuming some values for A, B, and C. The boundary conditions were checked at $\eta=0$. Shooting method was employed to correct the values of A, B, and C so that the boundary conditions were satisfied at $\eta=0$. The solution was assumed to have converged when the relative errors in A, B, and C, and the boundary conditions at $\eta=0$ were less than 10^{-6}.

The equations (3.35) to (3.37) describing the disturbance flow is a sixth order eigenvalue problem, linear in the disturbance amplitudes ϕ and s. α and β were chosen to be the eigenvalues of the system. The numerical method employed to solve the disturbance equations was the same as the one given by Hieber and Gebhart (1971).

The solutions to the equations (3.35) to (3.37) can be written as a linear combination of six independent integrals as,

$$\phi(\eta) = B_1\phi_1+B_2\phi_2+B_3\phi_3 \tag{3.40}$$

$$s(\eta) = B_1 s_1+B_2 s_2+B_3 s_3 \tag{3.41}$$

where B_1, B_2 and B_3 are complex constants. B_1 was taken as 1.0, thus fixing the disturbance level arbitrarily. The integrals were obtained from the solution of disturbance equations (3.35) to (3.37) at large values of η. They are given by

$$\phi_1 = e^{-\alpha\eta} \tag{3.42}$$

$$\phi_2 = e^{-\alpha_2\eta} \tag{3.43}$$

$$\phi_3 = \frac{q(\alpha_3/\lambda)e^{-\alpha_3\eta}}{[(\alpha_3^2-\alpha^2)(\alpha_3^2-\alpha_2^2)]} \tag{3.44}$$

$$s_1 = \frac{i\alpha PrG\theta'_\infty \; e^{-\alpha\eta}}{[\alpha_3^2 \;-(3APr+\alpha)^2]} \tag{3.45}$$

$$s_2 = \frac{i\alpha PrG\theta'_\infty \; e^{-\alpha_2\eta}}{[\alpha_3^2 \;-(3APr+\alpha_2)^2]} \tag{3.46}$$

$$s_3 = e^{-\alpha_3\eta} \tag{3.47}$$

where $\alpha_2 = +\left[\alpha^2-\frac{i\alpha cG}{\lambda}\right]^{1/2}$ and $\alpha_3 = +\left[\alpha^2-i\alpha cPrG\right]^{1/2}$.

For given values of G and β (β is a dimensionless real number), a complex value for α was assumed. Starting with (3.40) and (3.41) as the initial values, the equations (3.35) to (3.37) were integrated across the boundary layer using a fourth order Runge-Kutta method. B_2 and B_3 were determined by satisfying two of the three boundary conditions at $\eta=0$. The remaining boundary condition at $\eta=0$ is satisfied only if the assumed value of α is the eigenvalue of the equations (3.35) to (3.37) for the given values of G and β. The value of α which satisfied the third boundary condition at $\eta=0$ within 10^{-5} was found iteratively. The singularity that occurs in the disturbance equations at

(F'-c)=0 was stepped over by the numerical scheme.

The distributions for the disturbance velocity and temperature can be obtained from the equations (3.35) to (3.37). The disturbance equations are linear and homogeneous. Hence, the absolute magnitudes for the disturbance velocity and temperature cannot be obtained. Each distribution was normalized by the numerically obtained maximum value in the boundary layer. They are given by

$$\frac{\tilde{u}}{u_{max}} = \left[\frac{(\phi_r')^2+(\phi_i')^2}{\{(\phi_r')^2+(\phi_i')^2\}_{max}}\right]^{1/2} \tag{3.48}$$

$$\frac{\tilde{v}}{v_{max}} = \left[\frac{(\phi_r)^2+(\phi_i)^2}{\{(\phi_r)^2+(\phi_i)^2\}_{max}}\right]^{1/2} \tag{3.49}$$

$$\frac{\tilde{t}}{t_{max}} = \left[\frac{(s_r)^2+(s_i)^2}{\{(s_r)^2+(s_i)^2\}_{max}}\right]^{1/2} \tag{3.50}$$

3.2 Experimental Apparatus and Procedure

3.2.1 Experimental Apparatus

The experimental apparatus consisted mainly of a water tank, a test section, a coolant system, and a traversing mechanism. The photograph of the apparatus and test section is shown in Fig. 3.1. The schematic diagram is shown in Fig. 3.2.

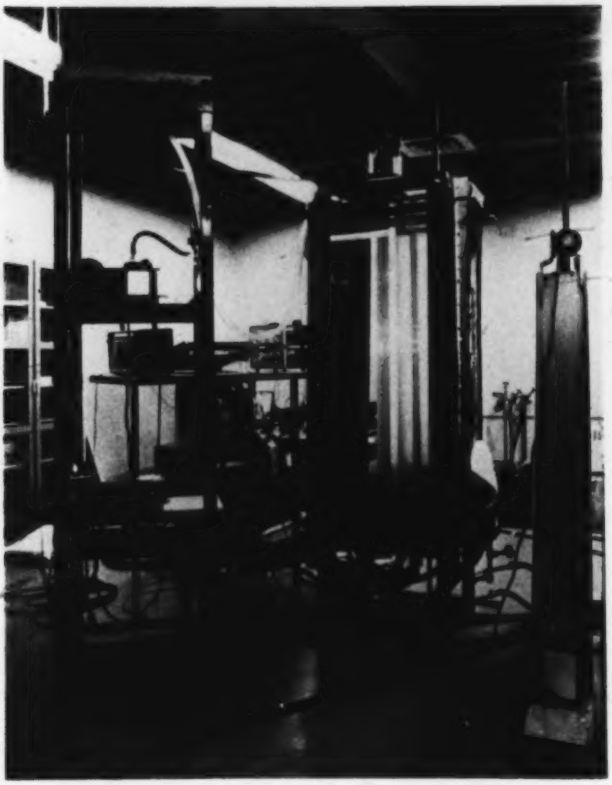

Fig. 3.1 Photograph of the experimental apparatus

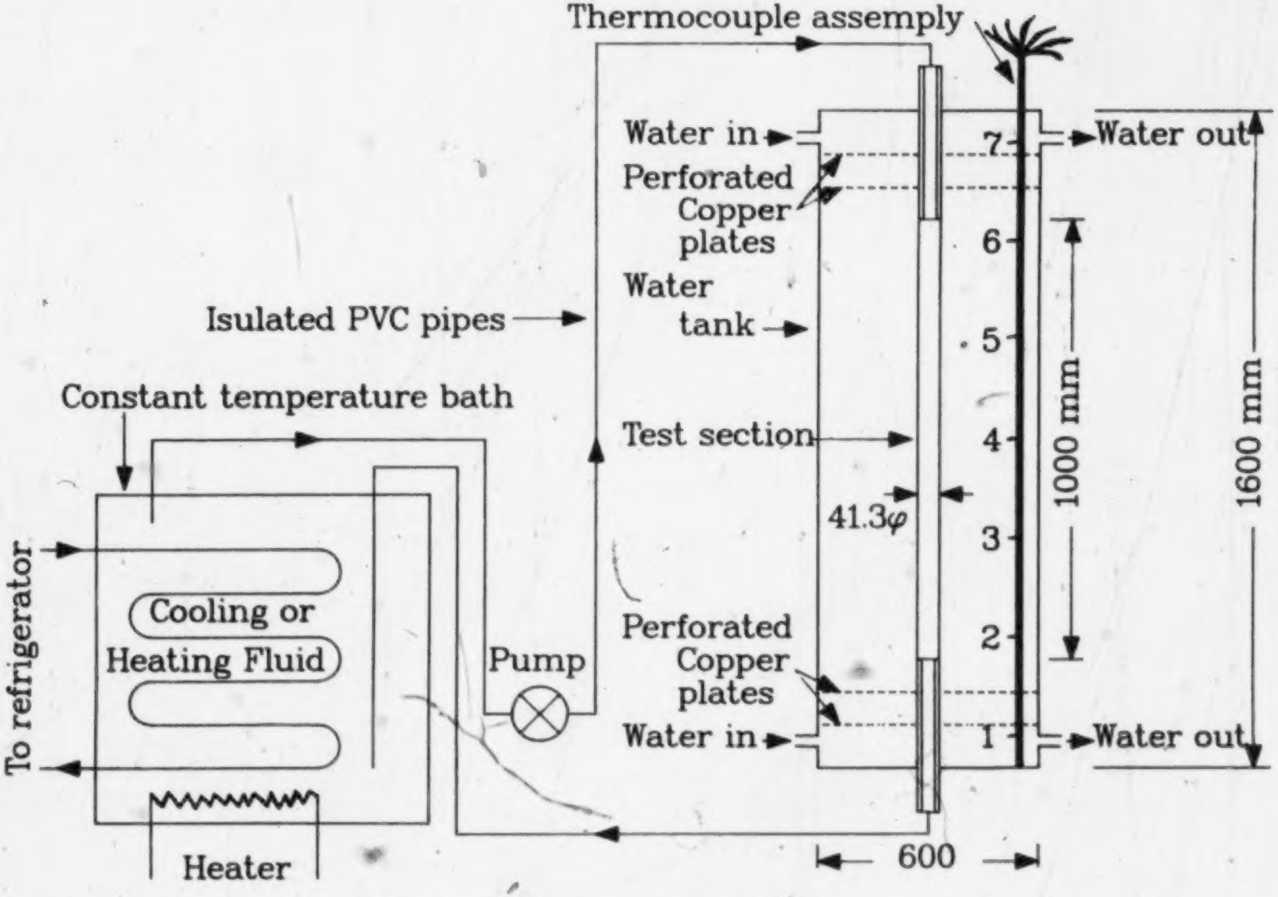
Thermocouple assemply
Water in
Perforated
Copper
plates
Water
tank
Isulated PVC pipes
Constant temperature bath
Test section
41.3φ
Perforated
Copper
plates
Water in
Water out
Water out
7
6
5
4
3
2
1
1000 mm
1600 mm
600
Pump
Cooling or
Heating Fluid
Heater
To refrigerator

Fig. 3.2 Schematic diagram of the experimental apparatus

The water tank was 0.6 m long, 0.6 m wide, and 1.6 m high. It was made up of galvanized mild steel plates of 4 mm thickness. It had 19 mm thick plexiglass windows on all four sides. Its sides were insulated with fiberglass leaving small portions for flow visualization (The photograph shows the apparatus without the insulation). To avoid the stratification of water inside the tank, water could be circulated near the top and the bottom of the tank. Perforated thin copper plates installed near the top and the bottom of the tank prevented any disturbance due to circulation reaching the center of the tank. The temperature of water inside the steel tank was measured by a copper-constantan thermocouple assembly consisting of seven thermocouples on a plexiglass tube, one for every 0.25 m height.

The test section consisted of a 1 m long copper pipe with an outside diameter of 41.3 mm and a wall thickness of 3 mm. It was connected to concentric PVC pipes at both ends. The air gap between the PVC pipes acted as an insulation. The whole arrangement was held vertically in the center of the water tank. The PVC pipes were connected to a coolant circulation loop at the top and the bottom of the tank. In order to obtain an isothermal surface over the entire length of the copper pipe, the coolant was circulated at a high flow rate ($(5\sim10) \times 10^{-3}$ m^3/s). Also, a helical copper wire was inserted inside the copper pipe to provide turbulent flow and heat transfer augmentation. The coolant temperatures at the inlet and the outlet of the test section were measured by iron-constantan thermocouples.

The coolant system consisted of a coolant tank, a refrigeration system (Tecumsh Refrigerator, Model AH 2511KU), a heater, a temperature controller (YSI Model 72 Proportional Controller), a centrifugal pump (Monarch Model BVE-30), and the associated piping arrangements. Plain tap water was used as the working fluid in the coolant system. The water could be cooled or heated to desired temperatures. The temperature controller controled the temperature of water within 0.1°C. The centrifugal pump was used to circulate the water through the test section. The pump and the associated pipings were insulated.

The temperature in the boundary layer was measured by a thermocouple mounted on a traversing mechanism. The traversing mechanism had two sliding arrangements, one moving in the horizontal direction and the other in the vertical direction. The horizontal sliding arrangement could be moved accurately to 0.0254 mm (0.001 inch) by manual rotation of a lead screw. A variable speed d. c. motor (Bodine Electric Gear Motor, Type NSH-33R) with a controller was used to move the vertical sliding mechanism. The whole arrangement was supported by an aluminium frame on levelling screws. A steel arm, supported by the horizontal sliding arrangement, carried the thermocouple and the dye injection rake.

The thermocouple probe was made up of a thin plexiglass rod in the form of a two-tined fork. The thermocouple, made by joining 0.076 mm copper and constantan wires, was suspended between the tips of the tines. The thermocouple junction had a diameter of about 0.1 mm. Fig. 3.3 shows a typical calibration curve for this thermocouple in the temperature range 0 to 20°C. This thermocouple had an accuracy of ±0.05°C. The iron-constantan thermocouples measuring the coolant temperatures and the copper-constantan thermocouples measuring the ambient water temperatures were accurate within ±0.1°C. A OMEGA TRC-III Ice Point Reference Chamber (accuracy 0 to 0.1°C) was used for the ice point reference temperature. A HP 3490A digital voltmeter with a resolution of 1 μV was used to measure the voltage outputs from the thermocouples.

3.2.2 Flow Visualization Techniques

Flow visualization techniques used were the shadowgraph and the dye injection methods. A slide projector fitted with a vertical line slit was used as the light source. A white foam card board at the back of the water tank served as the screen. A Nikon 35 mm camera with a motor drive, and a timer were used to take the shadowgraph pictures. Kodak 2475 recording film with a variable ASA was used. A dye, formed by dissolving methylene blue in water, was used. The traversing mechanism was used to inject the dye at the desired locations. When the temperature difference between the wall and the ambient water was small, the dye injection method was the only one used as the shadowgraph was not very clear under these conditions.

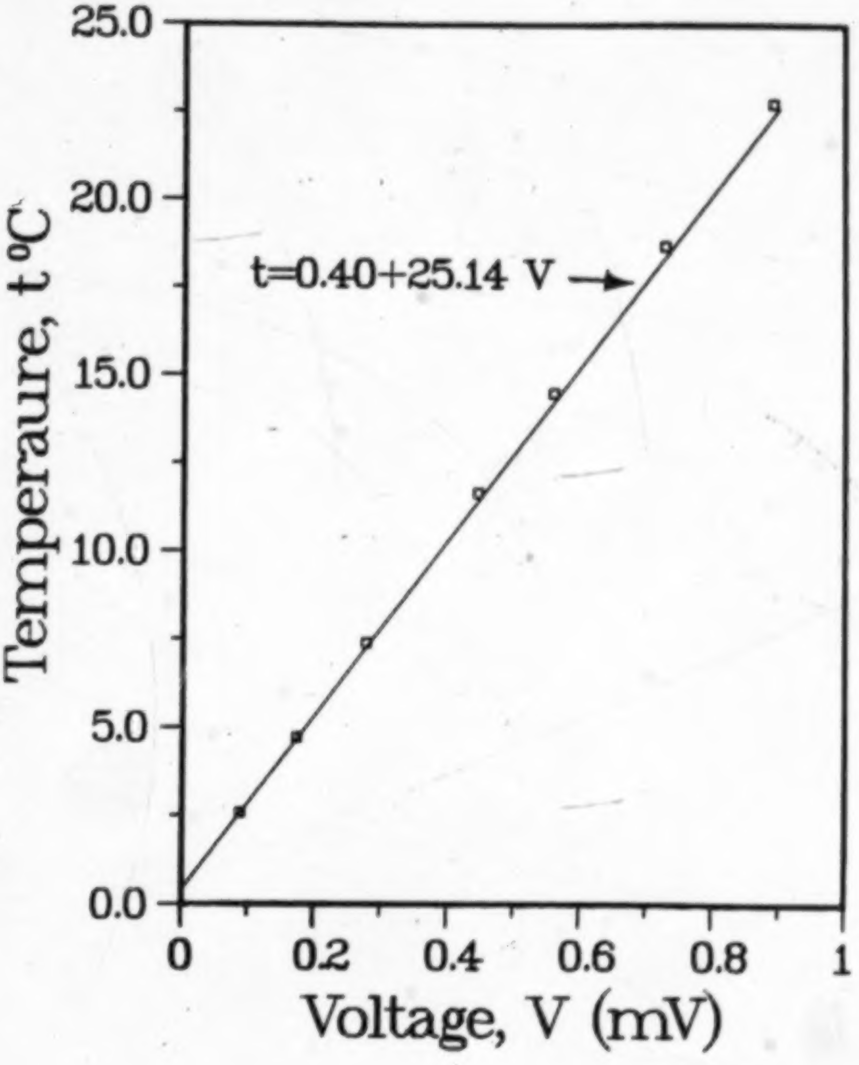

Fig. 3.3 Typical thermocouple calibration curve

3.2.3 Experimental Procedure

The steel tank was filled with deaerated plain tap water and allowed to equilibrate for about one to two hours. The constant temperature fluid was brought down to the desired temperature and then the fluid was allowed to circulate through the test section. The bulk temperatures of the fluid at the inlet and the outlet of the test section were always within 0.2°C. The surface temperature of the copper pipe was taken as the average of these two temperatures. The dye was injected continuously for flow visualization studies.

After about 15 minutes of starting the experiment, thus allowing ample time for the initial disturbances to die away, the light source was turned on and the flow was visualized. The locations of the onset of instability and the transition to turbulent flow were closely observed. The onset of instability was taken as the nearest point to the leading edge where small oscillations on the dye were observed. As the disturbances moved downstream they amplified and became vortices. The vortices, as they moved downstream, broke down into turbulent flow. The point of transition to turbulent flow was taken as the nearest point to the leading edge below which the flow was always turbulent. The flow was considered to be turbulent when it had a larger boundary layer and exhibited the nature of complete disorder and mixing.

The temperature of the ambient water was measured by the copper-constantan thermocouple assembly. It was always within 0.25°C in the range of the test section. The experiments were repeated for various combinations of ambient and wall temperatures in the range 5 to 35°C. Both heated and cooled walls were examined. The experiments were conducted late at night to minimize the disturbances due to normal activities in the building during the day time.

3.3 Results and Discussion

The equations (3.20) to (3.24) and (3.35) to (3.37) were solved numerically and the stability plane was obtained for various values of Pr, γ_f and ϵ_f. The numerical solutions corresponding to Boussinesq approximations ($\gamma_f=\epsilon_f=0$) agreed very well with those given by Nachtsheim (1963) for Pr=0.733 and Pr=6.7.

3.3.1 The Effects of Variation of Viscosity with Temperature

The effects of temperature-dependent viscosity on the laminar flow were discussed in Chapter 2 in terms of the dimensionless parameter γ_f. The larger the absolute value of γ_f, the more pronounced are the effects of temperature-dependent viscosity. The effects of γ_f on the stability of the laminar flow are shown in Figs. 3.4(a) to (f) for Pr=10. Fig. 3.4(a) shows the stability plane for $\gamma_f=0$ (Boussinesq approximations), Figs. 3.4(b) and (c), the stability planes for positive values of γ_f (cooled walls), and Figs. 3.4(d) and (e), the stability planes for negative values of γ_f (heated walls). Fig. 3.4(f) compares the neutral stability curves for various values of γ_f and it is

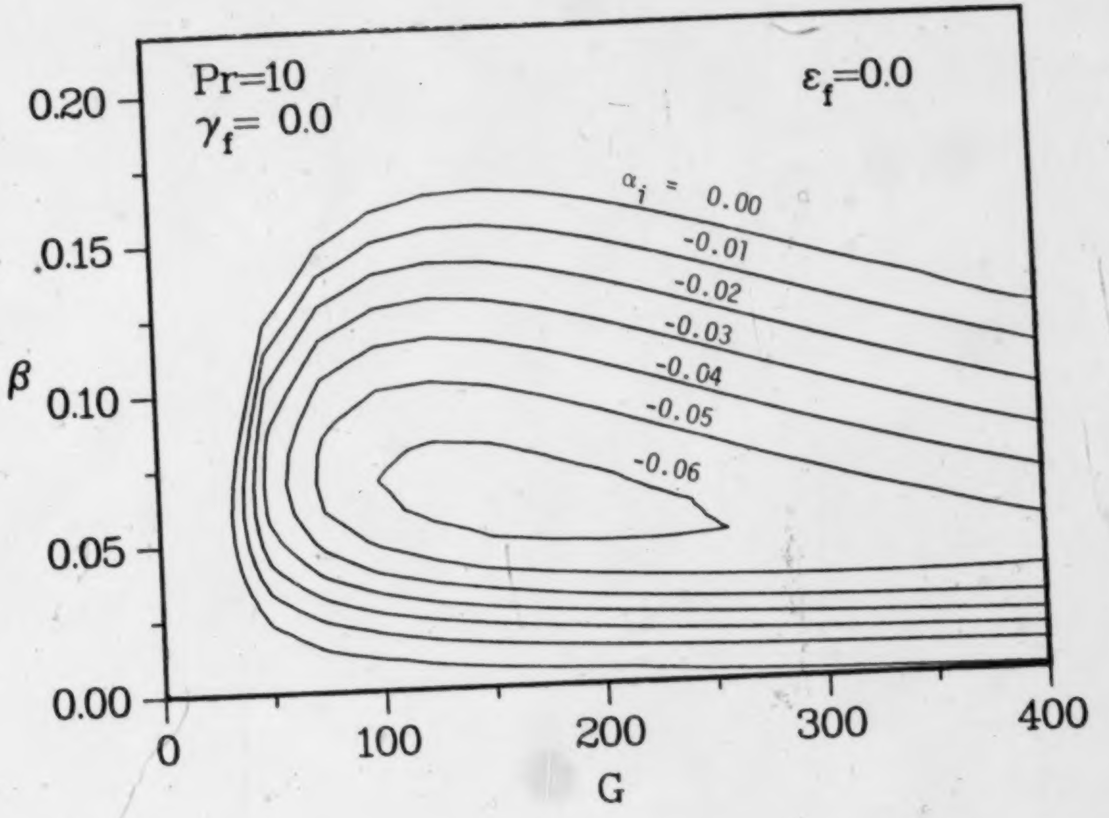

Fig. 3.4(a) The stability plane for Pr=10 and γ_f=0.0

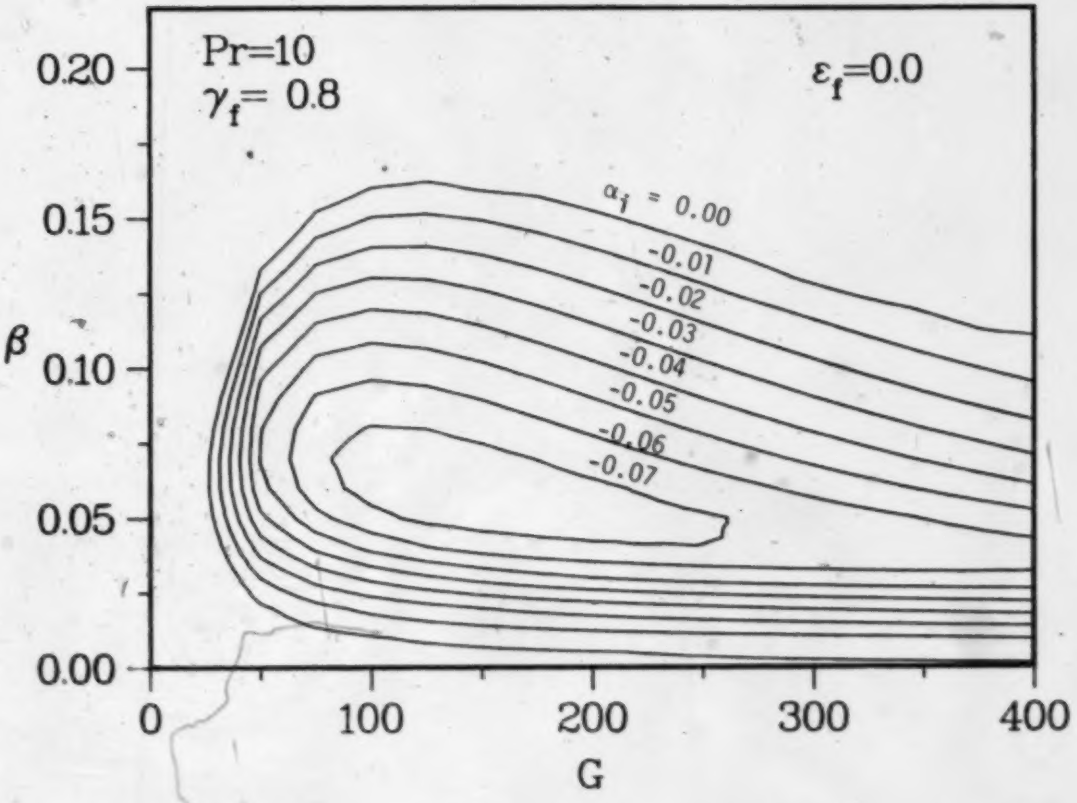

Fig. 3.4(b) The stability plane for Pr=10 and γ_f=0.8

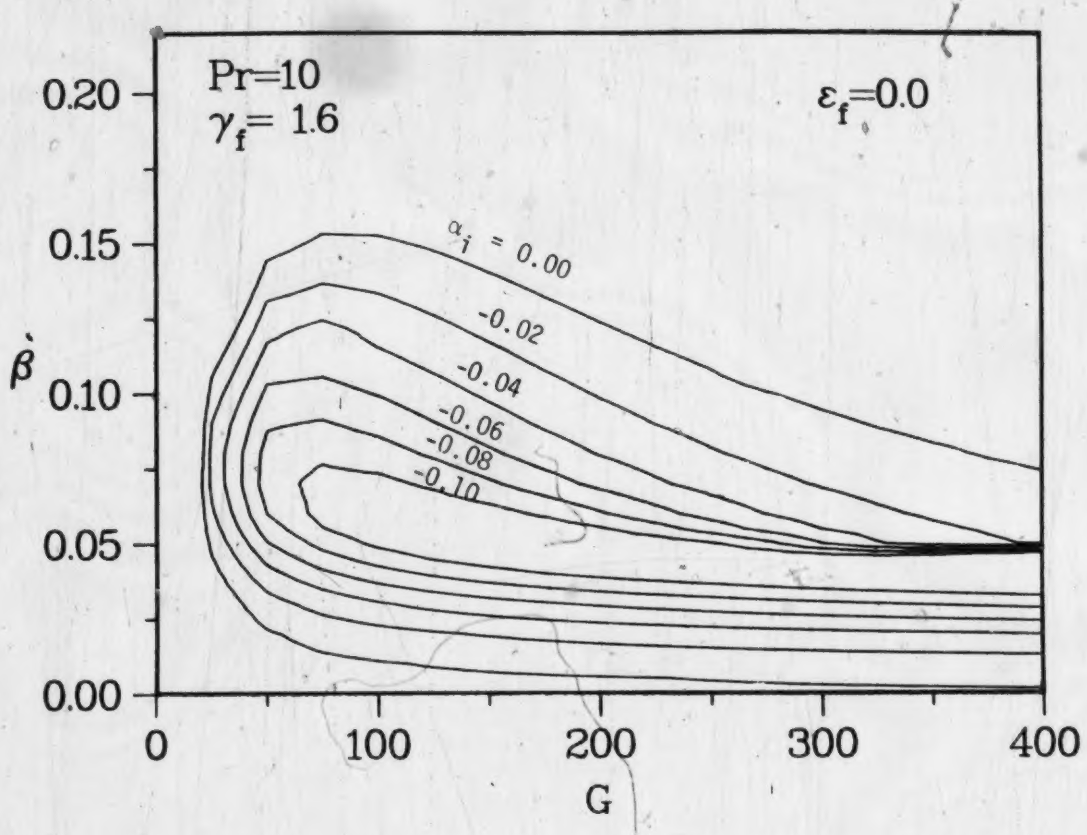

Fig. 3.4(c) The stability plane for Pr=10 and γ_f=1.6

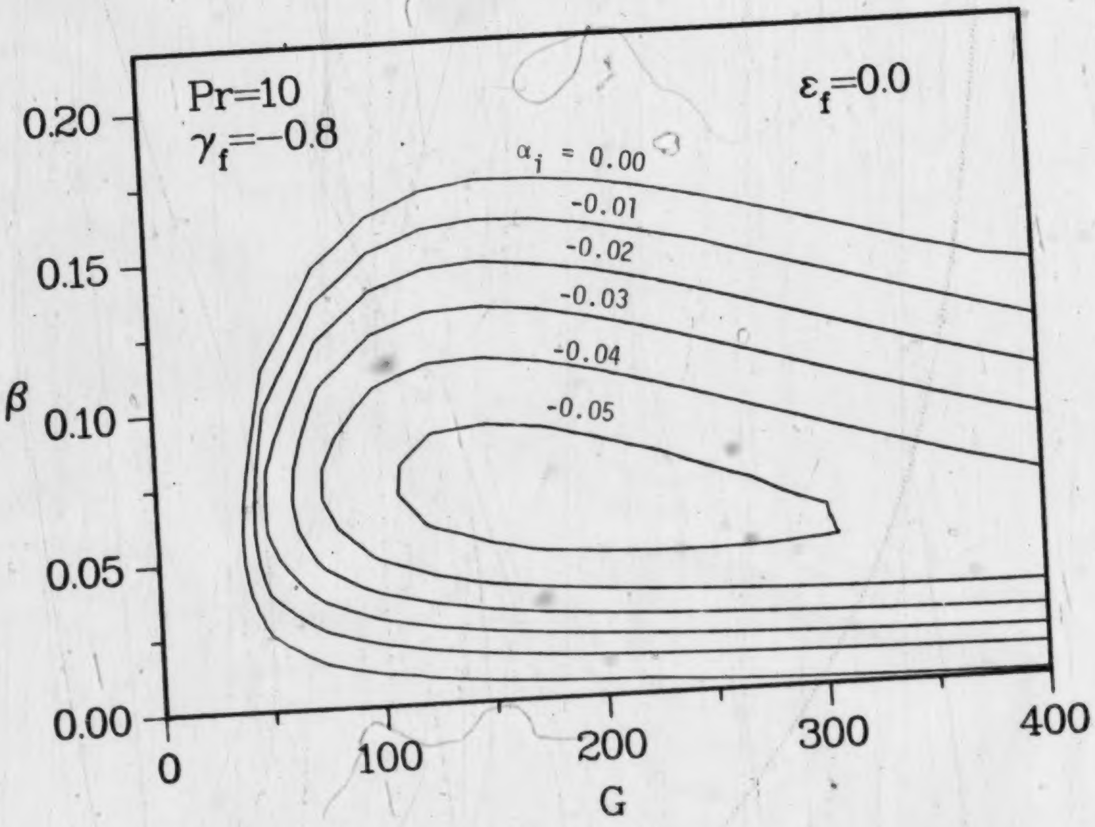

Fig. 3.4(d) The stability plane for Pr=10 and γ_f=-0.8

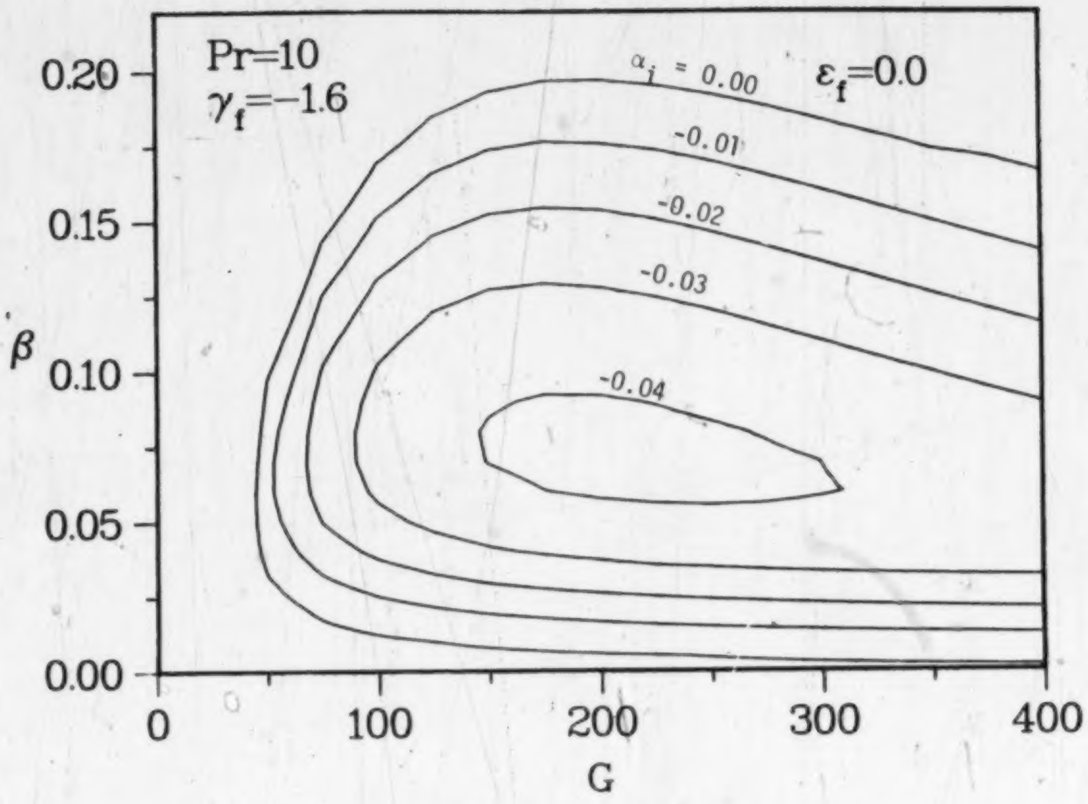

Fig. 3.4(e) The stability plane for Pr=10 and γ_f=-1.6

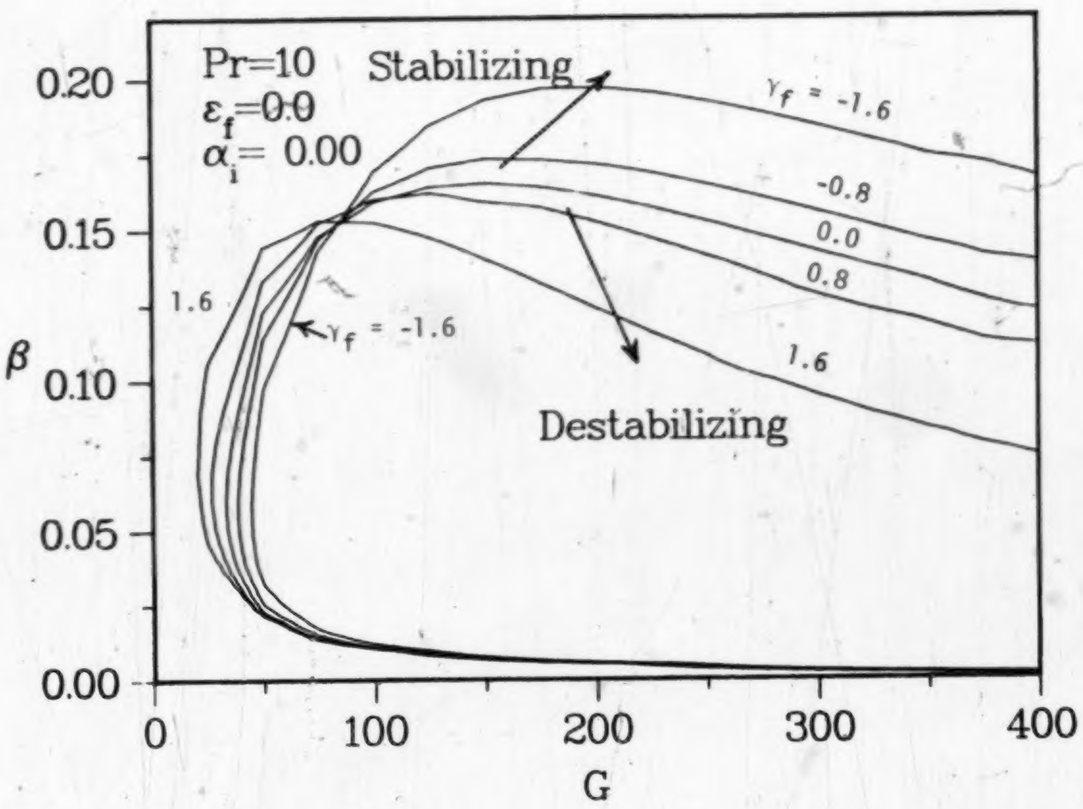

Fig. 3.4(f) The effects of γ_f on the neutral stability curve for Pr=10

seen that the curves for the positive values of γ_f lie to the left of the ones for the negative values. Hence, for the same temperature difference between the wall and the ambient liquid, the location at which the laminar flow first becomes unstable to disturbances is nearer to the leading edge for a cooled wall than for a heated wall.

The transtion of laminar flow into turbulent flow depends on the growth of the disturbance as it moves downstream. The disturbances with frequencies higher than the one corresponding to the critical value of G normally amplify faster (Hieber and Gebhart, 1971). If A_0 is the amplitude of a disturbance frequency at the neutral curve ($G=G_0$), its amplitude, A_G, at a location G is given by (Jaluria, 1980)

$$\frac{A_G}{A_0} \propto \exp(A) \tag{3.51}$$

$$\text{where } A=\int_{G_0}^{G} (-\alpha_i)dG$$

At the neutral curve A is equal to zero and contours of constant A may be determined by following various constant frequency paths and evaluating the above integral along these paths. By comparing the contours and values of α_i in Figs. 3.4(a) to (e), it can be easily seen that disturbances amplify faster for positive vaules of γ_f (cooled walls, for liquids) than for the the negative values (heated walls, for liquids).

The naturally occurring disturbances of varying frquency and amplitude enter the flow at various distances from the leading edge. As the disturbances move downstream, only those within a narrow range of frequencies amplify faster depending on the local Grashof number and the distance from the leading edge. That is, the natural convective flow favours disturbances having specific frquencies and transfers more energy into them. This frequency filtering phenomenon has received considerable experimental support and the details can be found in Jaluria (1980). Comparing the contours of a_i in Figs 3.4(a) to (e), it can be easily seen that for positive values of γ_f, the frequency filtering mechanism is more pronounced. The larger the positive value, the more pronounced are the effects.

Figs. 3.5(a) and (b) show the effects of variable viscosity for Prandtl numbers 20 and 50. The same trends are observed as for the case of Pr=10. Hence, as in forced convection, for liquids, the natural convective flow along a cooled vertical isothermal wall is more unstable than the flow along a heated wall. The frequency filtering mechanism is more pronounced for a cooled wall than for a heated wall. Also, as the disturbances amplify faster for a cooled wall, the transition to turbulent flow may occur earlier.
Figs. 3.6(a) to (d) show typical disturbance velocity and temperature profiles for Pr=10 and for γ_f=0.0, 0.8 and -0.8.

The base flow velocity boundary layer thickness is larger for a negative value of γ_f than for a positive value (see Fig. 2.5(d)). Previous experimental studies (Fujii et

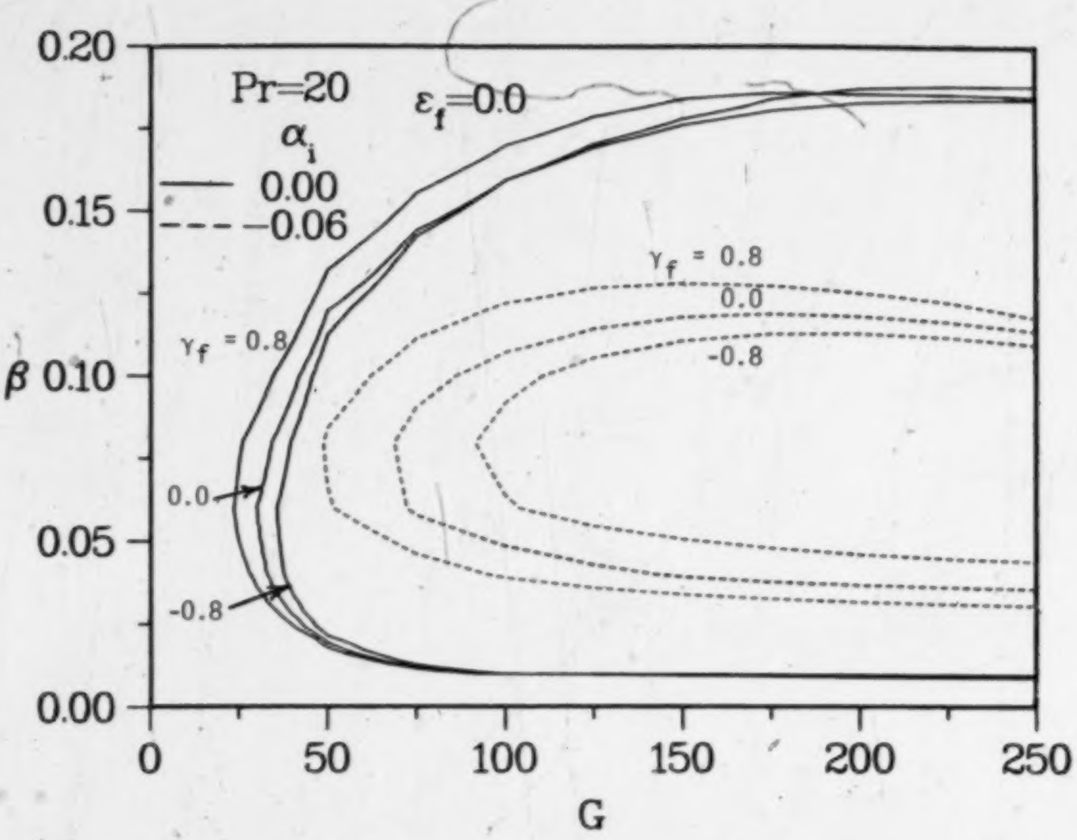

Fig. 3.5(a) The effects of γ_f on the contours of α_i=0.0 and -0.06 for Pr=20

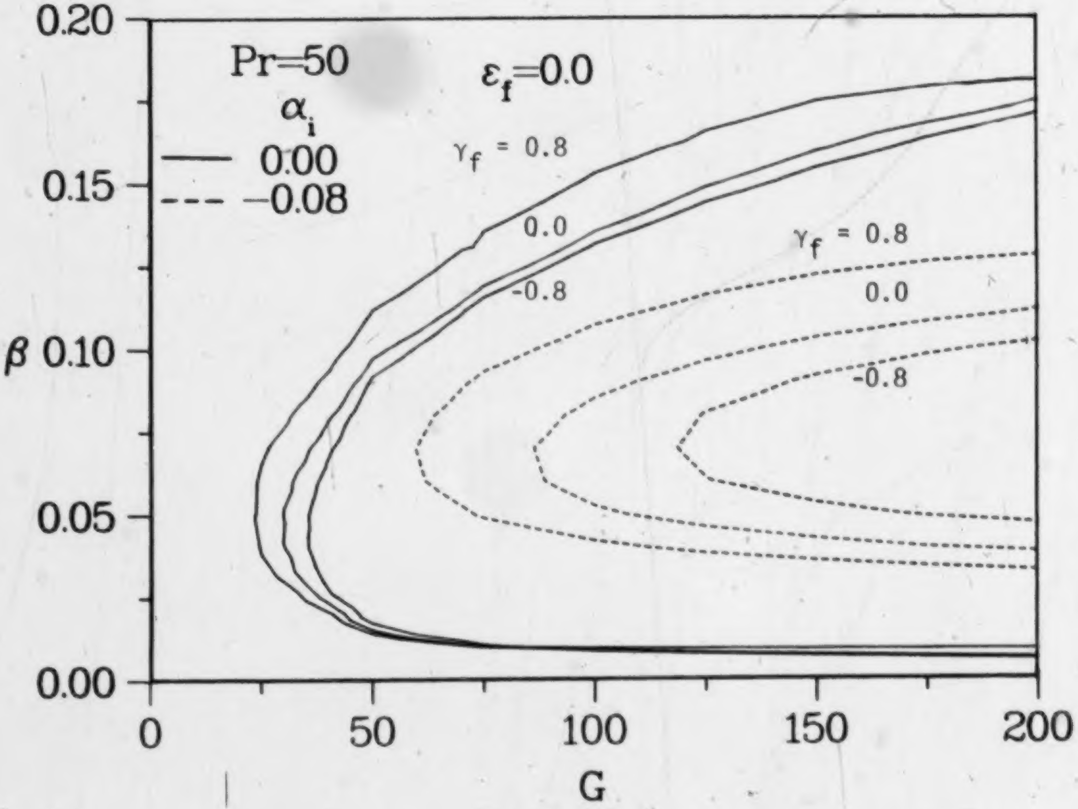

Fig. 3.5(b) The effects of γ_f on the contours of a_i=0.0 and -0.08 for Pr=50

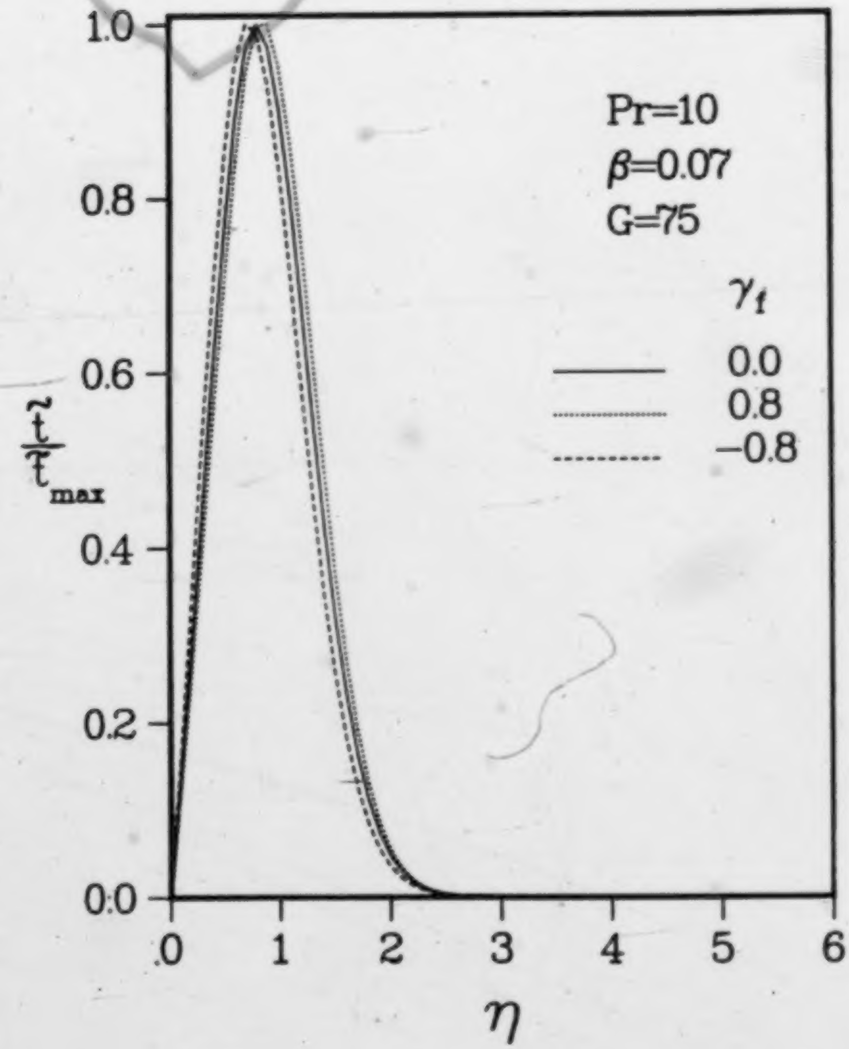

Fig. 3.6(a) The disturbance temperature profile for various values of γ_f when β=0.07, G=75 and Pr=10

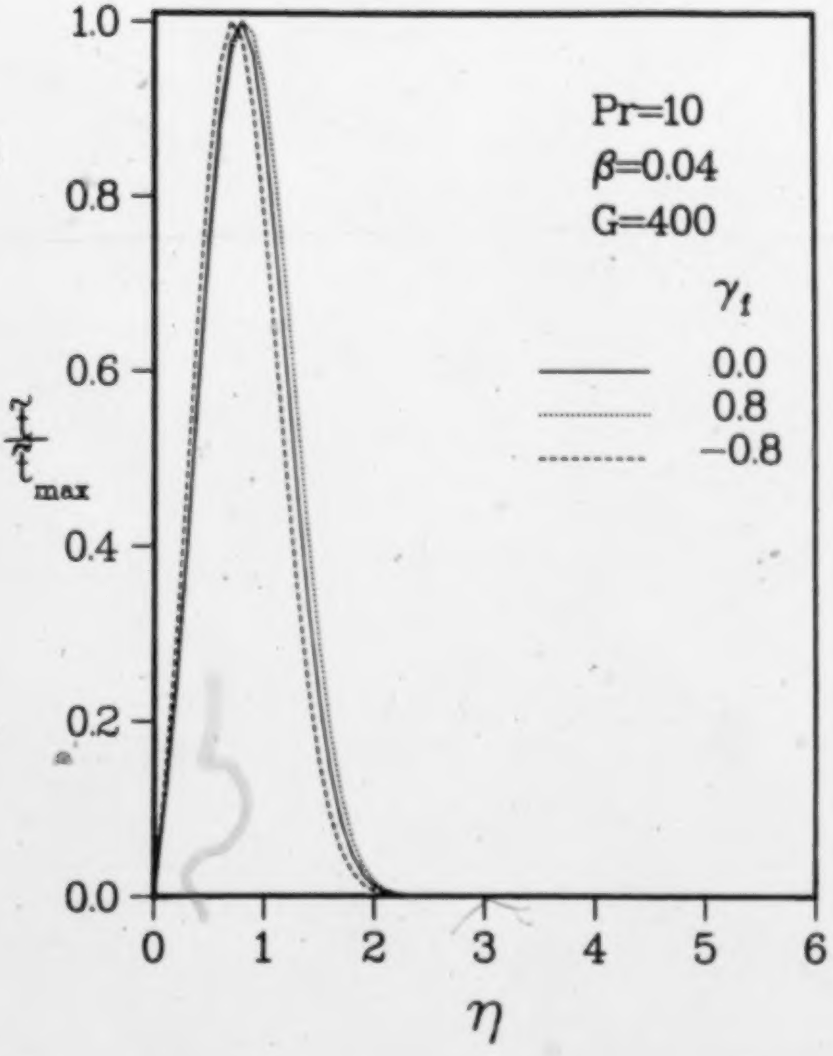

Fig. 3.6(b) The disturbance temperature profile for various values of γ_f when β=0.04, G=400 and Pr=10

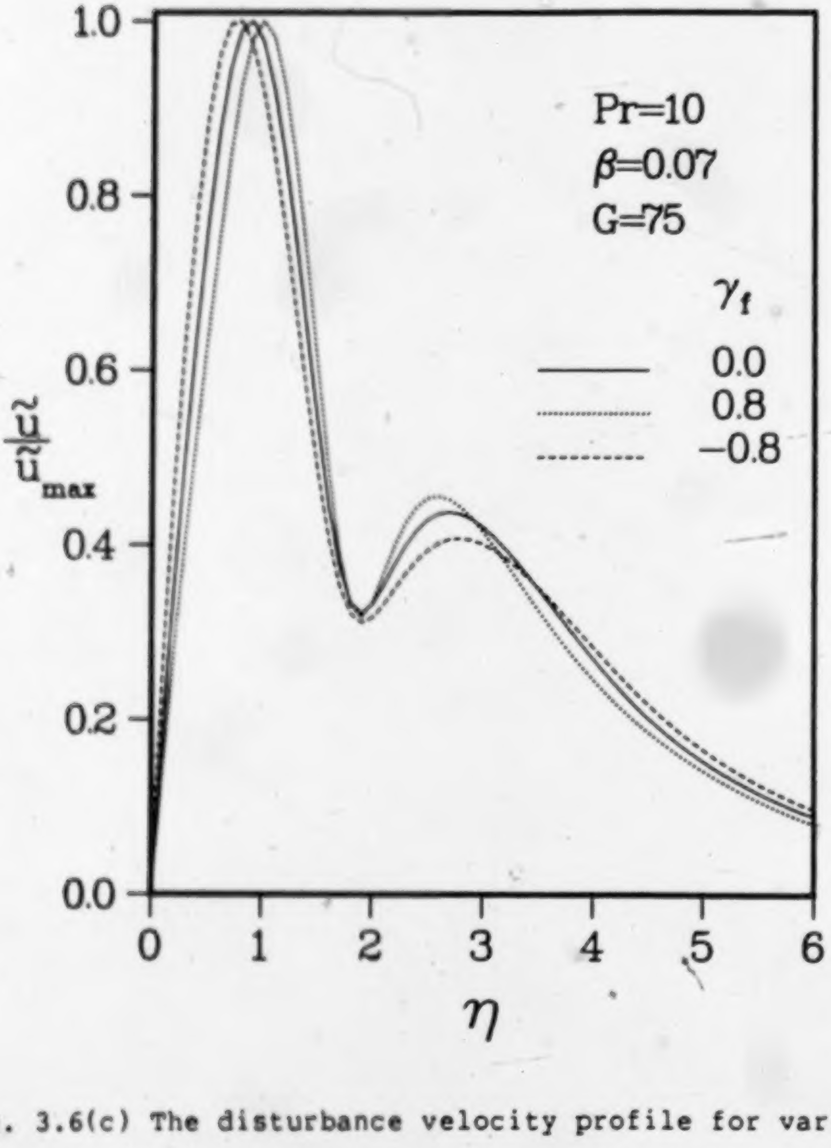

Fig. 3.6(c) The disturbance velocity profile for various values of γ_f when β=0.07, G=75 and Pr=10

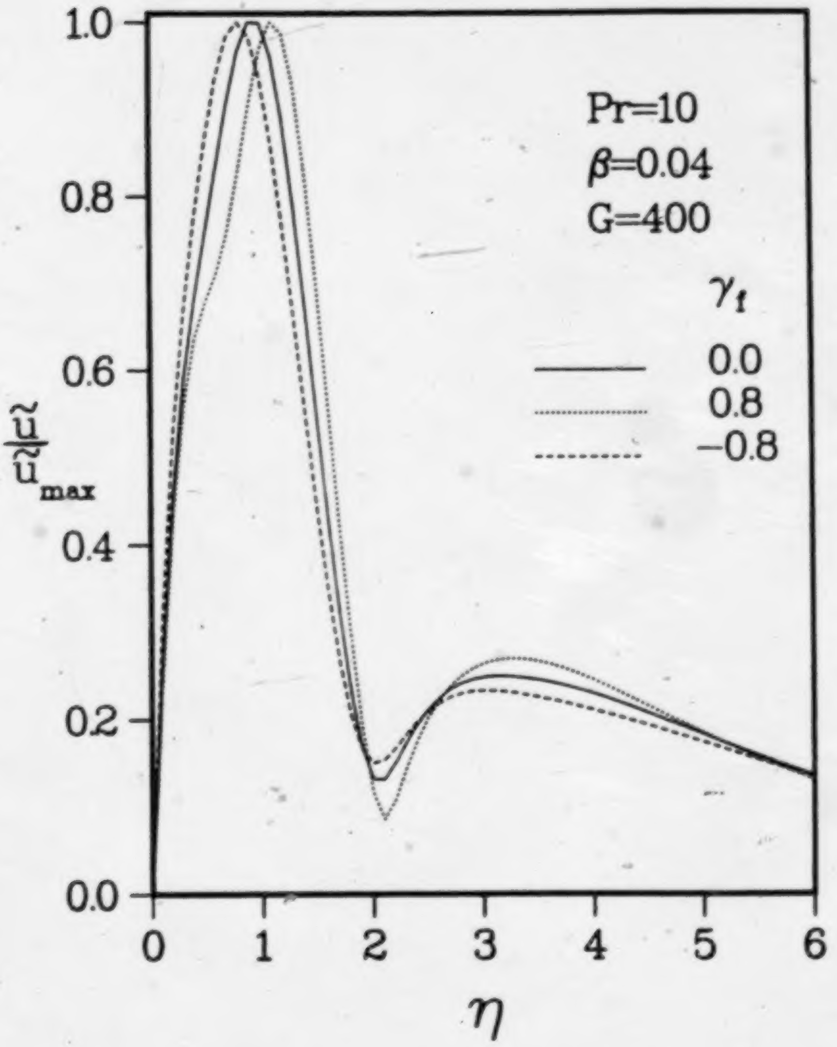

Fig. 3.6(d) The disturbance velocity profile for various values of γ_f when β=0.04, G=400 and Pr=10

al., 1970, and Colak-Antic and Gortler, 1971) and the present flow visualization studies (to be discussed later) indicate that the break-down of the vortices in the outer part of the laminar boundary layer causes the flow to become turbulent. Hence the base flow velocity boundary layer thickness may have an effect on the stability of the flow. But this is not evident from the disturbance velocity and temperature profiles. This may be due to the fact that the linear stability theory is valid only in the region where the flow is two-dimensional whereas the vortices acquire a three-dimensional character before breaking down into turbulent flow.

3.3.2 The Effects of Variation of Coefficient of Thermal Expansion with Temperature

As indicated earlier, for most liquids, and for water when both t_0 and t_∞ are larger than t_m, a negative value of ϵ_f denotes a cooled wall (down flow) and a positive value denotes a heated wall (up flow). The effects of ϵ_f on the base flow temperature and velocity profiles are shown in Figs. 2.4(c) and (d) and were discussed in detail in Chapter 2.

Figs. 3.7(a) to (d) show the stability planes for the cases of ϵ_f=0.5, -0.5, 1.0 and -1.0. Fig. 3.7(e) compares the neutral stability curves for various values of ϵ_f. A negative value of ϵ_f lowers the critical Grashof number for the onset of instability and a positive value increases it (see Fig. 3.7(e)). Hence a heated wall stabilizes the flow

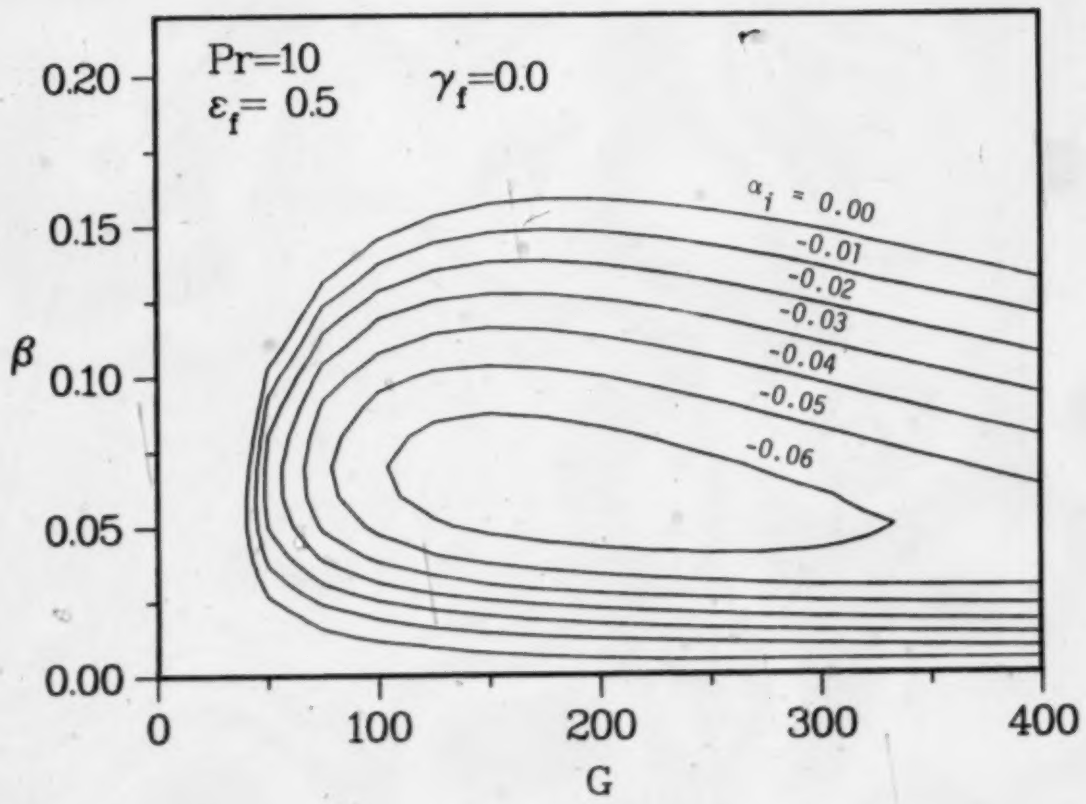

Fig. 3.7(a) The stability plane for Pr=10 and ϵ_f=0.5

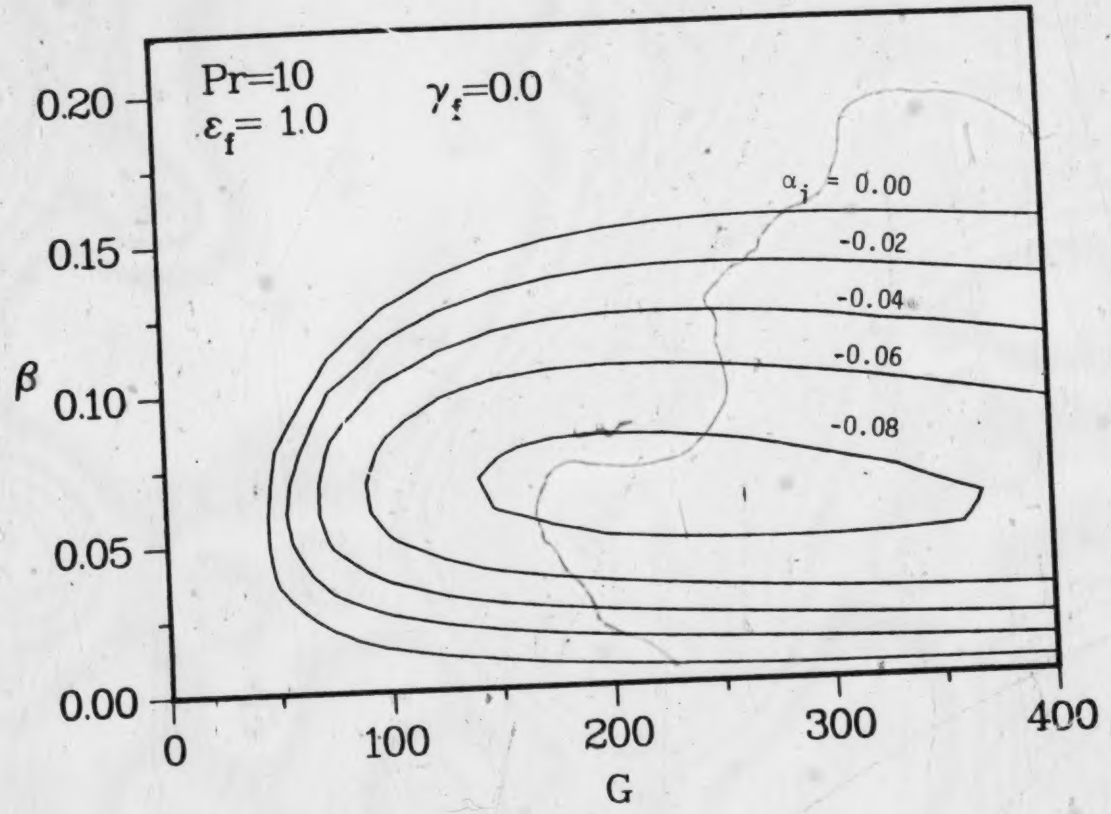

Fig. 3.7(b) The stability plane for Pr=10 and ϵ_f=1.0

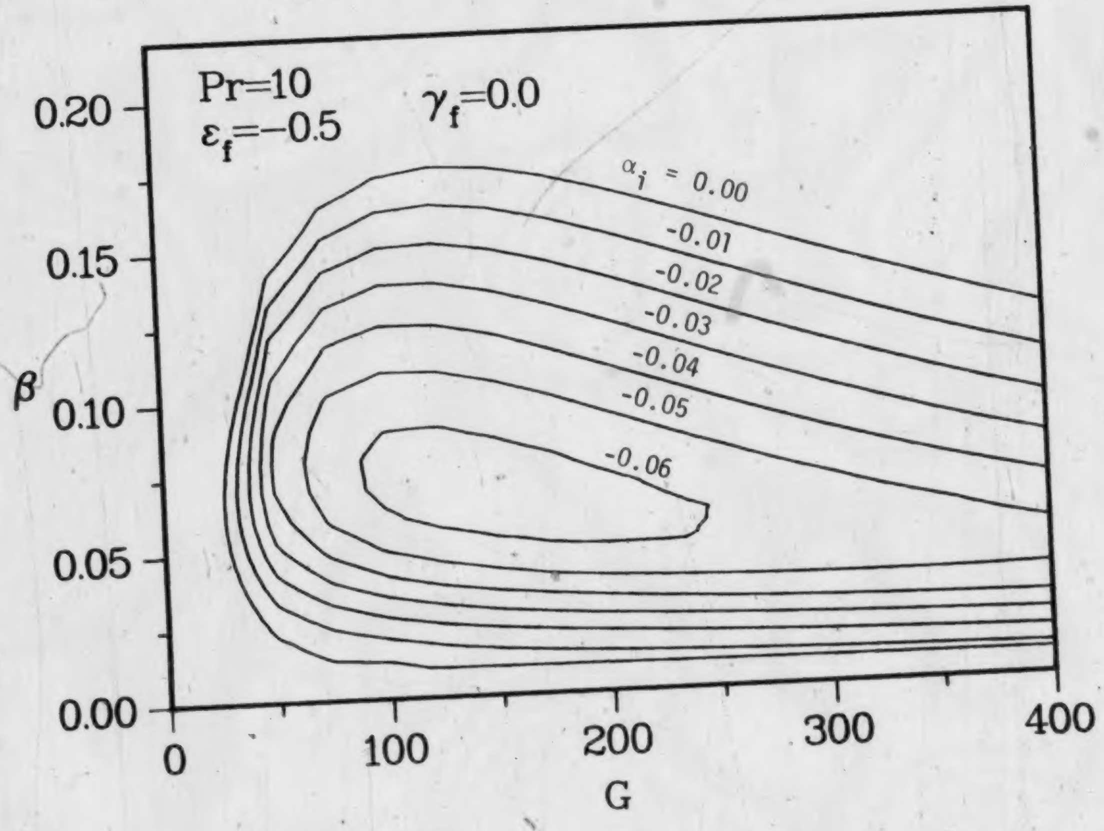

Fig. 3.7(c) The stability plane for Pr=10 and ϵ_f=-0.5

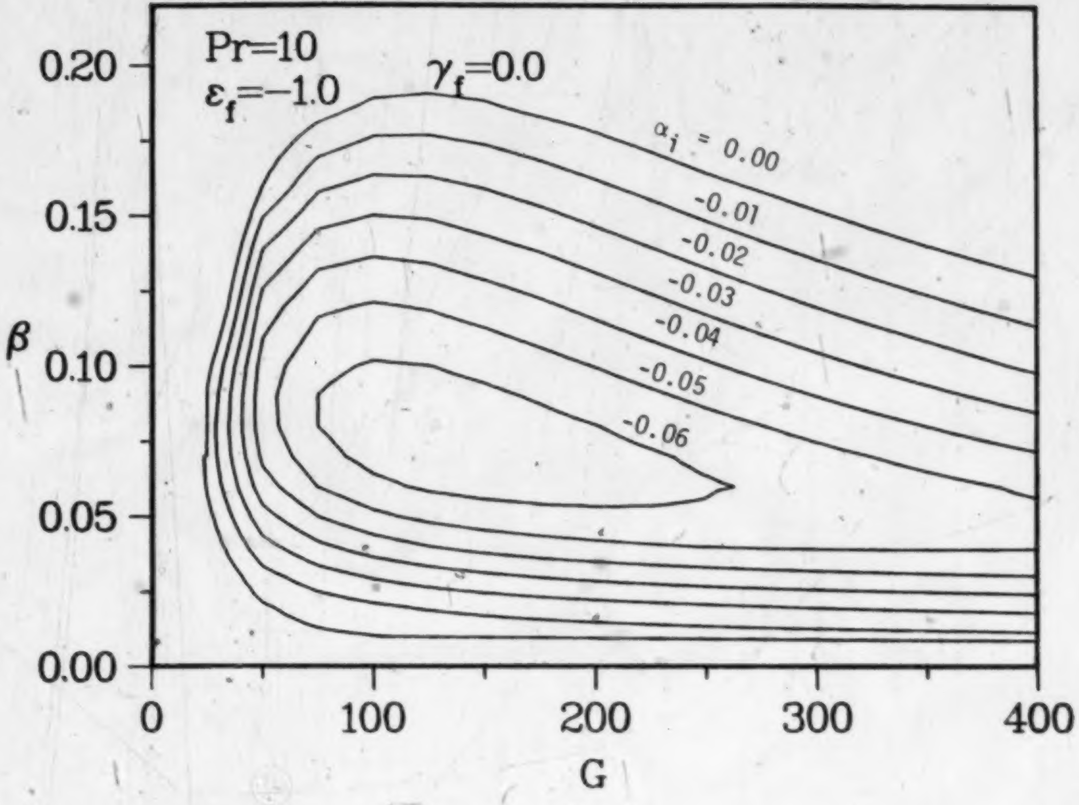

Fig. 3.7(d) The stability plane for Pr=10 and ϵ_f=-1.0

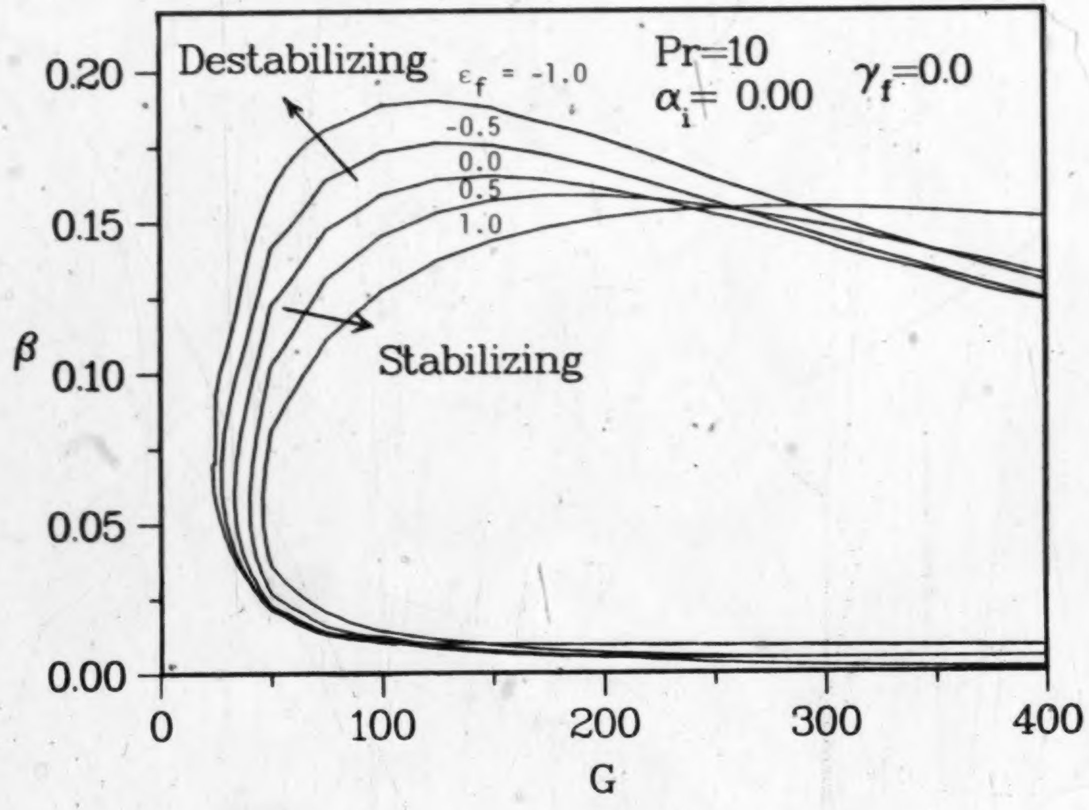

Fig. 3.7(e) The effects of ϵ_f on the neutral stability curve for Pr=10

initially and the cooled wall destabilizes it. But the values of α_i are lower for a heated wall (ϵ_f positive) than those for a cooled wall (ϵ_f negative) for the same temperature difference between the wall and the ambient liquid (see Figs. 3.7(b) and (d), for example). Hence, from eq. (3.51), the rate of amplification of the disturbance may be faster for a positive value of ϵ_f than for a negative value, at larger values of G.

It is also seen that the effect of ϵ_f is not as pronounced as that of γ_f (compare Figs. 3.4(c) and (e), and Figs. 3.7(b) and (d), for example). Hence, for most liquids, when the variation of the coefficient of thermal expansion is taken into consideration, the flow is initially more unstable for a cooled wall. But, as the disturbances amplify faster for a heated wall than for a cooled wall at downstream locations, the transition to turbulence may occur earlier for a heated wall than for a cooled wall.

Figs. 3.8(a) to (d) show typical disturbance temperature and velocity profiles. As before, the effect of the base flow velocity or temperature boundary layer thickness on the onset of instability and transition to turbulent flow is not evident from the disturbance profiles.

3.3.3 The Effects of Variations of Both the Viscosity and the Coefficient of Thermal Expansion with Temperature

For many liquids, in particular for water and aqueous solutions, both the viscosity and the coefficient of thermal expansion are strong functions of temperature. Hence it is

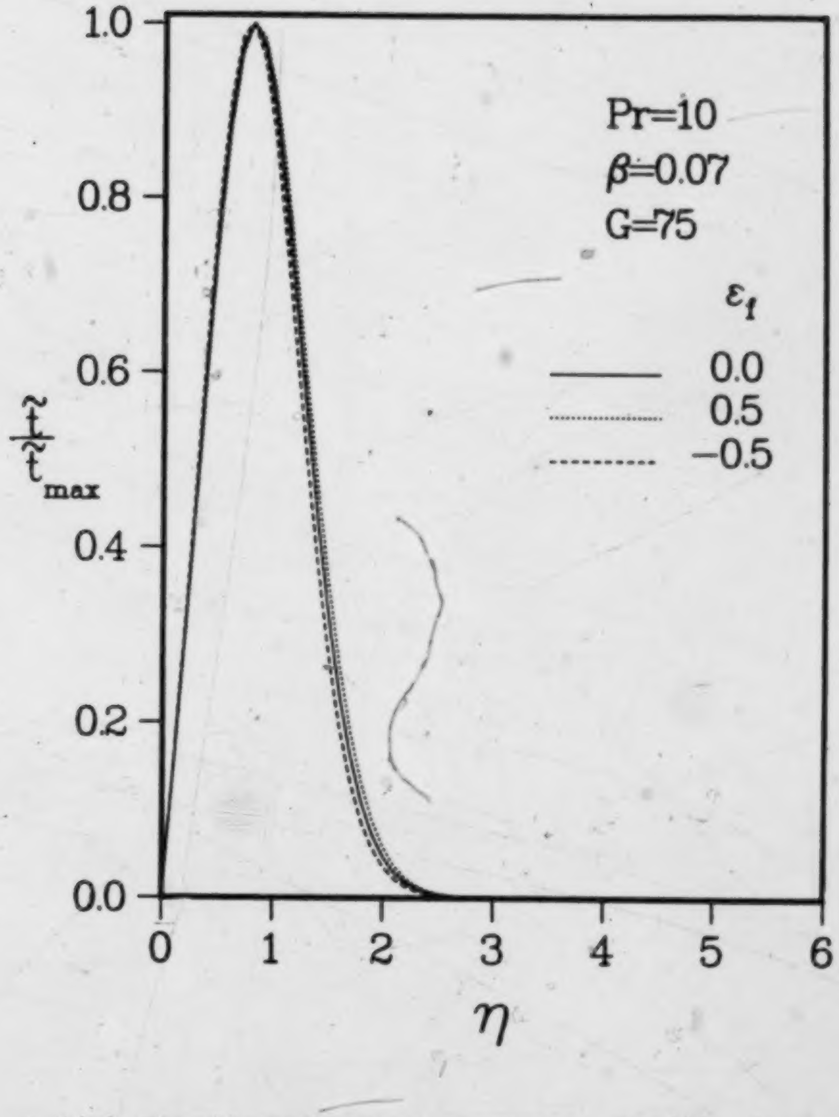

Fig. 3.8(a) The disturbance temperature profile for various values of ϵ_f when β=0.07, G=75 and Pr=10

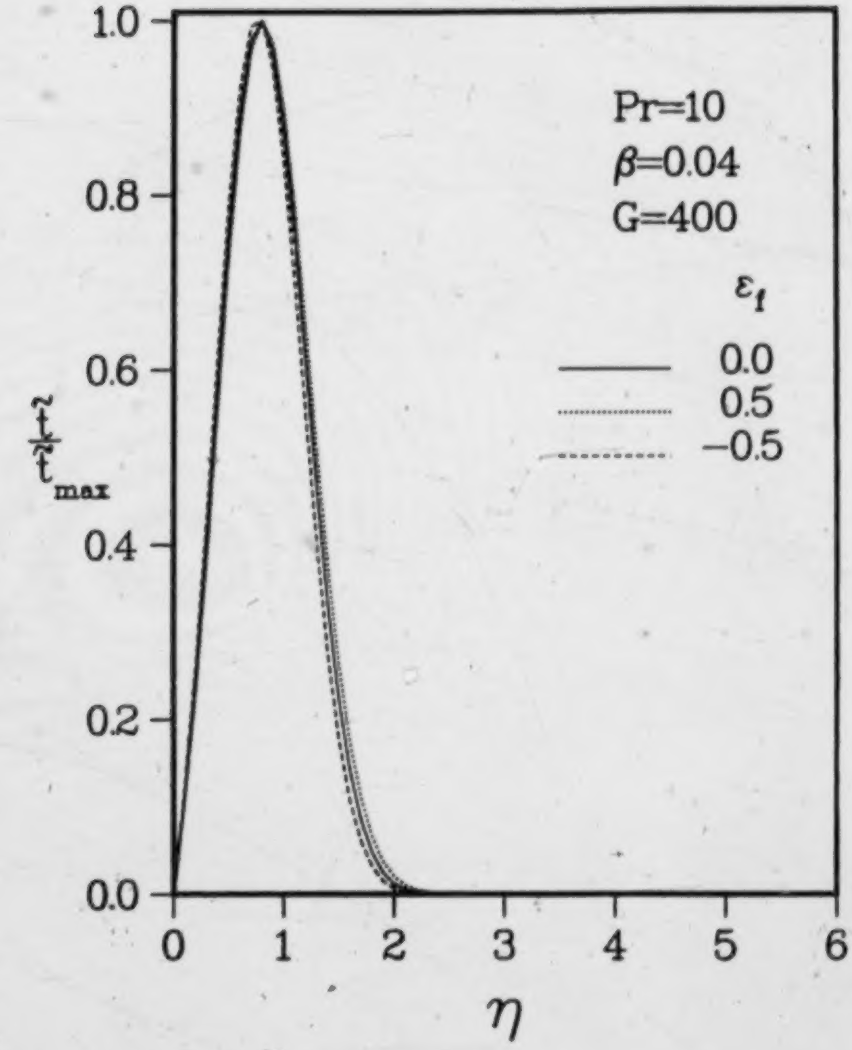

Fig. 3.8(b) The disturbance temperature profile for various values of ϵ_f when β=0.04, G=400 and Pr=10

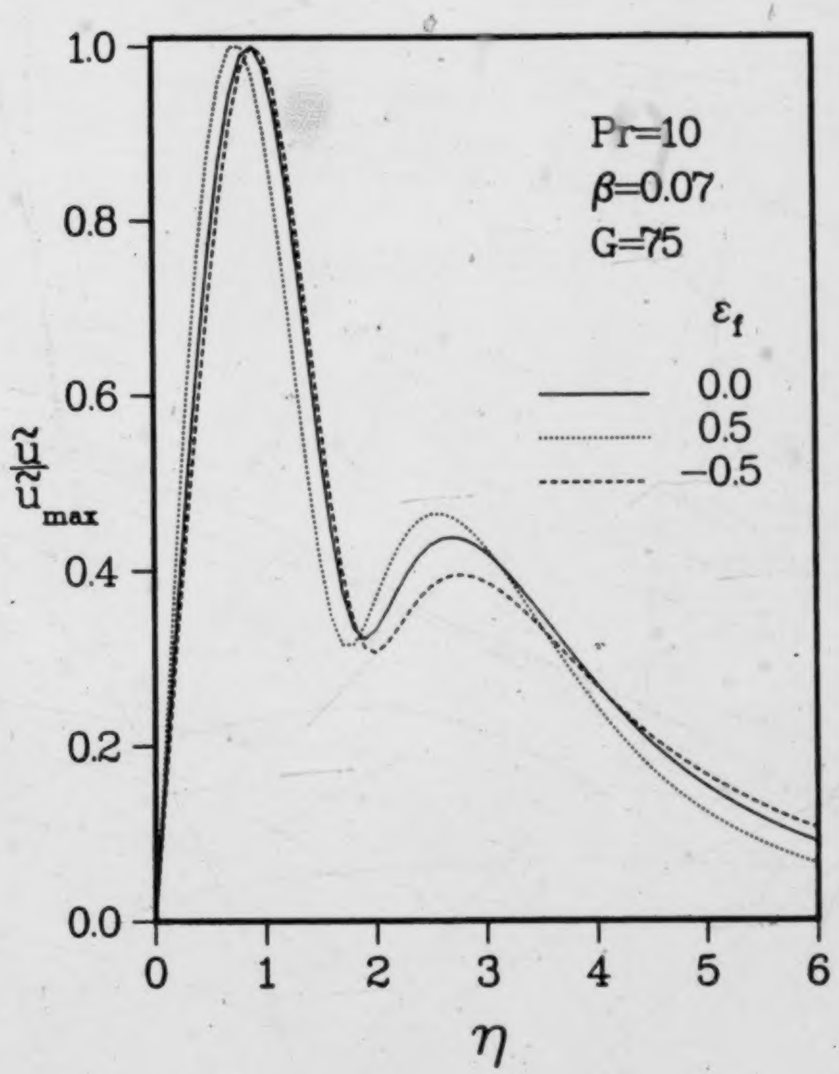

Fig. 3.8(c) The disturbance velocity profile for various values of ϵ_f when β=0.07, G=75 and Pr=10

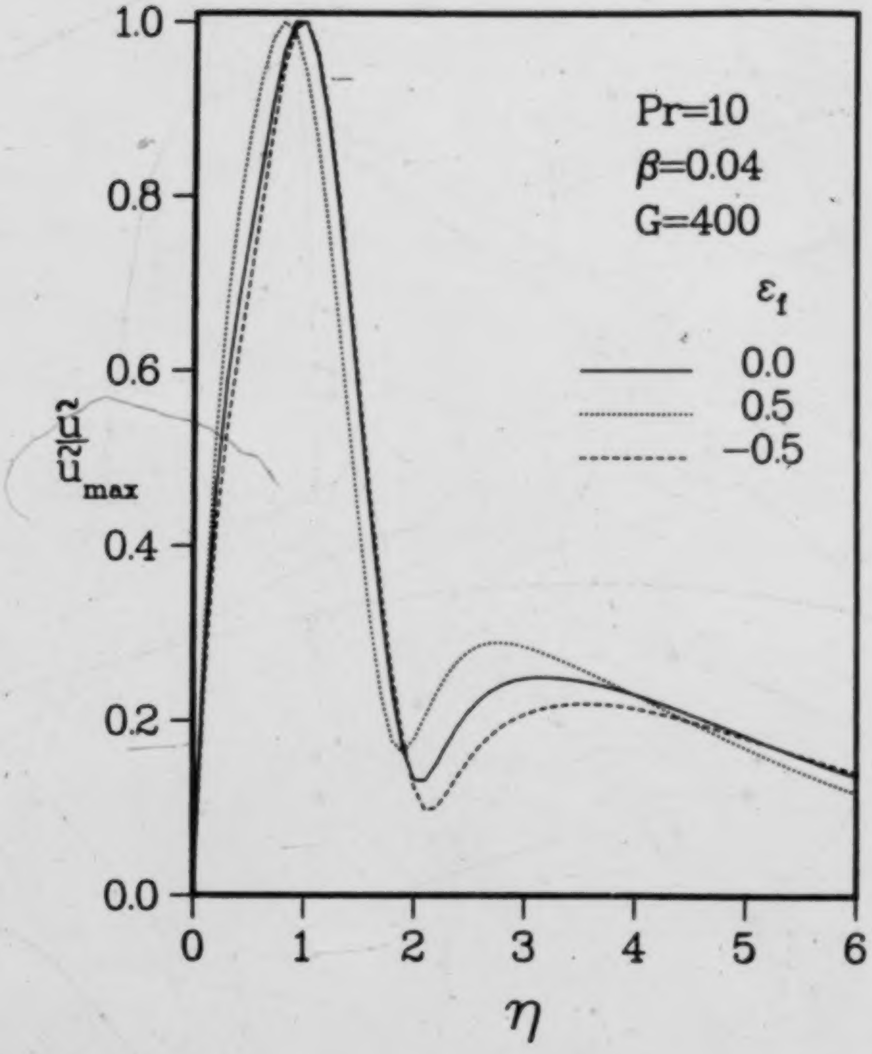

Fig. 3.8(d) The disturbance velocity profile for various values of ϵ_f when β=0.04, G=400 and Pr=10

important to study the effects of both γ_f and ϵ_f on the stability of laminar natural convective flow along an isothermal vertical flat plate.

Numerical results were obtained for a typical case of natural convective flow from an isothermal vertical flat plate in water for $t_f=20°C$ and $|t_0-t_\infty|=20°C$, with and without the variations of viscosity and coefficient of thermal expansion with temperature. The approximate values of γ_f and ϵ_f for a cooled wall are 0.50 and -0.55, respectively and for a heated wall, -0.50 and 0.55, respectively. The Prandtl number is approximately equal to 7. The case of $\gamma_f=\epsilon_f=0$ corresponds to Boussinesq approximations. The base flow temperature and velocity profiles are similar to the ones shown in Figs. 2.8(a) and (b).

Fig. 3.9 compares the contours of $\alpha_i=0.00$ and -0.05 for both heated and cooled walls with and without the effects of variable properties. It can be seen that for the cooled wall the critical Grashof number for the onset of instability is lower and the rate of amplification of disturbance is faster for the variable property case than for the constant property case. The frequency filtering mechanism is also more pronounced for the cooled wall. It is to be noted that when ϵ_f is positive the amplification of disurbances may be faster at downstream locations. Hence, the transition to turbulent flow may occur earlier for a heated wall when the effects of variable properties are considered.

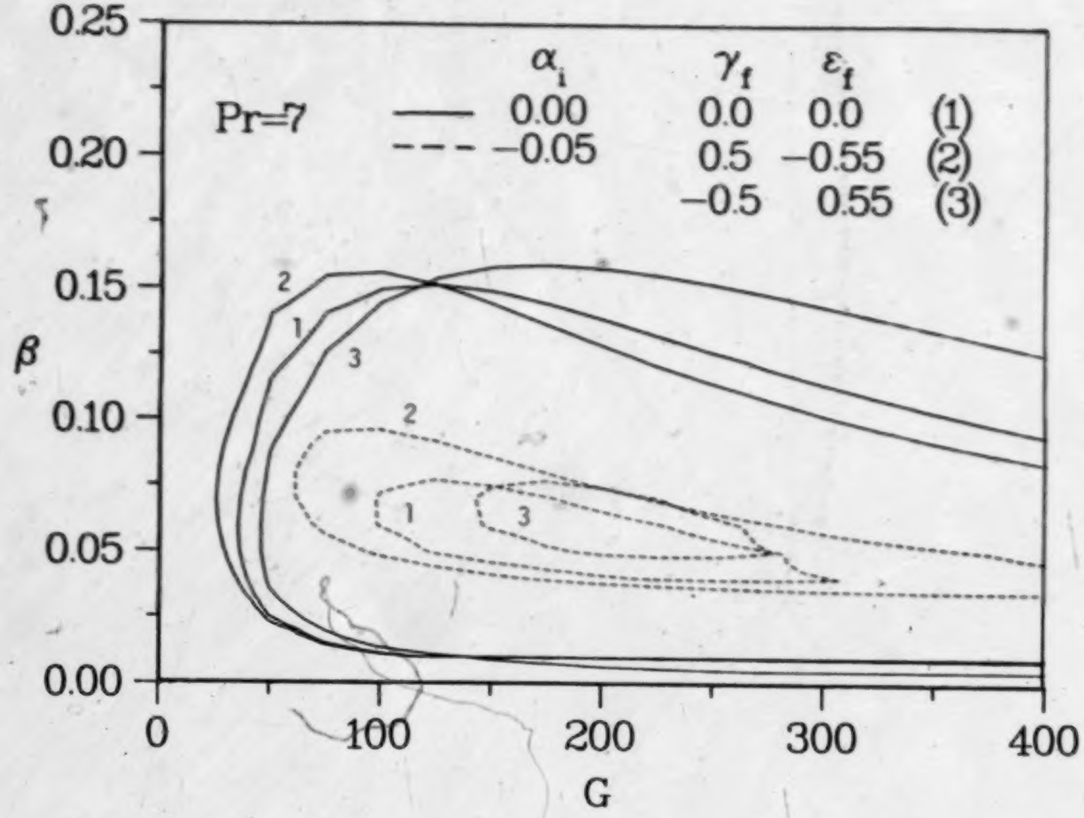

Fig. 3.9 The effects of both γ_f and ϵ_f on the stability of laminar natural convective flow of water, when t_f=20°C and $|t_0-t_\infty|$=20°C

3.3.4 Experimental Results

Experiments were conducted with an isothermal vertical circular cylinder of diameter 43.3 mm and length 1 m in water for various combinations of wall and ambient temperatures in the range 5 to 35°C. The flow was visualized by shadowgraph and dye injection techniques. Fig. 3.10(a) shows a typical shadowgraph when t_0=5.0°C and t_∞=28.0. The flow was completely laminar near the leading edge. For this case, at approximately 16.0 cm from the leading edge small oscillations on the dye were detected. This point was taken as the point of onset of instability.

As the disturbances moved downstream, they amplified with time and distance and became vortices. The vortices can be clearly seen in the range 30 cm to 55 cm from the leading edge. The vortices were mainly confined to the outer part of the boundary layer. This observation agrees with previous experimental studies in water by Fujii et al. (1970) and Colak-Antic and Gortler (1971). The break-down of these vortices causes the flow to become turbulent and it occurred in the range 55.0 cm to 57.5 cm from the leading edge, for the case shown in Fig. 3.10(a). As the flow was completely turbulent below 57.5 cm from the leading edge, this point was taken as the point of transition to turbulence for this case.

Fig. 3.10(b) shows the critical values of Rayleigh number for the onset of instability and the transition to turbulence for various temperature differences between the wall and the ambient medium. Fujii et al. (1970) showed that

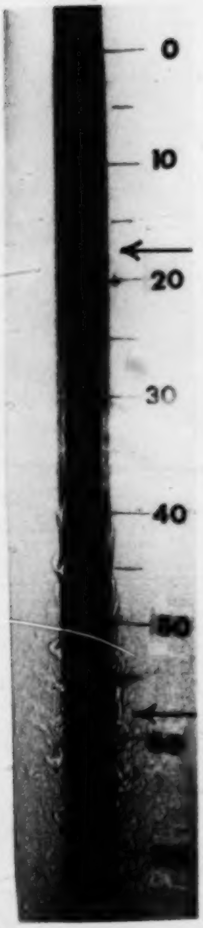

Onset of Instability

Transition to Turbulence

Fig. 3.10(a) Typical shadowgraph flow visualization photograph in water for $t_0=5.0°C$, and $t_\infty=28.0°C$ at steady state

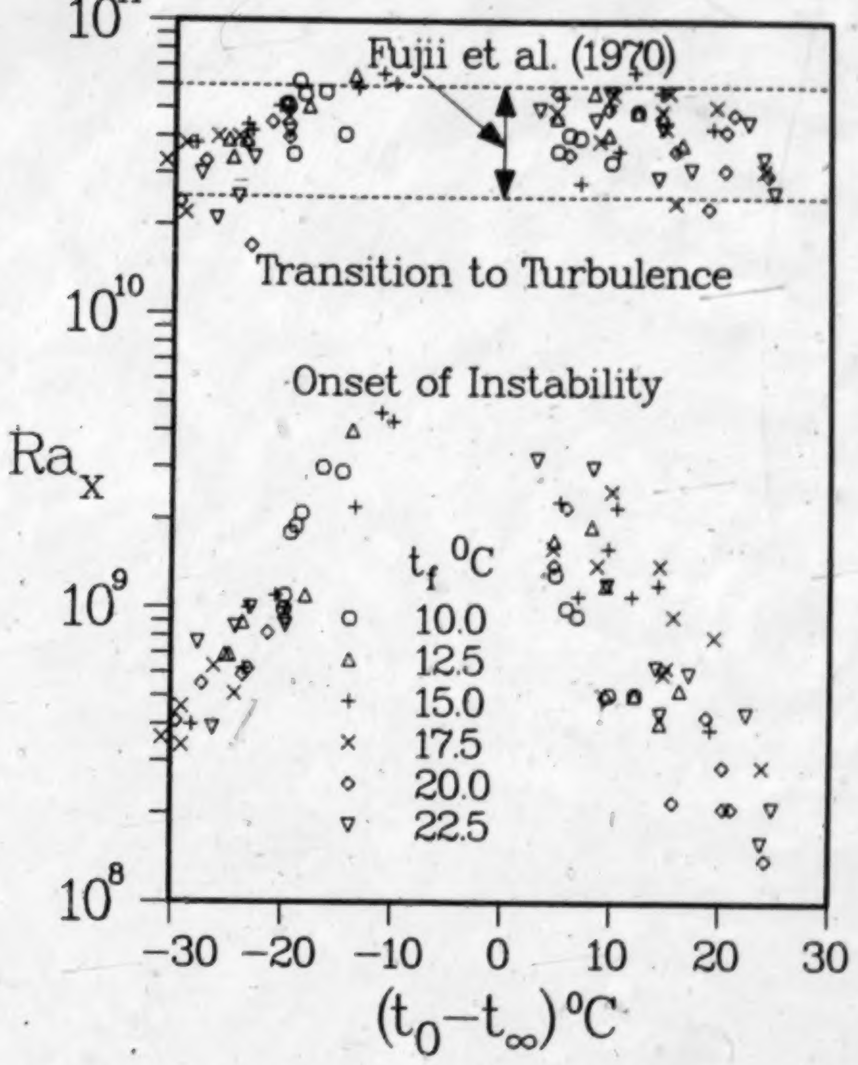

Fig. 3.10(b) The experimentally obtained critical values of Ra_x in water

the transition to turbulent flow occurs when the value of Ra_x is between (2 to 6) X 10^{10}. They also found this value to be independent of the liquids they studied (water, Mobiltherm oil and spindle oil). The critical values of Ra_x for the transtion to turbulent flow obtained in the present study are within the range of Fujii et al. (1970).

The critical values of Ra_x for the onset of instability obtained experimentally are 2 to 3 orders of magnitude higher than those obtained from the linear stability analysis (not shown in the figure). This is due to the fact that the naturally occurring disturbance can be detected experimentally only when its amplitude is finite whereas the linear stability theory assumes a infinitesimal value. From Fig. 3.10(b), it can be seen that the larger the temperature difference between the wall and the ambient medium, the lower is the critical value for both cooled and heated walls.

The theoretical analysis was done for a vertical flat plate whereas the experimental results were obtained for a vertical circular cylinder. The experimental values for the cylinder can assumed to be those of a vertical flat plate if the value of the parameter $(d/x)(Ra_x)^{1/4} > B$, where d is the outside diameter of the cylinder, x is the distance from the leading edge to the point of measurement and B is a constant (Jaluria, 1980). The local Nusselt numbers at the surface obtained experimentally by Fujii et al. (1970) for a circular cylinder (o. d. 80 mm) were within 1.3% of the values for a flat plate. The value of the constant B for the experiments conducted in the present study was within range of Fujii et al. (10 to 30 in the present experiments and 5 to 80 in Fujii et al.). Hence, the present experimental results for the cylinder may be assumed to correspond to those of a vertical flat plate.

3.4 Conclusions

The effects of temperature-dependent viscosity and coefficient of thermal expansion on the stability of laminar natural convective boundary layer flow of a liquid along an isothermal vertical flat plate were investigated numerically for various Prandtl numbers. The results indicated that the variation of viscosity with temperature destabilized the flow for a cooled wall and stabilized it for a heated wall. The frequency filtering mechanism was more pronounced for a cooled wall.

The variation of coefficient of thermal expansion with temperature lowered the critical Grashof number for the onset of instability for a cooled wall but the disturbance growth rate was faster for a heated wall. Hence, the variation of coefficient of thermal expansion with temperature initially stabilized the flow for a heated wall. But farther downstream it destabilized the flow. The trends of experimentally obtained critical values of Grashof number for the onset of instability and the transition to turbulent flow agreed with the numerical predictions.

It should be pointed out that the instability mode and the transition mechanism for the cylinder may be somewhat different from those of the flat plate. Hence, eventhough the flat plate is a special case of a circular cylinder with an infinite radius, the experimental results obtained in this study should be interpreted under this light.

4. The Effects of Maximum Density and Temperature-Dependent Viscosity on the Stability of Laminar Natural Convective Flow of Cold Water Along an Isothermal Vertical Surface

As the natural convective flows arise due to a density difference arising from a temperature or concentration difference, an accurate description of the density as a function of temperature or concentration is important. This is especially true in the case of water near its density maximum. In Chapter 3, the effects of temperature-dependent viscosity and coefficient of thermal expansion on the stability of laminar natural convective flow along an isothermal vertical surface were studied. As explained in Chapter 2, the theoretical formulation for the variation of coefficient of thermal expansion with temperature that was used in Chapter 3 may not be valid when there is a density maximum.

In this Chapter, the stability of laminar natural convective boundary layer flow of cold water along an isothermal vertical flat plate is studied employing the new density relationship suggested by Mollendorf and Gebhart (1977). The effects of both the density maximum and the temperature-dependent viscosity are examined. Various combinations of wall and ambient temperatures in the range 0 to 20°C are considerd. In particular, the flow from an isothermal wall at 0°C, corresponding to an ice surface, is studied in detail. The stability characteristics of the flow with and without buoyancy force reversals inside the thermal boundary layer are analyzed.

4.1 Theoretical Analysis

4.1.1 Variations of Density and Viscosity of Cold Water with Temperature

For pure water at 1 atmospheric pressure, Gebhart and Mollendorf (1977) have shown that the following the density-temperature relationship accurately correlates the density in the temperature range 0 to 20°C.

$$\rho(t)=\rho_m(1-\alpha_t|t-t_m|^q) \qquad (4.1)$$

where $q=1.8949$, $\alpha_t=9.2972 \times 10^{-6}$ and $t_m=4.0293°C$ (t_m is the temperature corresponding to the density maximum).

The viscosity of water is a strong function of temperature. For example, the viscosity of water decreases by 80% as the temperature increases from 0°C to 20°C. Hence, it is important to include the effects of temperature-dependent viscosity in the analysis. For moderate temperature differences between the wall and the ambient water (~ 10 to 20°C), one can assume that the viscosity may be approximated by a linearized Taylor series expansion about a reference temperature, say, the film temperature. The linearized approximation about the film temperature was given in eq. (3.24).

4.1.2 Governing Equations

The coordinate system is the same as the one shown in Fig. 2.1. With the density formulation for the cold water as shown in eq. (4.1), the base flow equations and the boundary conditions, corresponding to eqs. (3.20) to (3.22) are,

$$\frac{d}{d\eta}\left[\frac{\mu}{\mu_f} F''\right] + 3FF'' - 2(F')^2 \pm [|\theta - R|^q - |R|^q] = 0 \quad (4.2)$$

$$\theta'' + 3PrF\theta' = 0 \quad (4.3)$$

$$F(0)=F'(0)=\theta(0)-1=F'(\infty)=\theta(\infty)=0 \quad (4.4)$$

where $$Gr_x = \frac{g\alpha_t |t_0 - t_\infty|^q \, x^3}{\rho_0 \nu_f^2}, \quad G = 4\left[\frac{Gr_x}{4}\right]^{1/4}$$

$$\eta = \frac{Gy}{4x}, \quad \bar{\psi} = \nu_f G \, F(\eta), \quad \theta = \frac{\bar{t} - t_\infty}{t_0 - t_\infty}$$

$$R = \frac{t_m - t_\infty}{t_0 - t_\infty}, \quad \bar{u} = \frac{\partial \bar{\psi}}{\partial y}, \text{ and } \bar{v} = -\frac{\partial \bar{\psi}}{\partial x}$$

The prime denotes differentiation with respect to η and ± denotes up and down flows, respectively. The temperature parameter R indicates the proximity of the temperatures t_0 and t_∞ to t_m. For given values of t_0 and t_∞, a large absolute value of R (say, $|R|>8$) indicates a condition remote from the maximum density region. For smaller values of |R|, the effect of maximum density becomes important. The range of values of R for which the flow reversals occur has been discussed in detail by Carey et al. (1980).

As shown in the previous chapter, the disturbance equations were obtained by employing the assumptions involved in linear stability theory, such as small disturbances and parallel flow approximation. Assuming the disturbances to be two-dimensional travelling waves and non-dimensionalizing the variables the disturbance equations become,

$$\begin{aligned} \left[\frac{\mu}{\mu_f}\right]\left[\phi'''' - 2\,\alpha^2\phi'' + \alpha^4\phi\right] = \\ i\alpha G[(F'-c)(\phi''-\alpha^2\phi)-F'''\phi] \\ - 2\left[\frac{\mu}{\mu_f}\right]'(\phi'''-\alpha^2\phi') - \left[\frac{\mu}{\mu_f}\right]''(\phi''+\alpha^2\phi) \\ \mp\left[q\frac{(\theta-R)}{|\theta-R|}\,|\theta-R|^{q-1}s' + q(q-1)|\theta-R|^{q-2}s\theta'\right] \end{aligned} \tag{4.5}$$

$$s'' - \alpha^2\,s = i\alpha GPr[(F'-c)s - \phi'\theta'] \tag{4.6}$$

$$\phi(0)=\phi'(0)=s(0)=\phi(\infty)=\phi'(\infty)=s(\infty)=0 \tag{4.7}$$

Higgins and Gebhart (1983) studied the stability of laminar natural convective boundary flow of cold water along an isothermal vertical flat plate for small temperature differences (~5°C). They neglected the effects of variation of viscosity with temperature. In the present study, a more detailed analysis of the stability of the natural convective boundary layer flow along a vertical flat plate is done including the effects of variation of viscosity with temperature. Various combinations wall and ambient water temperatures in the range 0° to 20°C are considered. In particular, the flow from a wall at 0°C corresponding to an ice surface is studied in detail.

4.1.3 Numerical Method

The numerical method employed to solve the base flow and the disturbance equations is the same as the one shown in the previous chapter. With the density formulation as shown in eq. (4.1), the solutions to the base flow eqs. (4.2) to (4.4) at large η, corresponding to eqs. (3.38) and (3.39), are given by,

$$F = A + C\, e^{-3A\eta/\lambda} \pm \frac{B\, R\, |R|^{q-2}}{[27A^3 Pr^2 (\lambda Pr-1)]}\, e^{-3APr\eta} \qquad (4.8)$$

$$\theta = B\, e^{-3APr\eta} \qquad (4.9)$$

where $\lambda = 1-\frac{\gamma_f}{2}$, and A, B, and C are real constants.

The integrals ϕ_1, ϕ_2, ϕ_3, s_1, s_2 and s_3, corresponding to eqs. (3.42) to (3.47), were obtained from the solution of disturbance eqs. (4.5) to (4.7) at large values of η. They are given by

$$\phi_1 = e^{-\alpha\eta} \tag{4.10}$$

$$\phi_2 = e^{-\alpha_2\eta} \tag{4.11}$$

$$\phi_3 = \pm\,\frac{q(\alpha_3/\lambda)\ R|R|^{q-2}\ e^{-\alpha_3\eta}}{[(\alpha_3^2-\alpha^2)(\alpha_3^2-\alpha_2^2)]} \tag{4.12}$$

$$s_1 = \frac{i\alpha PrG\theta'_\infty\ e^{-\alpha\eta}}{[\alpha_3^2\ -(3APr+\alpha)^2]} \tag{4.13}$$

$$s_2 = \frac{i\alpha PrG\theta'_\infty\ e^{-\alpha_2\eta}}{[\alpha_3^2\ -(3APr+\alpha_2)^2]} \tag{4.14}$$

$$s_3 = e^{-\alpha_3\eta} \tag{4.15}$$

where $\alpha_2 = +\left[\alpha^2-\frac{i\alpha cG}{\lambda}\right]^{1/2}$ and $\alpha_3 = +\left[\alpha^2-i\alpha cPrG\right]^{1/2}$

4.2 Results and Discussion

The equations (4.3) to (4.8) were solved numerically, and the neutral stability curves and the constant amplification contours were obtained for three diiferent cases,

(a): both t_0 and t_∞ are below t_m,

(b): both t_0 and t_∞ are above t_m, and

(c): t_0 and t_∞ are on the opposite sides of t_m.

There is no buoyancy force reversal across the thermal boundary layer for the cases (a) and (b). The buoyancy force may reverse inside the thermal boundary layer in case (c) due to the presence of the density maximum. Both cooled and heated walls were examined. Stability analysis was done only for the cases with no flow reversals. When there is a flow reversal, the boundary layer approximation itself may not be valid and flow may not be steady as shown by Carey et al. (1980).

Fig. 4.1 shows typical base flow temperature and velocity profiles for various t_∞ when $t_0=0$°C. For up flows there is a buoyancy force reversal at the edge of the boundary layer when t_∞ is greater than t_m. For down flows the buoyancy force reversal occurs near the wall.

4.2.1 Neutral Stability Curves When Both t_0 and t_∞ are Below or Above t_m

Figs. 4.2(a) and 4.3(a) show the nose region of the neutral stability curves for various values of t_∞ when $t_0=0$°C and 5°C, respectively. Figs. 4.2(b) and 4.3(b) show the nose region of the neutral stability curves for various values of t_0 when $t_\infty=0$ and 5°C, respectively. Figs. 4.2(c) and 4.3(c) show the dimensionless buoyancy force at all points inside the thermal boundary layer for the cases shown in Figs. 4.2(a) and (b), and Figs. 4.3(a) and (b), respectively. The flow is up for the cases shown in Figs. 4.2(a) and 4.3(b), and is down in Figs. 4.2(b) and 4.3(a). For given values of t_f and $|\Delta t|$, the down flows are more unstable than up flows. This is due to the fact that the

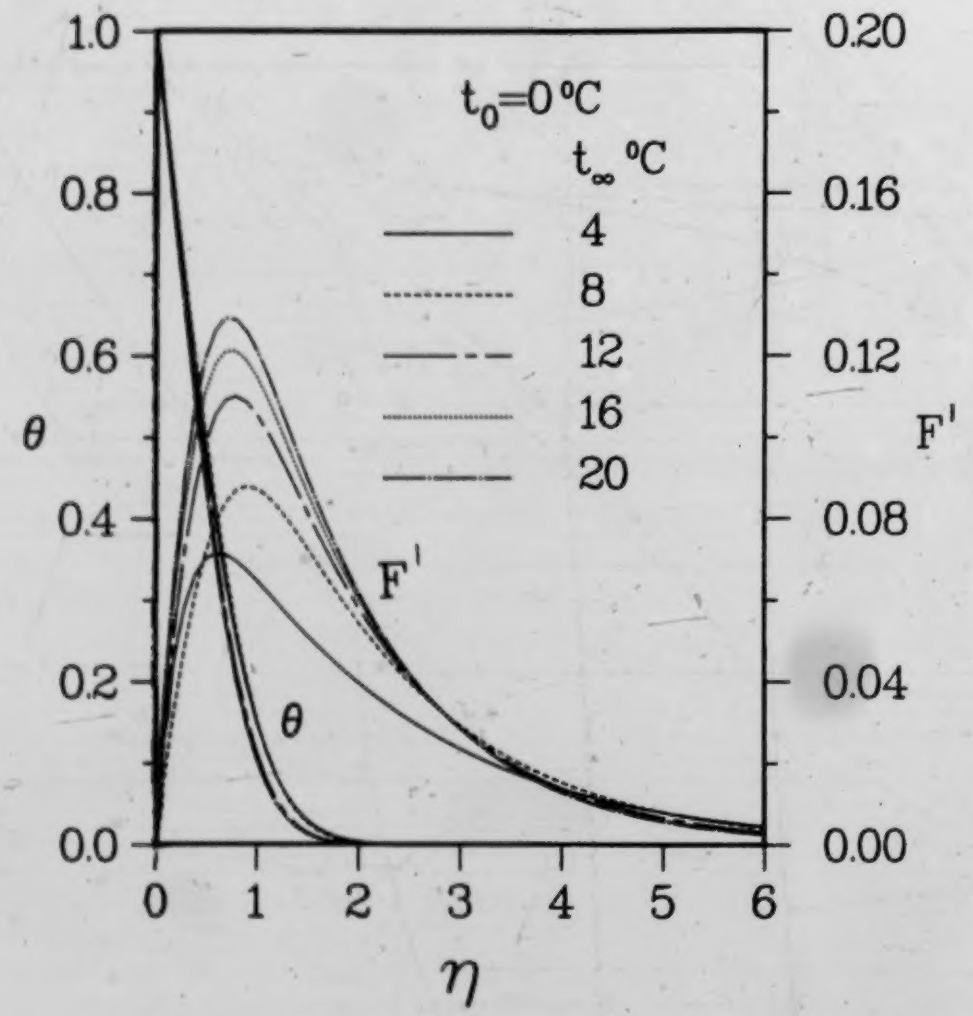

Fig. 4.1 Typical base flow temperature and velocity profiles for various values of t_∞ when t_0=0°C

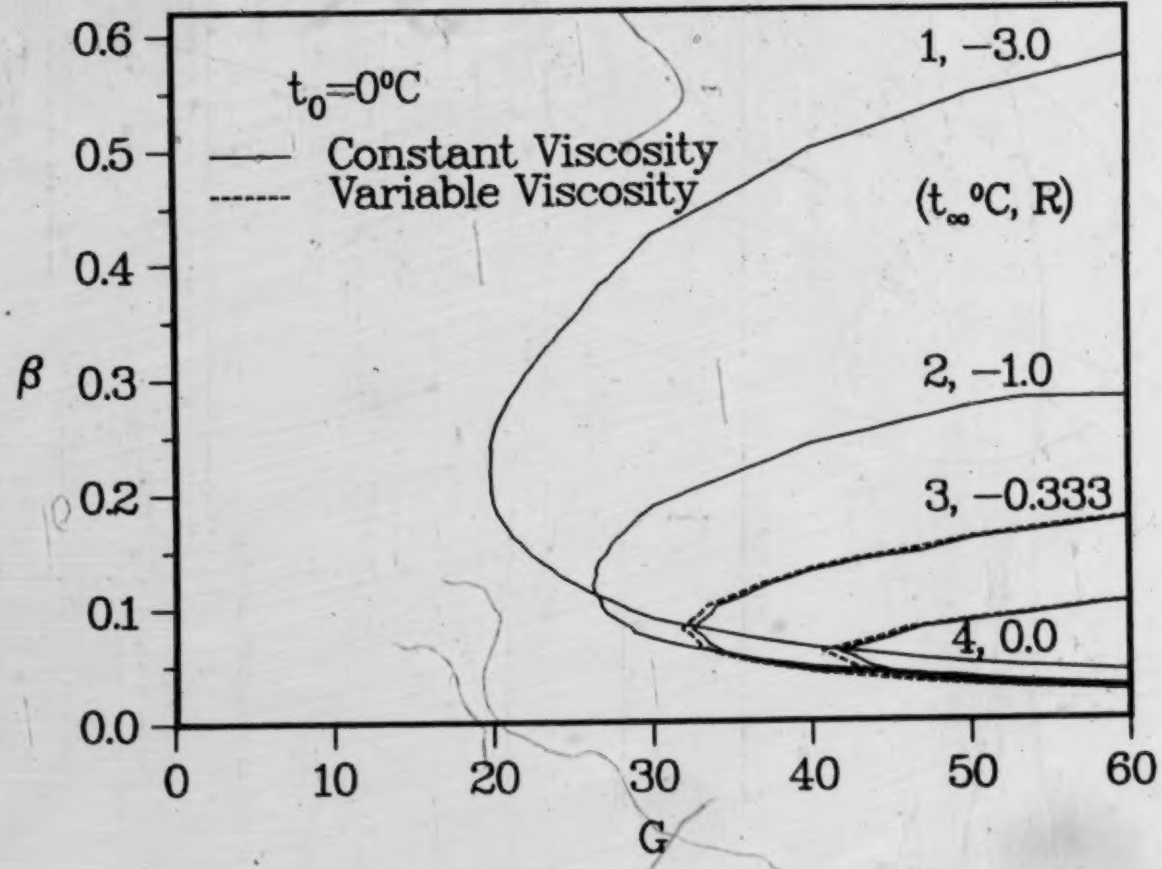

Fig. 4.2(a) The neutral stability curves for various values of $t_\infty (< t_m)$ when $t_0 = 0$°C

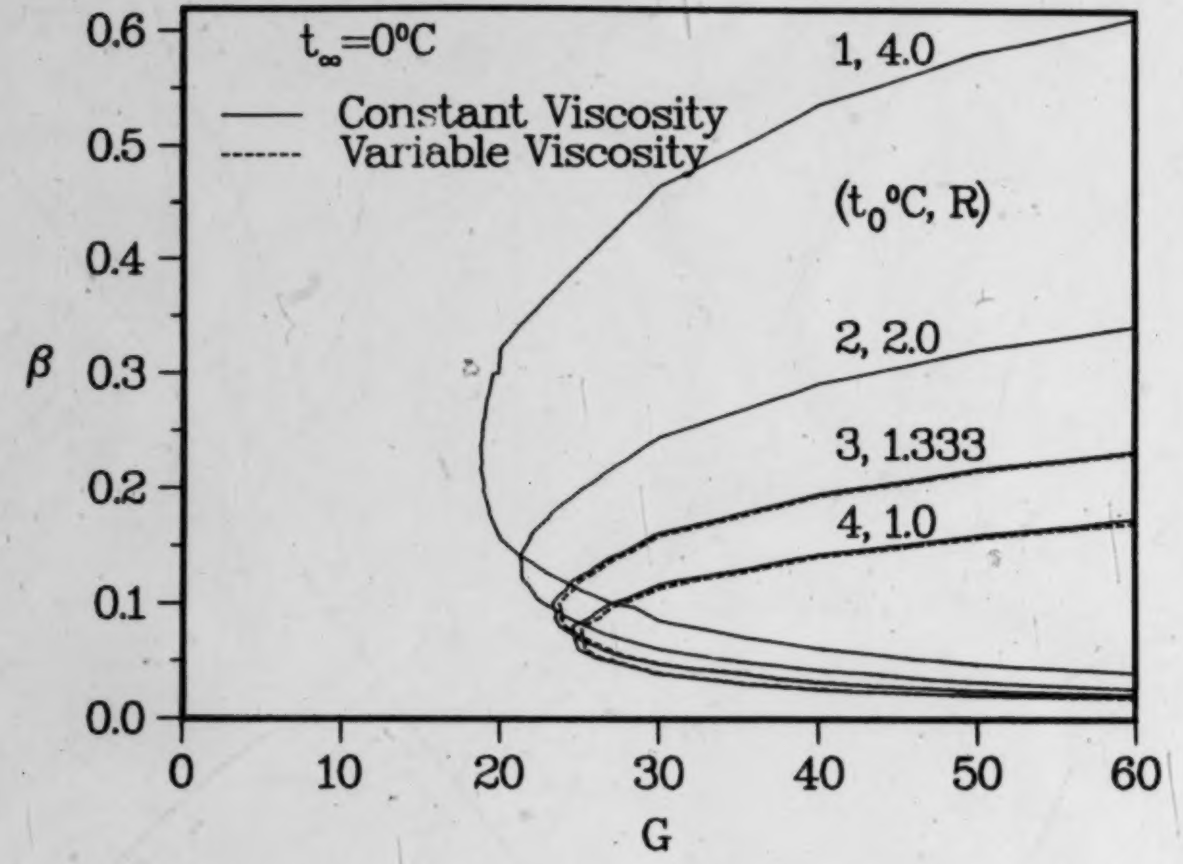

Fig. 4.2(b) The neutral stability curves for various values of $t_0(<t_m)$ when $t_\infty=0$°C

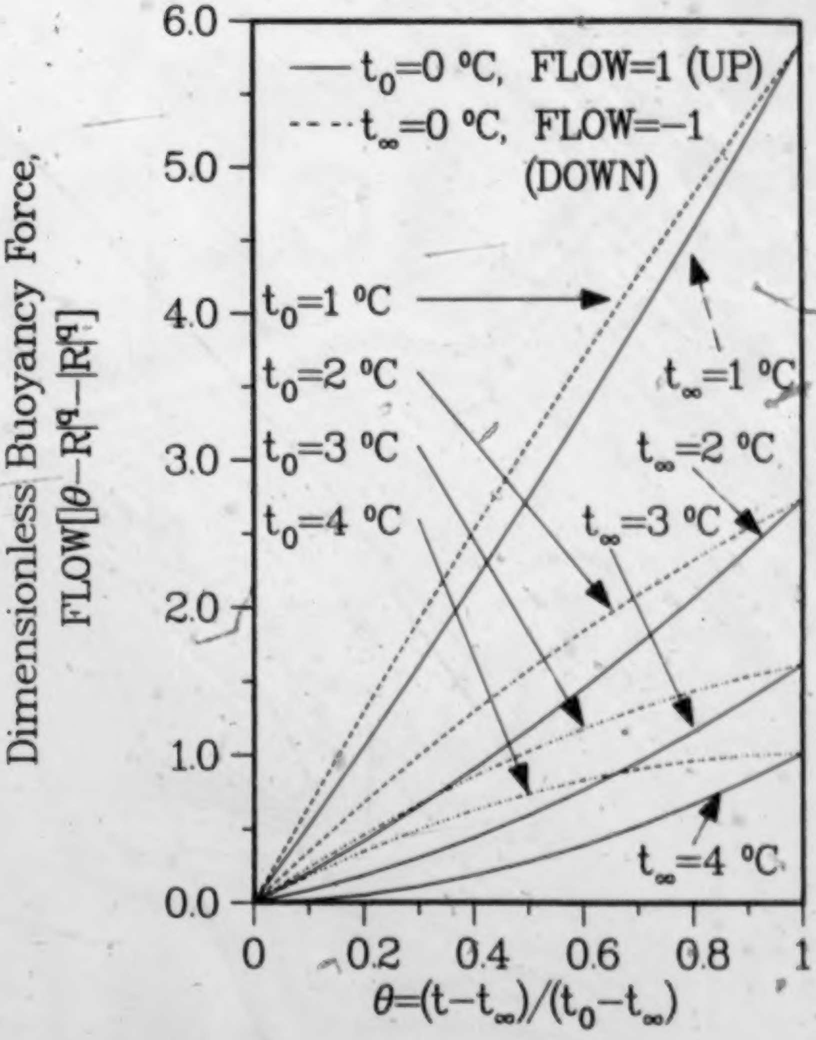

Fig. 4.2(c) The dimensionless buoyancy force when both t_0 and t_∞ are below t_m

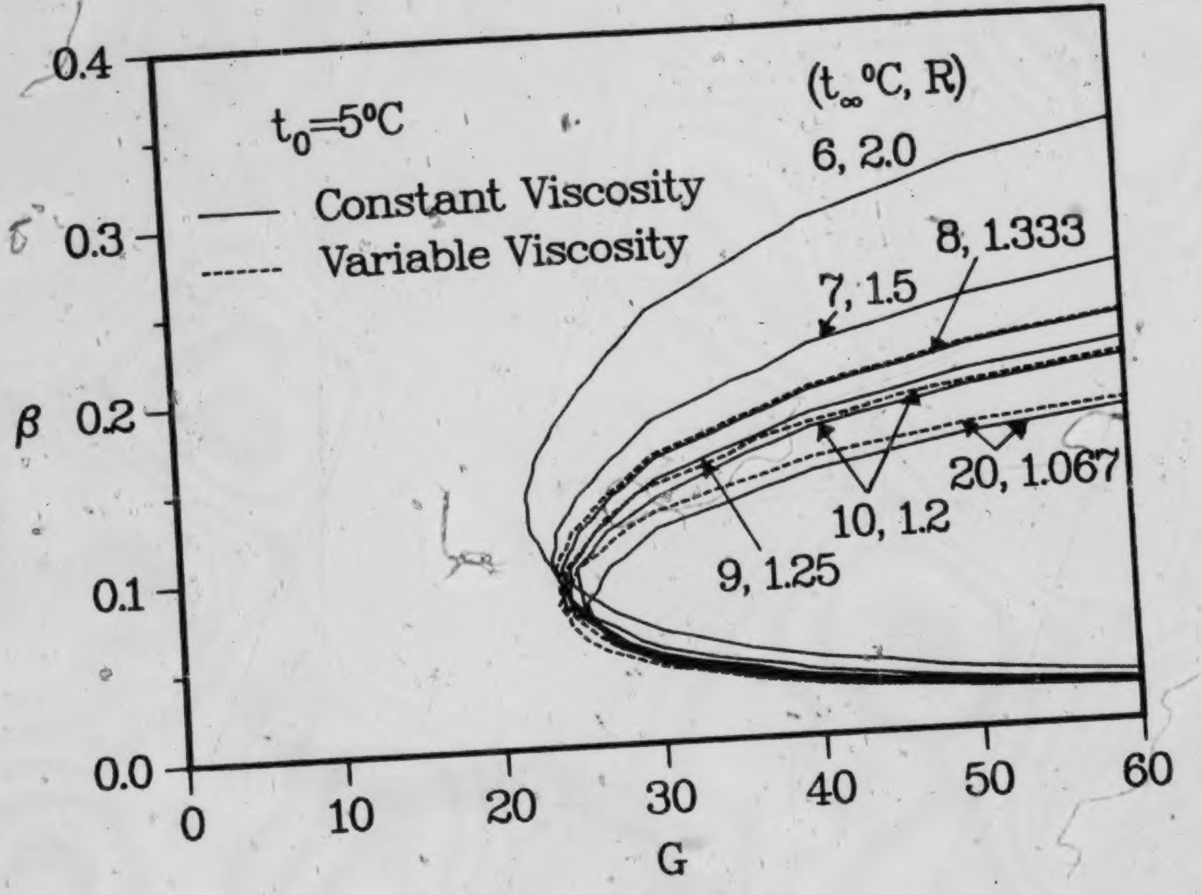

Fig. 4.3(a) The neutral stability curves for a cooled wall with t_0=5°C

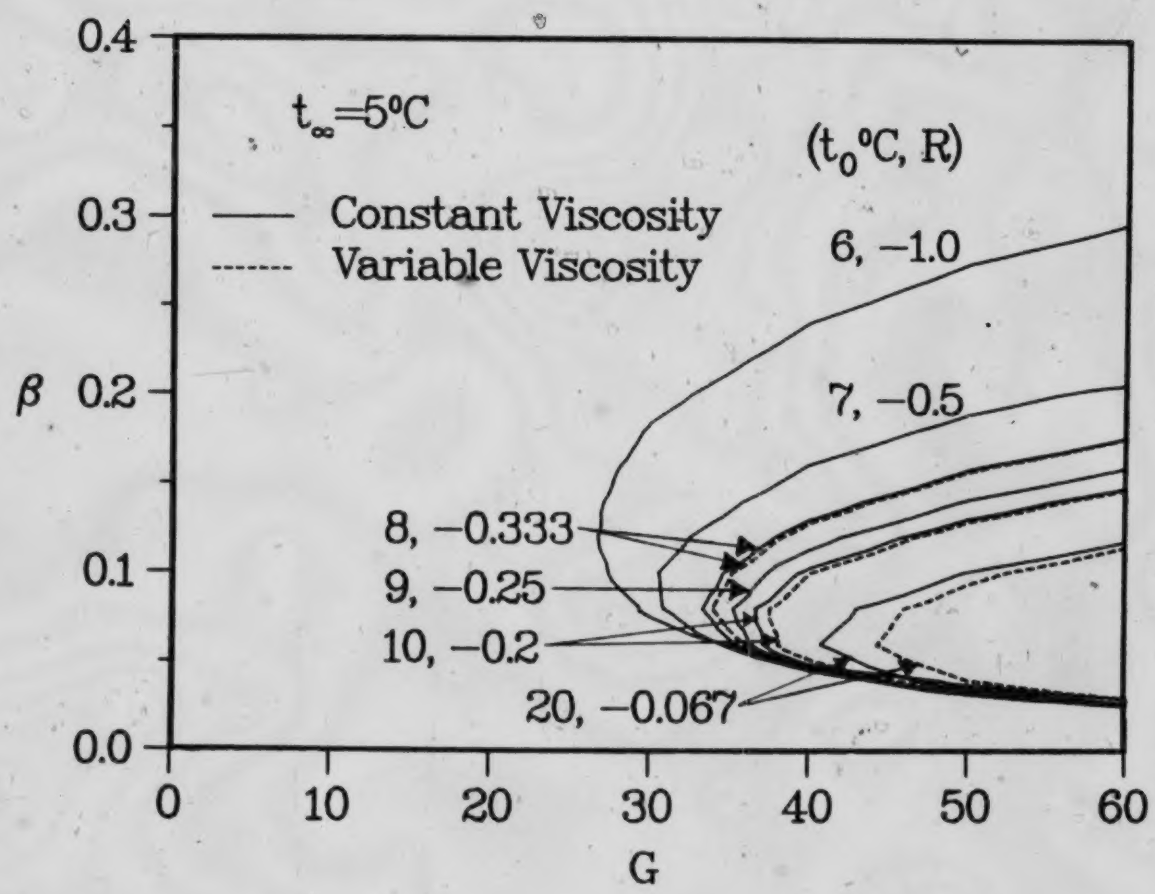

Fig. 4.3(b) The neutral stability curves for a heated wall when t_∞=5°C

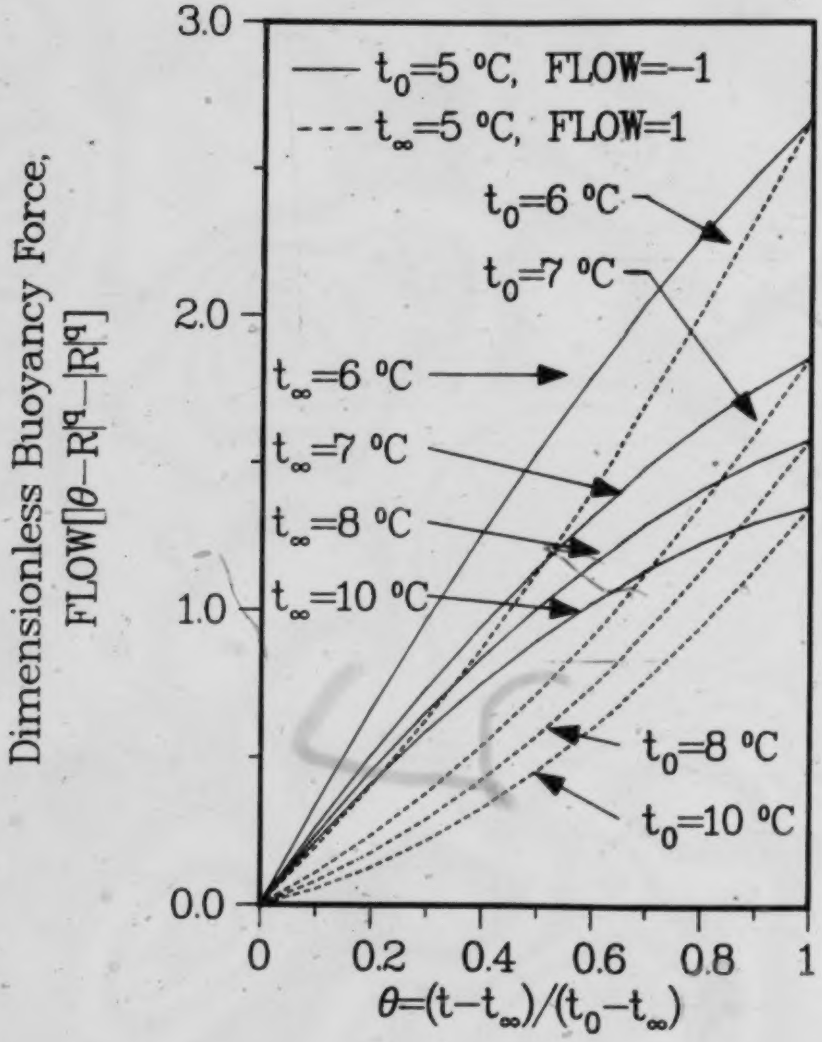

Fig. 4.3(c) The dimensionless buoyancy force when both t_0 and t_∞ are above t_m

dimensionless buoyancy force is larger for down flows than for up flows (see Figs. 4.2(c) and 4.3(c)). This is similar to the effect of variation of coefficient of thermal expansion with temperature which was discussed in the previous chapter. For a given value of t_0 or t_∞, the flow is more unstable for smaller values of $|\Delta t|$ than for larger ones. Also the flow is unstable to a wide range of frequencies for smaller values of $|\Delta t|$.

4.2.2 Neutral Stability Curves When t_0 and t_∞ are on the Opposite sides of t_m

The instability analysis was done only for those combinations of t_0 and t_∞ for which there are no flow reversals. Fig. 4.4(a) shows the nose region of the neutral stability curves for various values of t_∞ ($>t_m$) when $t_0=0°C$. The flow is down for the cases shown. The flow is more unstable when t_∞ is closer to t_m. Also, the frequency filtering mechanism is more pronounced when t_∞ is closer to t_m. Fig. 4.4(b) shows the nose region of the neutral stability curves for various values of t_0 ($>t_m$) when $t_\infty=0°C$. The flow is down for the cases shown. The flow is more unstable when t_0 is farther away from t_m than when it is nearer to t_m. The flow is unstable to a wider range of frequencies when t_0 is farther away from t_m.

Fig. 4.4(c) shows the dimensionless buoyancy force at all points inside the thermal boundary layer for the cases shown in Figs. 4.4(a) and (b). When t_0 and t_∞ are on the opposite sides of t_m, the flow becomes more unstable when

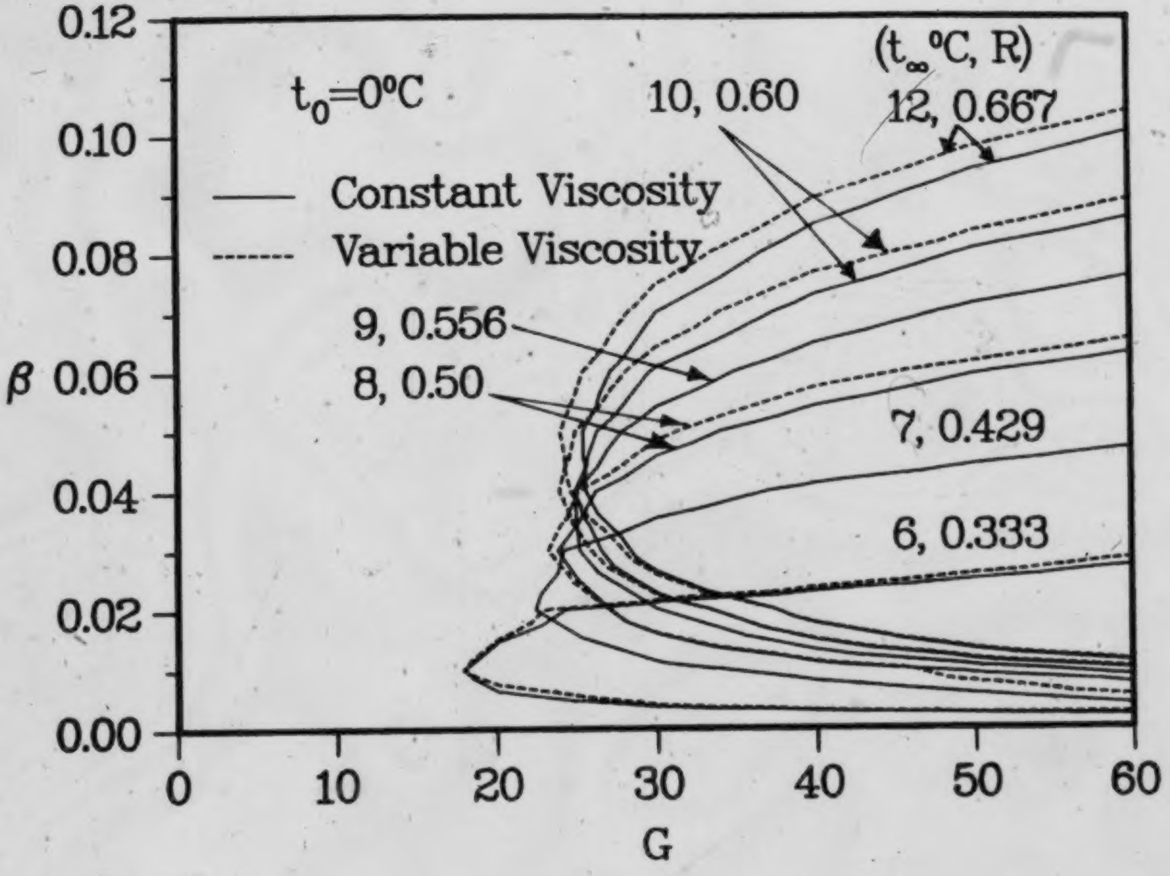

Fig. 4.4(a) The neutral stability curves for various values of t_∞($>t_m$) when t_0=0°C

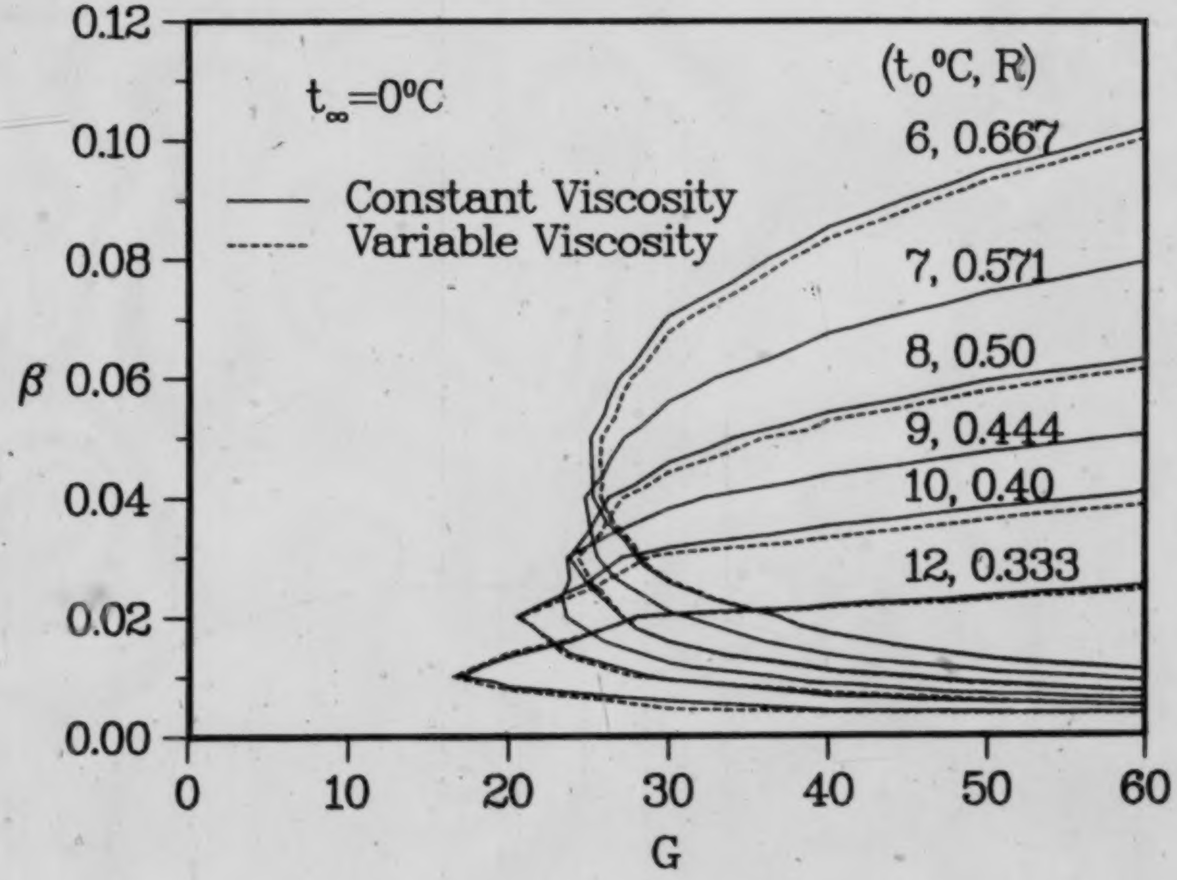

Fig. 4.4(b) The neutral stability curves for various values of $t_0(>t_m)$ when t_∞=0°C

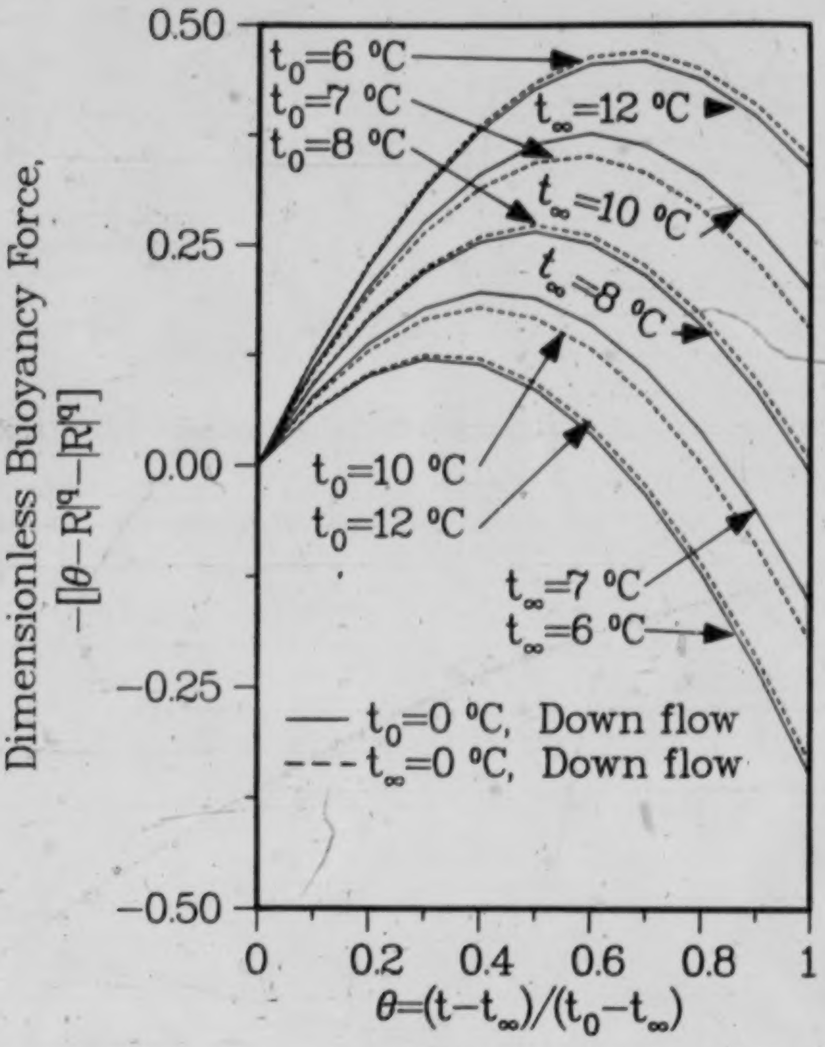

Fig. 4.4(c) The dimensionless buoyancy force when t_0 and t_∞ are on the opposite sides of t_m

there is a buoyancy force reversal inside the thermal boundary layer. Also, the frequency filtering mechanism is more pronounced when there is a buoyancy force reversal. The more significant is the buoyancy force reversal, the lower is the value of critical G for the onset of instability (compare the cases for t_∞=7.0 and 6.0°C in Figs. 4.4(a) and (c), for example).

4.2.3 The Effects of Variation of Viscosity with Temperature

Figs. 4.2(a) to 4.5(b) show the effects of variation of viscosity with temperature on the stability of the laminar flow for various combinations of wall and ambient temperatures. The temperature-dependent viscosity stabilizes the flow for heated walls and destabilizes the flow for cooled walls. Moreover, the disturbances amplify faster for a cooled wall than for a heated wall (see Fig. 4.5(a)). These effects (particularly the disturbance amplification rate) are more pronounced for larger temperature differences between the wall and the ambient water. Fig. 4.5(b) shows the critical values of G and β obtained from the linear stability analysis. The critical value of G is discontinuous and the value of β is lower in the flow reversal region. As the disturbances amplify faster for a cooled wall, the transition to turbulent flow may occur at a lower value of Gr_x.

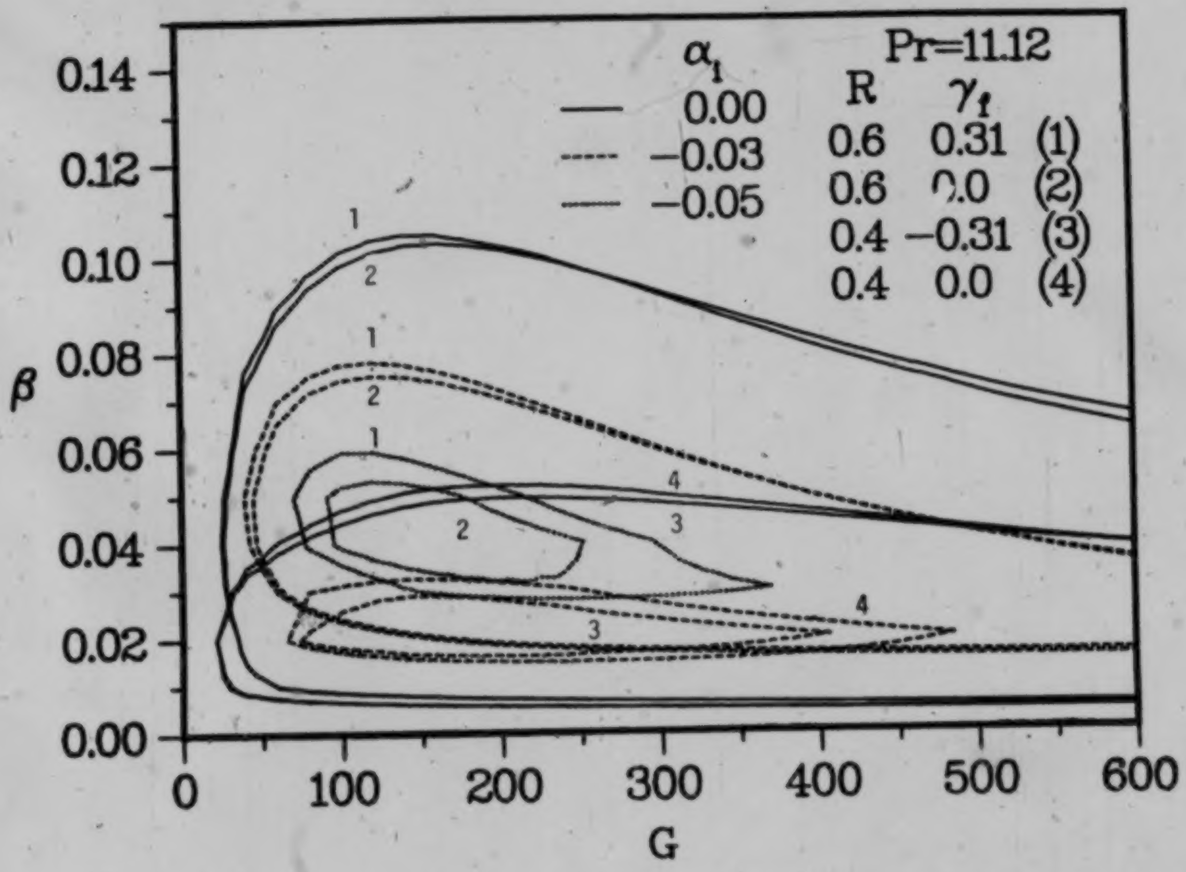

Fig. 4.5(a) The effects of temperature-dependent viscosity when t_0=0°C and t_∞=10°C, and t_0=10°C and t_∞=0°C

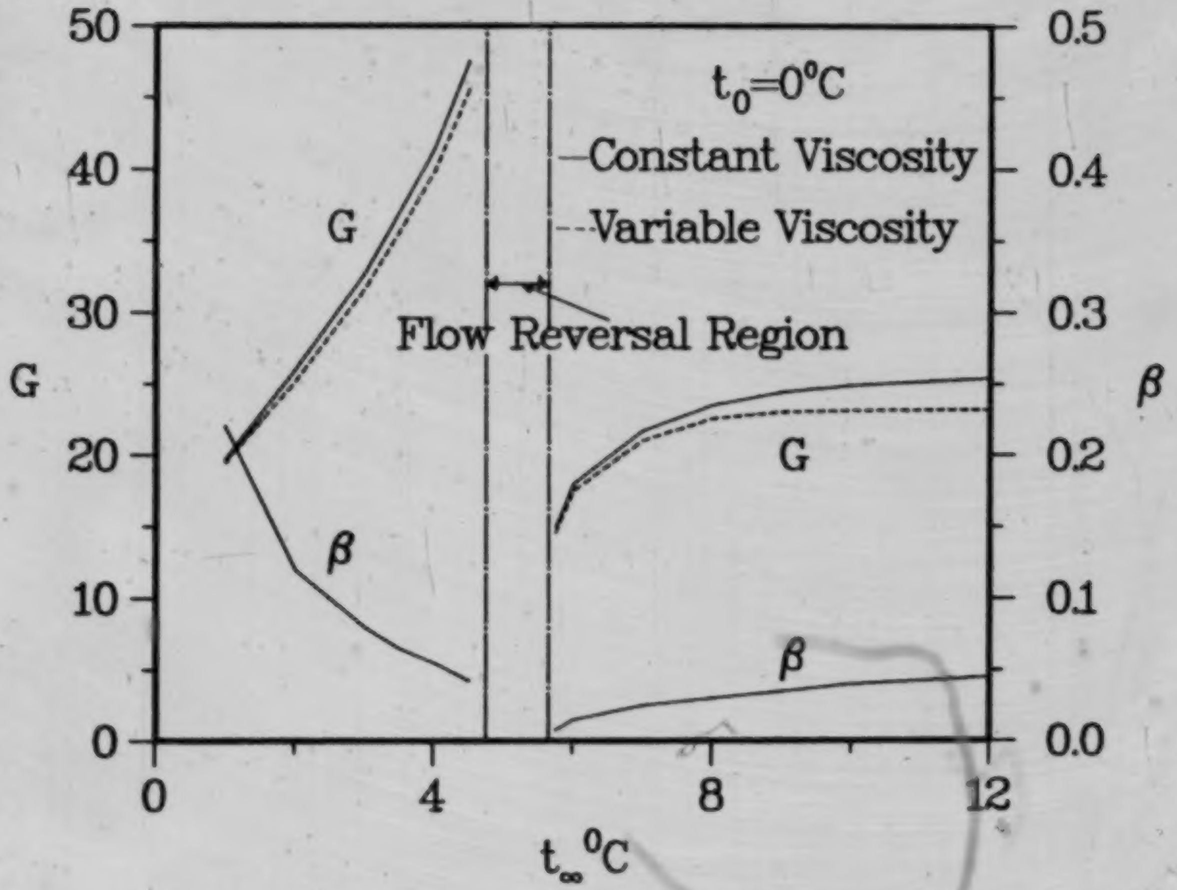

Fig. 4.5(b) The critical values of G and β for various t_∞ when $t_0=0°C$

4.2.4 Flow Visualization Studies

The points of onset of instability and transition to turbulent flow were obtained for the natural convective flow along an isothermal vertical circular cylinder in water for various values of t_∞ and t_0 in the range 0°C to 20°C. Dye injection and shadowgraph flow visualization techniques were used to obtain the critical values. The experimental apparatus and test section was the same the one described in the previous chapter except that a second coolant system consisting of a mixture of 60% (by volume) ethylene glycol, 30% water and 10% methanol was used to cool the cylinder for low temperatures (near 0°C) and for ice formation over the cylinder. The experimental procedure was the same as described in the one described in Chapter 3. When a thin ice layer was present on the test section the surface temperature was taken to be 0°C.

Fig. 4.6(a) shows typical dye injection photographs (t_∞=15.5°C, t_0=0°C). The oscillations and the eventual break down of the dye are clearly seen. The critical values of Ra_x for the onset of instability and the transition to turbulent flow for different values of t_∞ for an ice surface (t_0=0°C) are shown in Fig. 4.6(b). The experimentally obtained critical values of Ra_x for the transition to turbulent flow appear to be slightly higher than the range of values given by Fujii et al. (1970). This may be due to the fact that a density maximum was present for the cases shown in Fig. 4.7(b) whereas Fujii et al. (1970) studied cases far away from a density maximum. The variation of the observed

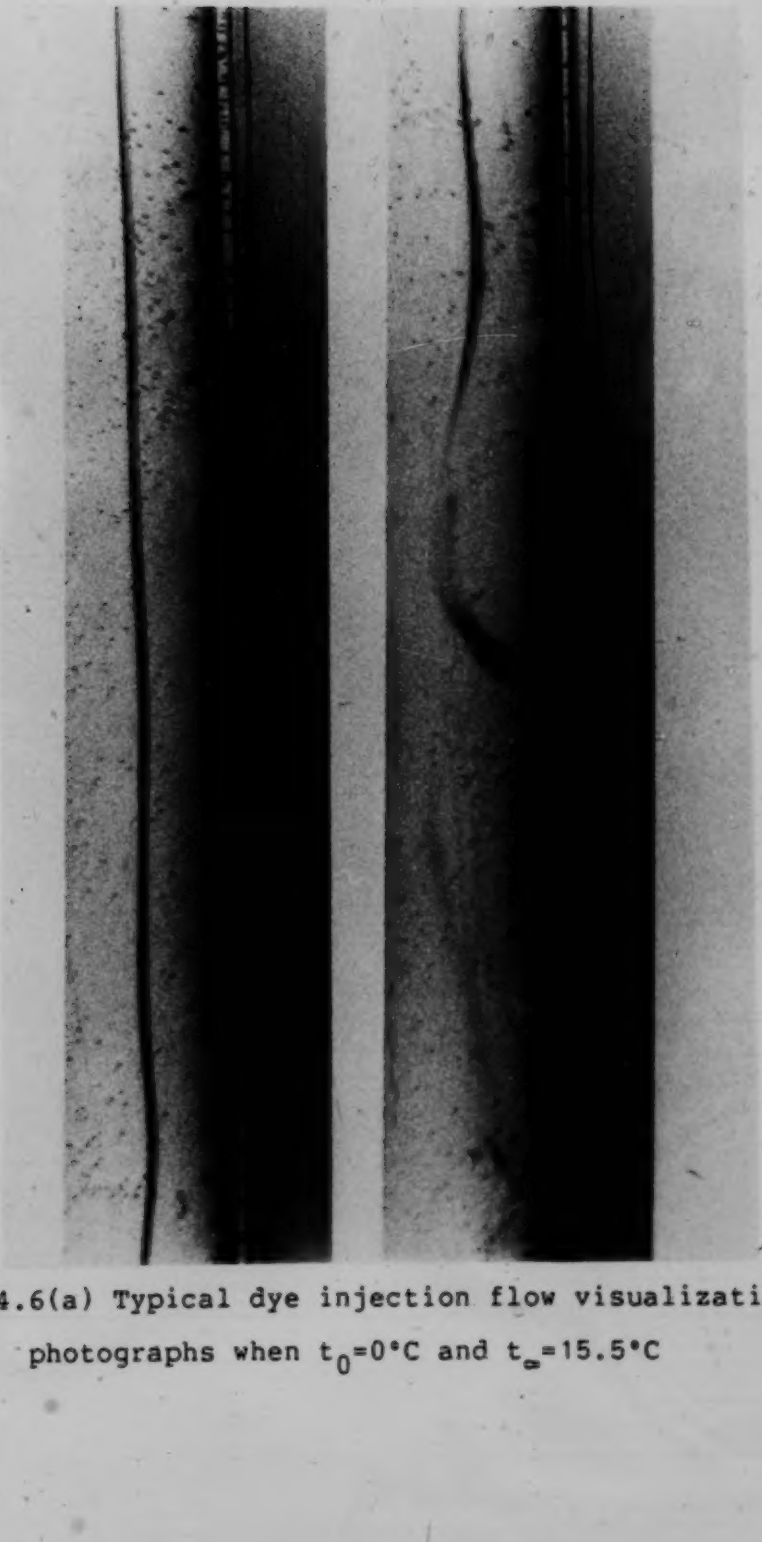

Fig. 4.6(a) Typical dye injection flow visualization photographs when t_0=0°C and t_∞=15.5°C

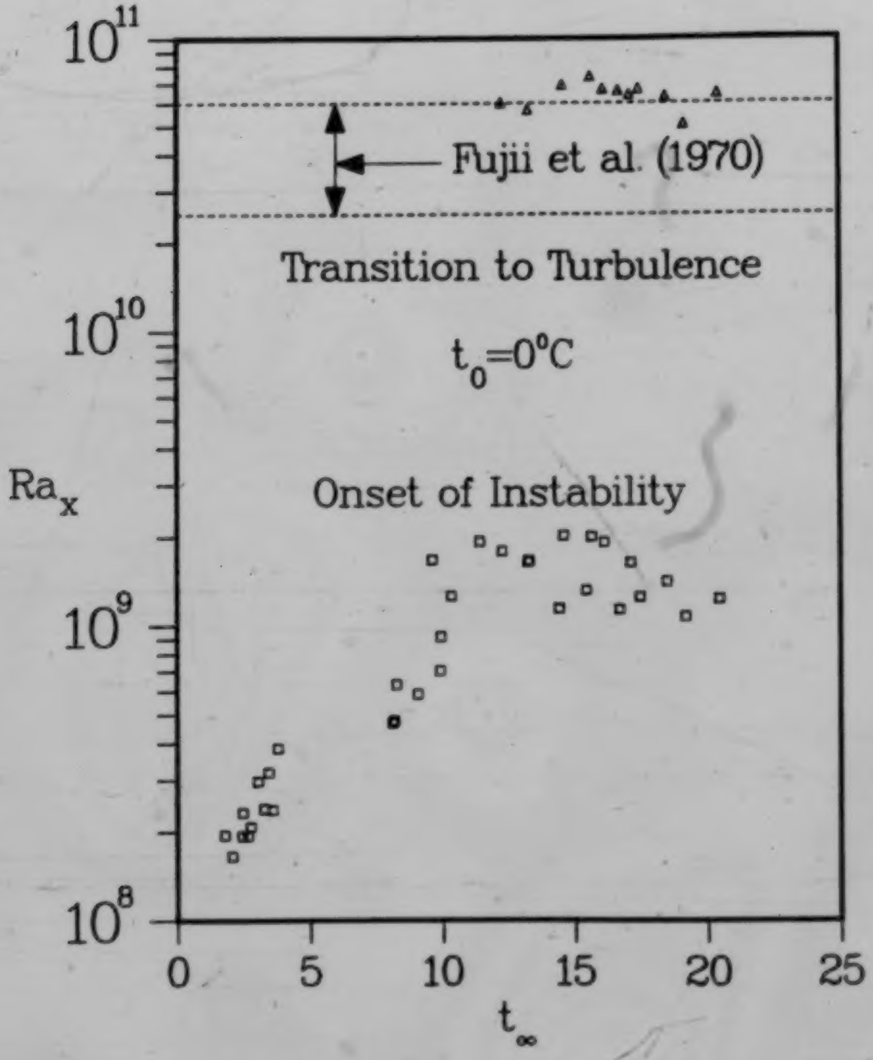

Fig. 4.6(b) The experimentally obtained critical values of Ra_x for the onset of instability and the transition to turbulent flow in water for an ice surface

critical Ra_x with t_∞ for the onset of instability is similar to that of G with t_∞ as shown in Fig. 4.6(b).

It should be stressed again that the experiments were conducted with a vertical circular cylinder whereas the instability analysis was done for a flat plate. Hence, the comparison between the theoretically obtained critical values and the experimentally obtained values has to be made under this light.

4.3 Conclusions

The stability of buoyancy induced flow along an isothermal vertical flat surface in cold water has been studied in detail for heating and cooling situations. The numerical results reveal that the critical Grashof number for the onset of instability may be discontinous in the region where flow reversals occur. The temperature-dependent viscosity stabilizes the flow for a heated wall and destabilizes it for a cooled wall. The trends of experimentally obtained critical values of Rayleigh number for the onset of instability and the transition to turbulent flow support the numerical predictions.

5. Transient Laminar Natural Convective Flow Along a Vertical Circular Cylinder Subjected to a Step Change in Surface Temperature

In this Chapter, the transient laminar natural convective flow along a vertical circular cylinder subjected to a step change in surface temperature is investigated numerically for various curvatures of the cylinder and Prandtl numbers 0.1, 0.72, 1.0 and 10.0. In addition, experiments were done in water with a smooth vertical circular copper pipe (outside diameter 41.3 mm and length 1 m) for a step change in surface temperature. The transient and the steady state temperatures were measured at various locations inside the thermal boundary layer and the flow was visualized using the shadowgraph flow visualization technique.

5.1 Theoretical Analysis

5.1.1 Governing Equations

The physical model and the coordinate system are shown in Fig. 5.1. The quiescent ambient medium and the surface of the vertical circular cylinder are at a constant temperature t_∞. At time $\bar{\tau}=0$, the surface temperature of the cylinder is changed from t_∞ to t_0. (It appears that there are no approximate analytical or numerical solutions available in the literature for the transient laminar natural convective

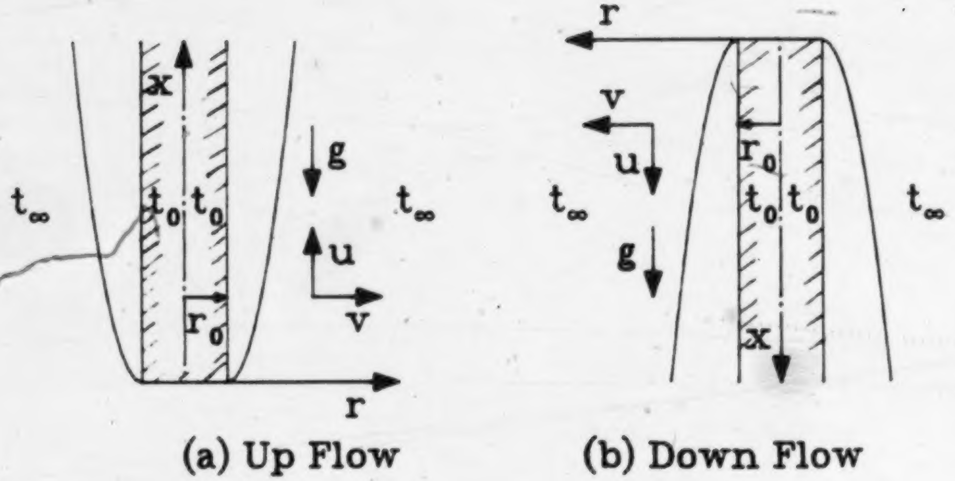
x
g
t∞
t0 t0
u
v
r0
r
t∞
r
v
r0
u
t∞
t0 t0
t∞
g
x

(a) Up Flow (b) Down Flow

Fig. 5.1 The coordinate system

flow adjacent to a vertical circular cylinder subjected to a step change in surface temperature). The transient flow that arises as a result of the step ~~change in~~ surface temperature can be briefly described as follows (Siegel, 1958). At a finite distance from the leading edge, the flow initially develops as if the cylinder were infinite in extent. Owing to the wavelike nature of the unsteady boundary layer equations, a finite time elapses before the leading edge influences the flow development at that section; thereafter a transition to the steady state solution takes place. The initial stage of transient flow develoment for the semi-infinite vertical circular cylinder is discussed in detail Appendix D.

Employing the familiar Boussinesq and boundary layer approximations, the equations governing the conservation ~~of~~ mass, momentum, and energy for the transient natural convective flow along the cylinder are given by

$$\frac{\partial u}{\partial x} + \frac{\partial v}{\partial r} + \frac{v}{r} = 0 \tag{5.1}$$

$$\frac{\partial u}{\partial \bar{\tau}} + u\frac{\partial u}{\partial x} + v\frac{\partial u}{\partial r} = g\beta(t-t_\infty) + \nu\left[\frac{1}{r}\,\frac{\partial u}{\partial r} + \frac{\partial^2 u}{\partial r^2}\right] \tag{5.2}$$

$$\frac{\partial t}{\partial \bar{\tau}} + u\frac{\partial t}{\partial x} + v\frac{\partial t}{\partial r} = \alpha\left[\frac{1}{r}\,\frac{\partial t}{\partial r} + \frac{\partial^2 t}{\partial r^2}\right] \tag{5.3}$$

The initial and the boundary conditions are, for $\bar{\tau} < 0$,

$$u = v = 0 \text{ and } t = t_\infty \text{ for all } x \text{ and } y \tag{5.4}$$

for $\bar{\tau} \geq 0$,

$$u = v = 0 \text{ and } t = t_0 \text{ at } y = 0, \text{ for all } x \tag{5.5}$$

$$u \to 0 \text{ and } t \to t_\infty \text{ as } y \to \infty, \text{ for all } x \tag{5.6}$$

$$u = v = 0 \text{ and } t = t_\infty \text{ at } x = 0, \text{ for all } y > 0 \tag{5.7}$$

The equations are the similar to the ones given in Sparrow and Gregg (1958) except for the additional unsteady terms. It is to be noted that the boundary layer approximations are not valid near the leading edge. Introducing the following dimensionless variables,

$$X = xG, \ Y = yG, \ R_0 = r_0G, \ U = \frac{u}{\nu G} \tag{5.8}$$

$$V = \frac{v}{\nu G}, \ \tau = \nu G^2\bar{\tau}, \ \theta = \frac{t-t_\infty}{t_0-t_\infty} \tag{5.9}$$

where $y = r-r_0$ and $G = \left[\frac{g\beta(t_0-t_\infty)}{\nu^2}\right]^{1/3}$ (5.10)

the governing equations become,

$$\frac{\partial U}{\partial X} + \frac{\partial V}{\partial Y} + \frac{V}{R_0+Y} = 0 \tag{5.11}$$

$$\frac{\partial U}{\partial \tau} + U\frac{\partial U}{\partial X} + V\frac{\partial U}{\partial Y} = \theta + \frac{1}{R_0+Y}\frac{\partial U}{\partial Y} + \frac{\partial^2 U}{\partial Y^2} \tag{5.12}$$

$$\frac{\partial \theta}{\partial \tau} + U\frac{\partial \theta}{\partial X} + V\frac{\partial \theta}{\partial Y} = \frac{1}{Pr}\left[\frac{1}{R_0+Y}\frac{\partial \theta}{\partial Y} + \frac{\partial^2 \theta}{\partial Y^2}\right] \tag{5.13}$$

The initial and the boundary conditions become,

for $\tau < 0$,

$$U = V = 0 \text{ and } \theta = 0 \text{ for all X and Y} \tag{5.14}$$

for $\tau \geq 0$,

$$U = V = 0 \text{ and } \theta = 1 \text{ at } Y = 0, \text{ for all X} \tag{5.15}$$

$$U \to 0 \text{ and } \theta \to 0 \text{ as } Y \to \infty, \text{ for all X} \tag{5.16}$$

$$U = V = 0 \text{ and } \theta = 0 \text{ at } X = 0, \text{ for all } Y > 0 \tag{5.17}$$

For a given value of X, the value of R_0 determines the effect of curvature; the smaller the value, the more pronounced is the effect of curvature. When $R_0 \to \infty$, the equations reduce to the ones corresponding to a vertical flat plate. The relation between R_0 and ξ, the curvature parameter of Sparrow and Gregg (1958), is given by

$$\xi = 2(2)^{1/2} \frac{X^{1/4}}{R_0} \tag{5.18}$$

The local Nusselt number is given by

$$Nu_x = \frac{hx}{k} = X \left[-\frac{\partial \theta}{\partial Y} \Big|_{Y=0} \right] \tag{5.19}$$

$$\text{or} \quad \frac{Nu_x}{(Gr_x)^{1/4}} = X^{1/4} \left[-\frac{\partial \theta}{\partial Y} \Big|_{Y=0} \right] \tag{5.20}$$

5.1.2 Numerical Method

An explicit finite difference method similiar to the one discussed in Hellums and Churchill (1962) was used to solve the equations (5.11) to (5.17). The space under investigation was divided into a grid dimension of M X N in

X and Y coordinate directions, respectively. A variable grid system with grid sizes varying in geometric progression was used. Finer grids near the leading edge and the surface, and coarser grids away from the leading edge and the surface were used. The smallest and the largest grid sizes in the X-direction were between 2 and 2.5, and between 6 and 7 respectively. The maximum value of X varied from 215 to 250. In the Y-direction, the smallest grid size varied from 0.5 to 1 depending on Pr. The maximum grid size in the Y direction was between 2 and 4.5. The maximum value of Y varied from 45 to 90. The value of M was between 55 and 65, and that of N was between 35 to 45.

The governing equations, and the initial and the boundary conditions were finite differenced and solved for each grid point starting at time $\tau=0$. The solution was then marched in time with sufficiently small time steps until the values of U, V, and θ attain their steady state values. The steady state was considered to have been achieved when the change in two cosecutive values of U, V, and θ was less than 0.5 percent at all points in the solution region. When the convergence criterion was taken as 0.25 percent, there was not any appreciable difference in the solution from that of 0.5 percent except that at the outer edge of the boundary layer U converged rather slowly.

5.2 Experimental Apparatus and Procedure

The experimental apparatus was the same as the one described in detail in Chapter 3.

The steel tank was filled with deaerated plain tap water. The water was allowed to equilibrate for about one to two hours. The coolant was brought down to the desired temperature and was kept circulating in the bypass loop. The thermocouple was positioned at the desired location at which the transient temperature was to be recorded. The light source was switched on. The flow was then allowed to circulate through the test section. The output of the thermocouple, and the temperatures of the coolant at the inlet and the outlet were continuously recorded. The transient flow was photographed. The flow became steady within 5 minutes of starting the experiment for temperature differences larger than 10°C. The steady state natural convective flow was photographed after 10 minutes of starting the experiment. The inlet and the outlet coolant temperatures were always found to be within 0.25°C. The surface temperature was taken to be the average of these temperatures. The steady state temperature profile in the boundary layer was measured at various axial locations.

5.3 Results and Discussion

The equations (5.11) and (5.17) were solved numerically for Pr=0.1, 0.72, 1.0 and 10.0, and R_0=2.0, 10.0 and 100.0. The transient and the steady state solutions were obtained for Grashof numbers up to 10^7.

5.3.1 Steady State Temperature and Axial Velocity Profiles

Figs. 5.2(a) to 5.4(b) show the steady state temperature and axial velocity profiles for typical values of Pr, R_0, and Gr_x. For larger values of R_0(>100), the steady state temperature and velocity profiles agreed very well with those obtained from the similarity solution for a flat plate. For example, when Gr_x was equal to 10^7 and R_0 was equal to 100, the velocity and temperature profiles agreed very closely with those obtained for a flat plate for the Prandtl numbers studied (solutions for a flat plate were given in Chapter 2). This ensured the validity and the accuracy of the numerical scheme.

For given values of Pr and Gr_x, the thicknesses of the temperature and the velocity boundary layers were larger for smaller values of R_0 as seen from Figs. 5.2(a) and (b), and Figs. 5.4(a) and (b). Also, the temperature gradients near the wall were larger and the maximum velocities were lower for smaller values of R_0. For example, at $Gr_x=10^7$ the maximum velocities for $R_0=2$ were about 14 to 18% lower than those of $R_0=100$ for the Prandtl numbers investigated. As in the case of a flat plate, for given values of R_0 and Pr, the thicknesses of velocity and temperature boundary layers were smaller for lower values of Gr_x as seen from Figs. 5.3(a) and (b), and Figs. 5.4(a) and (b). Also, the maximum velocities were lower for these cases.

Fig. 5.5 compares the steady state local Nusselt number at the surface with that of Aziz and Na (1982) for typical values of the curvature parameter ξ. It is seen that the

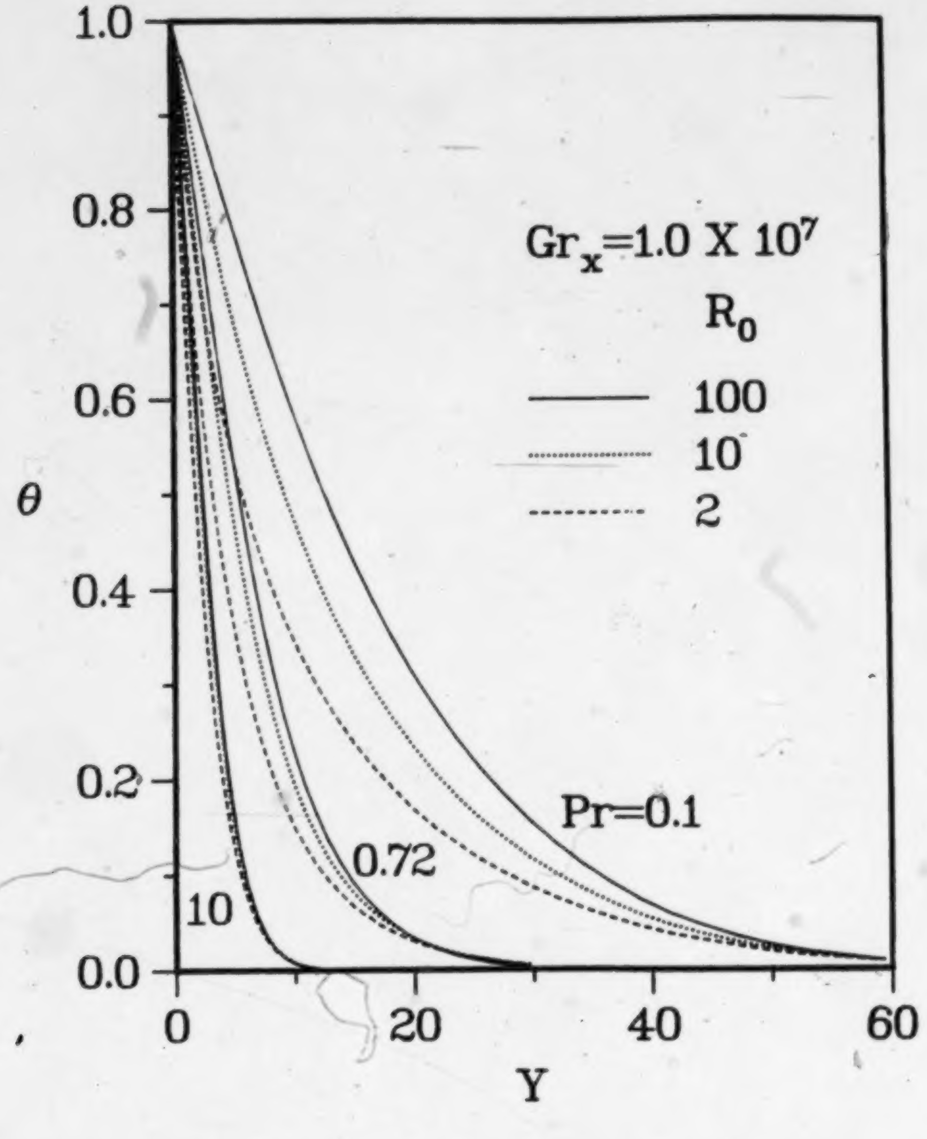

Fig. 5.2(a) The steady state temperature profiles for various values of R_0 and Pr when Gr_x=1 X 10^7

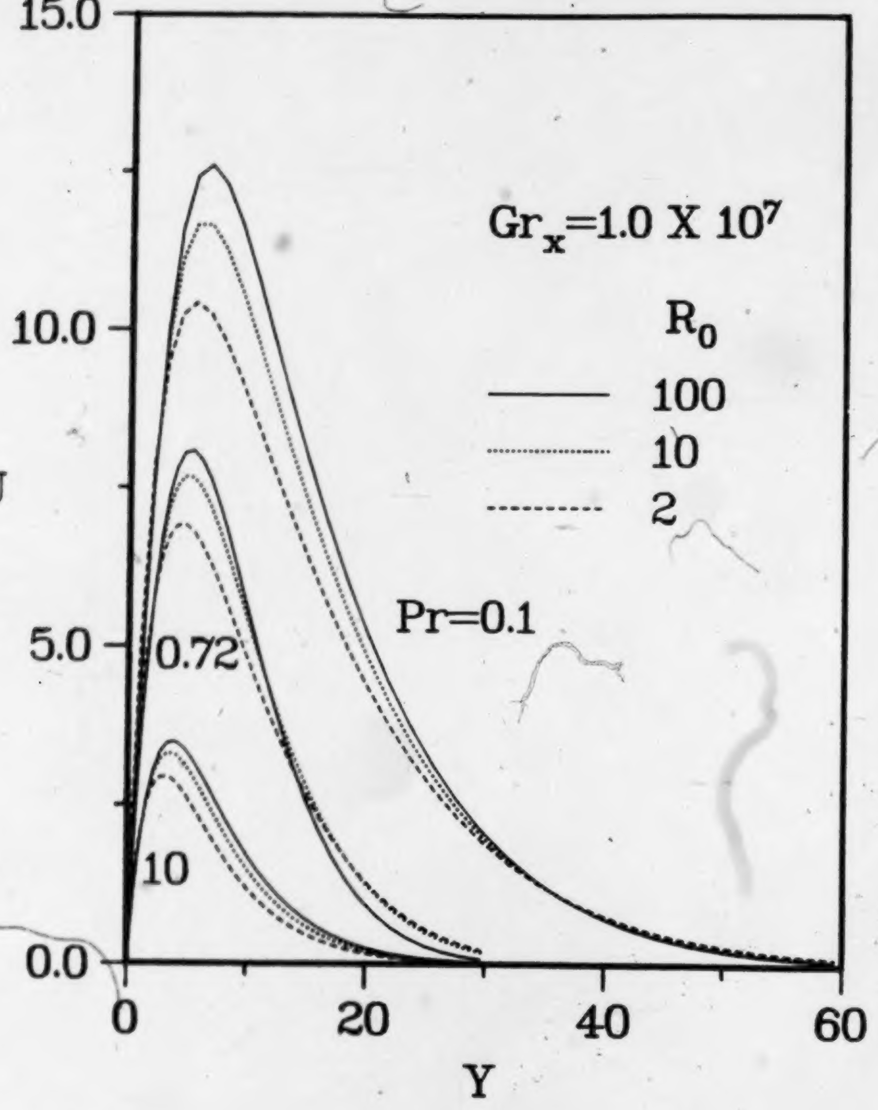

Fig. 5.2(b) The steady state velocity profiles for various values of R_0 and Pr when Gr_x=1 X 10^7

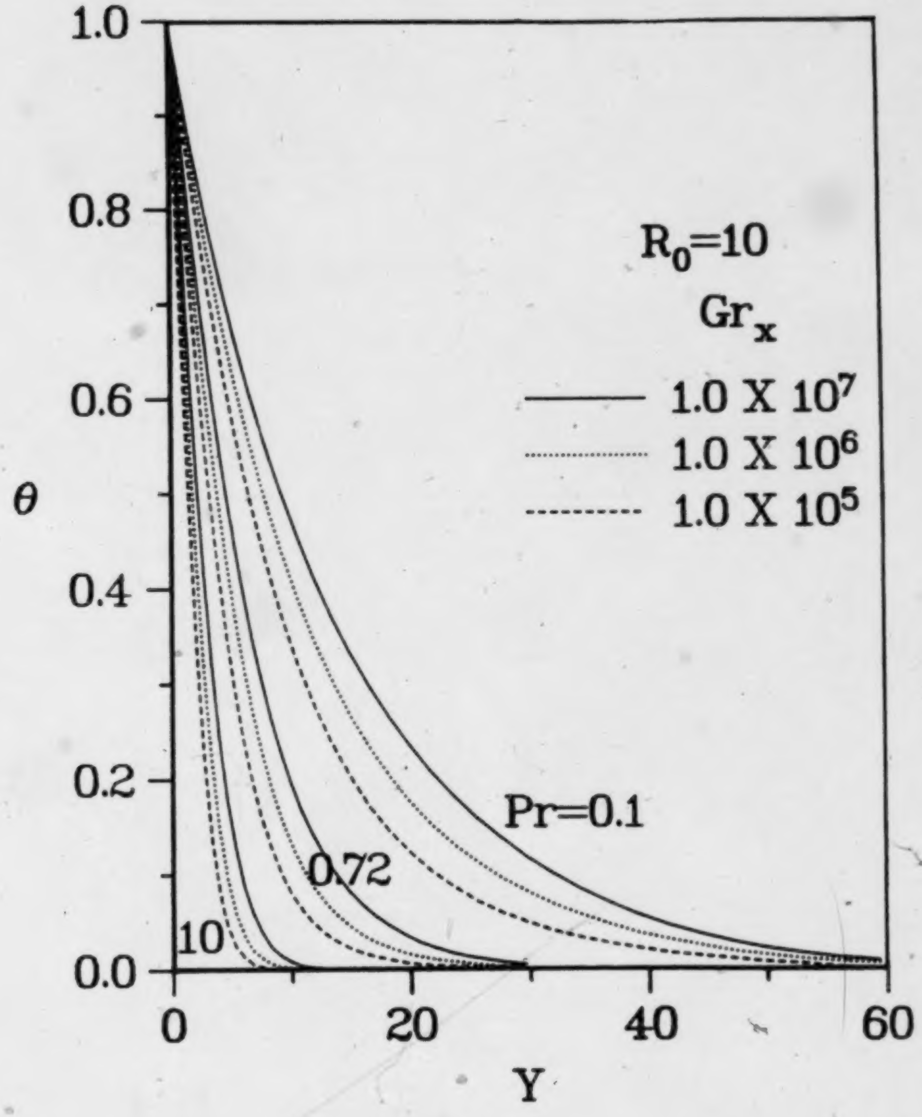

Fig. 5.3(a) The steady state temperature profiles for various values of Gr_x and Pr when R_0=10

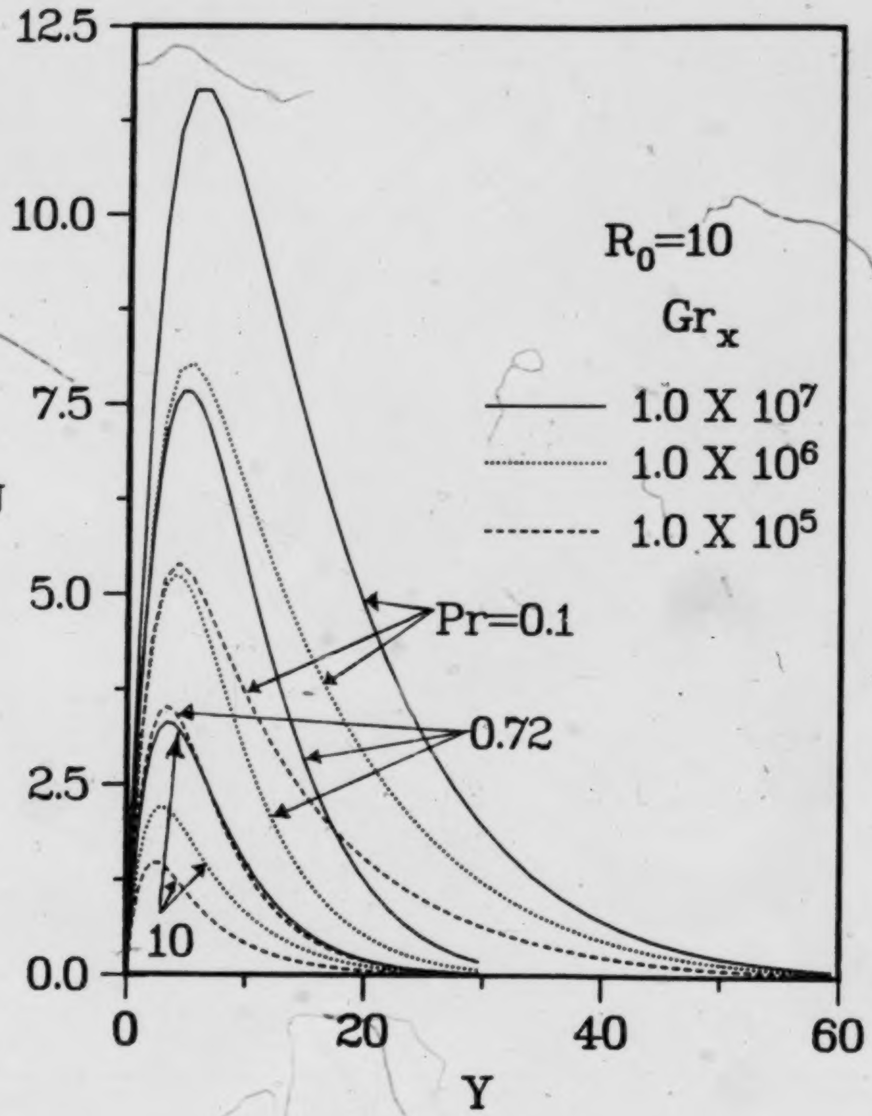

Fig. 5.3(b) The steady state velocity profiles for various values of Gr_x and Pr when R_0=10

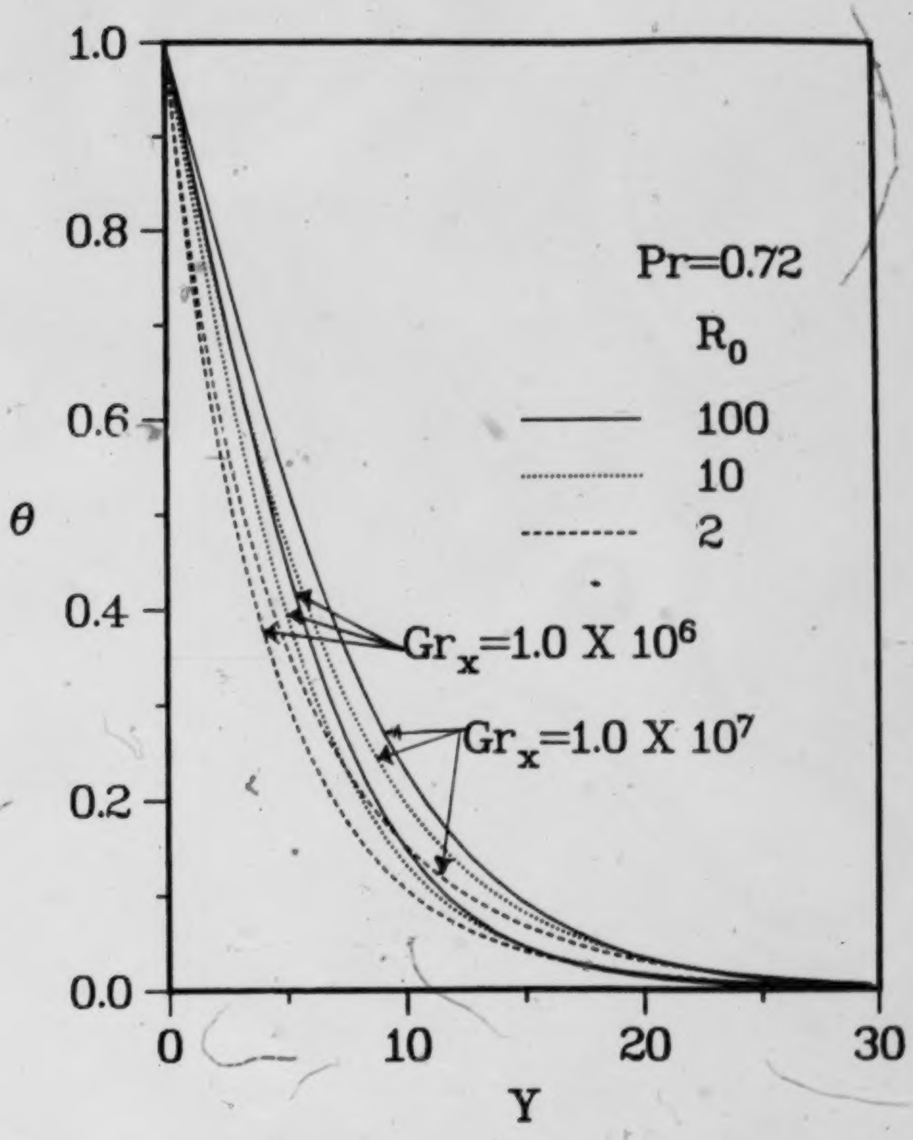

Fig. 5.4(a) The steady state temperature profiles for various values of R_0 and Gr_x when Pr=0.72

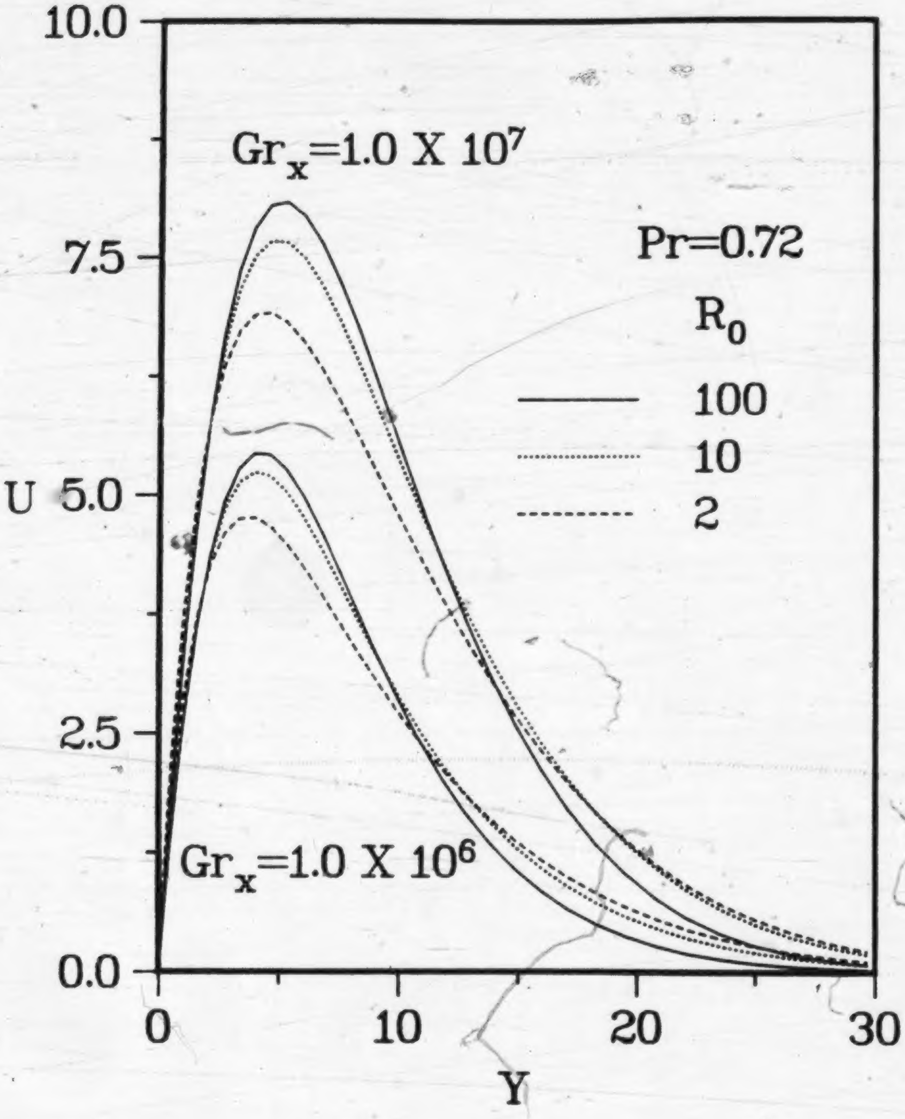

Fig. 5.4(b) The steady state velocity profiles for various values of R_0 and Gr_x when Pr=0.72

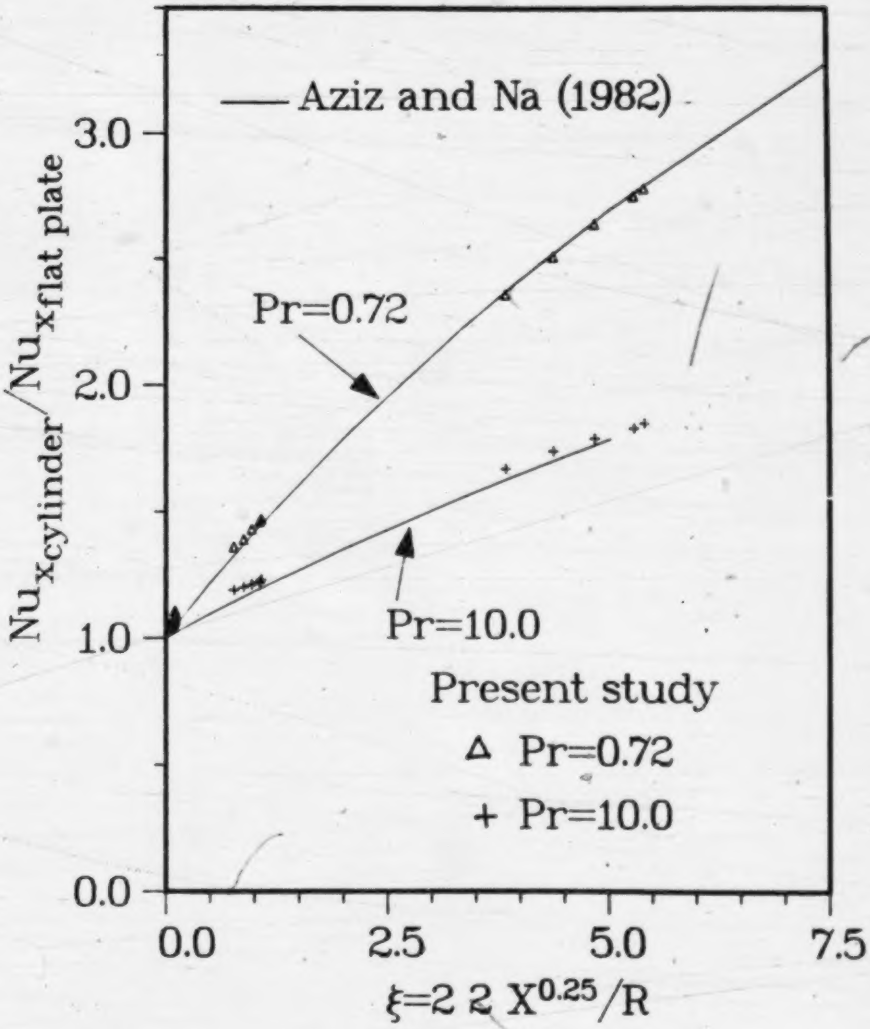

Fig. 5.5 The steady state local Nusselt number for various values of ξ

present numerical solution agrees fairly well with the perturbation solution of Aziz and Na.

5.3.2 Transient Temperature and Axial Velocity Profiles

The transient temperature and velocity profiles obtained numerically for typical values of Pr, R_0 and Gr_x are shown in Figs. 5.6(a) to 5.9(d). During the initial stages of the transient state, the heat transfer process is mainly by conduction and hence the diffusion of heat was slower for larger Pr and smaller R_0. For given values of R_0 and Gr_x, the transients lasted longer for larger Pr as shown in Figs. 5.6(a) and (b). The larger the value of Gr_x, the longer was the time required for the effect of leading edge to be felt. Hence, the transients lasted longer at larger values of Gr_x for given values of Pr and R_0 as shown in Figs. 5.7(a) and (b), and Figs. 5.8(a) and (b). For given Gr_x and Pr, the transients lasted longer for smaller values of R_0 as seen from Figs. 5.9(a) to (d). The boundary layers developed slowly, especially in the outer region when R_0 was smaller.

The dimensionless temperature at points in the inner portion of the thermal boundary layer went through a maximum during the transient period. This overshoot in temperature was found to be larger in the region where the velocity is maximum. The temperature overshoot was larger for Prandtl numbers 0.72 and 1.0 for given values of R_0 and Gr_x. For a given value of Pr, the temperature overshoot was found to be larger when the values of Gr_x and R_0 are larger. Also, for

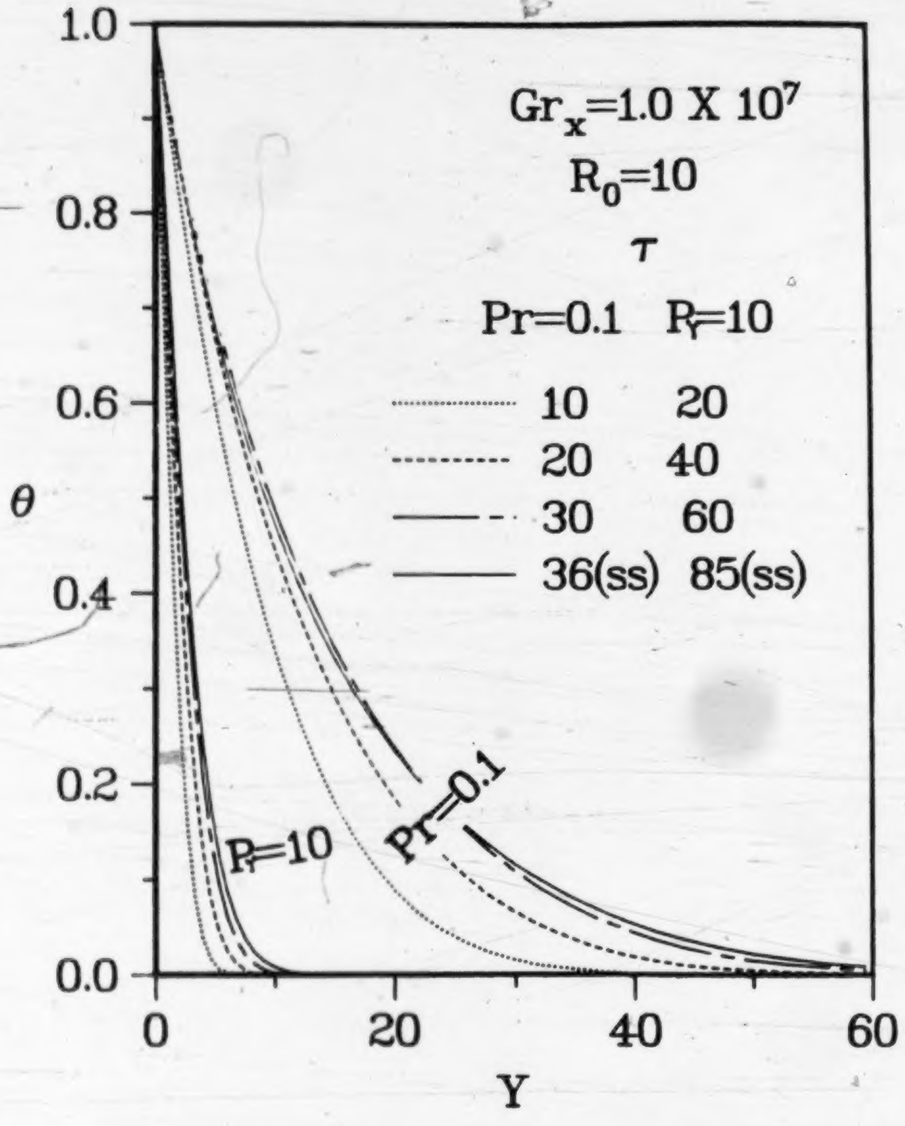

Fig. 5.6(a) The transient temperature profiles for Pr=0.1 and 10.0 when Gr_x=1 X 10^7 and $\tilde{R}_0$=10

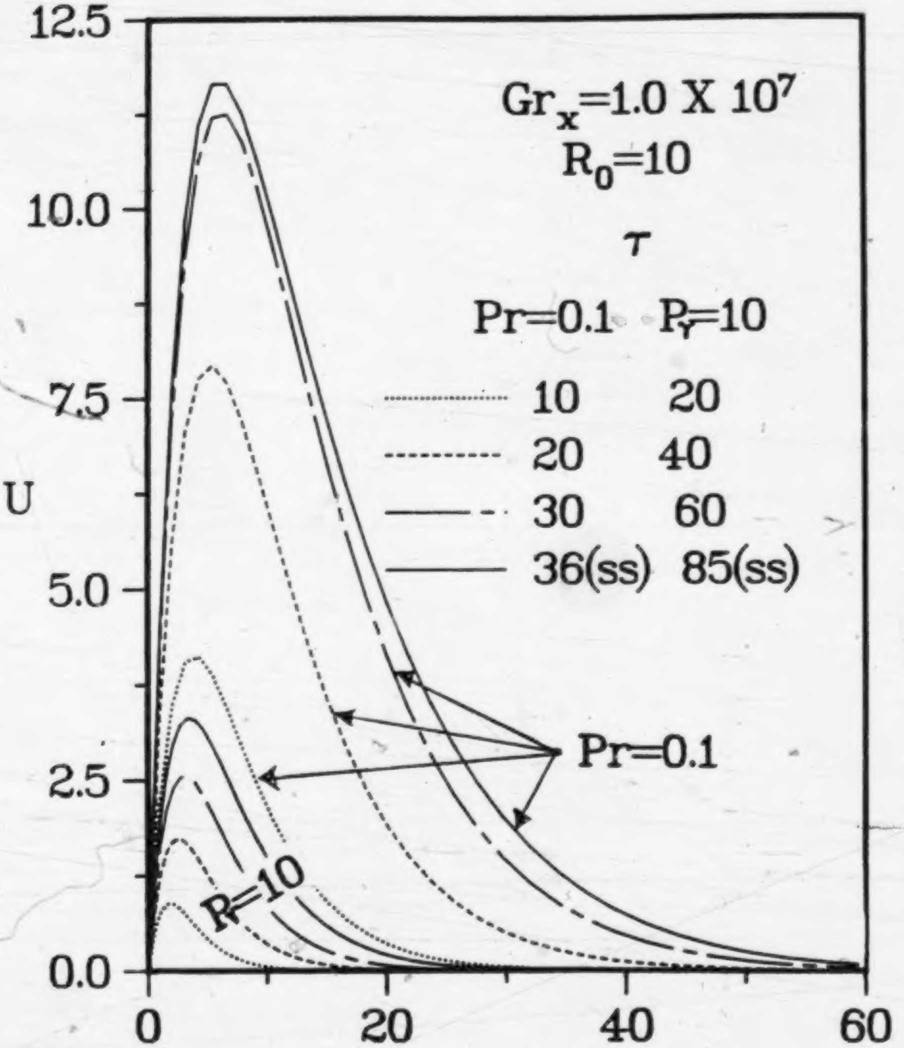

Fig. 5.6(b) The transient velocity profiles for Pr=0.1 and 10.0 when $Gr_x = 1 \times 10^7$ and $R_0 = 10$

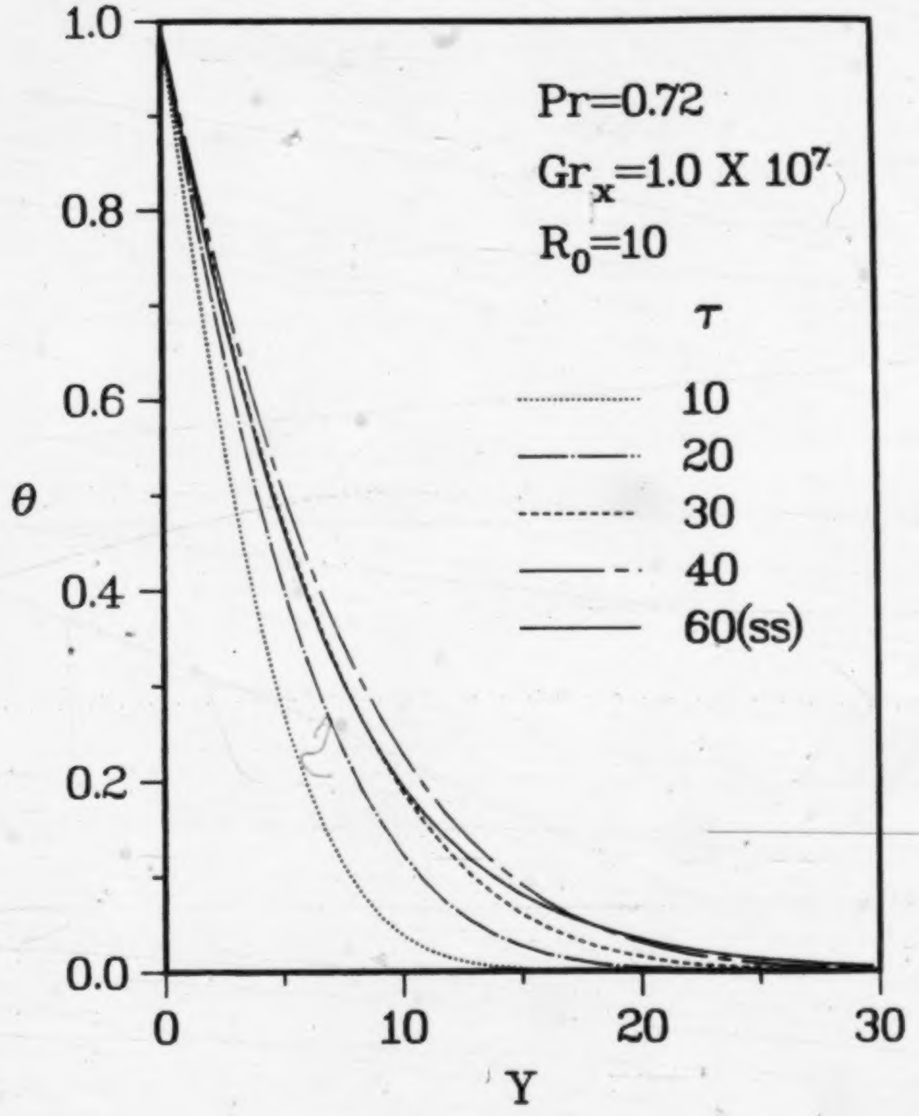

Fig. 5.7(a) The transient temperature profiles at $Gr_x=1 \times 10^7$ when $R_0=10$ and $Pr=0.72$

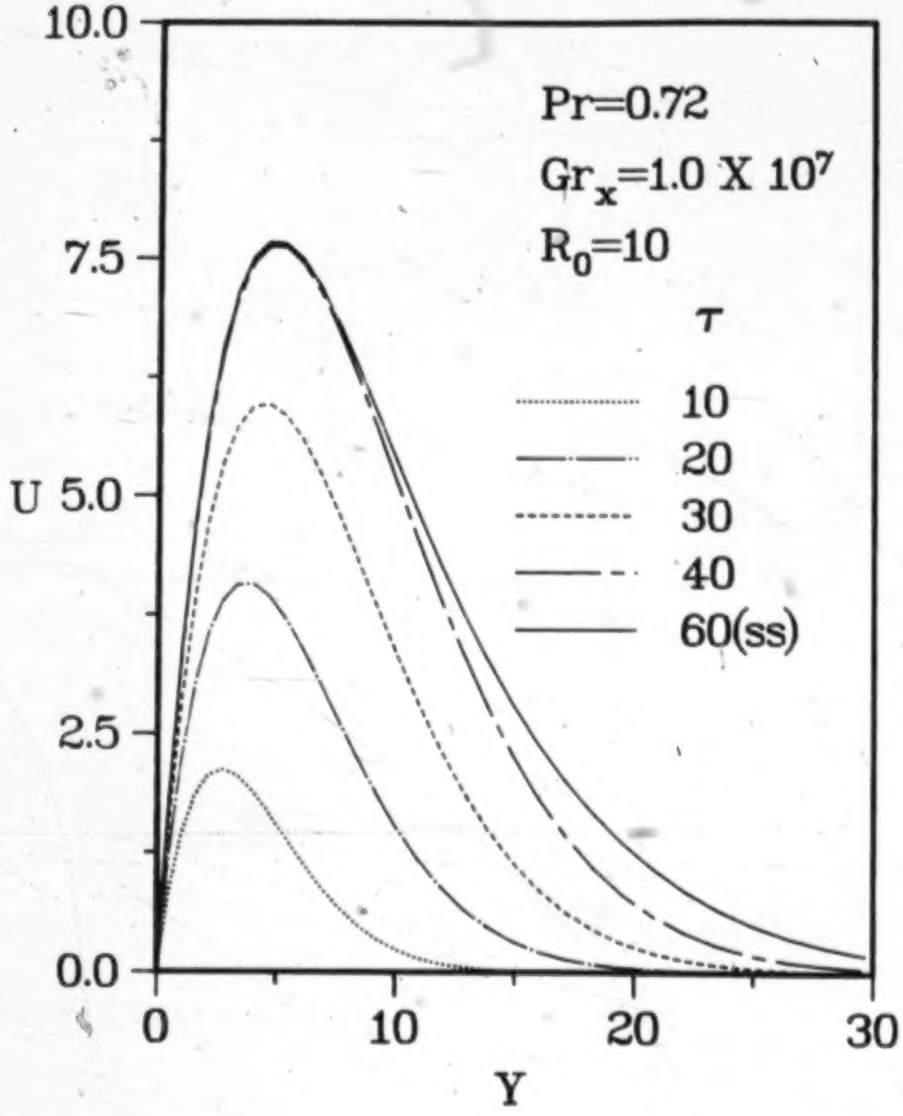

Fig. 5.7(b) The transient velocity profiles at $Gr_x=1 \times 10^7$ when $R_0=10$ and $Pr=0.72$

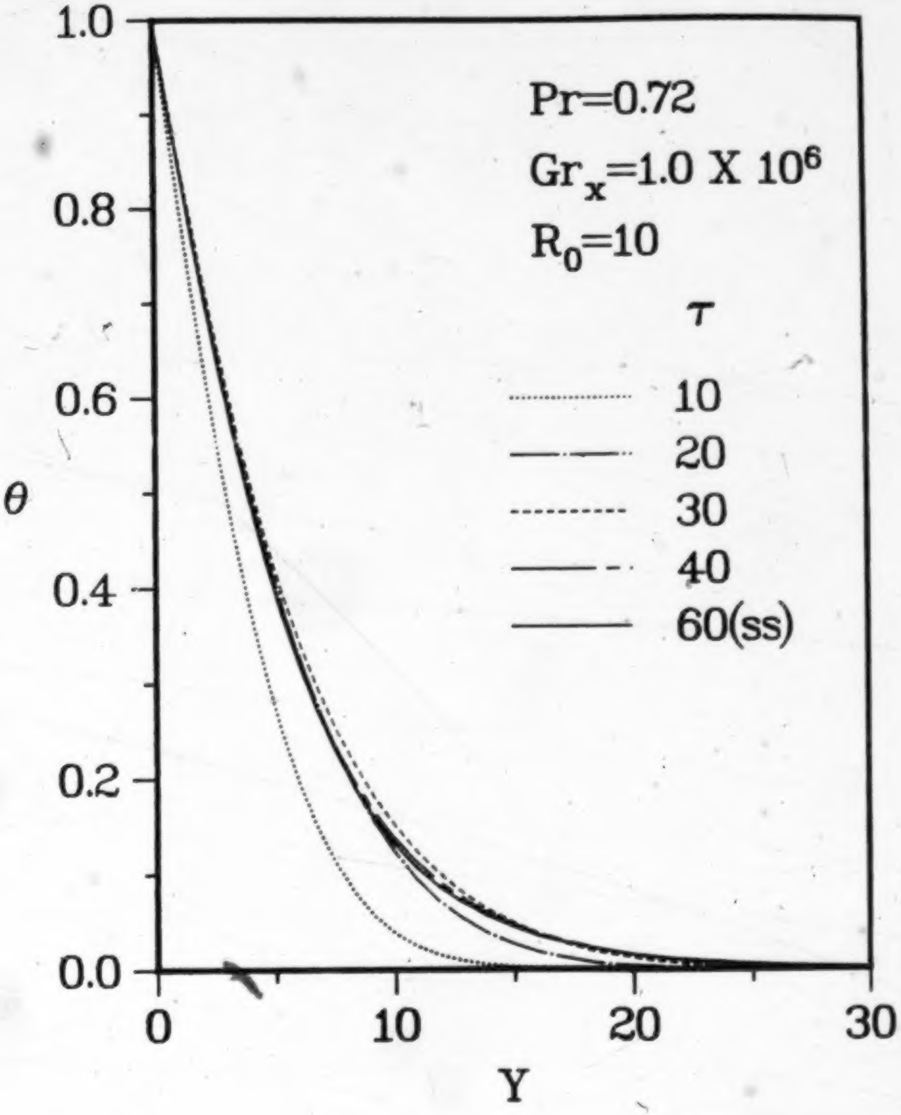

Fig. 5.8(a) The transient temperature profiles at $Gr_x = 1 \times 10^6$ when $R_0 = 10$ and $Pr = 0.72$

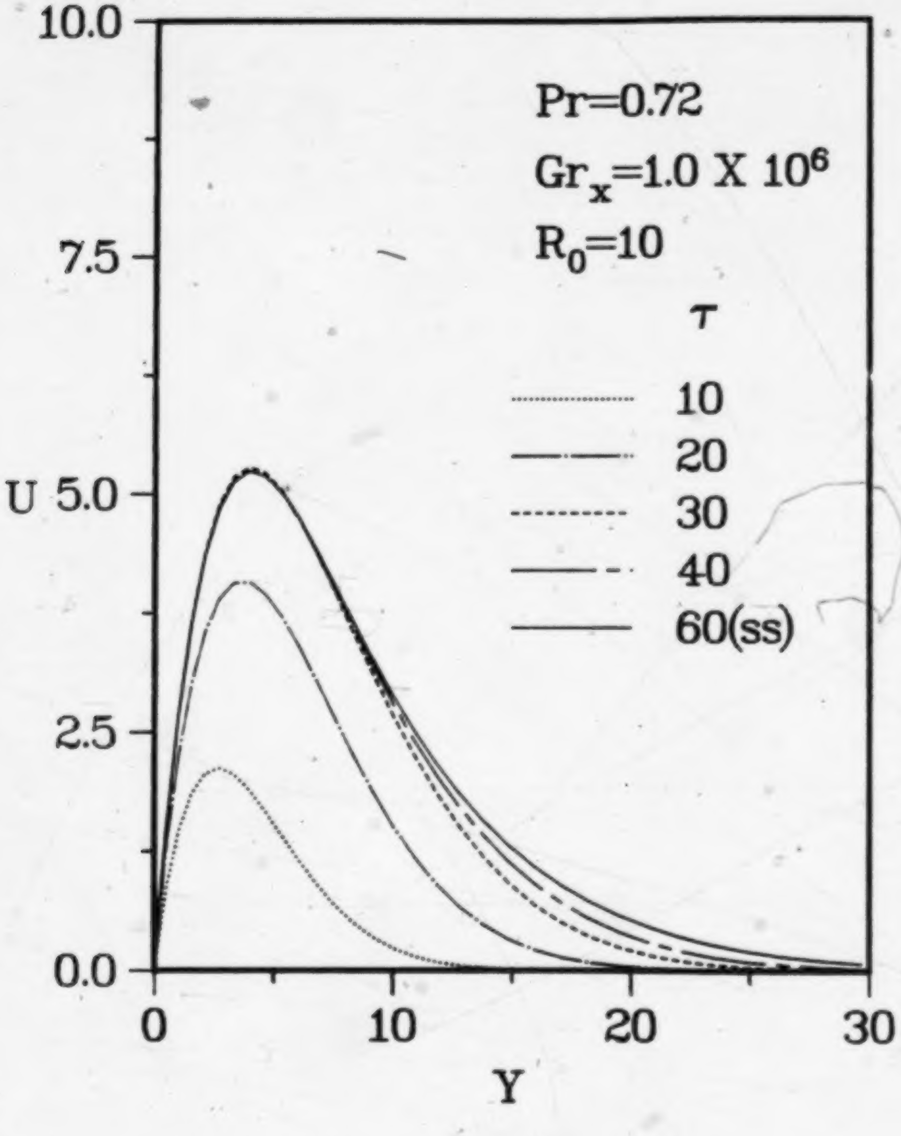

Fig. 5.8(b) The transient velocity profiles at $Gr_x=1 \times 10^6$ when $R_0=10$ and $Pr=0.72$

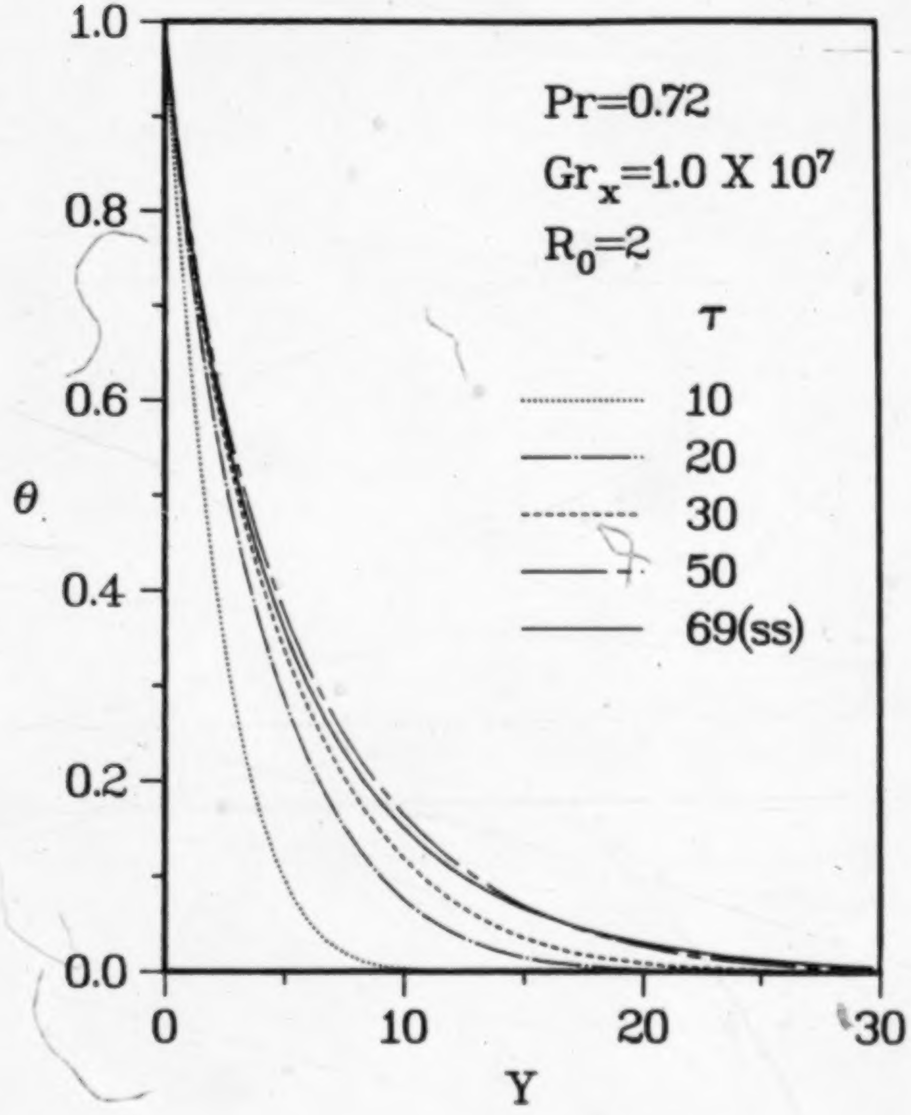

Fig. 5.9(a) The transient temperature profiles at $Gr_x = 1 \times 10^7$ when $R_0 = 2$ and Pr=0.72

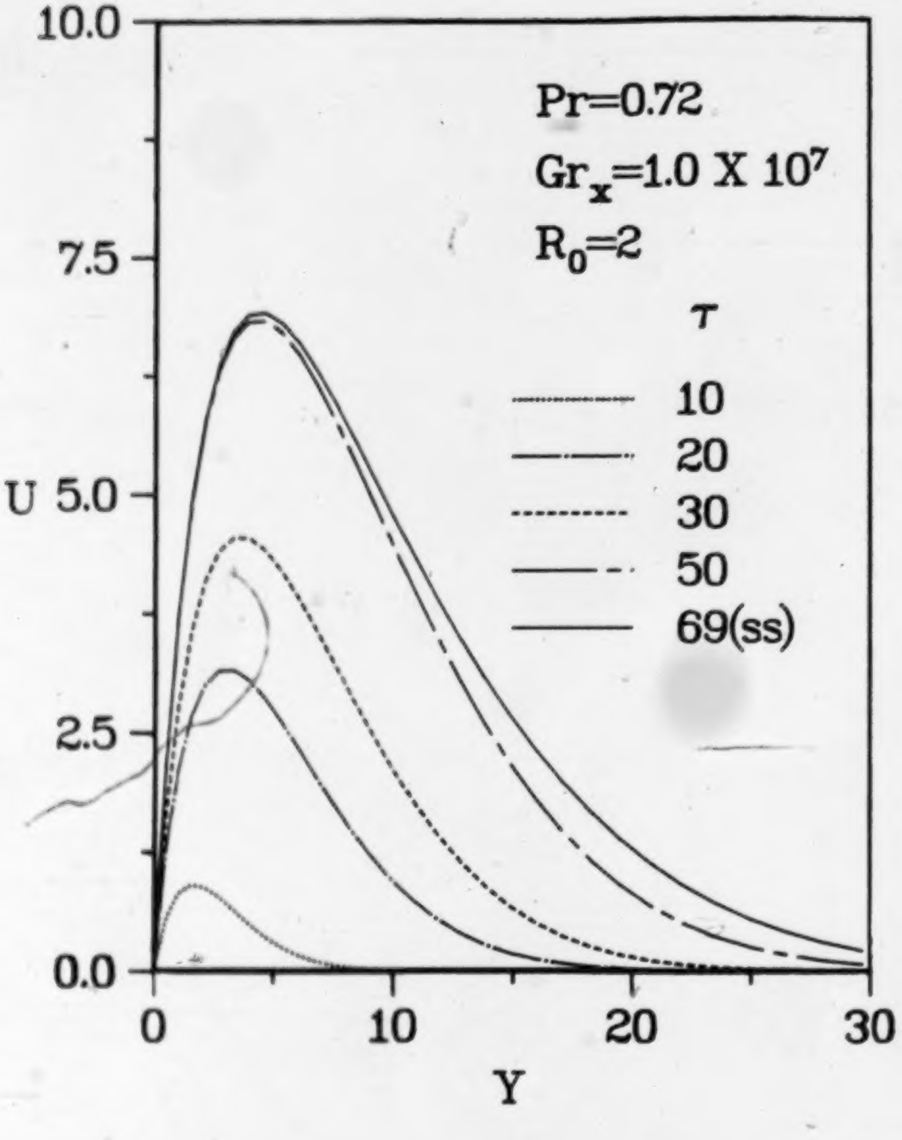

Fig. 5.9(b) The transient velocity profiles at $Gr_x=1 \times 10^7$ when $R_0=2$ and $Pr=0.72$

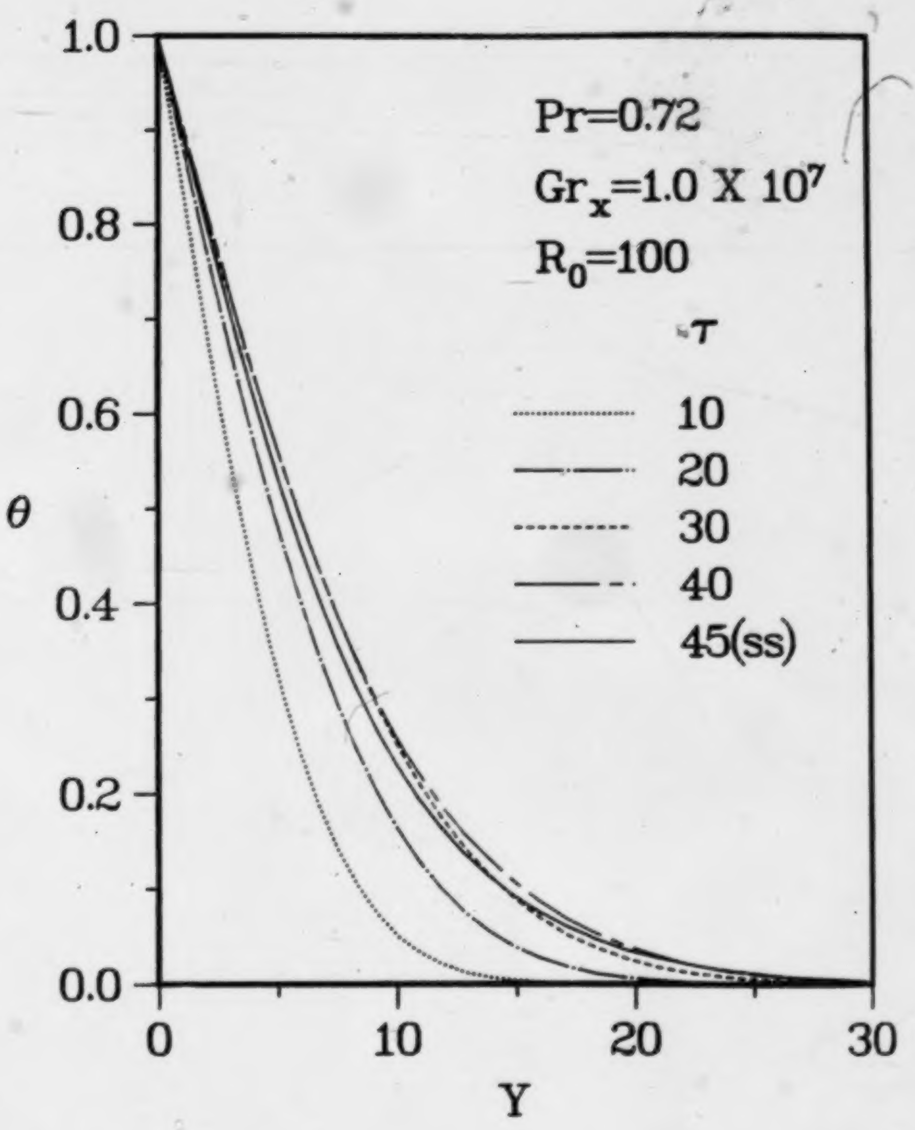

Fig. 5.9(c) The transient temperature profiles at $Gr_x=1 \times 10^7$ when $R_0=100$ and $Pr=0.72$

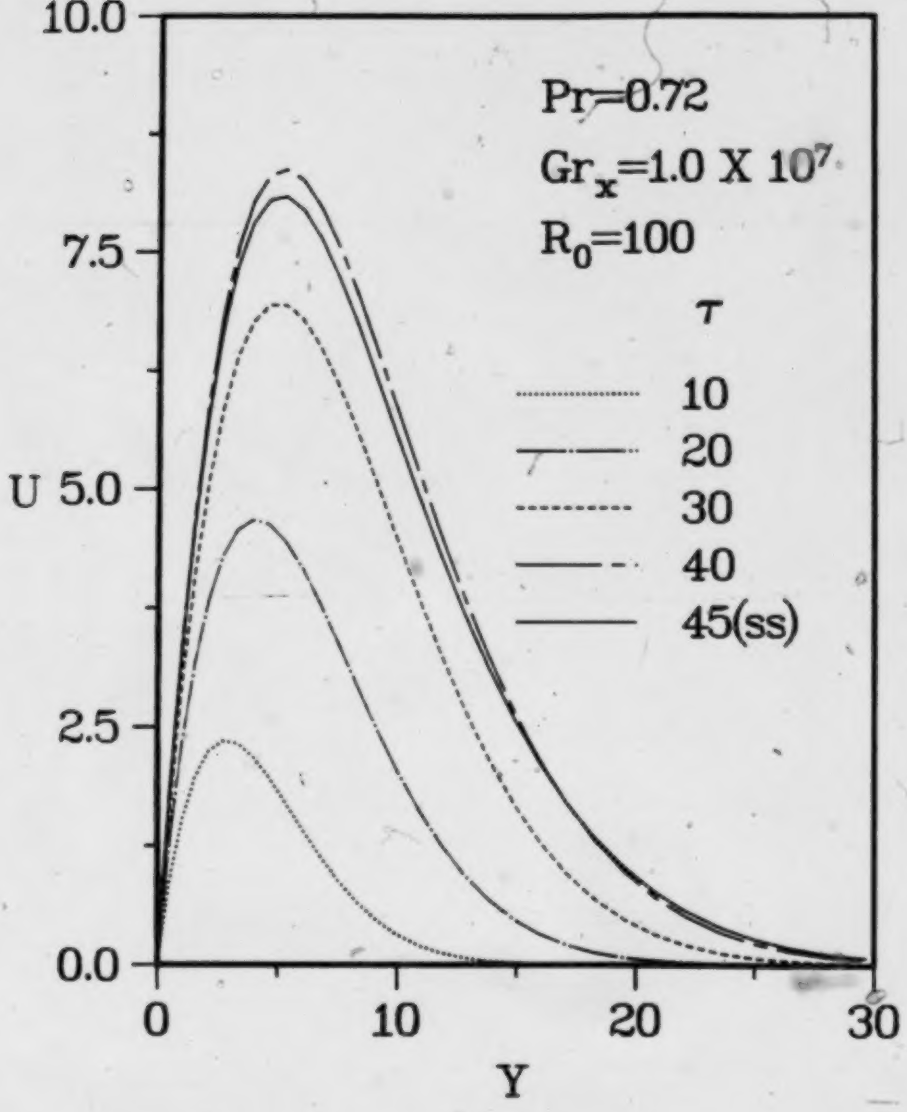

Fig. 5.9(d) The transient velocity profiles at $Gr_x=1 \times 10^7$ when $R_0=100$ and $Pr=0.72$

smaller Prandtl numbers a slight overshoot in U occurred near the region where the value is maximum. As before, the overshoot in U was larger for Prandtl numbers 0.72 and 1.0, and for larger values of Gr_x and R_0. This is due to the fact that at a given position along the cylinder, the heat conduction process is sufficiently rapid to enable the boundary layer thickness to grow beyond the steady state thickness before the constaints induced by the leading edge can propagate to that location and prevent the growth from continuing as if the cylinder were infinite in length. The overgrowth in boundary layer thickness causes a minimum in the heat transfer coefficient at the surface.

5.3.3 Transient Local Nusselt Numbers

The variation of local Nusselt number with dimensionless time τ for different values of R_0, Pr and Gr_x is shown in Figs. 5.10(a) to (c). When R_0 was smaller, the effect of curvature was more pronounced and hence the steady state value of Nu_x was larger than that of a flat plate. As shown in Fig. 5.5, the steady state values of Nu_x obtained in the present study agreed fairly well with the recent improved perturbation solutions by Aziz and Na (1982). The difference in the steady state values of Nu_x between the present numerical solutions and those given Aziz and Na was less than 5% except near the leading edge. The agreement was better for larger values of R_0 and Gr_x. The Nusselt number Nu_x went through a minimum value during the transient period. For larger values of Gr_x and R_0, the difference

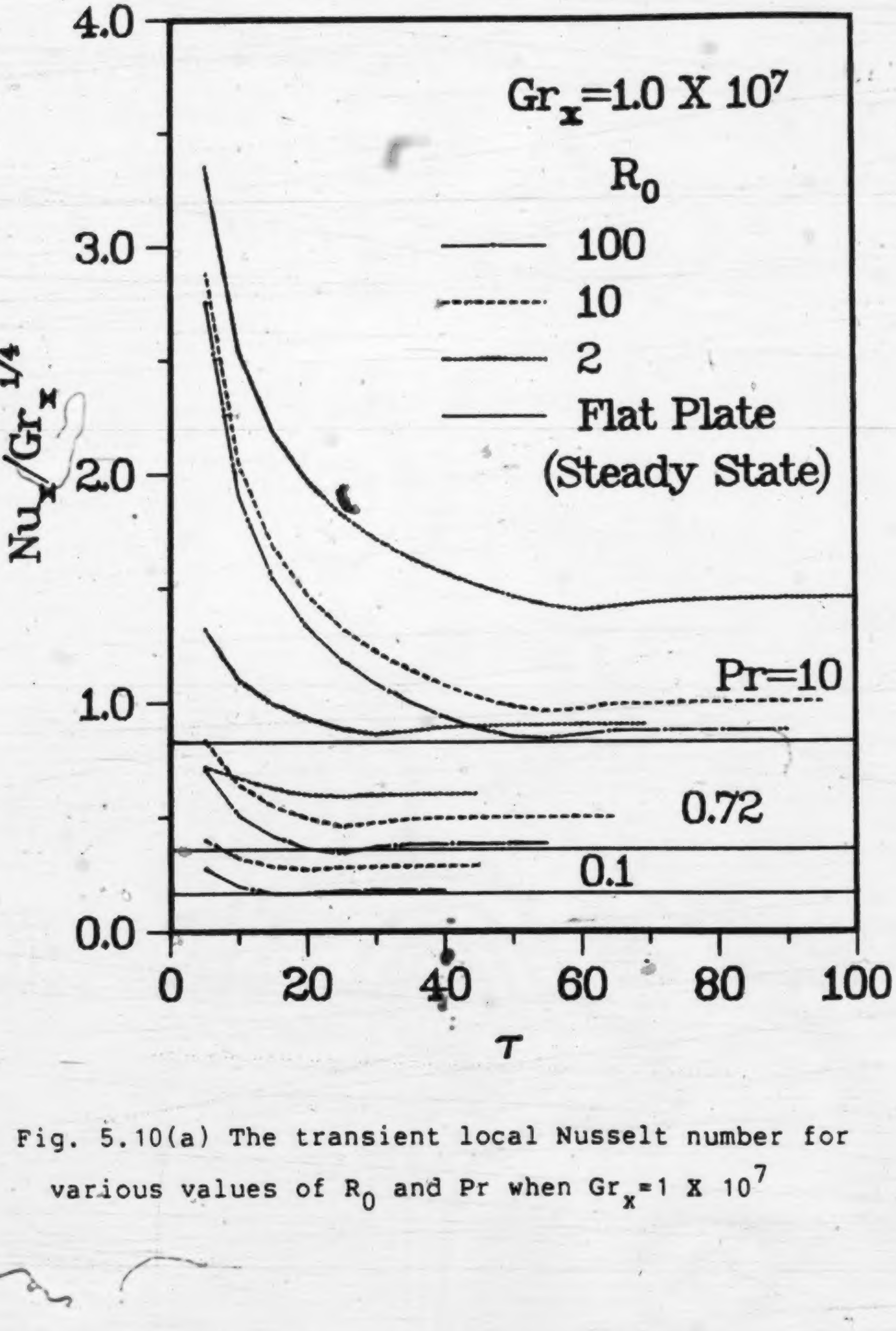

Fig. 5.10(a) The transient local Nusselt number for various values of R_0 and Pr when Gr_x=1 X 10^7

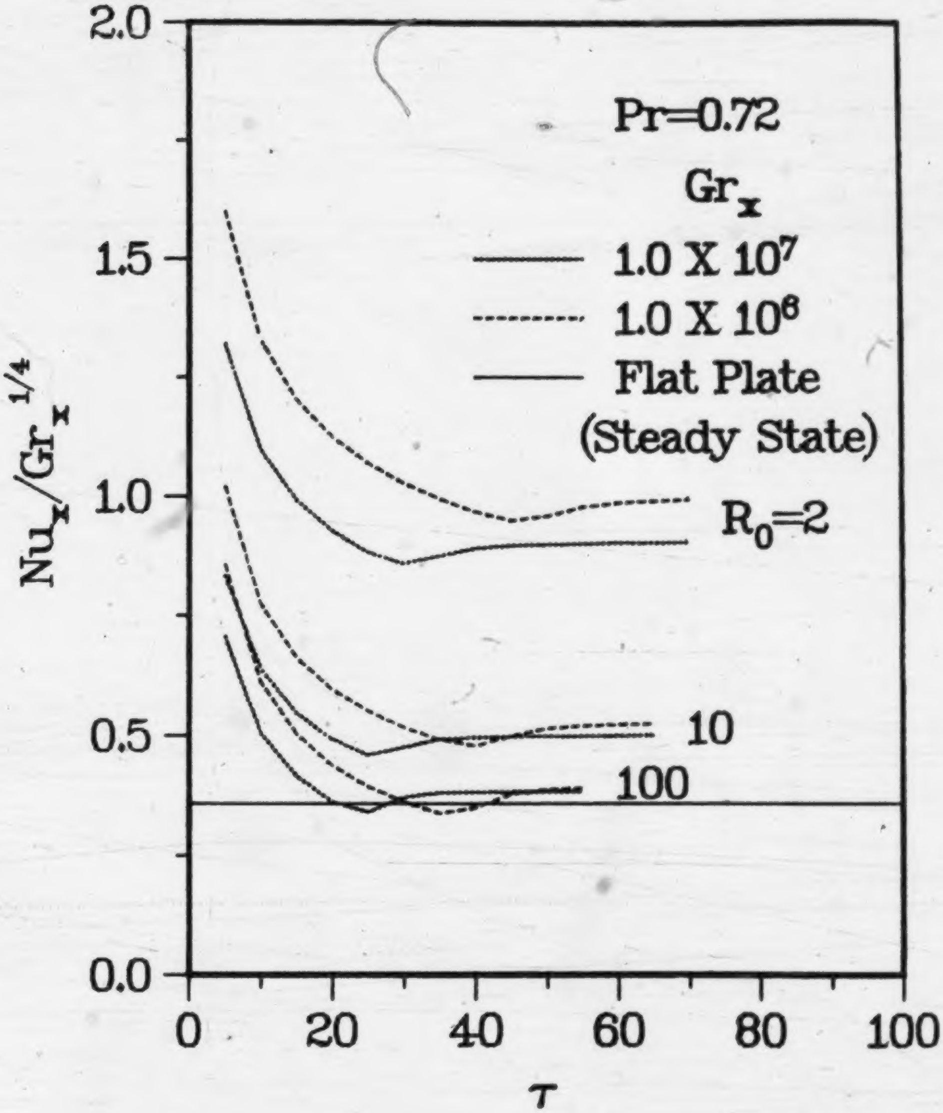

Fig. 5.10(b)The transient local Nusselt number for various values of Gr$_x$ and R$_0$ when Pr=0.72

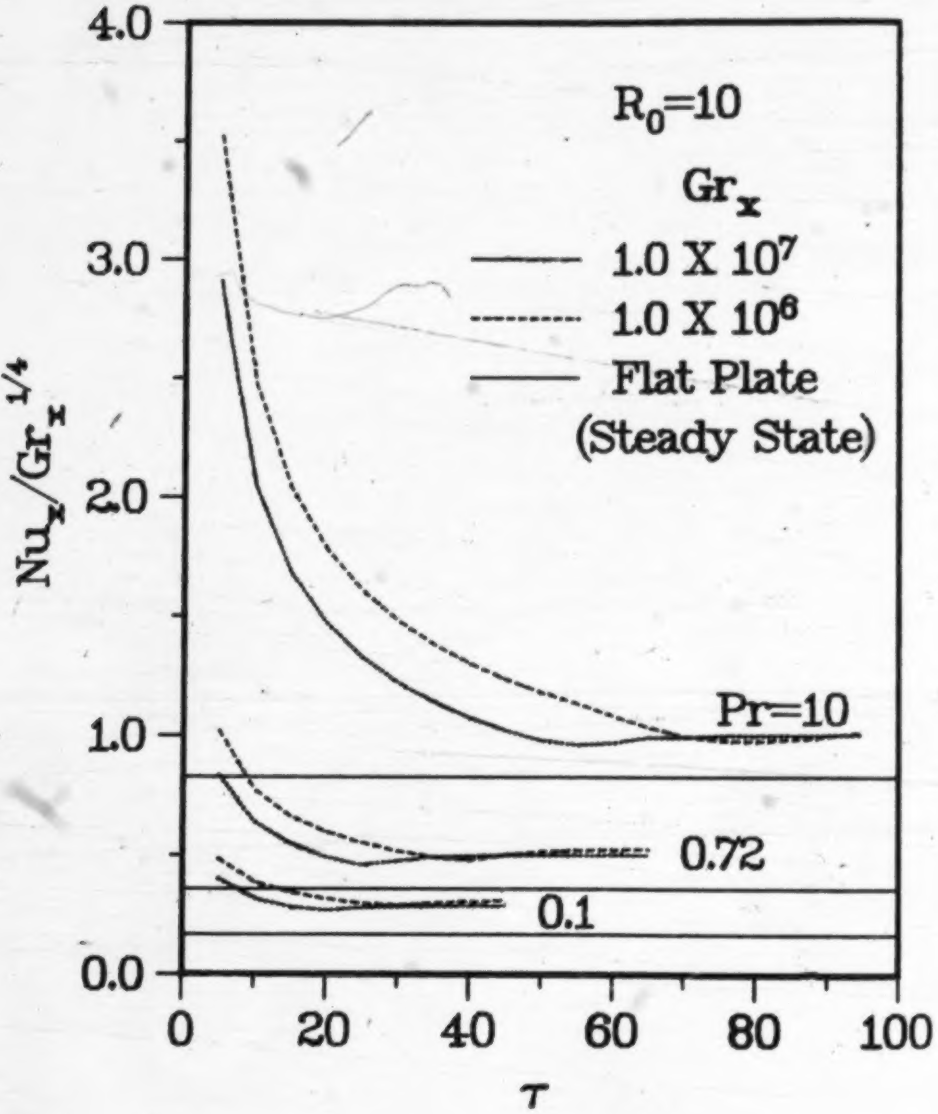

Fig. 5.10(c)The transient local Nusselt number for various values of Gr_x and Pr when R_0=10

between the steady state Nu_x and the minimum value that occurred during the transient period was slightly larger. This undershoot in Nu_x was not as large as the overshoot in temperature that occurred away from the surface, as indicated in the previous section.

5.3.4 Temperature Measurements

Figs. 5.11(a) to (j) show the analog records of the transient and the steady state temperatures at various locations inside the thermal boundary layer when the wall was suddenly cooled. For the experimental records shown, the ambient temperature was at a constant value between 20.0 and 22.5°C. The wall temperature was kept at a constant value between 10.0 and 12.5°C except for the case (j) where it was 5.0°C. Each of these measurements were taken separately with the same thermocouple. The steady state value of Gr_x varied from 1.5×10^7 to 7.4×10^9. (The properties were calculated at the corresponding film temperature). The time taken to cool the wall from the ambient temperature to the the coolant temperature was about 5 seconds. As the transients lasted longer than 1 minute, it was assumed that there was a step change in wall temperature.

During the initial transient period, the mode of heat transfer was conduction and hence the temperature dropped smoothly. As time increased, the effect of the presence of the leading edge propagated downstream. At lower values of Gr_x the flow was laminar during the transient and the steady state periods as seen from Figs. 5.11(a) and (b). At points

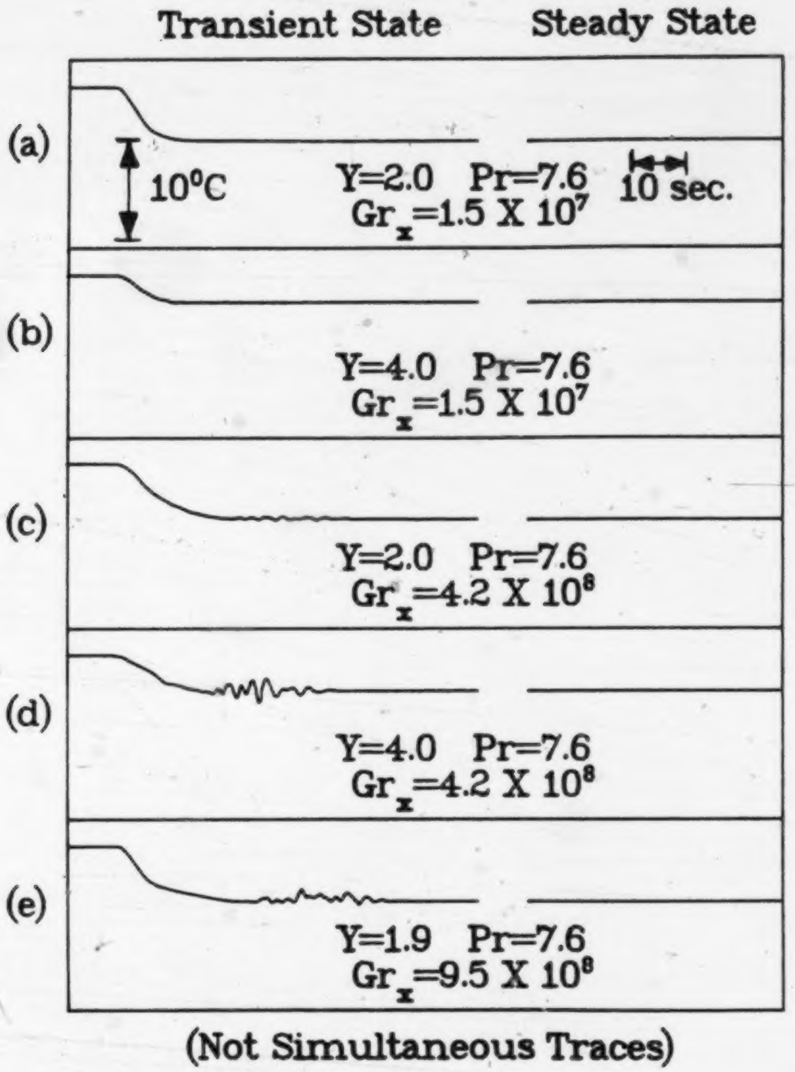

Fig. 5.11 The experimental temperature records at various locations inside the thermal boundary layer when the wall was suddenly cooled

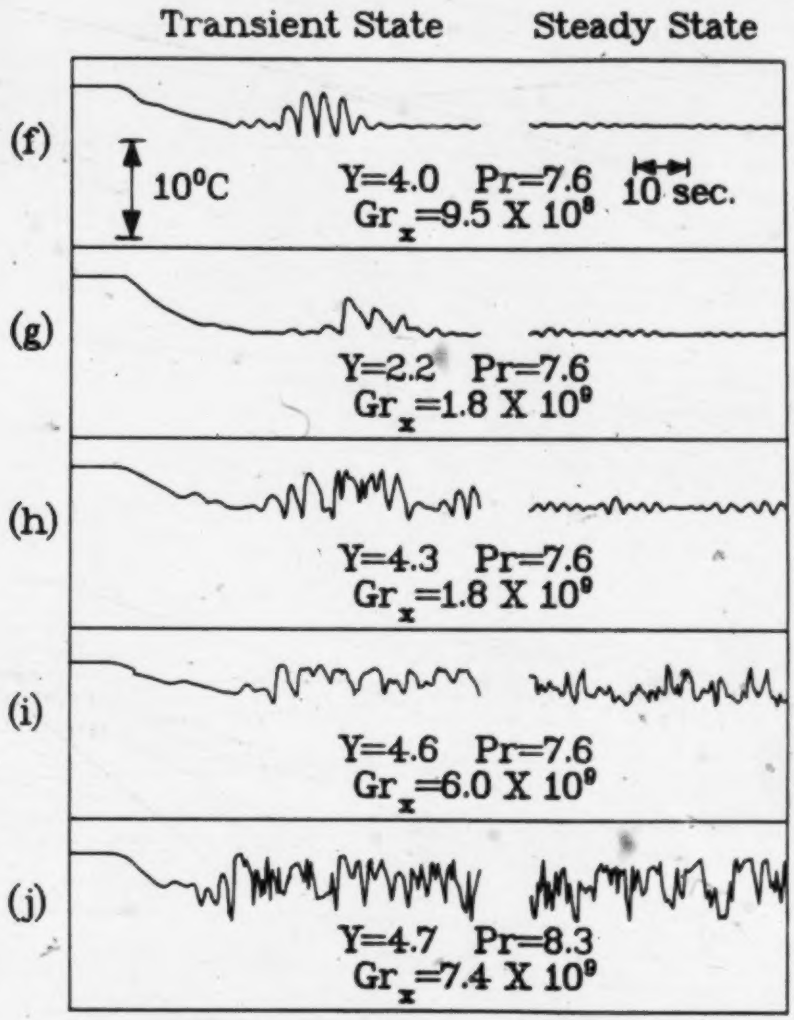

(Not Simultaneous Traces)

Fig. 5.11 The experimental temperature records at various locations inside the thermal boundary layer when the wall was suddenly cooled

farther away from the leading edge the flow became unstable to disturbances that were present in the system. The flow became unstable at a lower value of Gr_x during the transient period than that at steady state period as seen from Figs. 5.11(c) to (f). Figs. 5.11(g) to (i) show that for a particular value of Gr_x the disturbance temperature level was larger during the transient period than at steady state, Also, the transition to turbulent flow occurred at a lower Gr_x during the transient period than at the steady state period.

Fig. 5.12 shows the numerically computed transient and steady state temperature profiles and the experimental measurements for the case with Gr_x=1.56 X 10^7 and Pr=7.4. The value of R_0 in this case was 102. The agreement between the numerical predictions and the experimental measurements was fairly good.

5.3.5 Flow Visualization Studies

Figs. 5.13(a) to (p) show the transient development of the natural convective flow as visualized by shadowgraph for the case when t_0=5.0°C and t_∞=28.0°C. The temperature difference between the ambient water and the wall was kept large so that the flow can be visualized clearly. As expected, during the early period the flow was laminar everywhere as shown in Figs. 5.13(b) and (c).

As the boundary layer grew and the rate of flow increased with time, at distances away from the leading edge, the flow became unstable to disturbances that are

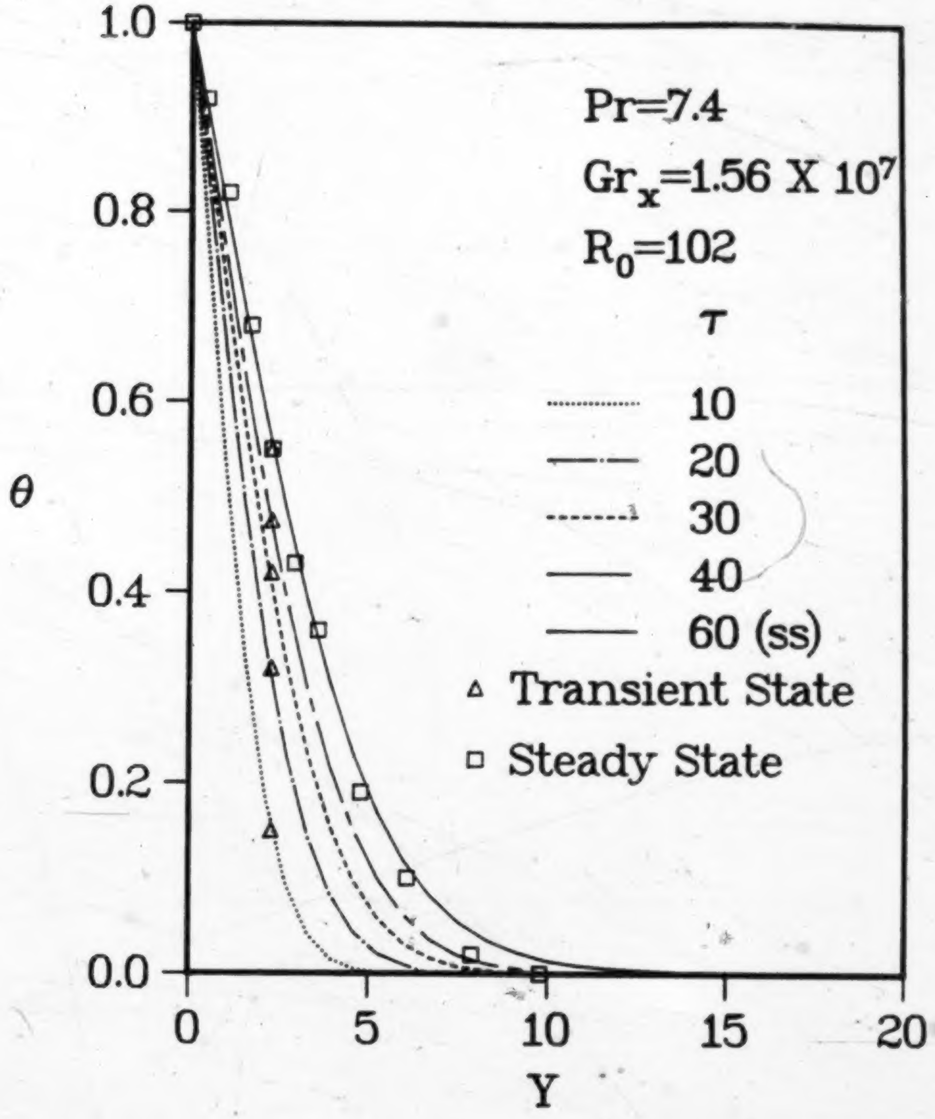

Fig. 5.12 A comparison between the numerical and the experimental temperatures for transient and steady state conditions

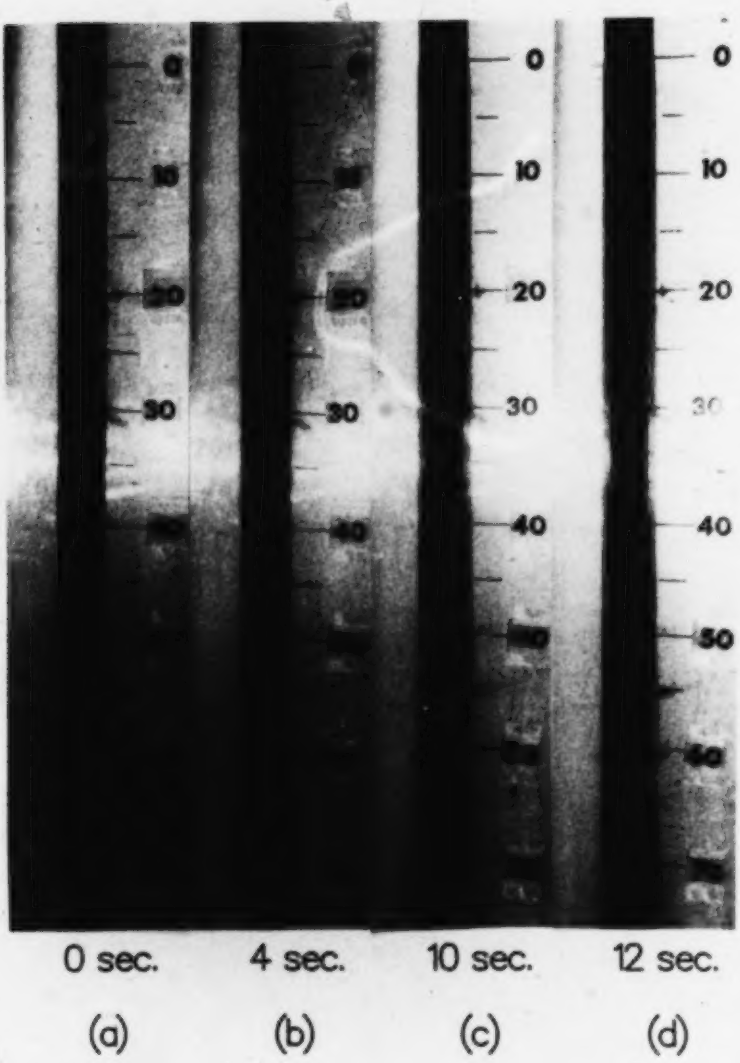
0
10
20
30
40
50
60
0 sec.
4 sec.
10 sec.
12 sec.
(a)
(b)
(c)
(d)

Fig. 5.13 Flow visualization photographs of transient flow development in water

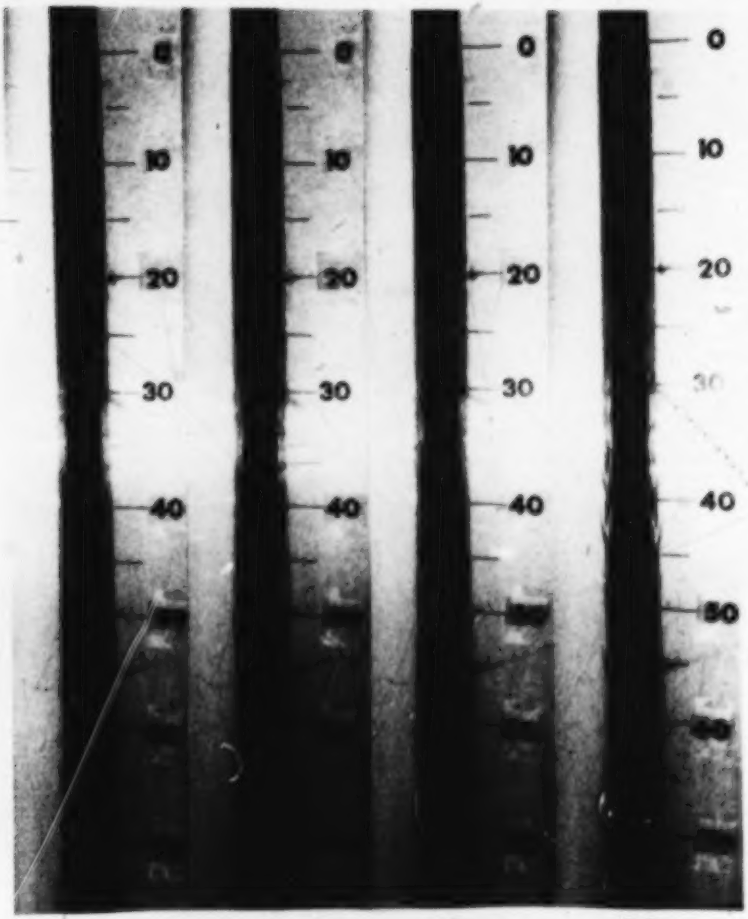
0
10
20
30
40
50

14 sec. 16 sec. 18 sec. 20 sec.

(e) (f) (g) (h)

Fig. 5.13 Flow visualization photographs of transient flow development in water

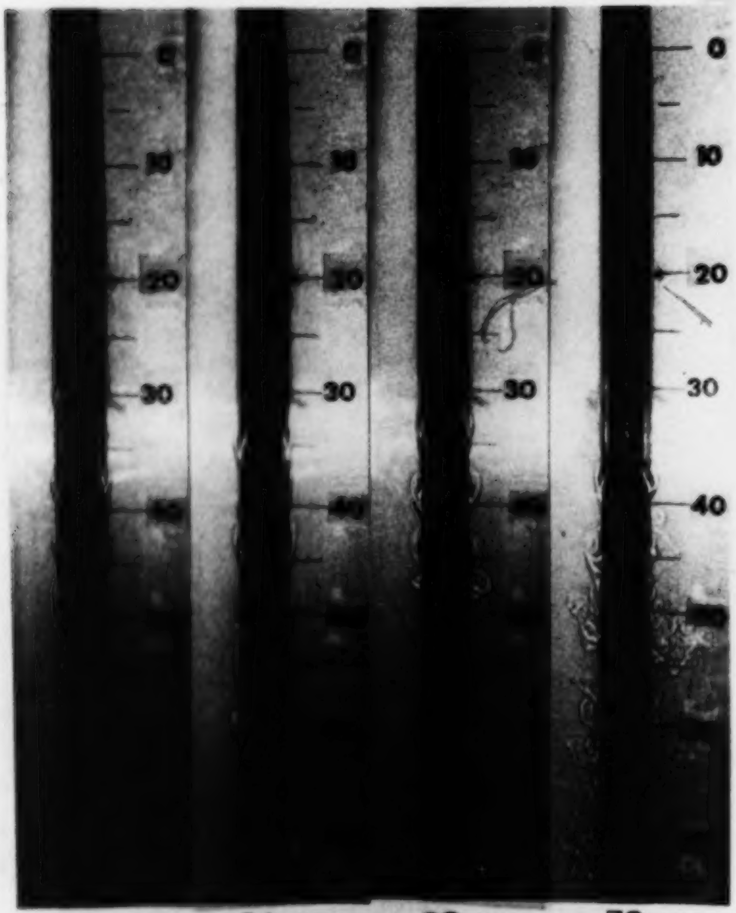
0
10
20
30
40
50

22 sec. 24 sec. 28 sec. 32 sec.

(i) (j) (k) (l)

Fig. 5.13 Flow visualization photographs of transient flow development in water

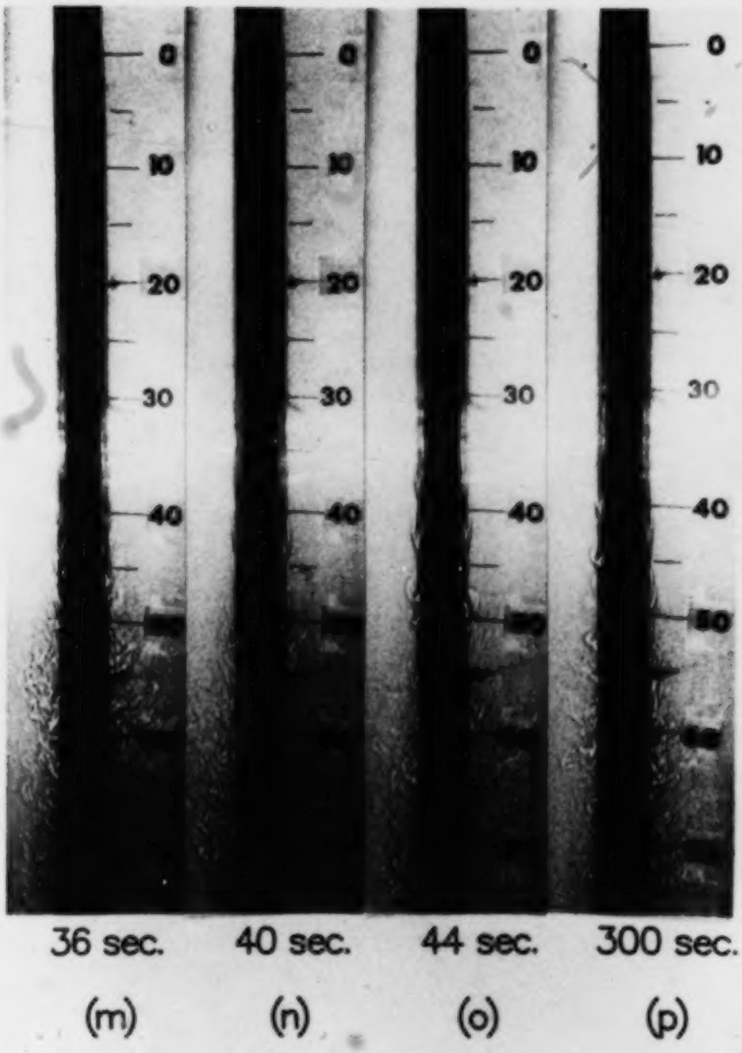
0
10
20
30
40
50
0
10
20
30
40
50
0
10
20
30
40
50
0
10
20
30
40
50
36 sec.
40 sec.
44 sec.
300 sec.
(m)
(n)
(o)
(p)

Fig. 5.13 Flow visualization photographs of transient flow development in water

present in the system. These disturbance waves can be seen in Fig. 5.13(d) in the range 47.5 cm and 52.5 cm from the leading edge. These disturbances amplified as they moved downstream and are clearly seen in Fig. 5.13(e) in the range 52.5 cm and 57.5 cm from the leading edge. Soon these disturbances became vortices. Also, disturbances appeared at many locations and this can be seen in Figs. 5.13(f) and (g). As these vortices moved downstream, they broke down into turbulence, as shown in Fig. 5.13(h) at approximately 75 cm from the leading edge. As more vortices broke down into turbulence the point of transition to turbulent flow moved closer to the leading edge as shown in Figs. 5.13(i), (j) and (k).

It was found that during the transient period the flow could be locally turbulent at some locations and be laminar at points above and below them. In Fig. 5.13(k) at approximately 47.5 cm from the leading edge the disturbance is on the verge of breaking down into turbulent flow whereas the flow is still laminar at 50 cm and this can be also seen in Fig. 5.13(l). At 36 seconds, the flow was turbulent at all locaitions below 50 cm from the leading edge as shown in Fig. 5.13(m). During the transient period, the point of transition to turbulent flow moved down slightly and this can be seen from Figs. 5.13(n) and (o). The flow at steady state is shown in Fig. 5.13(p) and it can be seen that the flow was turbulent below 56 cm from the leading edge. Also, during the transient period the thickness of the boundary layer was larger than that during the steady state period as seen from Figs. 5.13(n) and (p).

5.4 Conclusions

The transient laminar natural convective flow along a smooth vertical circular cylinder subjected to a step change in surface temperature was investigated numerically and experimentally. Numerical results indicate that during the transient period there is an overshoot in temperature in the thermal boundary layer and an undershoot in the local Nusselt number at the surface. The temperature measurements in water during the transient and the steady state periods agree fairly well with those obtained numerically. The flow visualization studies and the temperature measurements show that the critical values of Gr_x for the onset of instability and the transition to turbulent flow are lower during the transient period than at the steady state period.

6. Determination of Local Heat Transfer Coefficients at the Solid-Liquid Interface by Heat Conduction Analysis of the Solidified Region[1]

In this Chapter, it will be demonstrated that when freezing or melting takes place over (or inside) various geometries, the local transfer coefficient at the solid-liquid interface can be obtained fairly accurately from a one-dimensional heat conduction analysis of the solidified region. This is shown by comparing the two-dimensional numerical solution with the one-dimensional analytical solution for a few example problems taken from the literature. The conditions for the validity of the one-dimensional approximation are also given. The example problems involve freezing of water over a planar plate in longitudinal flow (Hirata et al., 1978a and 1978b), a cylinder in cross flow (Okada et al., 1978, and Cheng et al., 1981) and freezing of water inside a pipe with ice bands (Gilpin, 1979,1981).

6.1 Theoretical Analysis

When solidification or melting occurs under external or internal, laminar or turbulent conditions involving various geometrical shapes, the solid-liquid interface is often irregular and can be oscillatory (Gilpin et al., 1980, for example). Thus, in experimental investigations involving solidification or melting processes, it is generally difficult to determine the heat transfer coefficients at the interface by direct measurement of the temperature profiles. Under many circumstances, the shape of the solidified region can be obtained by photographic method. The boundary wall temperatures at any instant are either known or can be measured. The interface is at a constant freezing point temperature. Then the local heat transfer coefficient at the interface can be determined by solving the Laplace equation with Dirichlet boundary conditions for the temperature field inside the solidified region.

---

[1] A version of this chapter has been published: Cheng, K. C., and Sabhapathy, P., *Transactions of ASME, J. Heat Transfer*, Vol. 107, pp. 703-706, 1985.

For the solution of the Laplace equation inside a complex geometry, one can employ various approximate analytical or numerical methods. At steady state or quasi-steady state, the local convective heat transfer coefficient at the ice-water interface can be obtained from a heat balance equation at the interface as

$$h(t_\infty - t_f) - k_i \left.\frac{\partial t}{\partial n}\right|_f = 0 \qquad (6.1)$$

$\left.\frac{\partial t}{\partial n}\right|_f$ is the local temperature gradient for the ice layer at the interface and it can be found from the heat conduction analysis of the ice layer. This involves finding a solution of Laplace equation in an arbitary geometry. The steady two-dimensional heat conduction equation for the solidified region is

$$\nabla^2 t = 0 \tag{6.2}$$

where $\nabla^2 = \frac{\partial^2}{\partial x^2} + \frac{\partial^2}{\partial y^2}$ or $\frac{\partial^2}{\partial r^2} + \frac{1}{r}\frac{\partial}{\partial r} + \frac{\partial^2}{\partial x^2}$

The boundary conditions are

$$t = t_f \quad \text{at the interface} \tag{6.3}$$

$$t = t_0 \quad \text{at the cooled wall} \tag{6.4}$$

Other boundary conditions such as a convective boundary condition at the cooling wall may be specified depending on the particular phase change problem.

By employing the method of boundary-fitted coordinate systems, the irregular or complicated physical domain for the solidified region such as the one shown in Fig. 6.1(a) can be transformed into a regular domain such as the one shown Fig. 6.1(b). This technique is based on the automatic numerical generation of a curvilinear coordinate system. A detailed account of this method can be found in Thompson (1978). When the solidified region is specified by the Cartesian system, the boundary-fitted coordinate system is generated by numerically solving the following system of elliptic equations.

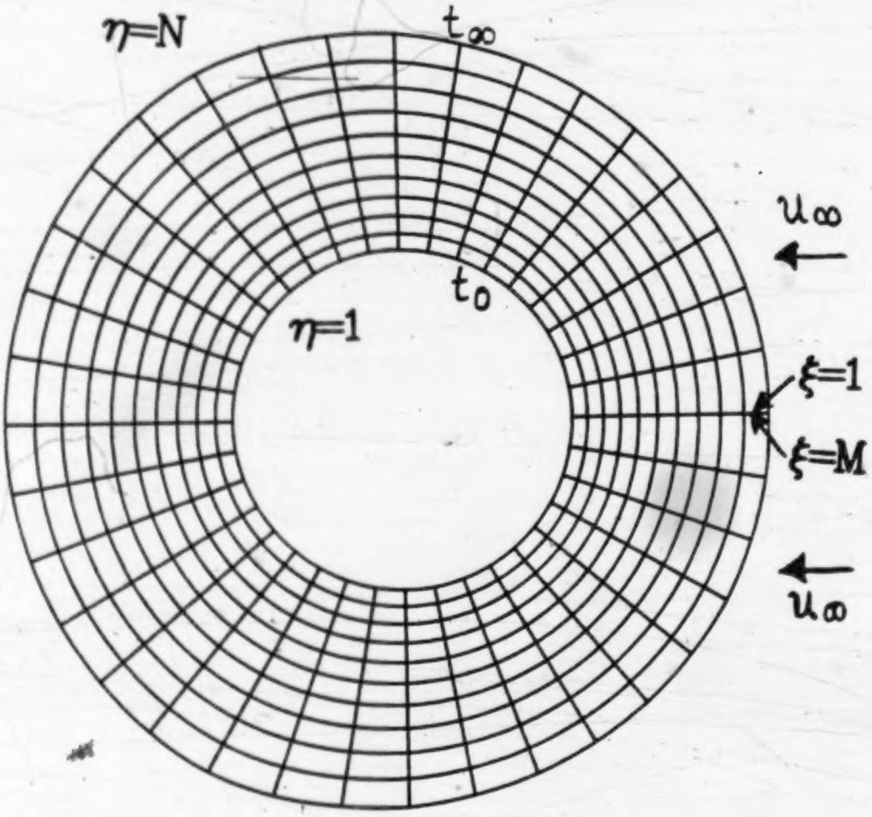
η=N
t_∞
u_∞
t_0
η=1
ξ=1
ξ=M
u_∞

Fig. 6.1(a) The physical plane for ice formation around a cooled cylinder

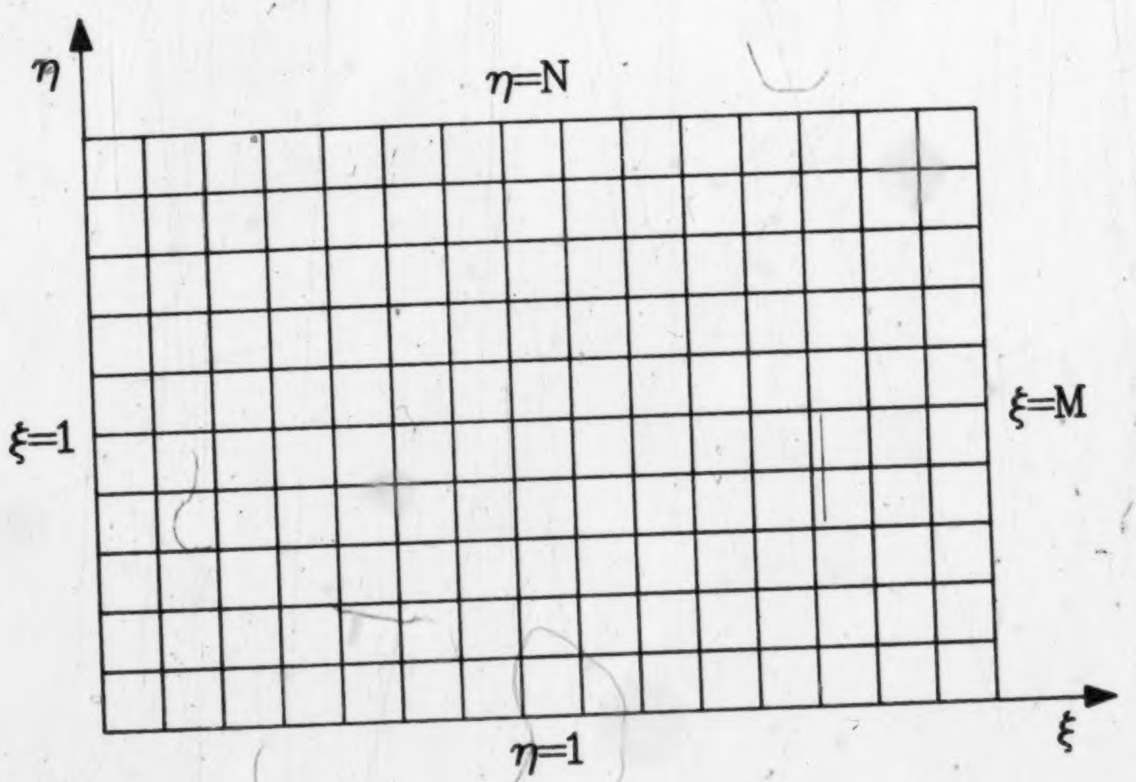

η
η=N
ξ=1
ξ=M
η=1
ξ

Fig. 6.1(b) The transformed plane of the ice layer

$$\alpha x_{\xi\xi} - 2\beta x_{\xi\eta} + \gamma x_{\eta\eta} + J^2(Px_\xi + Qx_\eta) = 0 \qquad (6.5)$$

$$\alpha y_{\xi\xi} - 2\beta y_{\xi\eta} + \gamma y_{\eta\eta} + J^2(Py_\xi + Qy_\eta) = 0 \qquad (6.6)$$

Dirichlet boundary conditions are prescribed at the boundaries. The coordinate control functions P and Q allow node points to be concentrated in some desired part of the domain such as the layer near the ice-water interface. The equation for the temperature field inside the transformed plane becomes,

$$\alpha t_{\xi\xi} - 2\beta t_{\xi\eta} + \gamma t_{\eta\eta} + J^2(Pt_\xi + Qt_\eta) = 0 \qquad (6.7)$$

The ice-water interface corresponds to $\eta(x,y)=N$ in Fig. 6.1(b) and a constant temperature $t=t_f$ is specified there. Other boundray conditions are transformed in a similar manner. Then the finite-differenced equations and the boundary conditions can be solved easily, using a successive over-relaxation procedure, for example. The temperature derivative in the outward normal direction at the ice-water interface can be shown to be (Thompson, 1978),

$$\frac{\partial t}{\partial n}\Big|_f = \frac{\gamma t_\eta - \beta t_\xi}{J(\gamma)^{1/2}}\Big|_{\eta=N} \qquad (6.8)$$

Thus, the normal derivative at the interface, and hence the local heat transfer coefficient, can be obtained more easily than the collocation method or direct finite difference method. The total heat transfer rate per unit axial distance can be obtained from

$$Q' = \int [h(\gamma)^{1/2}] d\xi \tag{6.9}$$

Similarly the local heat transfer coefficient at the cooled wall and the corresponding heat transfer rate can be found.

In this study, the square mesh sizes (M,N) were chosen by trial and error. (M=25, N=11,16) for the flat plate, (M=37, N=11,16) for the cylinder and (M=20, N=11) for the pipe were used to obtain the numerical solution. The convergence criterion used in finding the coordinates was 1×10^{-3} of the maximum value of the coordinate in that particular direction and that for the dimensionless temperature (1.0 at the interface and 0.0 at the cooled wall) was also 1×10^{-3}. The maximum difference in the total heat transfer rates at the cooled wall and the interface was found to be less than 0.5 percent in all cases studied.

An approximate solution to the local heat transfer coefficients at the interface can be found from a one-dimensional analysis of the solidified region. For the case of ice formation on a cooled flat plate, the local heat transfer coefficient h can be computed from the following equation

$$h = \frac{\theta_c k_i}{\delta} \tag{6.10}$$

For ice formation outside a cooled cylinder, it can be shown that (Carslaw and Jaeger, 1956),

$$h = \frac{\theta_c k_i}{r_0}\left[\frac{1}{S\ (1/Bi+\ln S)}\right] \tag{6.11}$$

$$h = \frac{\theta_c k_i}{r_0}\left[\frac{1}{S\ \ln S}\right] \quad \text{for } Bi \to \infty \tag{6.12}$$

For the ice formation inside a cooled pipe, it can be shown that

$$h = \frac{\theta_c k_i}{r_0}\left[\frac{1}{S\ \{1/Bi+\ln(1/S)\}}\right] \tag{6.13}$$

$$h = \frac{\theta_c k_i}{r_0}\left[\frac{1}{S\ \ln(1/S)}\right] \quad \text{for } Bi \to \infty \tag{6.14}$$

The validity of one-dimensional model is assessed against the two-dimensional model.

6.2 Results and Discussion

6.2.1 Ice Formation Over an Isothermally Cooled Planar Plate

The transition from laminar to turbulent flow on a frozen layer formed on an isothermally cooled flat plate placed in a stream of warm water was studied in (Hirata et al., 1978a, 1978b). Due to the interaction between the ice surface and the convective heat transfer, two modes of transition, namely smooth transition and step transition, were observed in the transition flow regime. For both modes, the transition Reynolds number was found to be substantially lower than that for flow on a flat plate. The local heat transfer coefficient at the ice-water interface was determined by the analysis of the temperature field in the ice layer for two cases shown in Hirata et al. (1979b) and the results are given in Fig. 6.2. For smooth transition, the local heat tranfer coefficients from the one-dimensional solution and the two-dimensional solution agreed within 1 percent. For the step transition, the two solutions were within 1 percent for Nu_x at all positions except near the region where there was a sudden change in the ice layer thickness. Near that region, the one-dimensional solution was found to overpredict the local Nusselt number at points near a local maximum ice layer thickness and to underpredict at points near a local minimum. Hence, a one-dimensional analysis can be applied when the thickness of the ice layer changes smoothly and a two-dimensional analysis is needed when there is a sudden change of ice layer thickness.

6.2.2 Ice Formation Around an Isothermally Cooled Cylinder in Crossflow

When water freezes over an isothermally cooled cylinder in cross flow, the ice layer formed has a complex shape (Okada et al., 1978, and Cheng et al., 1981). The local heat transfer coefficient at the interface of the frozen layer was determined by finite difference method in (Okada et al., 1978) and by a collocation method in (Cheng et al., 1981) using the two-dimensional heat conduction equation in cylindrical coordinates for the doubly connected region. The shapes of the frozen layers were determined by measurements

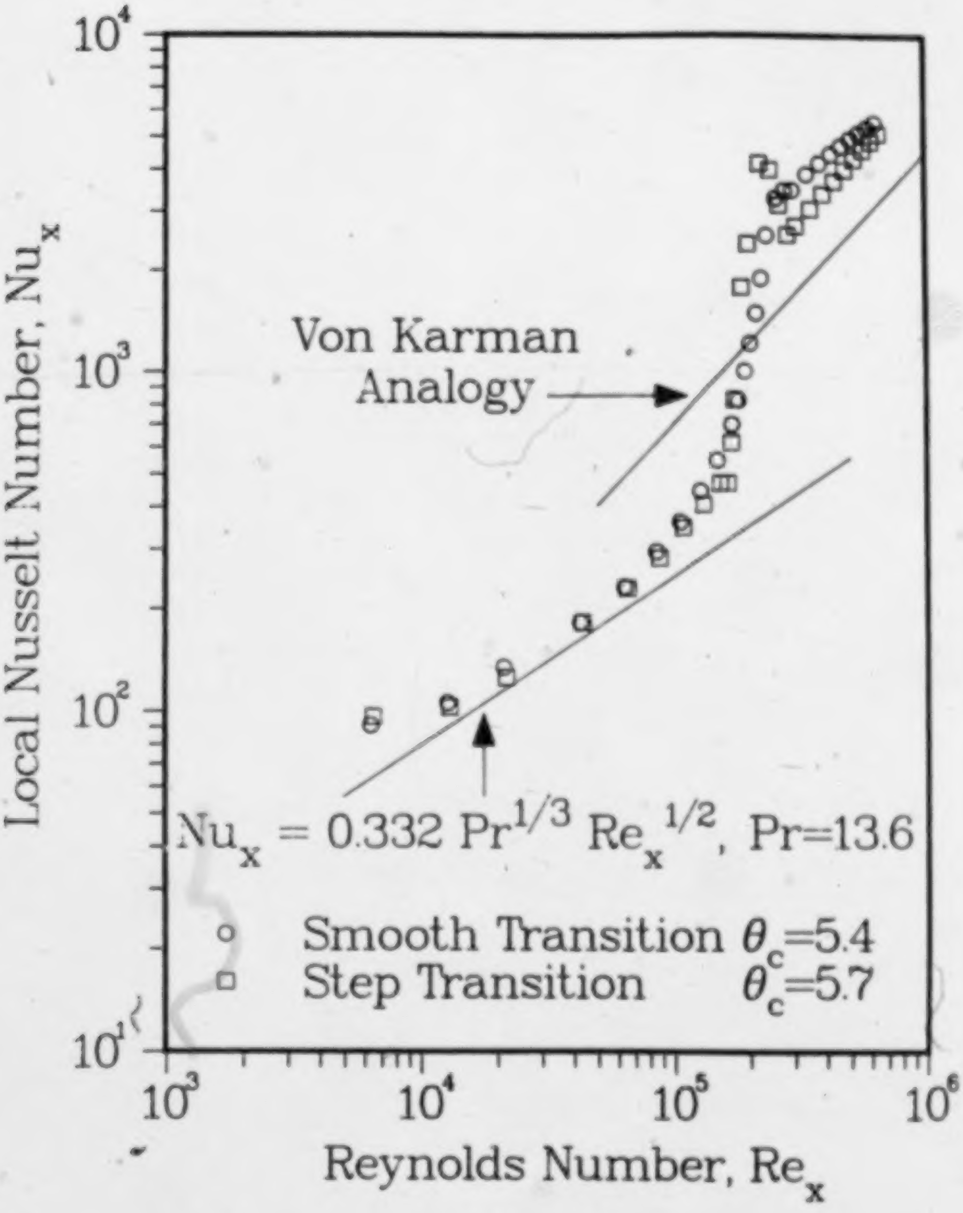

Fig. 6.2 The local Nusselt number at the interface for freezing of water over an isothermally cooled planar plate

in Okada et al. (1978) and by photographs in Cheng et al. (1981). For the profiles given in the above two studies, the local heat transfer coefficients at the interface were determined by both the method of boundary-fitted coordinate systems and the one-dimensional analysis. The results are shown in Figs. 6.3(a) and (b). (The local heat transfer coefficients, rather than the local Nusselt numbers, are plotted in the figures for easy comparison with literature). The present two-dimensional solution agreed fairly well with the values given in the above studies. As noted earlier, that the one dimensional-analysis overpredicts the local heat transfer coefficients where the ice layer thickness was locally maximum and gave fairly accurate results when the ice layer thickness changes smoothly.

6.2.3 Ice Formation Inside a Convectively Cooled Pipe

Freezing of water inside a cooled vertical pipe is of considerable technical importance particularly in the blockage of water pipes in cold regions. The ice-band structure in the form of surface waves at the ice-water interface inside a cooled pipe was first reported by Gilpin (1979, 1981) for the Reynolds number range 3.7×10^2 to 1.4×10^4. The local heat transfer coefficients at the ice-water interface for a typical steady-state ice layer profile shown in Gilpin (1981) were determined by the method of the boundary-fitted coordinate systems. As noted in previous cases, the one-dimensional solution predicted a higher value for the local heat transfer coefficient at

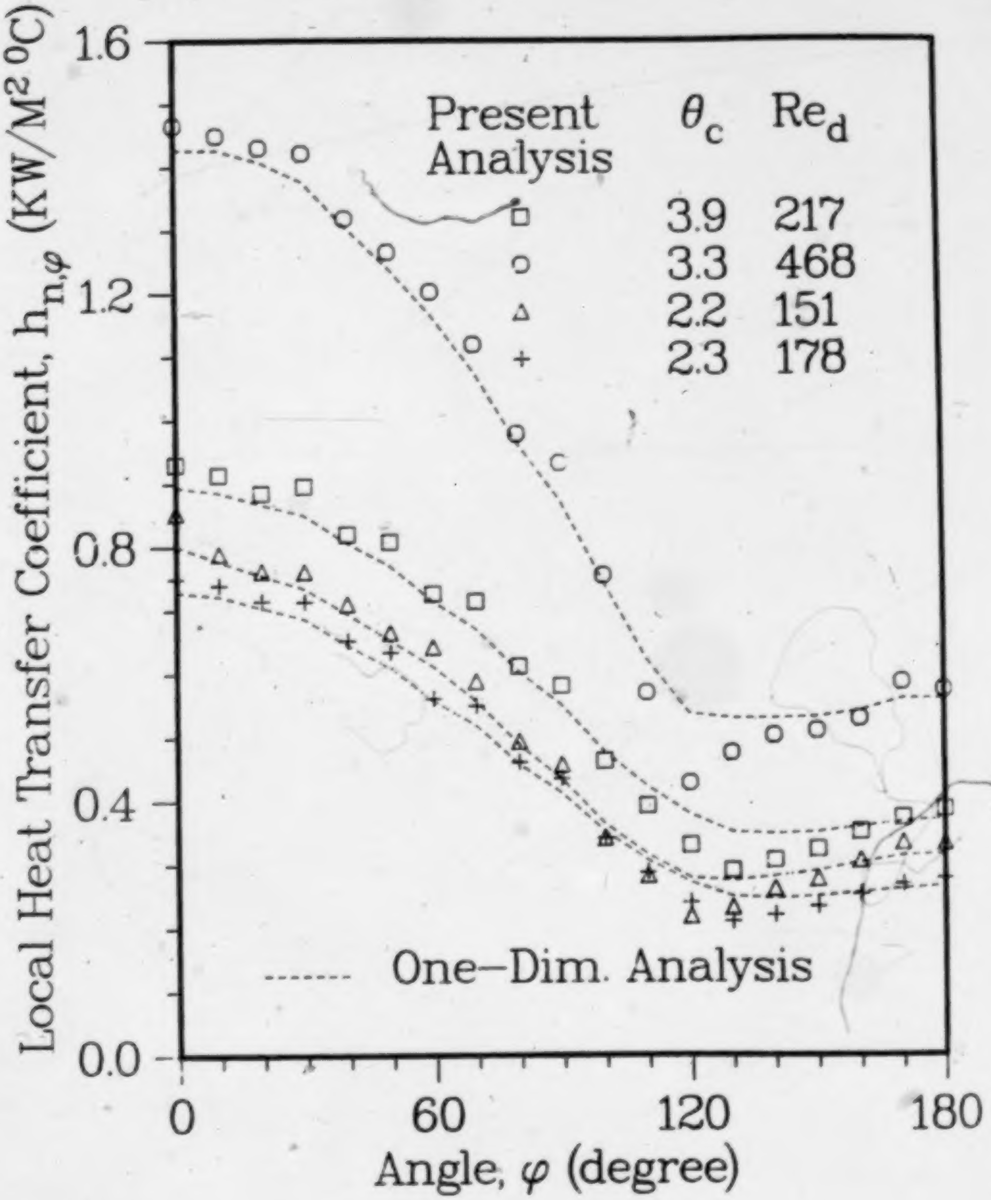

Fig. 6.3(a) The local heat transfer coefficient at the interface for freezing of water over an isothermally cooled cylinder in cross flow

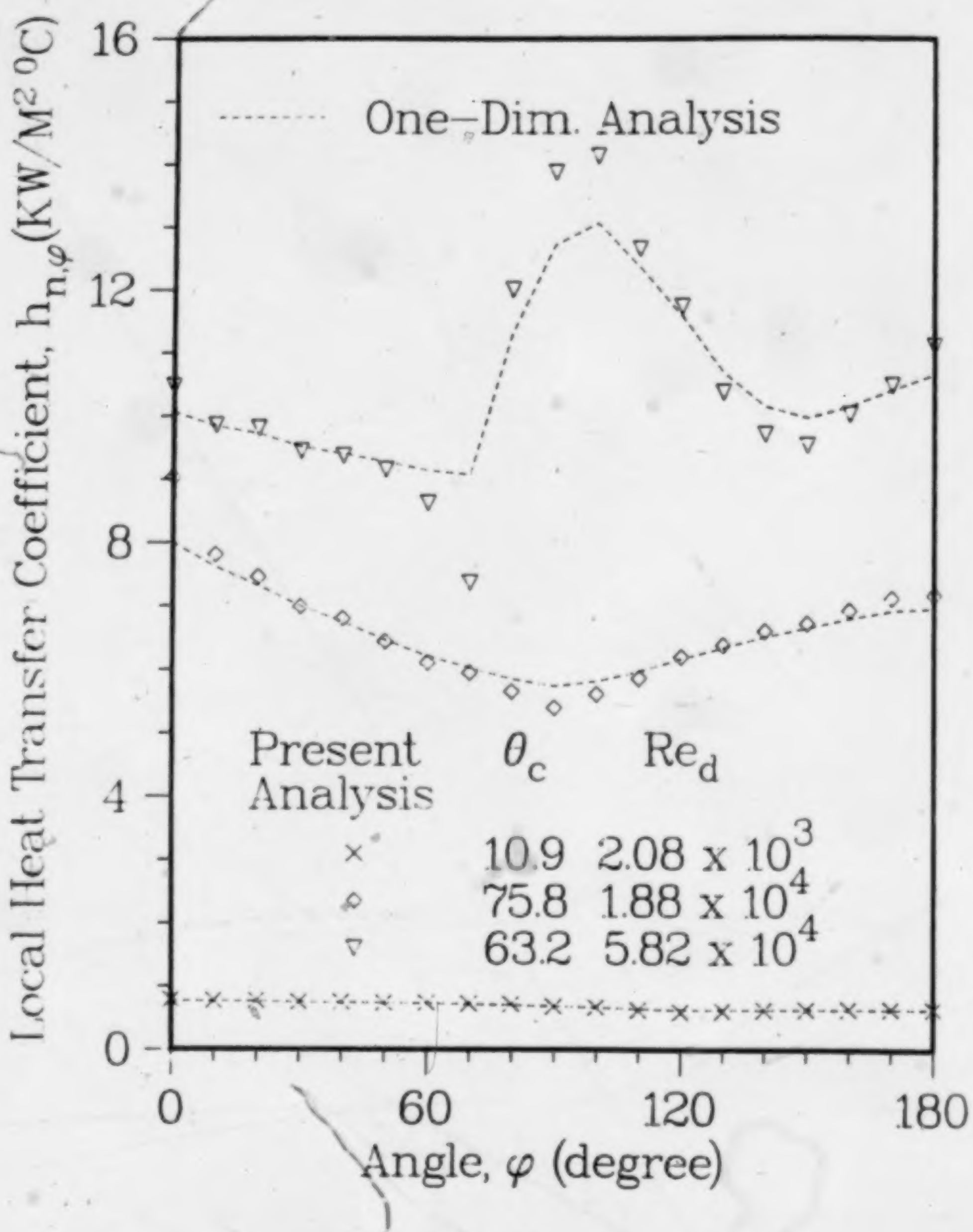

Fig. 6.3(b) The local heat transfer coefficient at the interface for freezing of water over an isothermally cooled cylinder in cross flow

points near the maximum ice layer thickness and agreed fairly well with the two-dimensional analysis when the ice layer thickness changed smoothly (see Fig. 6.4). It is noted that the determination of the local heat transfer coefficients by temperature profile measurements would be extremely difficult for this case.

6.3 Conclusions

The method of boundary-fitted coordinate systems was applied to a class of steady-state ice formation problems involving simply or doubly connected solidified regions in determining the local heat transfer coefficients at the solid-liquid interface. It was also shown that a one-dimensional analysis gives fairly accurate results for the local heat transfer coefficients at the ice-water interface except at points near a local maximum or minimum ice layer thickness. It is to be noted that the determination of the local heat transfer coefficient at the solid-liquid interface from the heat conduction analysis of the solid region has not been widely employed in the past. This method may be very useful in situations where it is very difficult to measure the temperature profile.

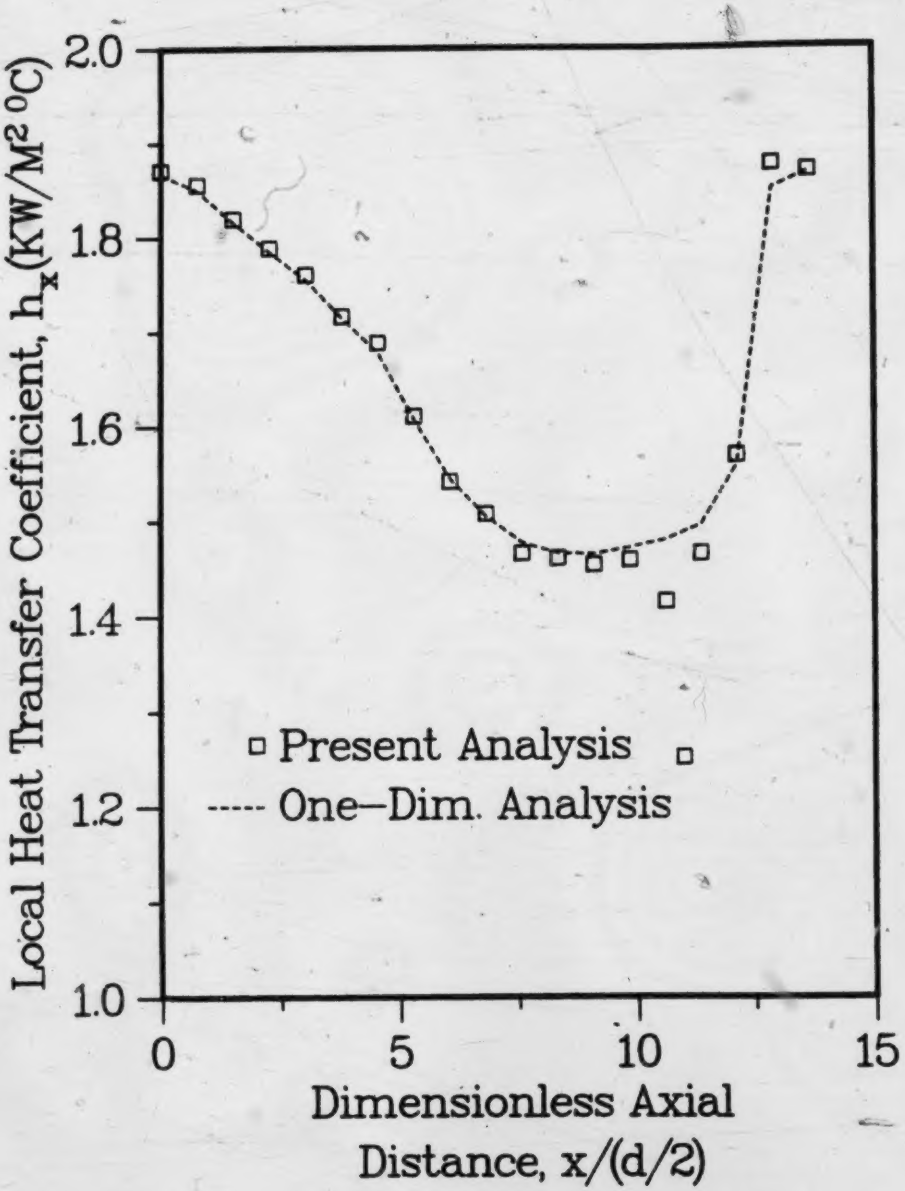

Fig. 6.4 The local heat transfer coefficient along one wave length for ice surface waves inside a cooled pipe

7. An Experimental Investigation of Ice Formation Over a Convectively Cooled Vertical Circular Cylinder in Natural Convection[1]

In this Chapter, a one-dimensional analysis of the transient development of the solid-liquid interface when a superheated liquid solidifies on a convectively cooled vertical pipe is presented. Experimental results for freezing of water (8 to 17.5°C) over a cooled vertical pipe (coolant temperature range -10 to -20°C) are given. Photographs of transient and steady state ice layer profiles are presented. The effects of natural convection in all the three regimes of the flow (laminar, transition, and turbulent) are examined. The effects of stratification and dissolved air in the ambient water, and the stability of the interface to artificially induced disturbances are also investigated.

7.1 A One-Dimensional Analysis of the Transient Development of the Solid-Liquid Interface

When a warm quiescent liquid solidifies over a cooled vertical cylindrical surface, the presence of natural convection in the liquid adjacent to the interface affects the position and the shape of the interface at any time.

---

[1] A version of this chapter has been presented: Cheng, K. C., and Sabhapathy, P., *the 23rd ASME National Heat Transfer Conference*, Denver, Colorodo, Aug. 4-7, 1985, and published as ASME Paper 85-HT-1

Experiments on freezing of water, to be described in detail later, indicate that the surface of the interface is smooth and the ice thickness changes gradually with distance except near the leading edge. Hence, the temperature distribution inside the solid layer can be assumed to be one-dimensional at any time except near the leading edge. Previous studies on solidification or melting over a convectively cooled or heated cylindrical pipe have mainly employed finite difference numerical methods (Yuen and Kleinman, 1980, for example). Also, these studies neglected the effect of natural convection in the liquid. In the present analysis, the effect of natural convection heat transfer in the liquid was included and the position of the solid-liquid interface was obtained by employing a perturbation method which was simpler and straightforward.

A schematic diagram of one-dimensional solidification of a warm liquid over a cooled vertical circular cylinder is shown in Fig. 7.1. The phase transition was assumed to take place at a constant temperature and the density difference between the solid and the liquid was neglected. The time taken for the steady natural convective flow to be established was assumed to be small and the natural convective heat transfer coefficient at the interface was assumed to be constant with time. (The heat transfer coefficient can be obtained from the correlations available in the literature for the natural convective flows over isothermal vertical surfaces and also, from the heat conduction analysis of the steady state solidified region).

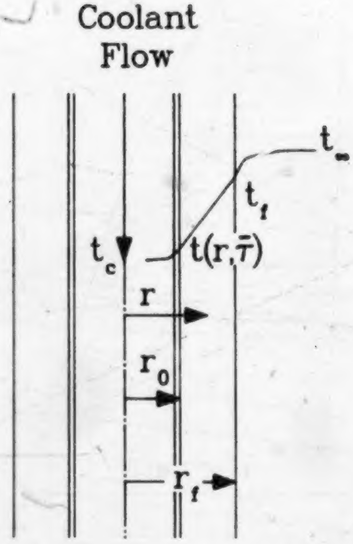
Coolant
Flow
t_∞
t_f
t_c
$t(r,\bar{\tau})$
r
r_0
r_f

Fig. 7.1 The coordinate system for a one-dimensional analysis of the ice layer

Also, the thermophysical properties of the solid were assumed to be independent of temperature.

The governing equations for the temperature distribution inside the solid layer, and the interface position are given by

$$\frac{\partial t}{\partial \bar{\tau}} = \alpha_s \left(\frac{\partial^2 t}{\partial r^2} + \frac{1}{r}\frac{\partial t}{\partial r}\right) \qquad (7.1)$$

$$\rho_s L \frac{\partial r_f}{\partial \bar{\tau}} = k_s \frac{\partial t}{\partial r}\bigg|_{r_f} - h_f(t_\infty - t_f) \qquad (7.2)$$

where L is the latent heat of freezing. (Other symbols are defined in the Nomenclature).

The boundary conditions are

$$\text{at } r = r_f, \quad t = t_f \qquad (7.3)$$

$$\text{at } r = r_0, \quad k_s \frac{\partial t}{\partial r} = h_c(t - t_c) \qquad (7.4)$$

$$\text{at } \bar{\tau} = 0, \quad r_f = r_0 \qquad (7.5)$$

When the convective heat transfer coefficient between the coolant and the wall, $h_c \to \infty$, the boundary condition (7.4) reduces to that of a constant wall temperature. Introducing the following dimensionless variables,

$$R = \frac{r}{r_0}, \qquad S = \frac{r_f}{r_0}, \qquad \tau = \frac{\bar{\tau}\ \epsilon a_s}{r_0^2},$$

$$\epsilon = \frac{c_s(t_f - t_c)}{L}, \qquad \theta = \frac{t - t_c}{t_f - t_c}$$

the equations and the boundary conditions become,

$$\frac{\partial^2\theta}{\partial R^2} + \frac{1}{R}\frac{\partial\theta}{\partial R} = \epsilon\ \frac{\partial\theta}{\partial\tau} \tag{7.6}$$

$$\frac{dS}{\partial\tau} = \frac{\partial\theta}{\partial R}\Big|_{R=S} - H \tag{7.7}$$

where $H = \dfrac{h_f r_0}{k_s\theta_c}$ and $\theta_c = \dfrac{t_f - t_c}{t_\infty - t_f}$

$$\frac{1}{Bi}\ \frac{\partial\theta}{\partial R}\Big|_{R=1} = \theta(R,\tau)\,\Big|_{R=1} \tag{7.8}$$

where $Bi = \dfrac{h_c r_0}{k_s}$

$$\theta(S,\tau) = 1 \tag{7.9}$$

$$S(\tau=0) = 1 \tag{7.10}$$

When Bi → ∞ the boundary condition (7.9) reduces to that of a constant wall temperature.

The dimensionless parameters of the problem are H and ϵ. H is a measure of heat transfer by convection at the interface. The larger the value of H, the smaller is the thickness of solidfied layer at steady state for a given wall temperature. When the liquid is at its freezing temperature, H is equal to zero. At steady state, the interface position and H are related by (from solving eqs. (7.6) to (7.10))

$$H = \frac{1}{S[1/Bi+\ln S]} \tag{7.11}$$

For an isothermal wall, ϵ is a measure of the ratio of the heat capacity of the solid layer to the latent heat of freezing and is called Stefan number. For water ϵ is less than 1.0 under normal freezing conditions. Hence, a perturbation technique similar to the one employed by Seeniraj and Bose (1982) for a flat plate can be used to obtain approximate solutions to the set of equations (7.6) to (7.10). As shown by Seeniraj and Bose, the independent variable τ was replaced by $S(\tau)$, and $G=dS/d\tau$ (G is the freezing speed). Employing ϵ as a perturbation parameter, θ and G can be written as,

$$\theta(R,S) = \theta_0(R,S) + \epsilon\theta_1(R,S) + \epsilon^2\theta_2(R,S) + \ldots. \tag{7.12}$$

$$G(S) = G_0(S) + \epsilon G_1(S) + \epsilon^2 G_2(S) + \ldots. \tag{7.13}$$

Substituting the above equations in equations (7.6) to

(7.10) and equating the terms with the same powers of ϵ, the resulting equations and the boundary conditions become,

$$\frac{\partial^2\theta_i}{\partial R^2} + \frac{1}{R}\frac{\partial\theta_i}{\partial R} = \begin{cases} 0 & \text{for } i = 0 \\ \sum_{j=1}^{i} G_{j-1}\frac{\partial\theta_{i-j}}{\partial S} & \text{for } i \geq 1 \end{cases} \tag{7.14}$$

$$G_i = \begin{cases} \left.\frac{\partial\theta_i}{\partial R}\right|_{R=S} - H & \text{for } i = 0 \\ \left.\frac{\partial\theta_i}{\partial R}\right|_{R=S} & \text{for } i \geq 1 \end{cases} \tag{7.15}$$

$$\text{at } R = 1,\ \frac{\partial\theta_i}{\partial R} = Bi\theta_i \text{ for } i \geq 0 \tag{7.16}$$

$$\text{at } R = S,\quad \theta_i = \begin{cases} 1 & \text{for } i = 0 \\ 0 & \text{for } i \geq 1 \end{cases} \tag{7.17}$$

and $\tau(S=1) = 0$ (7.18)

The solutions to the zeroth and the first order perturbations are

$$\theta_0 = \frac{1/Bi + \ln R}{1/Bi + \ln S} \tag{7.19}$$

$$G_0 = \frac{1}{S(1/Bi + \ln S)} - H \tag{7.20}$$

$$\theta_1 = \frac{FR^2}{4Bi} + \frac{F_1}{2}\left[\frac{R^2}{2}\ln R - \frac{R^2}{2} + F_2 \ln R + F_3\right] \quad (7.21)$$

$$G_1 = \frac{F_1 S}{2Bi} + \frac{F_1}{2}\left[S\ln S - \frac{S}{2} + \frac{F_2}{S}\right] \quad (7.22)$$

where $F_1 = -\dfrac{G_0}{S(1/Bi+\ln S)^2}$

$$F_2 = \frac{(S^2/2)[1-1/Bi-\ln S]+(1/Bi)[1-1/Bi-1/2]}{1/Bi+\ln S}$$

$$F_3 = \frac{1}{Bi}\left[\frac{1}{Bi} - 1 + F_2\right] + \frac{1}{2}$$

Higher order solutions can be obtained in a similar manner and a better approximation to θ and G can be obtained by employing the transformation suggested by Shanks (1953). Once G is known, τ can be obtained as a function of S, by inverting the equation $G=dS/d\tau$ and integrating it numerically.

At steady state, the heat conducted through the solid layer is exactly balanced by the heat convected from the liquid at the interface. Hence, the local and the average heat transfer coefficients at the interface for the steady state condition are given by

$$h_f = \frac{k_s\theta_c/r_0}{S[1/Bi + \ln S]} \quad (7.23)$$

$$\bar{h}_f = \frac{1}{x}\int_0^x h_f \, dx \tag{7.24}$$

The corresponding expressions for the local and the average Nusselt numbers at the interface are,

$$Nu_x = \frac{h_f x}{k_l} \tag{7.25}$$

$$\bar{Nu} = \frac{\bar{h}_f x}{k_l} \tag{7.26}$$

7.2 Experimental Apparatus and Procedure

The experimental apparatus was the same as the one described in Chapter 3 except that the coolant was a mixture of 60% (by volume) ethylene glycol, 10% methanol and 30% water. Fig. 7.2 shows the photograph of the probe used to measure the ice layer thickness. The probe was made up of two thin stainless steel shimstocks with a 'Delrin' tip so that the freezing front might not decay when touched. The steel arm mounted on the horizontal sliding arrangement carried the probe. When the tip touched the ice surface, the shimstocks made contact with each other and was sensed electronically for ice thickness measurement.

The steel tank was filled with deaerated (~27.5 in Hg. vacuum) tap water at a desired temperature and was allowed to equilibrate for about one to two hours. The coolant was brought down to a desired temperature and was kept circulating in the bypass loop. The flow was then allowed to circulate through the test section. The inlet and the outlet

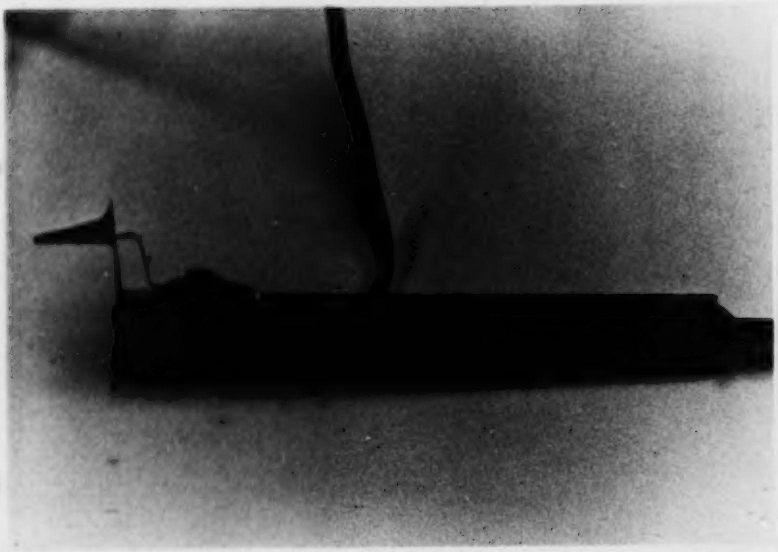

Fig. 7.2 Photograph of the probe used to measure the ice layer profile

temperatures of the coolant were continuously recorded. They were always within 0.1°C except during the initial cooling stage when the difference between them was as high as 0.5°C. The temperature of the ambient water was measured periodically. The ice profiles were also photographed at different times. The position of ice-water interface was measured with the probe at selected locations during transient and steady state periods.

7.3 Results and Discussion

7.3.1 Transient Development of the Interface

Experiments were done for various coolant temperatures from -10 to -20°C and ambient water temperatures from 8 to 17.5°C. An estimate of the convective heat transfer coefficient at the wall indicated that the Biot number was about 10 to 30. It is to be noted that the ice-water interface corresponds to a constant temperature at 0°C.

Figs. 7.3(a) to (c) show the photographs of transient ice layer growth for t_∞=9.9°C and t_c=-18.6°C. The thickness of the ice layer changed rapidly near the leading edge and increased slowly away from it. Visualization of the flow adjacent to the interface by shadowgraph technique for this case revealed that the flow was mainly laminar for the entire length of the cylinder with some disturbances on the laminar flow observed below 45 cm from the leading edge. The thickness of the ice layer continued to increase for the entire length of the cylinder.

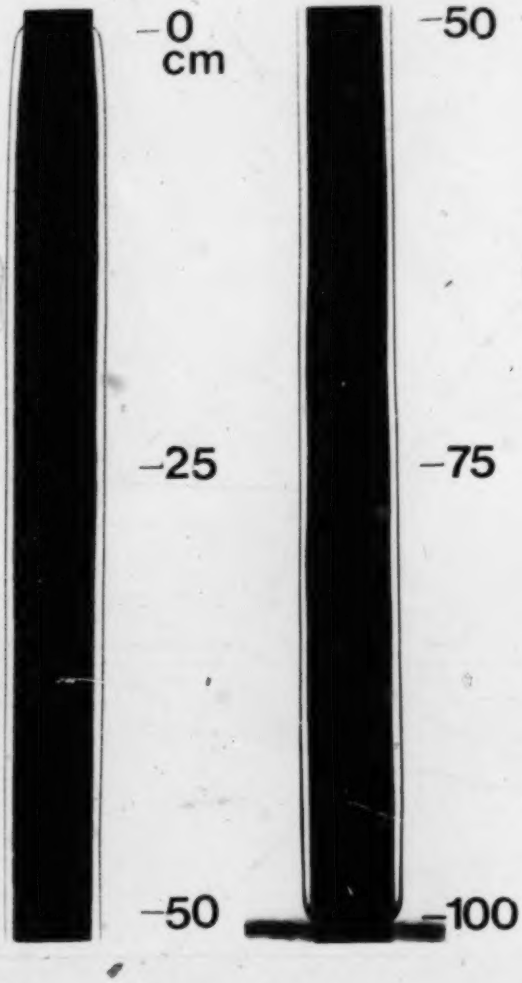
0
cm
25
50
50
75
100

$\bar{\tau}$ = 10 min

Fig. 7.3(a) Photographs of ice layer growth for t_∞=9.9°C and t_c=-18.6°C

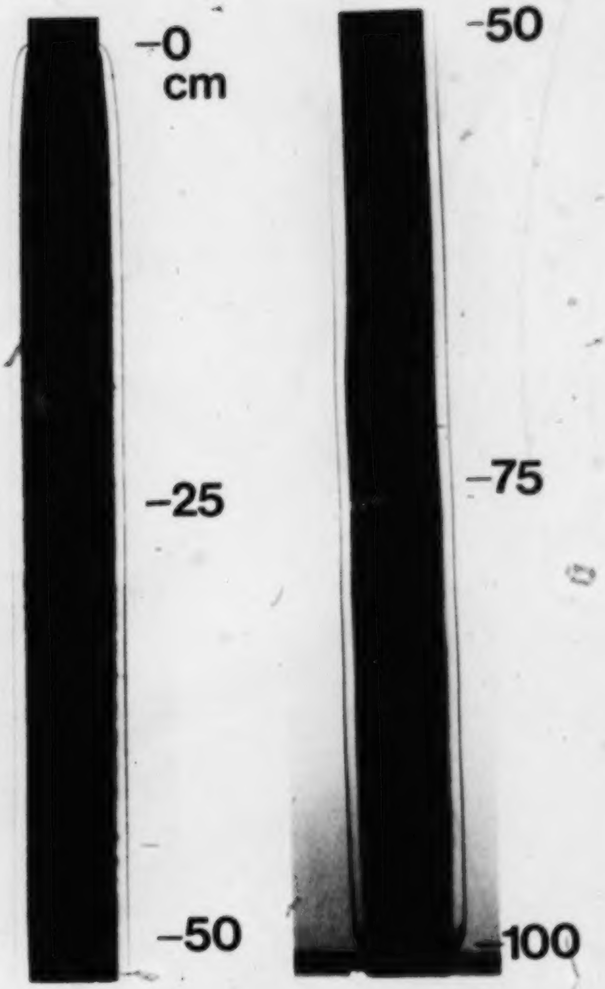
-0
cm
-25
-50
-50
-75
-100

$\bar{\tau}$ = 30 min

Fig. 7.3(b) Photographs of ice layer growth for t_∞=9.9°C and t_c=-18.6°C

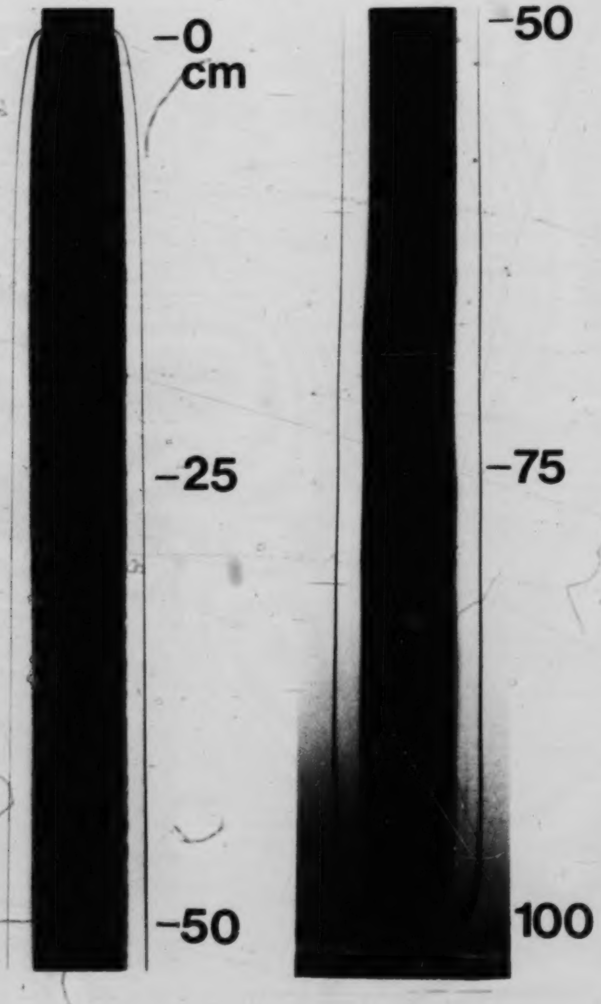
-0
cm
-25
-50
-50
-75
100

$\bar{\tau}$ = 120 min

Fig. 7.3(c) Photographs of ice layer growth for t_∞=9.9°C and t_c=-18.6°C

Figs. 7.4(a) to (c) show the photographs of the transient ice layer growth for t_∞=13.5°C and t_c=-16.7°C. The flow visualization by shadowgraph method indicated that the natural convective flow was laminar up to about x=30 cm. Small disturbances on the laminar flow were observed in the region x=30 cm to x=50 cm. As the disturbances moved downwards, they amplified with time and distance and became vortices. The vortices were observed below 50 cm from the leading edge. Below 85 cm from the leading edge, the vortices intermittently broke down into turbulence and hence the start of transition regime can be taken as x=85 cm approximately. The flow was not fully turbulent at x=100 cm. The thickness of the ice layer continued to increase in the laminar regime even when there were some small disturbances on the flow. It was of nearly uniform thickness when the disturbances on the laminar flow were large and also in the transition regime as seen from the photographs. Fig. 7.4(d) shows the ice layer profile 5 minutes after the the coolant circulation was cut off and the ice layer was allowed to melt in the ambient water. The ice layer near the leading edge of the copper pipe had already melted away.

Figs. 7.5(a) to (c) show the photographs of the transient ice layer growth for t_∞=17.5°C and t_c=-15.0°C. The natural convective flow was laminar up to about x=25 cm. Small disturbances on the laminar flow were present in the range x=25 to x=40 cm. Large disturbances on the laminar flow were present in the region x=40 cm to x=75 cm. In the region x=75 cm to x=90 cm, the vortices were observed to break down

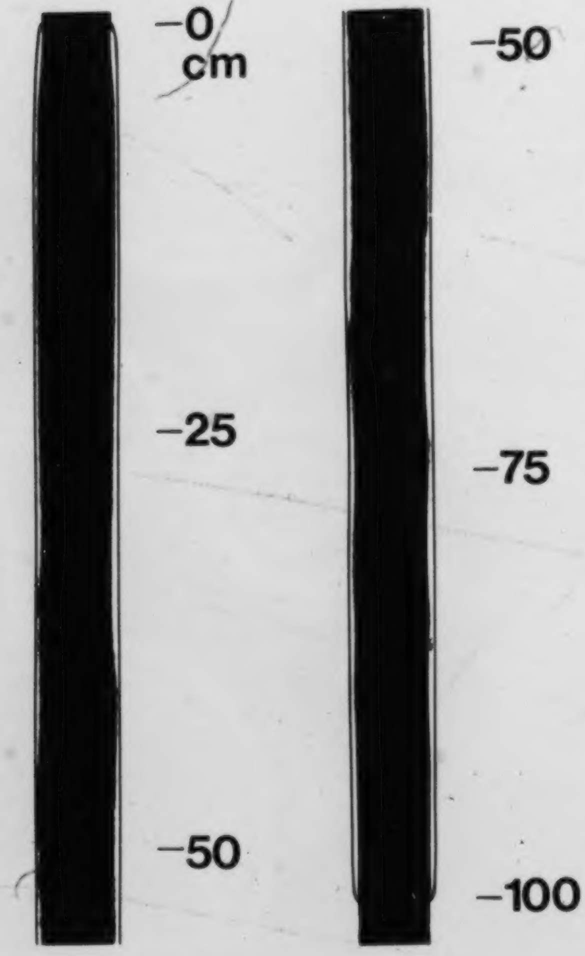

-0
cm
-25
-50
-50
-75
-100

$\bar{\tau}$ = 5 min

Fig. 7.4(a) Photographs of ice layer growth for t_∞=13.5°C and t_c=-16.7°C

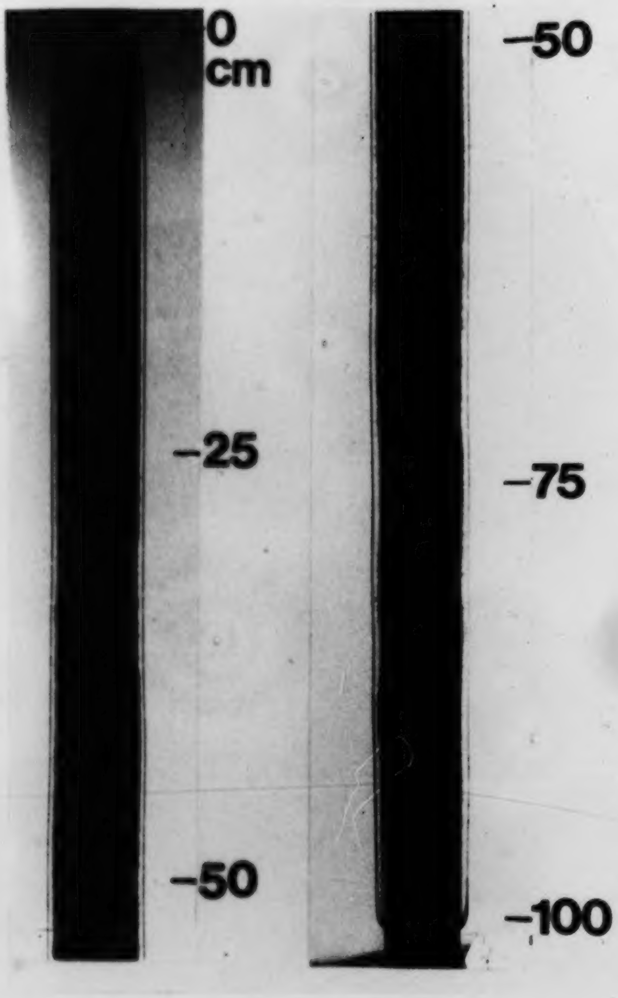
0
cm
−25
−50
−50
−75
−100

$\bar{\tau}$ = 15 min

Fig. 7.4(b) Photographs of ice layer growth for t_∞=13.5°C and t_c=-16.7°C

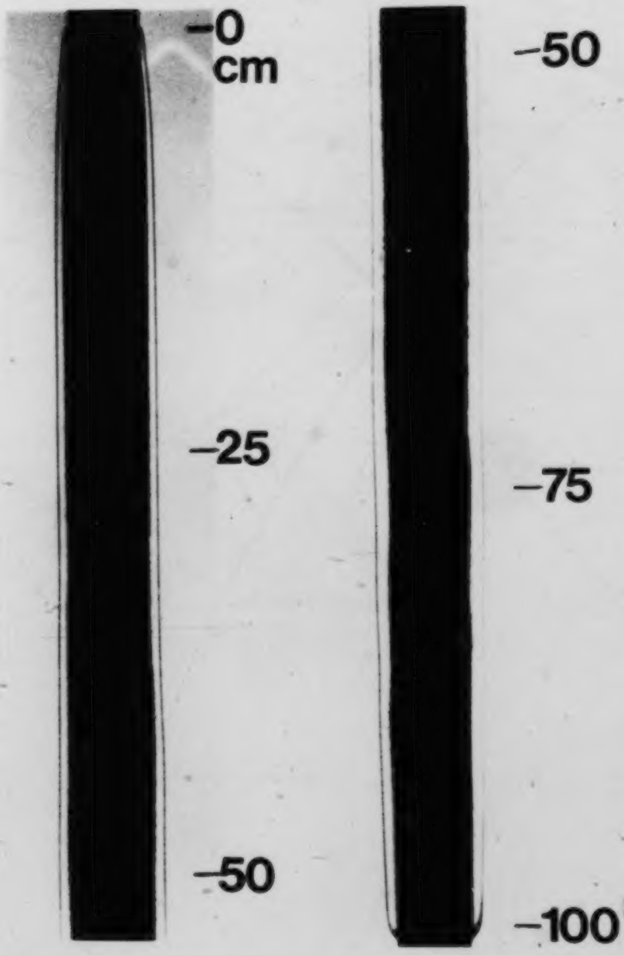
-0
cm
-25
-50
-50
-75
-100

$\bar{\tau}$ = 90 min

Fig. 7.4(c) Photographs of ice layer growth for t_∞=13.5°C and t_c=-16.7°C

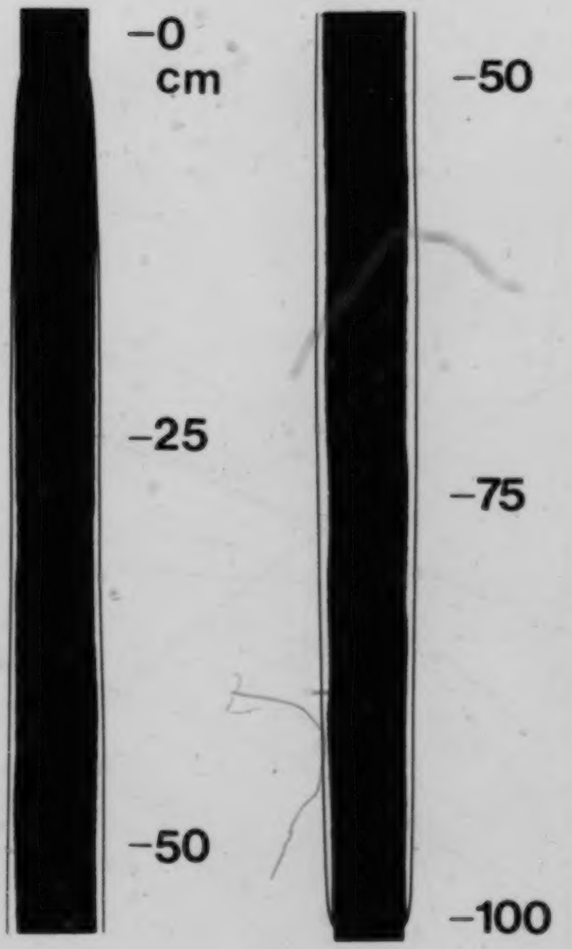
-0
cm
-25
-50
-50
-75
-100

Fig. 7.4(d) Photographs ice layer melting for t_∞=13.5°C and t_c=-16.7°C

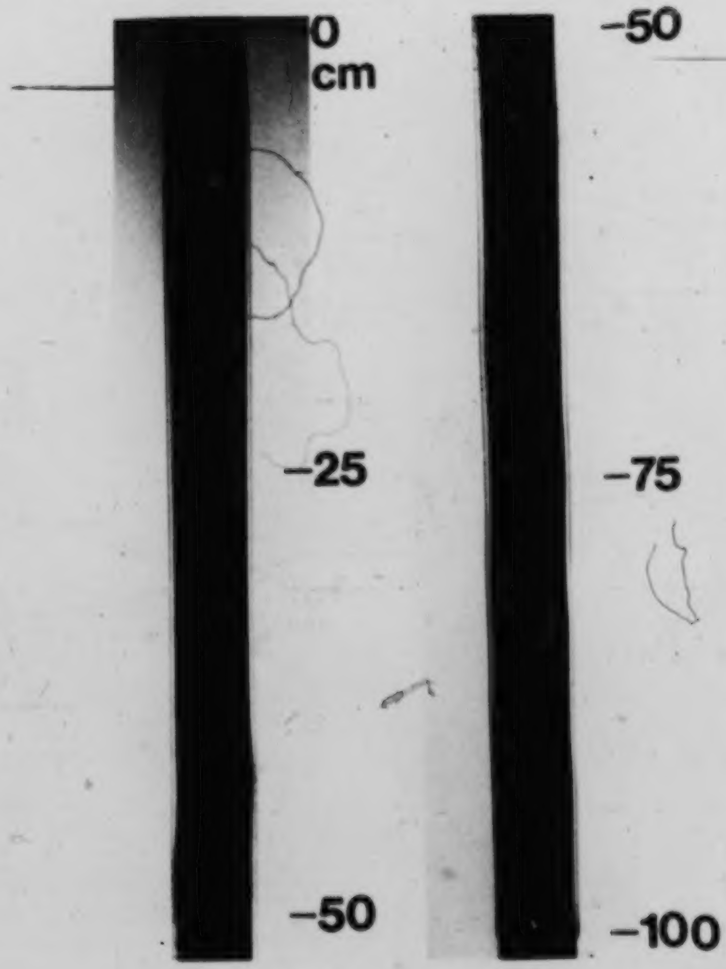
0
cm
-25
-50
-50
-75
-100

$\bar{\tau}$ = 5 min

Fig. 7.5(a) Photographs of ice layer growth for t_∞=17.5°C and t_c=-15.0°C

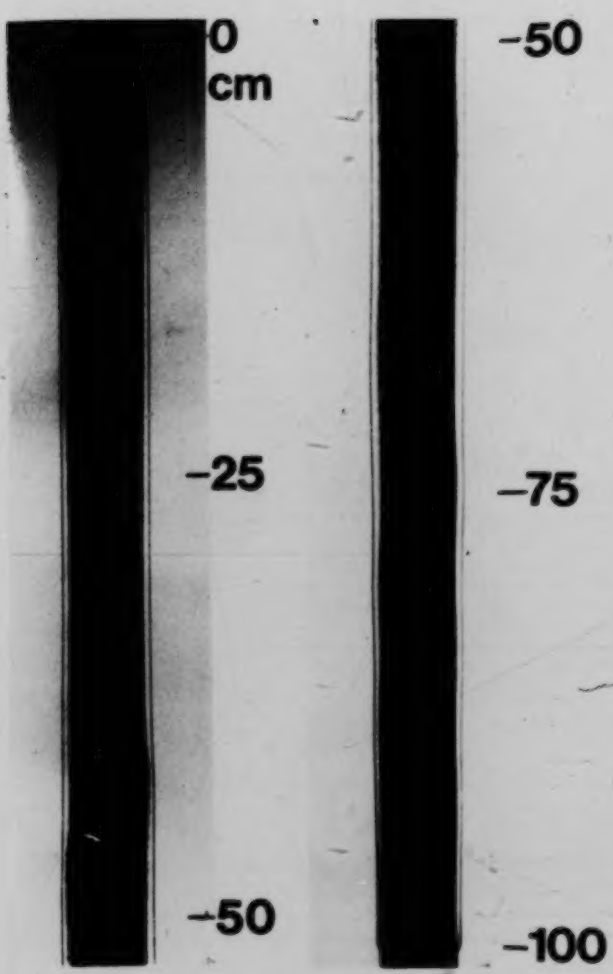
0
cm
-25
-50
-50
-75
-100

$\bar{\tau}$ = 15 min

Fig. 7.5(b) Photographs of ice layer growth for t_∞=17.5°C and t_c=-15.0°C

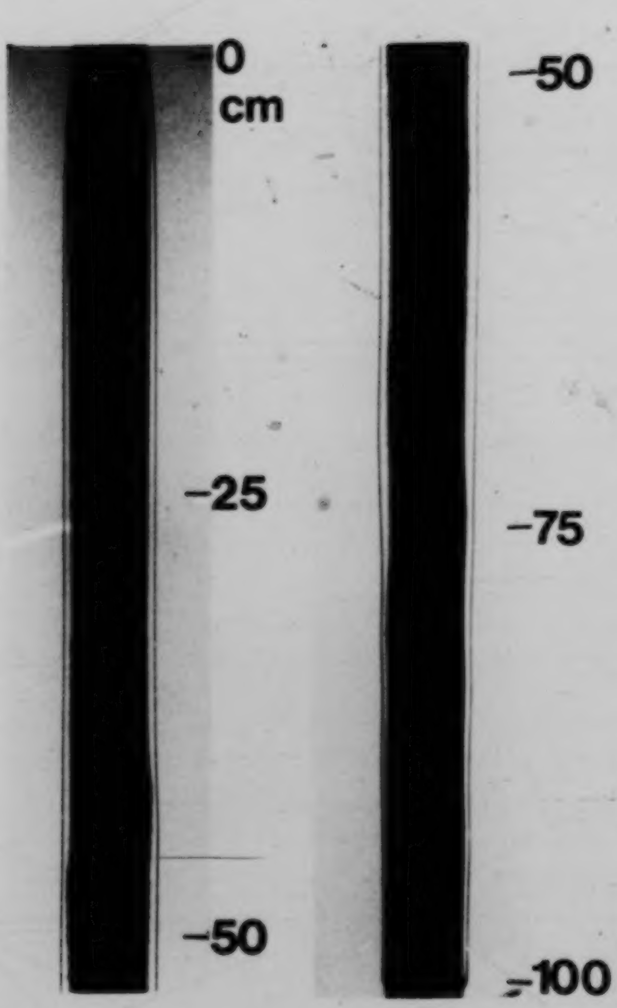
0
cm
–25
–50
–50
–75
–100

$\bar{\tau}$ = 45 min

Fig. 7.5(c) Photographs of ice layer growth for t_∞=17.5°C and t_c=-15.0°C

intermittently into turbulence. Hence, this region can be taken as the transition regime. The flow was fully turbulent below 90 cm from the leading edge. As before, the thickness of the ice layer continued to increase in the laminar regime of flow and was of nearly uniform thickness when the disturbances on the laminar flow were of large amplitude, and in the transition regime. It slowly decreased with distance in the turbulent regime. The change in ice layer thickness in the transition regime from laminar to turbulent flow was not as sharp as that observed in forced flow (Hirata et al., 1979b). Fig. 7.5(d) shows the photograph of the ice layer 5 minutes after the coolant flow was shut off and the ice layer was allowed to melt in the ambient water. The ice layer melted faster near the leading edge and in the turbulent flow regime.

In all the three regimes of the natural convective flow in water adjacent to the ice-water interface, the ice layer continued to grow until the conduction heat transfer through the ice layer was exactly balanced by the natural convection heat transfer in water at the interface. As expected, the ice layer growth slowed down as time progressed. The lower the ambient water temperature, the longer was the time required for the steady state condition to be achieved for a given wall temperature. For a given ambient water temperature the steady state thickness of the ice layer was larger for a lower wall temperature. Fig. 7.6 compares the theoretically predicted transient dimensionless ice layer thicknesses with those obtained experimentally for typical

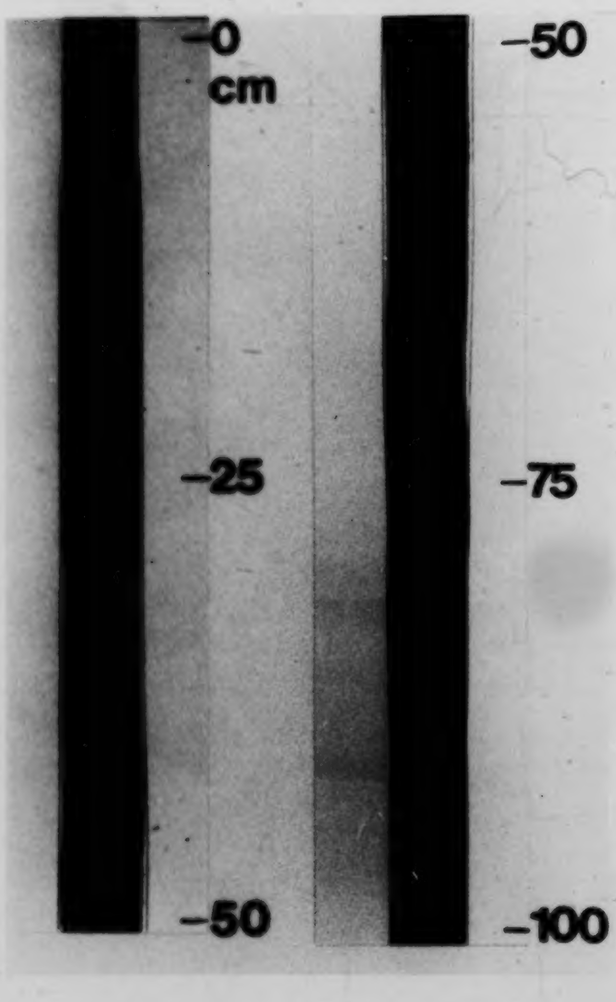
0
cm
-25
-50
-50
-75
-100

Fig. 7.5(d) Photographs of ice layer melting for t_∞=17.5°C and t_c=-15.0°C

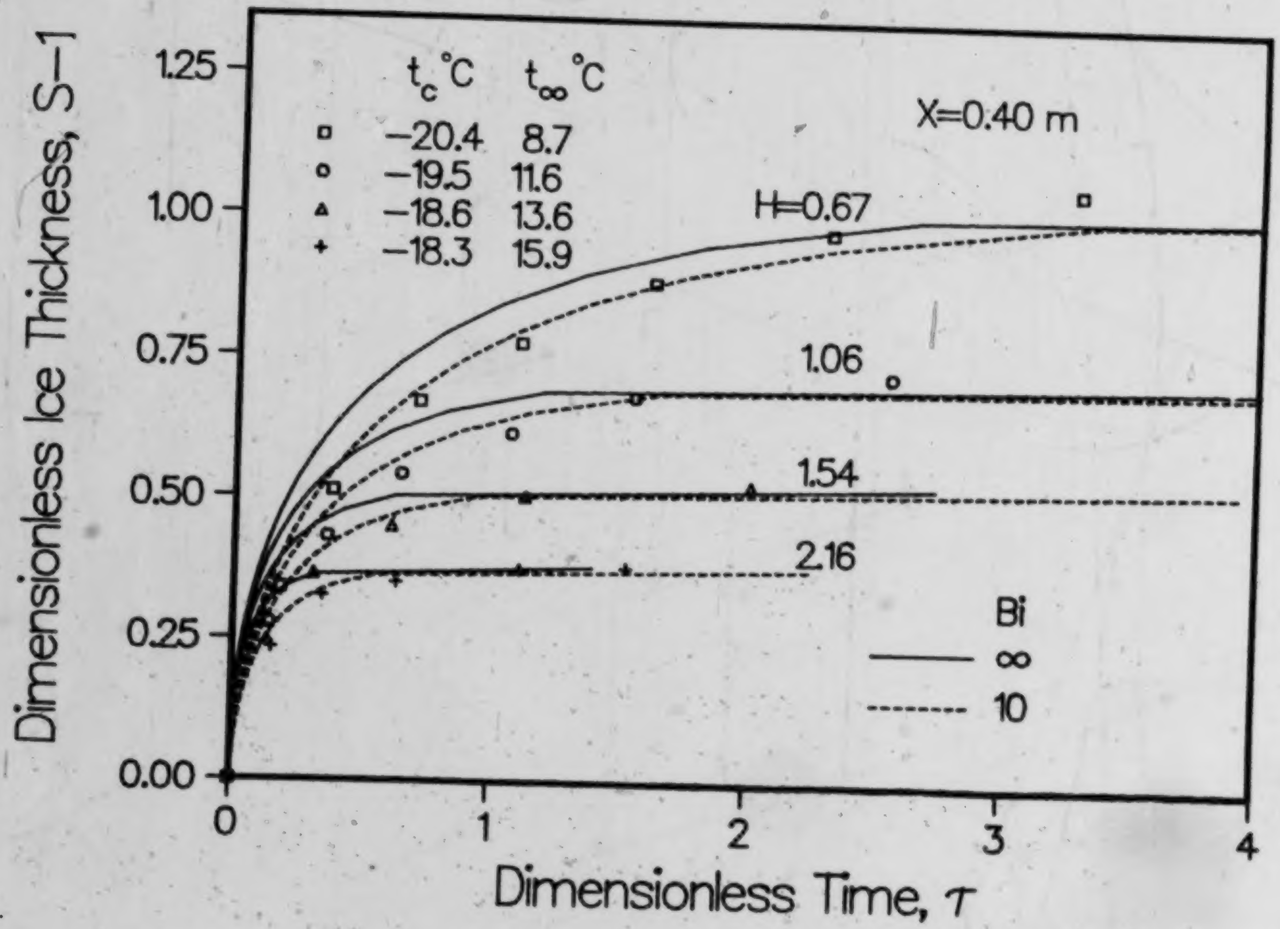

Fig. 7.6 A Comparison of experimentally obtained transient ice layer thickness with a one-dimensional analysis

coolant and ambient temperatures at x=40 cm. For numerical solutions the value of H was obtained from the corresponding experimentally measured steady state ice layer thickness (see eq. 7.11). The numerically predicted values are in fair agreement with the experimental values when Bi=10.

7.3.2 The Local and the Average Heat Transfer Coefficients at the Interface

As explained earlier, at steady state, the heat transfer by natural convection in water at the interface is exactly balanced by the heat transfer by conduction through the ice layer. Fig. 7.7 shows the variation of the local Nusselt number at the interface obtained from a one-dimensional heat conduction analysis of the ice layer with the Rayleigh number for typical ambient water temperatures. The wall temperature for these calculations was taken as the average of the inlet and the outlet coolant temperatures. (This is not strictly true and it will be explained later). The relation between the local Nusselt number and the Rayleigh number for the laminar natural convective flow from an isothermal vertical flat plate is also shown for comparison. (As discussed in Chapter 3, the results obtained in the present experiments may be assumed to those for a flat plate). The local Nusselt number obtained from the conduction analysis is seen to be higher than that of the natural convective flow from a vertical isothermal flat plate (the possible causes for this discrepancy will be examined later). The transition regime

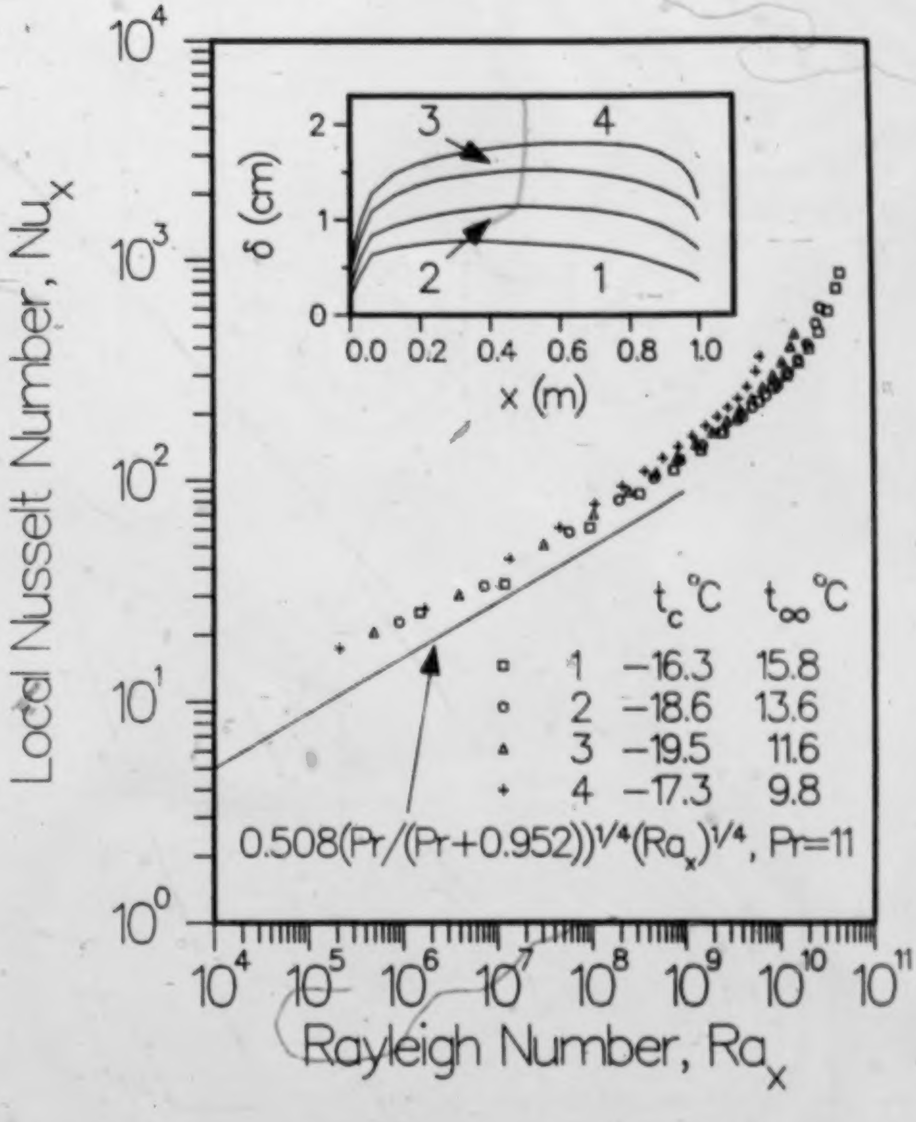

Fig. 7.7 The variation of local Nusselt number, Nu_x with Rayleigh number, Ra_x at the interface

of the natural convective flow can be taken as that of $Ra_x = (2 \text{ to } 6) \times 10^{10}$

Fig. 7.8 shows the average heat transfer coefficients at the interface for typical ambient water temperatures. As before, the values obtained from the conduction heat transfer analysis of ice layer are larger than those for the natural convective heat transfer from an isothermal vertical flat plate. The possible causes for the discrepancy may be due to one or several of the following reasons. The entrapped air bubbles in the ice layer during initial stage, to be explained later, impede the growth and reduce the steady state ice thickness. The assumption of constant wall temperature to have a value equal to the average of the inlet and the outlet coolant temperatures is not strictly true since a finite value of heat transfer coefficient exists between the wall and the coolant. Since the ice layer grows very slowly for larger times, the ice layer thickness measured for the steady state condition may be slightly lower than the actual value. Also, near the leading edge, the heat transfer process is two-dimensional. As explained in the previous Chapter, the one dimensional analysis predicts a lower value for the local heat transfer coefficient near that region.

7.3.3 The Effects of Stratification of Ambient Water

When solidification or melting takes place in a confined space, the ambient liquid tends to become stably stratified and hence it is of interest to know the effect of

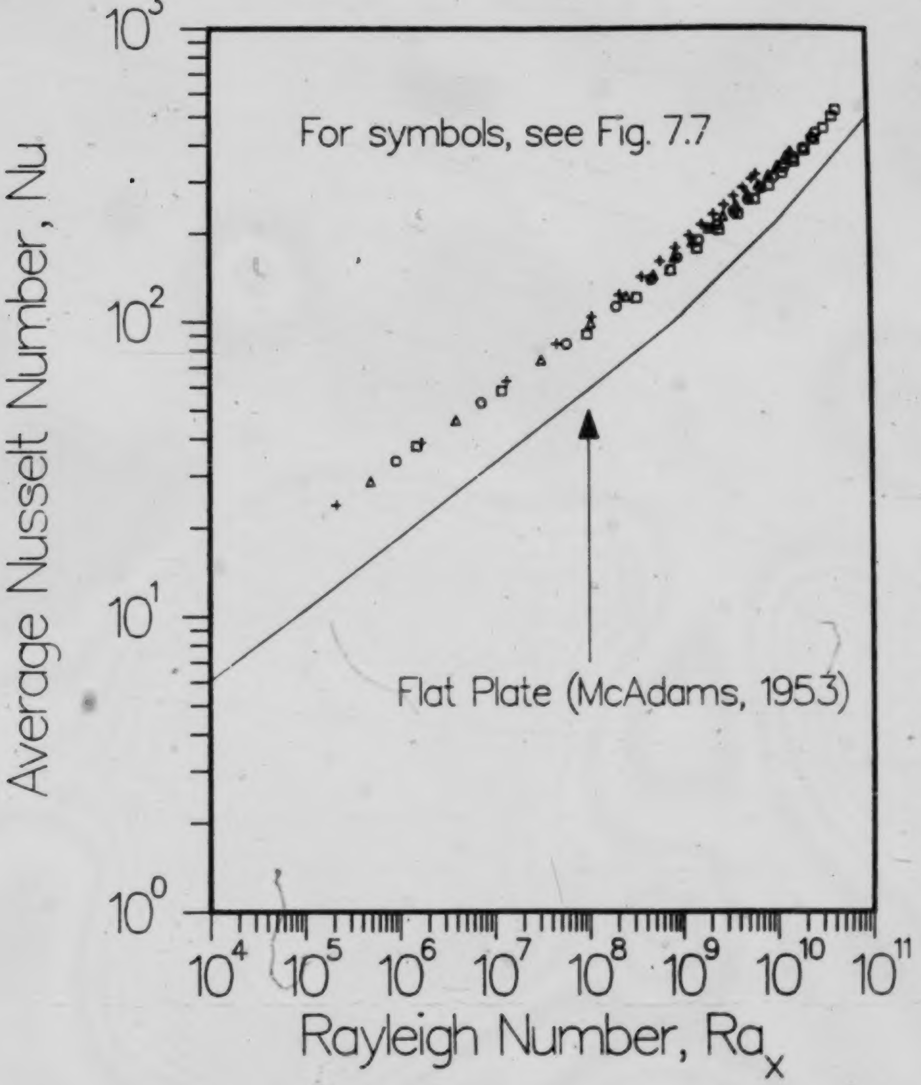

Fig. 7.8 The variation of average Nusselt number, $\bar{Nu}$ with Rayleigh number, Ra_x at the interface

stratification on the shape and the position of the solid-liquid interface. Fig. 7.9 shows the thickness of steady state ice layer for a typical case of a stratified ambient water with t_∞=16.0°C at x=0 cm and t_∞=9.4°C at x=100 cm, and when t_c=-16.8°C. The stratification of ambient water was nearly linear for this case. The ice layer thickness continued to increase over the entire length of the cylinder. The flow visualization by shadowgraph technique indicated that the flow was laminar up to x=30 cm and small disturbances were present on the laminar flow for x=30 cm to x=40 cm. Large disturbances were present in the region x=40 cm to x=80 cm. For distances greater than x=80 cm the vortices were observed to break down into turbulence. The flow was not fully turbulent at x=100 cm. The thickness of the ice layer continued to increase in the laminar and the transition regimes as shown in Fig. 7.9.

7.3.4 Cracking of Ice Layer During Melting

After stopping the coolant circulation, the ice layer was allowed to melt in the ambient water. In certain cases, after about 2 to 3 minutes of stopping the flow of coolant, the ice layer cracked with a fairly loud noise. The ice layer usually cracked when its thickness was larger (~15 to 25 mm). The larger the thickness of the ice layer, the louder was the cracking noise. For example, the ice layer cracked when t_∞=11.5°C and t_c=-16.0°C, and it melted without cracking for t_∞=9.0°C and t_c=-12.5°C. Figs. 7.10(a) to (b)

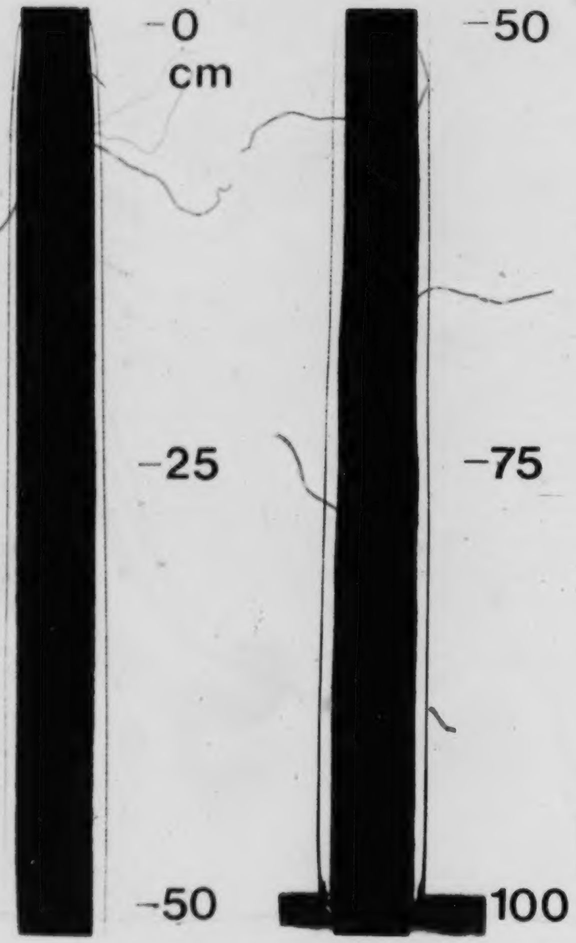
0
cm
25
50
50
75
100

Fig. 7.9 Photographs of ice layer growth in stratified ambient water

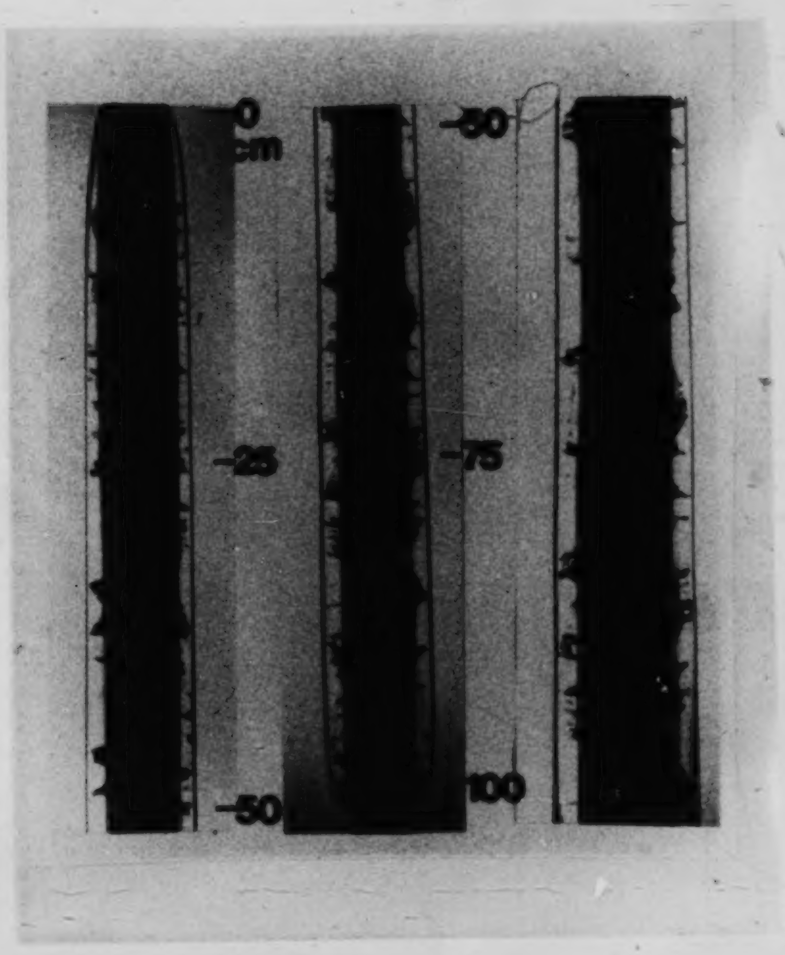
0
cm
25
50
50
75
100

Fig. 7.10 Photographs of cracked ice layer

show the cracked ice profile for the particular case when t_∞=9.8°C and t_c=-18.0°C. Cracks ran along the axial as well as the circumferential direction as seen from Fig. 7.10(c), which shows a section of this ice layer between x=60 and 85 cm clearly.

7.3.5 The Effects of Dissolved Air in Ambient Water

Under normal conditions water contains some dissolved air. When water freezes, the air is rejected at the ice-water interface due to the difference in solubility of air in water and in ice. The evolution of air results in entrapment of the air bubbles in the ice layer during the initial stage when the advancement of the interface is faster (Petrie et al., 1980). Also, the natural convective flow adjacent to the interface is in the transient stage and hence the velocity of the flow is lower. Although the water was deaerated before filling into the tank, there was still some air present in the ambient water. To find the effect of dissolved air in water, experiments were done with deaerated water, and with tap water without deaeration for the same coolant and ambient temperatures. It was found that the presence of air in water reduced the thickness of the ice layer at steady state condition slightly. For example, the thickness of the ice layer at steady state for t_∞=16.5°C and t_c=-16.0°C was about 5 percent less for water without deaeration than that for the deaerated water. The interface was observed to be smooth in both cases.

Fig. 7.11 shows a section of the ice layer containing air bubbles. The presence of air bubbles in the ice layer alters its heat transfer characteristics and this might be one of the reasons for the discrepancy in the heat transfer coefficients at the interface between those calculated from the heat conduction analysis of the ice layer and those obtained from the natural convective flow along an isothermal vertical flat plate. When the ice layer containing air bubbles was allowed to melt in the ambient water, the air bubbles are released from the ice layer into the natural convective boundary layer adjacent to the interface. The air bubbles enhanced the heat transfer from the ice layer to water and also caused the flow to become turbulent earlier. Hence, the ice layer melted faster with the presence of air bubbles than without them.

7.3.6 The Effects of Artificially-Induced Disturbances

When water freezes over an isothermally cooled flat plate in forced flow, it has been found that the ice layer is unstable to disturbances that are induced on the ice surface in the form of grooves at certain locations (Gilpin et al., 1980). In order to study the stability of ice layer to artificially-induced disturbances in natural convective flow, the ice layer was locally melted in the form of a groove for about one-half of the circumference. It was found that the ice layer remained stable in all regimes of the flow studied and the disturbance did not propagate downstream as found in the forced flow experiments. The ice

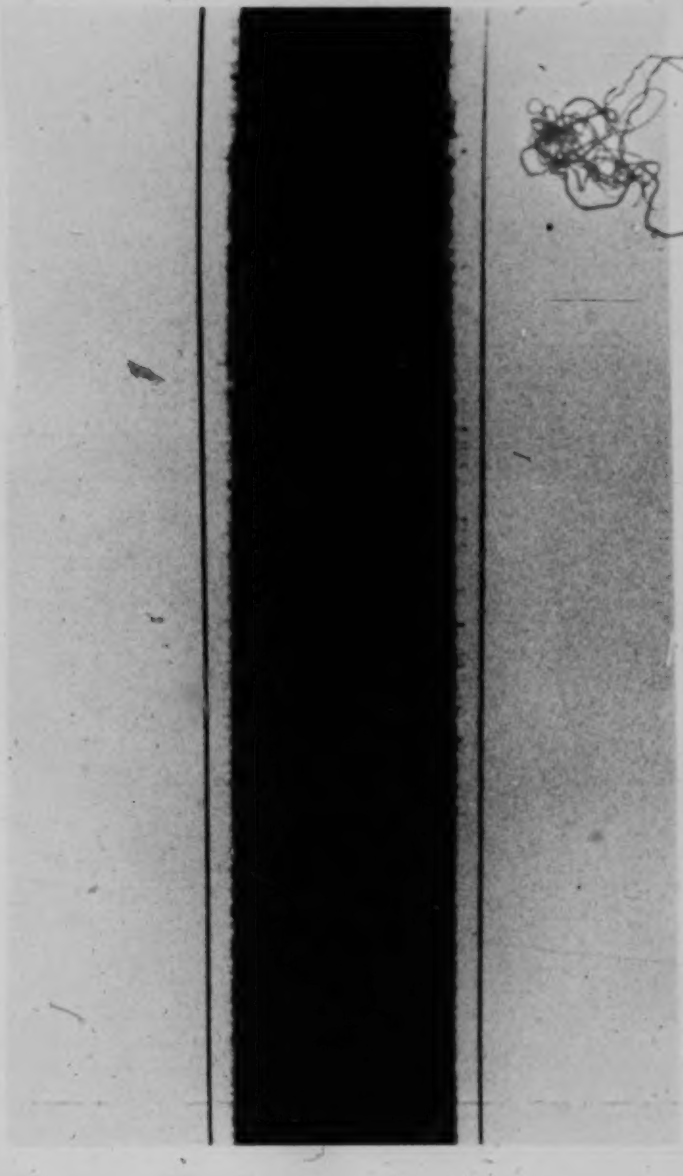

Fig. 7.11 Photograph showing the presence of air bubbles in the ice layer

layer grew back in the melted region and the disturbance disappeared completely. Figs. 7.12(a) to (d) show the artificially induced disturbance and its recovery process at x=50 cm when t_∞=16.1°C and t_c=-17.3°C under steady state ice layer conditions. The photographs were taken with a time interval of two minutes. The recovery time for this disturbance was about 10 minutes. If the coolant flow was stopped with the groove present, the ice layer melted very slowly around the groove until its thickness near the groove approached that of the groove and the groove disappeared entirely.

7.4 Conclusions

The effects of natural convection on freezing of water over a convectively cooled vertical circular cylinder were studied experimentally. In the laminar flow regime, the thickness of the ice layer increased with axial distance. In the transition regime, the ice layer had nearly uniform thickness. In the turbulent regime, the thickness decreased slowly with distance.

A one-dimensional analysis of transient solidification of a warm liquid over a cooled vertical circular cylinder with a convective boundary condition was also presented and the predicted results compared fairly well with those obtained experimentally. The local and the average heat transfer coefficients at the interface obtained by the conduction heat transfer analysis of the ice layer agreed fairly well with the values for the natural convective flow

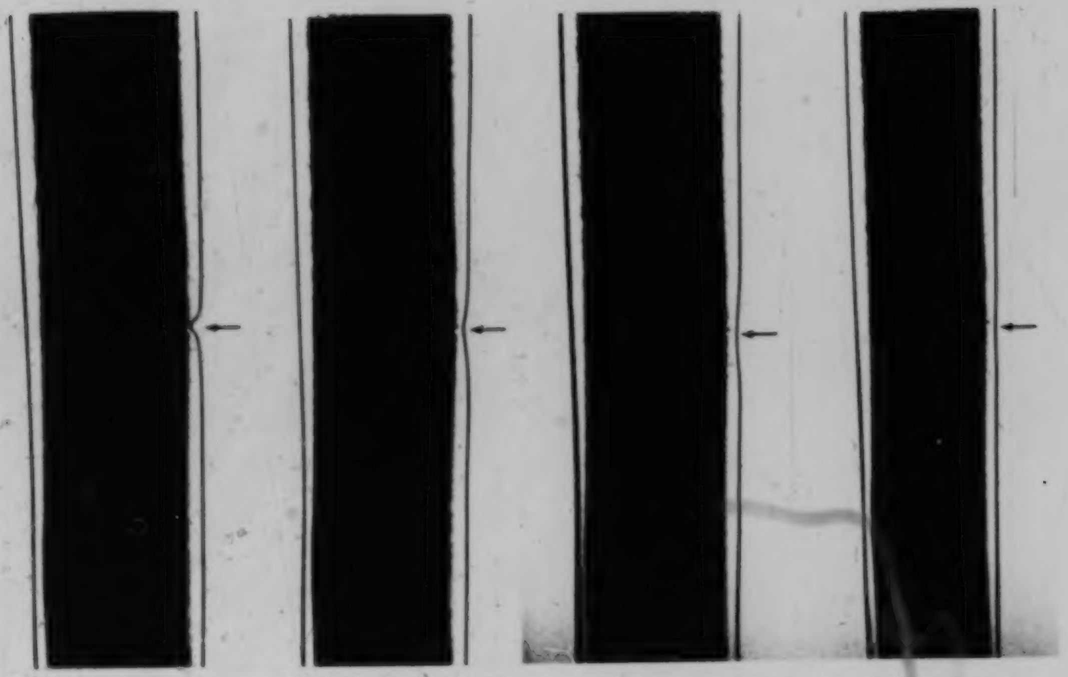

Figure 7.12 Photographs showing the artificially induced disturbance on the surface of the ice layer and its recovery process

along an isothermal vertical flat plate available in the literature. Hence, this method of determining the heat transfer coefficients at the interface by the heat conduction analysis of the solid region can be effectively used to study convective heat transfer problems in flows with recirculation, in flows over complex geometries, and inside pipes where the direct measurement of temperature profiles may be difficult.

The effects of stratification and dissolved air in the ambient water were also studied. When the ambient water was stably stratified the thickness of the ice layer continued to increase in the laminar and the transition regimes. The entrapment air bubbles in the ice layer due to the dissolved air in the ambient water reduced the steady state ice layer thickness slightly. The ice layer was found to be stable to disturbances induced on its surface in the form of a circumferential groove.

8. Conclusions

8.1 Scope of Results

The effects of temperature-dependent properties on the laminar natural convective boundary layer flow along an isothermal vertical flat plate were studied numerically for liquids with Prandtl numbers from 1 to ∞. All the relevant properties were considered in the form of dimensionless parameters. Both heated and cooled walls were examined. The effects of temperature-dependent properties on temperature and velocity profiles were also studied in detail.

The effects of temperature-dependent viscosity and the coefficient of thermal expansion on the stability of laminar natural convective boundary layer flow along an isothermal vertical flat plate were studied employing linear stability theory. The effect of maximum density was also investigated for various combinations of wall and ambient temperatures with and without the buoyancy force reversal inside the thermal boundary layer. The flow from a vertical wall at 0°C, corresponding to an ice surface, was investigated in detail. Experiments were conducted in water with a vertical circular copper cylinder (outside diameter 41.3 mm and length 1 m) for various combinations of wall and ambient temperatures from 0 to 35°C. The flow was visualized using shadowgraph and dye injection flow visualization techniques.

The transient natural convective flow along a vertical circular cylinder subjected to a step change in surface temperature was studied numerically for various radii of the cylinder with Prandtl numbers 0.1 to 10.0, and Grashof numbers up to 10^7. The transient temperature and velocity profiles and the local Nusselt number at the surface were obtained. The transient flow was also visualized in water using the shadowgraph technique.

The method of boundary-fitted coordinate systems was applied to a class of steady-state ice formation problems involving simply or doubly connected solidified regions in determining the local heat transfer coefficients at the ice-water interface. The two-dimensional solutions were compared with a simple one-dimensional analysis. The effects of natural convection on freezing of water over a convectively cooled vertical circular cylinder were studied experimentally. The transient solidification of a warm liquid over a convectively cooled vertical circular pipe was also analyzed employing a one-dimensional analysis.

8.2 Conclusions and Significance

It was shown clearly that for moderate temperature differences (~10 to 50°C for water, for example) between the wall and the ambient liquid, the density could be assumed to be constant in all terms of the governing equations except in the buoyancy force term. In the buoyancy force term, a better approximation of the variation of density with temperature than the conventional Boussinesq approximation was considered employing a dimensionless parameter.

The assumption that the density varies linearly with temperature in the buoyancy force term underpredicted the surface heat transfer, the surface shear stress, the total mass flow rate and the maximum velocity for down flows, and overpredicted them for up flows. The effects were more pronounced for large temperature differences between the wall and the ambient medium. The effects were significant for liquids with small as well as large Prandtl numbers.

The temperature-dependent viscosity increased the surface heat transfer, the total mass flow rate and the maximum velocity, and decreased the surface shear stress for a heated wall. When the thermal conductivity increased with temperature, the surface heat transfer and the surface shear stress increased for a heated wall. When the specific heat increased with temperature, the surface shear stress and the total mass flow rate increased, and the surface heat transfer decreased for a heated wall. The opposite remarks were true for a cooled wall. The effects of variable properties on the local Nusselt number at the surface were given in terms of the dimensionless parameters for various values of the Prandtl number.

The temperature-dependent viscosity destabilized the laminar natural convective boundary layer flow along a cooled wall and stabilized it along a heated wall. Moreover, the disturbances amplified faster for a cooled wall than for a heated wall. The frequency filtering mechanism was also more pronounced for a cooled wall. The variation of coefficient of thermal expansion with temperature lowered the critical Grashof number for the onset of instability for a cooled wall but the disturbance growth rate was faster for a heated wall. Hence, the temperature-dependent coefficient of thermal expansion initially stabilized the flow for a heated wall, but farther downstream it destabilized the flow. For water, the numerical results predicted that the critical Grashof number for the onset of instability was discontinous in the region where flow reversals occur due to the maximum density. The trends of experimentally obtained critical values of Grashof number for the onset of instability and the transition to turbulent flow supported the numerical predictions.

For the transient natural convective flow along a vertical circular cylinder, numerical results indicated that during the transient period there was an overshoot in temperature in the thermal boundary layer and an undershoot in the local Nusselt number at the surface. The experimental temperature measurements in water during the transient and the steady state periods agreed fairly well with those obtained numerically. The flow visualization studies and the temperature measurements showed that the critical values of Grashof number for the onset of instability and the transition to turbulence were lower during the transient period than at the steady state period.

When solidification or melting occurred under external or internal, laminar or turbulent conditions involving various geometrical shapes, a one-dimensional analysis gave fairly accurate results for the local heat transfer coefficients at the interface if the thickness of the solidified layer changed gradually.

When water froze over a convectively cooled vertical circular pipe in natural convection, the thickness of the ice layer increased with the axial distance in the laminar regime. In the transition regime, the ice layer had nearly uniform thickness. In the turbulent regime, the thickness decreased slowly with distance. The local and the average heat transfer coefficients at the interface obtained by the conduction heat transfer analysis of the ice layer agreed fairly well with the values for the natural convective flow along an isothermal vertical flat plate available in the literature. Hence, this method of determining the heat transfer coefficients at the interface by the heat conduction analysis of the solidified region can be effectively used to study convective heat transfer problems in flows with recirculation, in flows over complex geometries, and inside pipes where the direct measurement of temperature profiles may be difficult.

8.3 Recommendations

Experimental verification of the effects of temperature-dependent properties on the laminar natural convective flow along an isothermal vertical flat plate is necessary. For liquids with moderate and large Prandtl numbers, the effects are more pronounced on the velocity profile than on the temperature profile. Hence, they can be verified by measuring the velocity profiles for various combinations of wall and ambient temperatures. For water, both the viscosity and the coefficient of thermal expansion are strong functions of temperature. Under normal conditions, their effects oppose each other. Hence, different liquids, each with a particular property varying predominantly over others, have to be used for experiments. For example, for lubricating oils, the viscosity varies more predominantly than other proprties.

The experiments reported in this study on the stability of laminar natural convective flow along an isothermal vertical circular cylinder are qualitative in nature. Further experiments, especially on the amplification characteristics of disturbances are needed. This can be done by artificially inducing the disturbances and measuring their amplification rates for various combinations of wall and ambient temperatures.

In this study, numerical solutions were obtained the transient natural convective flow along a vertical circular cylinder subjected to a step change in surface temperature. Experimental measurements of transient velocity profiles for various radii of the cylinder are necessary to confirm the numerical predictions.

In solidification and melting problems the natural convection in the liquid plays a significant role on the shape and the position of the solid-liquid interface. In this study, experiments were done for freezing of water over a convectively cooled vertical circular pipe. This work can be easily extended to freezing of water over other geometries such as an inclined vertical flat plate and a horizontal cylinder.

References

Ackroyd, J. D., 1974, "Stress Work Effect in Laminar Flat Plate Natural Convection," *J. Fluid Mech.*, Vol. 62, pp. 677-695.

Aziz, A., and Na, T. Y., 1982, "Improved Perturbation Solution for Laminar Natural Convection on a Vertical Circular Cylinder," *Warme- und Stoffubertragung*, Vol. 16, pp. 83-87.

Bareiss, M., and Beer, H., 1980, "Influence of Natural Convection on the Melting Process in a Vertical Cylindrical Enclosure," *Letters in Heat and Mass Transfer*, Vol. 7, pp. 329-338.

Barrow, H., and Sitharamarao, T. L., 1971, "The Effect of Variation in the Volumetric Expansion Coefficient on Free Convection Heat Transfer," *Br. Chem. Eng.*, Vol. 16, pp. 704-705.

Batchelor, G. K., 1967, *An Introduction to Fluid Mechanics*, Cambridge University Press, London.

Boger, D. V., and Westwater, J. W., 1967, "Effect of Buoyancy on the Melting and Freezing Processes," *Trans. of ASME, J. Heat Transfer*, Vol. 89, pp. 81-89.

Brown, A., 1975, "The Effect on Laminar Free Convection Heat Transfer of the Temperature Dependence of the Coefficient of Volumetric Expansion," *Trans. of ASME, J. Heat Transfer*, Vol. 97, pp. 133-135.

Brown, S. N., and Riley, N., 1973, "Flow Past a Suddenly Heated Vertical Plate," *J. Fluid Mech.*, Vol. 59, pp. 225-237.

Carey, V. P., Gebhart, B., and Mollendorf, J. C., 1980, "Buoyancy Force Reversals in Vertical Natural Convection Flows in Cold Water," *J. Fluid Mech.*, Vol. 97, pp. 279-297.

Carey, V. P., and Gebhart, 1981, "Visualization of Flow Adjacent to a Vertical Ice Surface Melting in Cold Pure Water," *J. Fluid Mech.*, Vol. 81, pp. 37-55.

Carey, V. P., and Mollendorf, J. C., 1978, "Natural Convection in Liquids with Temperature Dependent Viscosity," *Proc. 6th Int. Heat Transfer Conf.*, Toronto, Vol. 2, *Paper* **NC5**, pp. 211-216.

Carey, V. P. and Mollendorf, J. C., 1980, "Variable Viscosity Effects in Several Natural Convection Flows," *Int.*

J. Heat Mass Transfer, Vol. 23, pp. 95-109.

Carnahan, B., Luther, H. A., and Wilkes, J. O., 1969, *Applued Numerical Methods*, John-Wiley & Sons, Inc., New York.

Carslaw, H. S., and Jaeger, J. C., 1959, *Conduction of Heat in Solids*, Oxford at the Clarendon Press, London.

Cebeci, T., 1974, "Laminar Free Convective Heat Transfer From the Outer Surface of a Vertical Slender Circular Cylinder," *Proc. 5th Int. Heat Tranfer Conf.*, Paper NC1.4, pp. 15-19.

Cheesewright, R., 1968, "Turbulent Natural Convection From a Vertical Plane Surface," *Trans. of ASME, J. Heat Transfer*, Vol. 90, pp. 1-8.

Cheng., K. C., Inaba, H., and Gilpin, R. R., 1981, "An Experimental Investigation of Ice Formation around an Isothermally Cooled Cylinder in Crossflow," *J. Heat Transfer*, Vol. 103, pp. 733-738.

Cheng, K. C., and Sabhapathy, P., 1985, "Determination of Local Heat Transfer Coefficients at the Solid-Liquid Interface by Heat Conduction Analysis of the Solidified Region," *Trans. of ASME, J. Heat Transfer*, Vol. 107, pp. 703-706.

Cheng, K. C., and Sabhapathy, P., 1985, "An Experimental Investigation of Freezing of Water Over an Isothermally Cooled Vertical Circular Cylinder in Natural Convection," *23rd ASME National Heat Transfer Conference*, Denver, Colorodo, Aug. 4-7.

Colak-Antic, P., and Gortler, H., 1971, "Flow Visualization Studies of Free Convection Laminar-to-Turbulent Transition along a Heated Vertical Plate in Water Induced by Two-Dimensional Forced Disturbances," *Warme-und Stoffubertragung*, Vol. 4, pp. 25-31.

Dring, R. P., and Gebhart, B., 1968, "A Theoretical Investigation of Disturbance Amplification in External Laminar Natural Convection," *J. Fluid Mech.*, Vol. 34, pp. 551-564.

Eckert, E. R. G., and Soehngen, E., 1951, "Interferometric Studies on the Stability and Transition to Turbulence of a Free-Convection Boundary Layer," *Proc. Gen. Disc. Heat Transfer, IME and ASME Meet. London, 11-13th Sept.*, pp. 321-323.

Fowle, F. E., 1944, *Smithsonian Physical Tables*, Smithsonian Institution, Washington, D. C.

Fujii, T., Nozu, S., and Honda, H., 1978, "Expressions of Thermodynamic and Transport Properties of Refrigerants R-11, R-12, R-22 and R-113," *Report No. 67*, Institue of Industrial Science, Kyaashu University.

Fujii, T., Takeuchi, M., Fujii, M., Suzaki, K., and Uehara, H., 1970, "Experiments on Natural Convective Heat Transfer From the Outer Surface of a Vertical Cylinder to Liquids," *Int. J. Heat Mass Transfer*, Vol. **13**, pp. 753-787.

Fujii, T., and Uehara, H., 1970, "Laminar Natural Convective Heat Transfer From the Outer Surface of a Vertical Cylinder," *Int. J. Heat Mass Transfer*, Vol. **13**, pp. 607-615.

Gaster, M., 1963, "A Note on a Relation Between Temporally Increasing and Spatially Increasing Disturbances in Hydrodynamic Stability," *J. Fluid Mech.*, Vol. **14**, pp. 222-224.

Gaster, M., 1965, "The Role of Spatially Growing Waves in the Theory of Hydrodynamic Stability," *Prog. Aeron. Sci*, Vol. **6**, pp. 251-270.

Gebhart, B., 1968, "Transient Natural Convection From Vertical Elements," *Trans. of ASME., J. Heat Transfer*, Vol. **83**, pp. 61-64.

Gebhart, B., and Mahajan, R. L., 1982, "Instability and Transition in Buoyancy Induced Flows," *Adv. in Appl. Mech.*, Vol. **22**, pp. 231-315.

Gebhart, B., and Mollendorf, J. C., 1977, "A New Density Relation for Pure and Saline Water," *Deep-Sea Res.*, Vol. **24**, pp. 831-848.

Gebhart, B., Mollendorf, J. C., 1978, "Buoyancy-Induced Flows in Water Under Conditions in Which the Density Extrema may Arise," *J. Fluid Mech.*, Vol. **89**, pp. 673-707.

Gilpin, R. R., 1979, "The Morphology of Ice Structure in a Pipe at or Near Transition Reynolds Numbers," *AIChE Symposium Series 189*, Vol. **75**, pp. 89-94.

Gilpin, R. R. 1981, "Ice Formation in a Pipe Containing Flows in the Transition and Turbulent Regimes," *Trans. of ASME, J. Heat Transfer*, Vol. **103**, pp. 363-368.

Gilpin, R. R., Hirata, T., and Cheng, K. C., 1980, "Wave Formation and Heat Transfer at an Ice-Water Interface in the Presence of a Turbulent Flow," *J. Fluid Mech.*, Vol. 99, pp. 619-640.

Goldstein, R. J., and Briggs, D. G., 1964, "Transient Free Convection About Vertical Plates and Cylinders," *Trans. of ASME, J. Heat Transfer*, Vol. 86C, pp. 490-500.

Goldstein, R. J., and Eckert, E. R. G., 1960, "The Steady and Transient Free Convection Boundary Layer on a Uniformly Heated Vertical Plate," *Int. J. Heat Mass Transfer*, Vol. 1, pp. 208-218.

Gray, D. D., and Giorgini, A., 1976, "The Validity of Boussinesq Approximation for Liquids and Gases," *Int. J. Heat Mass Transfer*, Vol. 19, pp. 545-551.

Griffiths, E., and Davis, A. H., 1931, "The Transmission of Heat by Radiation and Convection," *Food Investigation Board, Special Report No. 9*, Dept. Sci. Ind. Res., London.

Hale, N. W., and Viskanta, R., 1978, "Photographic Observaion of the Solid-Liquid Interfae During Melting of a Solid Heated From an Isothermal Vertical Wall," *Letters in Heat Mass Transfer*, Vol. 5, pp. 329-337.

Hama, F. R., Recesso, J. V., and Christiaens, J., 1959, "The Axisymmetric Free Convection Temperature Field Along a Vertical Thin Cylinder," *J. Aerospace Sci.*, Vol. 26, pp. 335-342.

Hara, T., 1958, "Heat Transfer by Laminar Free Convection About Vertical Flat Plate with Large Temperature Difference," *Bull. of JSME*, Vol. 1, pp. 251-254.

Hauptmann, E. G., 1968, "The Influence of Temperature Dependent Viscosity on Laminar Boundary-Layer Stability," *Int. J. Heat Mass Transfer*, Vol. 11, pp. 1049-1052.

Hellums, J. D., and Churchill, S. W., 1962, "Transient and Steady State, Free and Natural Convection, Numerical Solutions - Part 1: the Isothermal Vertical Plate," *AIChE Jl.*, pp. 690-692.

Hieber, C. A. and Gebhart, B., 1971, "Stability of Vertical Natural Convection Boundary Layers: Some Numerical Solutions," *J. Fluid Mech.*, Vol. 48, pp. 625-648.

Higgins, J. M., and Gebhart, B., 1982, "Measurements of Instability and Disturbance Growth in Vertical Buoyancy

Induced Flows in Cold Water," *Int. J. Heat Mass Transfer*, Vol. 25, pp. 1397-1409.

Higgins, J. M., and Gebhart, B., 1983, "Stability of Vertical Buoyancy Induced Flows in Cold Water," *Trans. of ASME, J. Heat Transfer*, Vol. 105, pp. 767-773.

Hirata, T., Gilpin, R. R., Cheng, K. C., and Gates, E., 1979, "The Steady State Ice Layer Profile on a Constant Temperature Plate in a Forced Convection Flow: I. Laminar Regime," *Int. J. Heat Mass Transfer*, Vol. 22, pp. 1425-1433.

Hirata, T., Gilpin, R. R., and Cheng, K. C., 1979, "The Steady State Ice Layer Profile on a Constant Temperature Plate in a Forced Convection Flow: II: The Transition and Turbulent Regime," *Int. J. Heat Mass Transfer*, Vol. 22, pp. 1435-1443.

Ho, C.-J. and Viskanta, R., 1984, "Heat Transfer During Melting From an Isothermal Vertical Wall," *Trans. of ASME, J. Heat Transfer*, Vol. 106, pp. 12-19.

Illingworth, C. R., 1950, "Unsteady Laminar Flow of Gas Near an Infinite Plate," *Proc. Cambridge Phil. Soc.*, Vol. 46, pp. 603-613.

Ingham, D. B., 1978, "Transient free convection on an Isothermal Vertical Flat Plate," *Int. J. Heat Mass Transfer*, Vol. 21, pp. 67-69.

Ito, T., Yamashita, H., and Nishikawa, K., 1974, "Investigation of Variable Property Problem Concerning Natural Convection From Vertical Plate with Prescribed Uniform Flux," *Proc. 5th Int. Heat Transfer Conf.*, Tokyo, Vol. 3, Paper NC2.3, pp. 49-53.

Jaluria, Y., 1980, *Natural Convection Heat and Mass Transfer*, Pergamon Press, New York, 1980.

Joseberger, E. G., and Martin, S., 1981, "A Laboratory and Theoretical Study of the Boundary Layer Adjacent to a Vertical Melting Ice Wall in Salt Water," *J. Fluid Mech.*, Vol. 111, pp. 439-473.

Kell, G. S., 1975, "Density, Thermal Expansivity, and Compressiblity of Liquid Water From 0° to 100°C: Correlations and Tables for Atmospheric Pressure and Saturation Reviewed and Expressed on 1968 Temperature Scale," *J. Chemical and Engineering Data*, Vol. 20, No. 1, pp. 97-105.

Knowles, C. P., and Gebhart, B., 1968, "The Stability of Laminar Natural Convection Boundary Layer," *J. Fluid Mech.*, Vol. **34**, pp. 657-686.

Kuiken, H. K., 1968a, "Axisymmetric Free Convection Boundary Layer Flow Past Slender Bodies," *Int. J. Heat Mass Transfer*, Vol. 11, pp. 11141-1153.

Kuiken, H. K., 1968b, "Boundary Layer Conditions in Free Convection," *J. Engrg. Math.*, No. 2, pp. 95-105.

Kuiken, H. K., 1968c,"An Asymptotic Solution for Large Prandtl Number Free Convection," *J. Engrg. Math.*, No. 4, pp. 355-371.

Lapadula, C. A., and Mueller, W. K., 1970, "The Effect of Buoyancy on the Formation of a Solid Deposit Freezing onto a Vertical Surfae," *Int. J. Heat Mass Transfer*, Vol. **13**, pp. 13-26.

Le Fevre, E. J., 1956, "Laminar Free Convection From a Vertical Flat Surface," *9th Int. Congr. Appl. Mech.*, Vol. **4**, pp.168-175.

Le Fevre, E. J., and Ede, A. J., 1956, "Laminar Free Convection From the Outer Surface of a Vertical Circular Cylinder," *Proc. 9th Int. Cong. Appl. Mech.*, Vol. **4**, pp. 176-183.

Lorenz. L., 1881, "Ueber das Leitungsvermogen der Mettalle fur Warme und Electricitat", *Annalen der Physik und Chemie*, **13**, 582-606.

Mahajan, R. L. and Gebhart, B., 1979, "An Experimental Determination of Transition Limits in a Vertical Natural Convection Flow Adjacent to a Surface," *J. Fluid Mech.*, Vol. **91**, pp. 131-154.

McAdams, W. H., 1954, *Heat Transmission*, 3rd. ed., McGraw-Hill, New York.

Menold, E. R., and Yang, K., 1962, "Asymptotic Solutions for Unsteady Laminar Free Convection on a Vertical Plate," *Trans. of ASME, J. App. Mech.*, Vol. **29**, pp. 124-126.

Minkowycz, W. J., and Sparrow, E. M., 1966, "Free Convection Heat Transfer to Steam Under Variable Property Conditions," *Int. J. Heat Mass Transfer*, Vol. **9**, pp. 1145-1147.

Minkowycz, W. J., and Sparrow, E. M., 1974, "Local Nonsimilar Solutions for Natural Convection on a Vertical

Cylinder," *Trans. of ASME, J. Heat Transfer*, Vol. 96, pp. 178-182.

Na, T. Y., 1979, *Computational Methods in Engineering Boundary Value Problems*, Academic Press, Toronto.

Nachtsheim, P. R., 1963, "Stability of Free-Convection Boundary Layer Flows," *NASA* **TN D-2089**.

Nishikawa, K., and Ito, T., 1969, "An Analysis of Free-Convection Heat transfer From an Isothermal Vertical Plate to Supercritical Fluids," *Int. J. Heat Mass Transfer*, Vol. 12, pp. 1149-1163.

Oberbeck, A., 1879, "Ueber die Warmeleitung der Flussigkeiten ber Berucksichtigung der Stromungen infolge von Temperaturdifferenzen", *Annalen der Physik und Chemie*, 7, 271-279.

Okada, M., Katayama, K., Terasaki, K., Akimoto, M., and Mabune, K., 1978, "Freezing Around a Cooled Pipe in Crossflow," *Bull. of JSME*, Vol. 21, No. 160, pp. 1514-1520.

Ostrach, S., 1953, "An Analysis of Laminar Free-Convection Flow and Heat Transfer about a Flat Plate Parallel to the Generating Body Force," *NACA*, Report No. 1111.

Ozisik, M. N., 1980, *Heat Conduction*, John Wiley and Sons, New York, ch. 10.

Padlog, R. D., and Mollendorf, J. C., 1983, "Variable Fluid Property Effects on Transport in Pure Water Around the Density Extremum," *Trans. of ASME, J. Heat Transfer*, Vol. 105, pp. 655-658.

Patterson, J., and Imberger, J., 1980, "Unsteady Natural Convection in a Rectangular Cavity," *J. Fluid Mech.*, Vol. 100, pp. 65-86.

Petrie, D. J., Linehan, J. H., Epstein, M., Lambert, G. A., and Stachyra, L. J., 1980, "Solidification in Two-Phase Flow," *Trans. of ASME, J. Heat Transfer*, Vol. 102, pp. 784-786.

Piau, J.-M., 1970, "Convection Naturelle Laminarie en Regime Permanent dans les Liquids. Influence des Vaiations des Proprietes Physiques avec la Temperature," *C. R. Acad. Sci. Ser. A*, Vol. 271, pp. 953-956.

Piau, J.-M., 1974, "Influence des Variations des Proprietes Physiques et de la Stratification en Convection

Naturelle," *Int. J. Heat Mass Transfer*, Vol. 17, pp. 465-476.

Plapp, J. E., 1957, "Laminar Boundary Layer Stability in Free Convection (part I) and Laminar Free Convection with Variable Fluid Properties (part II)," *Ph. D. Thesis*, California Institute of Technology.

Polymeropoulos, C. E., and Gebhart, B., 1967, "Incipient Instability in Free Convection Laminar Boundary Layers," *J. Fluid Mech*. Vol. 30, pp. 225-239.

Qureshi, Z. H., 1980, "Stability and Measurements in Fluid and Thermal Transport in Vertical Buoyancy-Induced Flows in Cold Water," Ph. D. Thesis, SUNYAB, Buffalo, NEW York.

Raithby, G. D. and Hollands, K. G. T., 1975, "A General Method of Obtaining Approximate Solutions to Laminar and Turbulent Free Convection Problems, *Adv. Heat Transfer*, Vol. 11, pp. 265-315.

Roache, P. J., 1982, *Computational Fluid Mechanics*, Hermosa Publishers, Albuquerque, N. M., U. S A.

Sammakia, B., and Gebhart, B., 1978, "Transient and Steady State Numerical Solutions in Natural Convection," *Numer. Heat Transfer*, Vol. 1, pp. 529-542.

Sammakia, B., and Gebhart, B., 1981, "Transient Natural Convection Along a Vertical Flat Surface: the Thermal Capacity Effect," *Numer. Heat Transfer*, Vol. 4, pp. 331-344.

Sammakia, B., Gebhart, B., and Qureshi, Z. H., 1982, "Measurements and Calculations of Transient Natural Convection in Water," *Trans. of ASME, J. Heat Transfer*, Vol. 104, pp. 644-648.

Saunders, O. A, 1939, "Natural Convection in Liquids," *Proc. Royal Soc. (London), Series A*, VOl. 172 pp. 55-71.

Schmidt, E., and Beckman, W., 1930, "Das Temperatur-und Geschwindigkeitsfeld von einer Warme abgebenden, senkrechten Platte bei naturlicher Konvektion," *Forsch-Ing.-Wes, Vol*. 1, p. 391.

Schetz, J. A., and Eichhorn, R., 1962, "Unsteady Natural Convection in the Vicinity of a Doubly Infinite Vertical Plate," *Trans. of ASME, J. Heat Transfer*, Vol. 84C, pp. 334-338.

Schuh, H., 1948, "Boundary Layers of Temperature," *Reps. and Trans. 1007, AVA Monograhs*, Bristish M. A. P.

Seeniraj, R. V., and Bose, T. K., 1982, "Planar Solidification of a Warm Flowing-Liquid Under Different Boundary Conditions," *Warme- und Stoffubertragung*, Vol. 16, pp. 105-111.

Shanks, D., 1955, "Non-linear Transformation of Divergent and Slowly Convergent Sequences," *J. Math. Phys.*, Vol. 34, pp. 1-42.

Shaukatullah, H., and Gebhart, B., 1979, "The Effect of Variable Properties on Laminar Natural Convection Boundary-Layer Flow Over a Vertical Isothermal Surface in Water," *Numerical Heat Transfer*, Vol. 2, pp. 215-232.

Siegel, R., 1958, "Transient Free convection From a Vertical Flat Plate," *Trans. of ASME.*, Vol. 80, pp. 347-359.

Sparrow, E. M., 1956, "Free Convection with Variable Properties and Variable Wall Temperature," *Ph. D. Thesis*, Harvard Univ., Cambridge, Mass.

Sparrow, E. M., and Gregg, J. L, 1956, "Laminar Free Convection Heat Transfer From the Outer Surface of a Vertical Cylinder," *Trans. of ASME*, Vol. 78, pp. 1823-1829.

Sparrow, E. M., and Gregg, J. L., 1958, "The Variable Fluid-Property Problem in Free Convection," *Trans. of ASME*, Vol. 80, pp. 879-886.

Sparrow, E. M., Patankar, S. V., and Ramadhyani, S., 1977, "Analysis of Melting in the Presence of Natural Convection in the Melt Region," *Trans. of ASME J. Heat Transfer*, Vol. 99, pp. 520-526.

Sparrow, E. M., Ramsey, J. W., and Kemink, R. G., 1979, " Freezing Controlled by Natural Convection," *Trans. of ASME, J. Heat Transfer*, Vol. 101, pp. 578-584.

Sparrow, E. M., Schmidt, R. R., and Ramsey, J. W., 1978, "Experiments on the Role of Natural Convection in the Melting of Solids," *Trans. of ASME, J. Heat Transfer*, Vol. 100, pp. 11-16.

Sugawara, S., and Michiyoshi, I., 1951, "The Heat Transfer by Natural Convection in the Unsteady State on a Vertical Flat wall," *Proc. 1st Japan Natl. Congr. Appl. Mech.*, pp. 501-506.

Szekely, J., and Chhabra, P. S., 1970, "The Effect of Natural Convection on the Shape and Movement of the Melt-Solid Interface in the Controlled Solidification of Lead," *Metallurgical Trans.*, Vol. 1, pp. 1195-1203.

Szewczyk, A. A., 1962, "Stability and Transition of the Free Convection Boundary Layer Along a Vertical Flat Plate," *Int. J. Heat Mass Transfer*, Vol. 5, pp. 903-914.

Thompson, J. F., 1978, "Numerical Solution of Flow Problems Using Boundary-Fitted Coordinate Systems," *Von Karman Inst. for Fluid Dynamics*, Lecture Series-4, pp. 1-100.

Tien, C. L. and Yen, Y., 1960, "An Approximate Solution of a Melting Problem with Natural Convection," *Chem. Engng. Prog. Symp. Series*, Vol. 62, No. 64, p. 166.

Touloukian, Y. S., and Ho, C. Y., 1972, *Thermophysical Properties of Matter, Vol. 1 to 8*, Plenum Press.

Van Buren, P. D., and Viskanta, R., 1980, "Interferometric Observation of Natural Convection During Freezing From a Vertical Flat plate," *Trans. of ASME, J. Heat Transfer*, Vol. 102, pp. 375-378.

Viskanta, R., 1983, "Phase-Change Heat Transfer," *Solar Heat Storage: Latent Heat Materials*, Vol. *1* edited by G. A. Lane, Uniscience Edition, CRC Press, Boca Raton.

Wazzen, A. R., Okamura, T., and Smith, A. M. O., 1968, "The Stability of Water Flow Over Heated and Cooled Flat Plates," *Trans. of ASME, J. Heat Transfer*, Vol. 68, pp. 109-113.

Weast, R. C., 1982, *CRC Handbook of Chemistry and Physics*, 63rd ed., CRC Press, Boca Raton.

Yuill, G. H., 1972, "Free Convection Heat Transfer From a Vertical Isothermal Plate to Water Near 4°C," *Ph. D. Thesis*, University of Minnesota.

Yuen, W. W., and Kleinman, A. M., 1980, "Application of a Variable Time-Step Finite-Difference Method for the One-Dimensional Melting Problem Including the Effect of Subcooling," *AIChE Jl.*, Vol. 26, pp. 828-832.

Appendix A

The Normalization and the Order-of-Magnitude Analysis of Laminar Flow Equations

The equations governing the conservation of mass, momentum, and energy for the two-dimensional laminar natural convective flow of an isotropic Newtonian fluid of variable properties along an isothermal vertical flat plate are given by (the dimensional quantities are given with a -) (Batchelor, 1967),

$$\frac{\partial(\bar{\rho}\ \bar{u}\ )}{\partial \bar{x}} + \frac{\partial \bar{\rho}\ \bar{v}}{\partial \bar{y}} = 0 \qquad (A.1)$$

$$\bar{\rho}\ (\bar{u}\ \frac{\partial \bar{u}}{\partial \bar{x}} + \bar{v}\ \frac{\partial \bar{u}}{\partial \bar{y}}) = - \frac{\partial \bar{p}_d}{\partial \bar{x}} + g(\rho_\infty - \bar{\rho}\ ) + \frac{\partial}{\partial \bar{x}}\left[2\bar{\mu}\ \frac{\partial \bar{u}}{\partial \bar{x}}\right.$$

$$\left. - \frac{2}{3}\ \bar{\mu}\ (\frac{\partial \bar{u}}{\partial \bar{x}} + \frac{\partial \bar{v}}{\partial \bar{y}})\right] + \frac{\partial}{\partial \bar{y}}\left[\bar{\mu}\ (\frac{\partial \bar{u}}{\partial \bar{y}} + \frac{\partial \bar{v}}{\partial \bar{x}})\right] \qquad (A.2)$$

$$\bar{\rho}\ (\bar{u}\ \frac{\partial \bar{v}}{\partial \bar{x}} + \bar{v}\ \frac{\partial \bar{v}}{\partial \bar{y}}) = - \frac{\partial \bar{p}_d}{\partial \bar{y}} + \frac{\partial}{\partial \bar{y}}\left[2\bar{\mu}\ \frac{\partial \bar{v}}{\partial \bar{y}}\right.$$

$$\left. - \frac{2}{3}\ \bar{\mu}\ (\frac{\partial \bar{u}}{\partial \bar{x}} + \frac{\partial \bar{v}}{\partial \bar{y}})\right] + \frac{\partial}{\partial \bar{x}}\left[\bar{\mu}\ (\frac{\partial \bar{u}}{\partial \bar{y}} + \frac{\partial \bar{v}}{\partial \bar{x}})\right] \qquad (A.3)$$

$$\bar{\rho}\ \bar{c}_p\ (\bar{u}\ \frac{\partial \bar{t}}{\partial \bar{x}} + \bar{v}\ \frac{\partial \bar{t}}{\partial \bar{y}}) = \frac{\partial}{\partial \bar{x}}(\bar{k}\ \frac{\partial \bar{t}}{\partial \bar{x}}) + \frac{\partial}{\partial \bar{y}}(\bar{k}\ \frac{\partial \bar{t}}{\partial \bar{y}})$$

$$- \frac{T}{\bar{\rho}}(\frac{\partial \bar{\rho}}{\partial \bar{t}})_p \left[\bar{u}\ \frac{\partial \bar{p}}{\partial \bar{x}} + \bar{v}\ \frac{\partial \bar{p}}{\partial \bar{y}}\right] + \bar{\mu}\ \bar{\phi} \qquad (A.4)$$

where

$$\bar{\phi} = \left[2\frac{\partial\bar{u}}{\partial\bar{x}} - \frac{2}{3}\left(\frac{\partial\bar{u}}{\partial\bar{x}} + \frac{\partial\bar{v}}{\partial\bar{y}}\right)\right]\frac{\partial\bar{u}}{\partial\bar{x}} + \left[\frac{\partial\bar{u}}{\partial\bar{y}} + \frac{\partial\bar{v}}{\partial\bar{x}}\right]^2 +$$

$$\left[2\frac{\partial\bar{v}}{\partial\bar{y}} - \frac{2}{3}\left(\frac{\partial\bar{u}}{\partial\bar{x}} + \frac{\partial\bar{v}}{\partial\bar{y}}\right)\right]\frac{\partial\bar{v}}{\partial\bar{y}}$$

and $\bar{p}_d = (\bar{p} - p_\infty)$

For the ambient fluid

$$\frac{\partial p_\infty}{\partial\bar{x}} = \rho_\infty g \qquad (A.5)$$

As a first step in seeking any simplification to the above set of steady two dimensional equations, an attempt is made to normalize the dependent and independent variables by introducing a set of characteristic quantities (given with subscript c). The definition of each of these characteristic quantities must come either from the boundary conditions and the governing equations or from the physical description of the problem. The normalized variables are defined as follows,

$$x = \frac{\bar{x}}{x_c},\ y = \frac{\bar{y}}{y_c},\ u = \frac{\bar{u}}{u_c},\ v = \frac{\bar{v}}{v_c},$$

$$\theta = \frac{t-t_\infty}{t_0-t_\infty}\ \rho = \frac{\bar{\rho}}{\rho_c},\ \mu = \frac{\bar{\mu}}{\mu_c},\ k = \frac{\bar{k}}{k_c},\ c_p = \frac{\bar{c}_p}{c_{pc}},$$

The normalized variables are substitued in the equations (A.1) to (A.4). The resulting equations are,

$$\frac{\rho_c u_c}{x_c} \frac{\partial(\rho u)}{\partial x} + \frac{\rho_c v_c}{y_c} \frac{\partial(\rho v)}{\partial y} = 0 \tag{A.6}$$

$$\begin{aligned}
\frac{\rho_c u_c^2}{x_c} \rho \left[u\frac{\partial u}{\partial x} + \frac{v_c x_c}{u_c y_c} v \frac{\partial u}{\partial y}\right] &= - \frac{\partial \bar{p}_d}{\partial x} + (\rho_\infty - \bar{\rho})g \\
&+ \frac{\mu_c u_c}{y_c^2} \left[\frac{y_c^2}{x_c^2} \frac{\partial}{\partial x}\{2\mu\frac{\partial u}{\partial x} - \frac{2}{3} \mu(\frac{\partial u}{\partial x} + \frac{v_c x_c}{u_c y_c} \frac{\partial v}{\partial y})\}\right. \\
&\left.+ \frac{\partial}{\partial y}\{\mu(\frac{\partial u}{\partial y} + \frac{y_c^2}{x_c^2} \frac{\partial v}{\partial x})\}\right]
\end{aligned} \tag{A.7}$$

$$\begin{aligned}
\frac{\rho_c u_c v_c}{x_c} \rho \left[u\frac{\partial v}{\partial x} + \frac{v_c x_c}{u_c y_c} v \frac{\partial v}{\partial y}\right] &= - \frac{\partial \bar{p}_d}{\partial y} \\
&+ \frac{\mu_c u_c}{y_c x_c} \left[\frac{y_c v_c}{x_c u_c} \frac{\partial}{\partial y}\{2\mu\frac{\partial v}{\partial y} - \frac{2}{3}\mu (\frac{\partial u}{\partial x} + \frac{v_c x_c}{u_c y_c} \frac{\partial v}{\partial y})\}\right. \\
&\left.+ \frac{\partial}{\partial x}\{\mu(\frac{\partial u}{\partial y} + \frac{y_c^2}{x_c^2} \frac{\partial v}{\partial x})\}\right]
\end{aligned} \tag{A.8}$$

$$\begin{aligned}
\frac{\rho_c c_{pc} u_c}{x_c}\Delta t \ \rho c_p \left[u\frac{\partial \theta}{\partial x} + \frac{v_c x_c}{u_c y_c} v \frac{\partial \theta}{\partial y}\right] &= \\
\Delta t\frac{k_c}{y_c^2} &\left[\frac{y_c^2}{x_c^2} \frac{\partial}{\partial x}(k\frac{\partial \theta}{\partial x}) + \frac{\partial}{\partial y}(k\frac{\partial \theta}{\partial y})\right] \\
&- \frac{T}{\bar{\rho}}(\frac{\partial \bar{\rho}}{\partial t})_p \left[\bar{u} \frac{\partial p}{\partial \bar{x}} + \bar{v} \frac{\partial p}{\partial \bar{y}}\right] + \bar{\mu} \bar{\phi}
\end{aligned} \tag{A.9}$$

There are only two groups of terms in the continuity eq. (A.7). As there is no special relationship between one of the velocities and the density, both groups must be of the same order. Hence,

$$\frac{u_c}{x_c} \sim \frac{v_c}{y_c} \tag{A.10}$$

The flow is thermally developed. Hence, in the energy eq. (A.9), the order of convection terms has to be equal to the order of the larger of the two conduction terms, namely the lateral conduction term.

$$\frac{\rho_c c_{pc} u_c}{x_c} \sim \frac{k_c}{y_c^2}$$

$$\text{i. e.} \qquad \frac{u_c}{x_c} \sim \frac{\nu_c}{\text{Pr}\ y_c^2} \tag{A.11}$$

For moderate and large Prandtl numbers, the viscous force term is of the same order as the buoyancy force term. Hence, in the momentum eq. (A.8),

$$\frac{\mu_c u_c}{y_c^2} \sim (\rho_\infty - \rho_0) g \tag{A.12}$$

It can be easily shown from eqs. (A.11) to (A.13) that

$$\frac{y_c}{x_c} \sim (Ra_x)^{-1/4} \tag{A.13}$$

where $$Ra_x = \frac{g(\rho_\infty - \rho_0)x_c^3}{\rho_0 \nu_c a_c}$$

Hence the condition for the boundary layer approximation

$$\frac{y_c}{x_c} < 1 \text{ is } Ra_x >> 1 \tag{A.14}$$

When the boundary layer approximation is employed the equations (A.1) to (A.4) become (dropping the - for the sake of convenience),

$$\frac{\partial}{\partial x}(\rho u) + \frac{\partial}{\partial y}(\rho v) = 0 \tag{A.15}$$

$$\rho(u\frac{\partial u}{\partial x} + v\frac{\partial u}{\partial y}) = g(\rho_\infty - \rho) + \frac{\partial}{\partial y}(\mu\frac{\partial u}{\partial y}) \tag{A.16}$$

$$\rho c_p(u\frac{\partial t}{\partial x} + v\frac{\partial t}{\partial y}) = \frac{\partial}{\partial y}(k\frac{\partial t}{\partial y}) - \frac{T}{\rho}(\frac{\partial \rho}{\partial t})_P \, u\frac{\partial p}{\partial x} + \mu\left[\frac{\partial u}{\partial y}\right]^2 \tag{A.17}$$

Appendix B

Variations of Properties of Liquids with Temperature

The properties of the liquids, density (kg/m^3), viscosity (cP), thermal conductivity (W/m^2/K), and specific heat at constant pressure (kJ/kg/K) used in Chapter 2 were taken from Fowle (1944), Touloukian and Ho (1972), Kell (1975), Fujii et al. (1978) and Weast (1982). In particular, the variations of properties with temperature employed in the numerical calculations are

Water

$$\rho(t)=(a_0+a_1t+a_2t^2+a_3t^3+a_4t^4+a_5t^5)/(1.0+a_6t)$$

where $a_0=999.83952$,

$a_1=+0.16945176 \text{ X } 10^{+02}$

$a_2=-0.79870401 \text{ X } 10^{-02}$

$a_3=-0.46170461 \text{ X } 10^{-04}$

$a_4=+0.10556302 \text{ X } 10^{-06}$

$a_5=-0.28054253 \text{ X } 10^{-09}$

$a_6=+0.16879850 \text{ X } 10^{-01}$

and t is the temperature in °C

If $t \le 20°C$

$$\log_{10}\mu(t)=b_1/(b_2+b_3(t-20.0)+b_4(t-20.0)^2)+b_5$$

If t > 20°C

$$\log_{10}\frac{\mu(t)}{\mu_{20}}=(b_6(20.0-t)+b_7(20.0-t)^2)/(b_8+t)$$

where $b_1=1301.0$

$b_2=998.333$

$b_3=8.1855$

$b_4=0.00585$

$b_5=-1.30233$

$b_6=1.3272$

$b_7=-0.001053$

$b_8=105.0$

$\mu_{20}=1.002$

$$k(t)=c_0+c_1\left[\frac{T}{T_0}\right]+c_2\left[\frac{T}{T_0}\right]^2+c_3\left[\frac{T}{T_0}\right]^3+c_4\left[\frac{T}{T_0}\right]^4$$

where $c_0=-0.92247$

$c_1=2.8395$

$c_2=-1.8007$

$c_3=0.52577$

$c_4=-0.07344$

$T=t+273.15$

$T_0=273.15$

$$c_p(t)=d_4\left[d_1+d_2(1.0+0.1t)^{(d_3)}+d_5 \text{ X } 10^{(d_6t)}\right]$$

where $d_1=0.996185$

$d_2=0.0002874$

$d_3=5.26$

$d_4=4.1855$

$d_5=0.01116$

$d_6=-0.036$

Ethyl Alcohol

$\rho(t)=a_0/(1.0+a_1t+a_2t^2+a_3t^3)$

where $a_0=806.0$

$a_1=0.10414 \times 10^{-02}$

$a_2=0.78360 \times 10^{-06}$

$a_3=0.17168 \times 10^{-07}$

$\mu(t)=b_0+b_1t+b_2t^2+b_3t^3$

where $b_0=1.77126$

$b_1=-0.335179 \times 10^{-01}$

$b_2=+0.291416 \times 10^{-03}$

$b_3=-0.101107 \times 10^{-05}$

$k(T)=(c_0+c_1T)c_2$

where $c_0=0.609512 \times 10^{03}$

$c_1=-0.70924 \times 10^{00}$

$c_2 = 0.41840 \times 10^{-03}$

$T = t + 273.15$

$$c_p(T) = (d_0 + d_1 T + d_2 T^2 + d_3{}^3) d_4$$

where $d_0 = 0.504351$

$d_1 = -0.481584 \times 10^{-03}$

$d_2 = -0.921631 \times 10^{-06}$

$d_3 = 0.114379 \times 10^{-07}$

$d_4 = 4.184$

$T = t + 273.15$

Benzene

$$\rho(t) = a_0 / (1.0 + a_1 t + a_2 t^2 + a_3 t^3)$$

where $a_0 = 899.0$

$a_1 = 0.11763 \times 10^{-02}$

$a_2 = 0.12775 \times 10^{-05}$

$a_3 = 0.80650 \times 10^{-08}$

$$\mu(t) = b_0 + b_1 t + b_2 t^2 + b_3 t^3 + b_4 t^4$$

where $b_0 = 0.908909$

$b_1 = -0.171538 \times 10^{-01}$

$b_2 = 0.246300 \times 10^{-03}$

$b_3=-0.217716 \times 10^{-05}$
$b_4= 0.786713 \times 10^{-08}$

$$k(T)=(c_0+c_1T)c_2$$

where $c_0=0.525278 \times 10^{03}$
$c_1=-0.604093 \times 10^{00}$
$c_2= 0.41840 \times 10^{-03}$
$T=t+273.15$

$$c_p(T)=(d_0+d_1T+d_2{}^2+d_3T^3)d_4$$

where $d_0=0.283708$
$d_1=0.275787 \times 10^{-03}$
$d_2=0.234387 \times 10^{-06}$
$d_3=0.106981 \times 10^{-08}$
$d_4= 4.184$
$T=t+273.15$

Freon R-12

$$\rho(t)=1000.0/(a_0+a_1t+a_2t_a^{3.25})$$

where $a_0=0.7080$
$a_1=0.115 \times 10^{-02}$
$a_2=0.140 \times 10^{-07}$

$$t_a = t + 60.0$$

$$\mu(t) = b_0 10^{\{b_1/(t+b_2)\}}$$

where

$b_0 = 0.179 \times 10^{-01}$

$b_2 = 0.341 \times 10^{+03}$

$b_3 = 0.292 \times 10^{+03}$

$$k(t) = c_0 + c_1 t$$

where $c_0 = +0.784 \times 10^{-01}$

$c_1 = -0.367 \times 10^{-03}$

$$c_p(t) = d_0 + d_1 t + d_2 t_a^{(d_3)}$$

where $d_0 = 0.926$ $d_1 = 0.944 \times 10^{-03}$

$d_2 = 0.750 \times 10^{-10}$

$d_3 = 4.45$

In Chapter 4, to study the effects of maximum density in the case of water, the density-temperature relationship proposed by Gebhart and Mollendorf (1977) was used.

$$\rho(t) = \rho_m (1 - a_t |t - t_m|^q)$$

where $q=1.8949$, $\alpha_t=9.2972 \times 10^{-6}$ and the temperature corresponding to the desity maximum, $t_m=4.0293$°C. The advantage of this relation is that the effect of maximum density is characterized by a single parameter R, as defined in Chpater 4. The above relation is valid in the temperature range 0 to 20°C for pure water at 1 atmospheric pressure.

Appendix C

The Error in the Local Heat Transfer Coefficient due to Boussinesq Approximations for a Typical Laminar Flow Situation in Water

In this section, the error in the local heat transfer coefficient due to Boussinesq approximations is calculated for the laminar natural convective boundary layer flow of water along an isothermal vertical flat plate at 10 cm from the leading edge when the film temperature and the temperature difference between the wall and the ambient medium are 20°C. The error is calculated for three reference temperatures, namely t_0, t_f and t_∞. Also, the error due to the model proposed by Piau (1974) to include the effects of variable properties is given. The functional variation of properties with temperature are given in Appendix B. The properties of water for the temperatures of interest are:

	10°C	20°C	30°C
Pr	9.3367	6.9437	5.3907
ρ (kg/m^3)	999.6995	998.2054	995.6562
μ (cP)	1.3072	1.0019	0.7976
$\nu \times 10^6$ (m^2/s)	1.3076	1.0038	0.8011
k (W/mK)	0.5869	0.6034	0.6182
c_p (kJ/kg/K)	4.1919	4.1816	4.1782
$\beta \times 10^3$ (K^{-1})	0.0880	0.2068	0.3032

Geometry: vertical flat plate
Fluid: water
$x=0.10$ m
$t_f=20°C$ and $|t_0-t_\infty|=20°C$

% Error in the local heat transfer coefficient due to Boussinesq approximations

	$t_r=t_0$	$t_r=t_f$	$t_r=t_\infty$
(a)heated wall	+21.7	+3.7	-22.0
(b)cooled wall	-26.2	-1.7	+15.0

$$\left[\ \% \text{ Error}=100\frac{h(x)_{B.A.}-h(x)}{h(x)}\ \right]$$

where $h(x)$ is the local heat transfer coefficient including the effects of variable properties and $h(x)_{B.A.}$ is the local heat transfer coefficient with Boussinesq approximations. (Eqs. (2.15) to (2.17) were solved to obtain the value of $h(x)$).

	Piau(1974)
(a)heated wall	-7.5

It is clearly seen that the error in the local heat transfer coefficient is more pronounced when either t_0 or t_∞ is selected as the reference temperature for both Boussinesq approximations and Piau's model.

Appendix D

The Initial Stage of the Transient Natural Convective Flow Adjacent to a Vertical Circular Cylinder

Points Away From the Leading Edge

The transient natural convective flow that arises as a result of a step increase in surface temperature can be descibed as follows. Heat is conducted into the fluid from the wall resulting in a thin vertical layer of heated fluid. The fluid moves up as the buoyancy force acclerates it. Momentum is both advected away by this velocity and diffused into the ambient fluid. Heat is also convected vertically by this velocity and the layer will continue to grow until the heat conducted in from the boundary balances that convected away. The scale analysis is similar to the transient flow inside a rectangular cavity described in detail by Patterson and Imberger (1980).

But for points at a finite distance from the leading edge, the initial stage of the transient natural convective flow development is a pure conduction phase. The flow is parallel to the axis of the cylinder and is independent of the axial coordinate, x. The transverse velocity component, v is zero. The temperature, t and the (axial) velocity, u are functions of the radial coordinate, r and time, $\bar{\tau}$. Employing Boussinesq approximations, the equations governing the conservation of momentum and energy for this regime are given by

$$\frac{\partial u}{\partial \bar{\tau}} = g\beta(t-t_\infty) + \nu\left[\frac{1}{r}\frac{\partial u}{\partial r} + \frac{\partial^2 u}{\partial r^2}\right] \qquad (D.1)$$

$$\frac{\partial t}{\partial \bar{\tau}} = \alpha\left[\frac{1}{r}\frac{\partial t}{\partial r} + \frac{\partial^2 t}{\partial r^2}\right] \qquad (D.2)$$

The initial and the boundary conditions are,

for $\bar{\tau} < 0$,

$u = 0$ and $t = t_\infty$ for all y (D.3)

for $\bar{\tau} \geq 0$,

$u = 0$ and $t = t_0$ at $y = 0$, for all x (D.4)

$u \to 0$ and $t \to t_\infty$ as $y \to \infty$ (D.5)

It should be stressed again that for a semi-infinite vertical circular cylinder the equations (D.1) to (D.5) are valid only for an initial short period of time before the leading edge effect is felt at that particular axial location. The propagation distance x_p of the leading edge may be estimated as follows (Siegel, 1958):

$$x_p(\bar{\tau}) = \int_0^{\bar{\tau}} [u(r,\bar{\tau})]_{max} d\bar{\tau} \qquad (D.5)$$

where the maximum value of the vertical velocity component is employed in determining the maximum distance propagated by the leading edge effect. This allows a determination of the time period for which the conduction solution may be expected to apply locally before convection effects become significant. Approximate solutions to eqs. (D.1) to (D.5) can be obtained by a perturbation technique.

Points Near the Leading Edge

During the initial stage, the flow velocities are smaller. Hence, near the leading edge, the effect of axial conduction terms may be important and the complete two-dimensional equations have to be solved to get an accutrate solution. This is especially true at low Prandtl numbers.

Appendix E

A Note on the Numerical Methods Employed in the Thesis

In this section a brief description of the numerical methods employed in different Chapters is given.

The base flow equations for the laminar natural convective flow along an isothermal vertical flat plate given in Chapters 2 to 4 constitute a system of fifth order ordinary differential equations, coupled in temperature through the buoyancy force term of the momentum equation. For example, the equations given in Chapter 3 are

$$\frac{d}{d\eta}\left[\{1+\gamma_f(\theta-0.5)\}\ F''\right] + 3FF''- 2(F')^2 + \theta[1+\epsilon_f(\theta-1)] = 0 \tag{C.1}$$

$$\theta'' + 3PrF\theta' = 0 \tag{C.2}$$

The corresponding boundary conditions are

$$F(0) = F'(0) = \theta(0) - 1 = F'(\infty) = \theta(\infty) = 0 \tag{C.3}$$

A number of numerical techniques can be employed to solve a system of ordinary differential equations with boundary conditions specified at two different points. In this analysis, the integration scheme employed was a fourth order Runga-Kutta method. The integration was performed starting from the outer edge of the boundary layer to the wall. A set of approximate solutions for F and θ when $\eta \to \infty$ were used as the starting values. The approximate solutions for F and θ when $\eta \to \infty$ can be found as follows:

From the boundary conditions at $\eta \to \infty$, $f(\infty) \to A$, the entrainment velocity, a constant. Hence, in the far field, the eqs. (C.1) to (C.3) can be written as,

$$\lambda F''' + 3AF'' = -q\theta \qquad \text{(C.4)}$$

$$\theta'' + 3PrA\theta' = 0 \qquad \text{(C.5)}$$

where $\lambda = 1 - \frac{\gamma_f}{2}$ and $q = 1 - \epsilon_f$.

The equation (C.5) can be integrated to obtain:

$$\theta = B \exp(-3PrA\eta)$$

The solution to eq. (C.4) can be written as the sum of a homogeneous solution and a particular solution. The homogeneous solution F_h is obtained from the homogeous part of eq. (C.4).

$$F_h = C_1 + C_2\eta + C_3\exp(-3A\eta/\lambda)$$

The particular solution F_p is given by

$$F_p = \frac{Bq}{[27A^3Pr^2(\lambda Pr - 1)]} e^{-3APr\eta}$$

The complete solution for $\eta \to \infty$

$$F=F_h+F_p$$

Employing the boundary conditions at $\eta\to\infty$, it can be easily shown that $C_1=A$; $C_2=0$, and let $C_3=C$.

Hence the solutions for $\eta\to\infty$ are

$$F = A + C\, e^{-3A\eta/\lambda} + \frac{Bq}{[27A^3Pr^2(\lambda Pr-1)]}\, e^{-3APr\eta} \qquad (3.38)$$

$$\theta = B\, e^{-3APr\eta} \qquad (3.39)$$

The asymptotic solutions provided effective starting values to an integration scheme beginning at large η (=10.0, for Pr=10, for example) and proceeding inward to $\eta=0$. The constants were guessed intially, and the integration was performed. The constants were corrected by a shooting technique. With correct gusses, the specified conditions at the wall $\eta=0$ would be satisfied.

The disturbance equations can be solved in a similar manner. The asymptotic solutions for the disturbance equations and further details are given Chapters 3 and 4 (see sections 3.1.5 and 4.1.3).

Chapter 5

The equations governing the transient natural convective flow along a vertical circular cylinder subjected to a step change in surface temperature are a system of partial differential equations. The numerical method employed to solve these equations was a straight forward upwind finite differene scheme. The details of the method can be found in Roache (1982) and Carnahan et al. (1969). (see also section 5.1.2, for further details).

Chapter 6

In Chapter 6, the method boundary-fitted coordinate systems was employed to find the temperature distribution inside the irregular solidified region. A detailed account of this method can be found in Thompson (1978). The finite differenced equations and the boundary conditions were solved using a successive over-relaxation (SOR) procedure (see section 6.1, for further details). The details of SOR can be found in any standard book on the numerical analysis (Carnahan et al., 1969, for example).